NTNU – Trondheim
Norwegian University of
Science and Technology

The Modelling of Suction Caisson Foundations for Multi-Footed Structures

Marijn Johannes Dekker

Wind Energy
Submission date: July 2014
Supervisor: Torgeir Moan, IMT
Co-supervisor: Gudmund Eiksund, BAT
Andrej Metrikine, TU Delft
Jeroen Hoving, TU Delft

Norwegian University of Science and Technology
Department of Marine Technology

Master Thesis of Science

The Modelling of Suction Caisson Foundations for Multi-Footed Structures

Marijn J. Dekker

Sponsored by SPT Offshore

15-07-2014

European Wind Energy Master - EWEM- Offshore Engineering Track

The Modelling of Suction Caisson Foundations for Multi-Footed Structures

Master of Science Thesis

For obtaining the degree of Master of Science in Offshore Engineering at Delft University of Technology and in Technology-Wind Energy at Norwegian University of Science and Technology.

Marijn J. Dekker

15-07-2014

European Wind Energy Master - EWEM
Delft University of Technology
Norwegian University of Science and Technology
SPT Offshore

Cover photo courtesy of SPT Offshore

European Wind Energy Master - EWEM
Of
Offshore Engineering Track

The undersigned hereby certify that they have read and recommend to the European Wind Energy Master - EWEM for acceptance a thesis entitled **"The Modelling of Suction Caisson Foundations for Multi-Footed Structures"** by **Marijn J. Dekker** in partial fulfillment of the requirements for the degree of **Master of Science**.

Dated: 15-07-2014

Supervisor: _____
Prof. A. Metrikine of Delft University of Technology

Supervisor: _____
Prof. T. Moan of Norwegian University of Science and Technology

Reader: _____
Prof. G.R. Eiksund of Norwegian University of Science and Technology

Reader: _____
Ir. J.S. Hoving of Delft University of Technology

Reader: _____
Ir. O.J. Dijkstra of SPT Offshore

Summary

Suction caisson foundations are becoming an increasingly used foundation solution for offshore structures, both as single anchor piles for floating structures and directly attached to a substructure for bottom-fixed offshore structures. For a structure founded on multiple caissons the foundation is statically indeterminate and the response to a load will depend on the stiffness of the suction caissons and the soil in which they are embedded, as well as the stiffness of the substructure and the topside. This soil-structure interaction dictates the use of an integrated approach for the design of the suction caissons.

The common practice for this integrated design is to model the caissons by means of a set of fixed-end linear springs connected to the substructure, as sketched in Figure 1. This way a design load can be applied on the substructure and the resulting reaction forces on and displacements of the suction caissons can be determined from the spring forces and deflections. This method does however not account for the non-linear load-displacement behaviour of soils, which can lead to incorrect load distributions for ultimate load conditions.

This thesis aims to develop a method that includes a more realistic foundation behaviour and can thus provide more accurate results for ultimate load conditions. In order to do this three different methods to model the foundation stiffness have been studied. First the currently used method with linear springs is studied. Next two methods taking non-linear soil behaviour into account have been developed, the first one using non-linear springs, the other using several load steps to solve the system. The methods have been applied for both a single suction caisson and a model of a jacket substructure resting on four suction caissons and compared with FEM calculations in the geotechnical software Plaxis. The FEM calculations come with their own inaccuracies and will not provide the exact behaviour of the system, however they have been used as a benchmark since model or full scale model tests are not feasible.

Linear spring method

In the linear-elastic method the caissons are assumed to act as a rigid body, which results in a system with 6 degrees of freedom that can be described by a 6x6 stiffness matrix.

The stiffness terms in this matrix can either be determined from analytical or empirical formulae based on the soil parameters and caisson dimensions or they can be computed using a FEM analysis. Three sets of analytical stiffness formulations have been compared with FEM calculations in Plaxis. The results showed that the analytical expressions give useful results that can be within a 10% range from the FEM results, provided that the soil is linear-elastic and uniform. This assumption is far from realistic and for other soil profiles the results can vary significantly.

Next the spring foundations have been applied in a structural model of a jacket founded on four suction caissons. The spring stiffnesses in this model have been based on the FEM results for a single caisson to allow for a fair comparison with FEM calculations of the full model. The models have been compared for shear moduli of 5, 20, 60 and 240 MPa. Additional springs between the caissons have been added in the structural model to account for the interaction between the caissons through the soil. The spring stiffnesses for these additional springs have been determined from a 24x24 flexibility matrix that has been determined in the full FE model of the four caissons. The resulting loads on the caissons correspond with an average difference of approximately 5% while the average caisson displacements match within an average range of 5 to 15%. These results show that the design method that is currently used provides accurate results for analytical soil profiles that are uniform and behave linear-elastic. The question is however whether this model can also be used for realistic soil profiles.

Non-linear spring method

There are various soil models that can be used to describe the non-linear behaviour of soils in a FE model. Two of these models, the Mohr-Coulomb model and the Hardening Soil model, have been compared and the Hardening Soil model has been selected for further use in the calculations since it gives a better correspondence with model tests and includes more aspects of realistic soil behaviour. The first approach to include the non-linear behaviour of the soil in the structural model that has been considered is the replacement of the linear springs by non-linear ones defined by load-displacement curves. Two models, each with a different configuration of non-linear springs, have been developed and the curves for the springs have been determined using FEM calculations for a single caisson. Since it is not possible to use a stiffness matrix, which allows for coupling between the degrees of freedom, in the non-linear spring models the springs have to be attached at the rotation centres of the caissons. In the first model all springs are connected to the centre rotation for an overturning moment. In the second model the lateral and rotational springs are combined into two springs, one of which is applied at mudline and the other at the rotation centre for a lateral load. The models therefore assume that these rotation centres have a fixed position. This assumption has been checked and is only valid for a limited load range, as the rotation centres vary with the applied load. Another assumption that the models rely on is that the load-displacement curves are a function of a single load component and not influenced by any other load components. A series of FEM calculations has been carried out to test this assumption and it can be concluded that the assumption is not valid. The loading in other directions can lead to a change of the stiffness for a degree of freedom by as much as a factor two. An additional vertical load will lead to an increased lateral and rotational stiffness whereas an overturning moment reduces the lateral stiffness and vice versa.

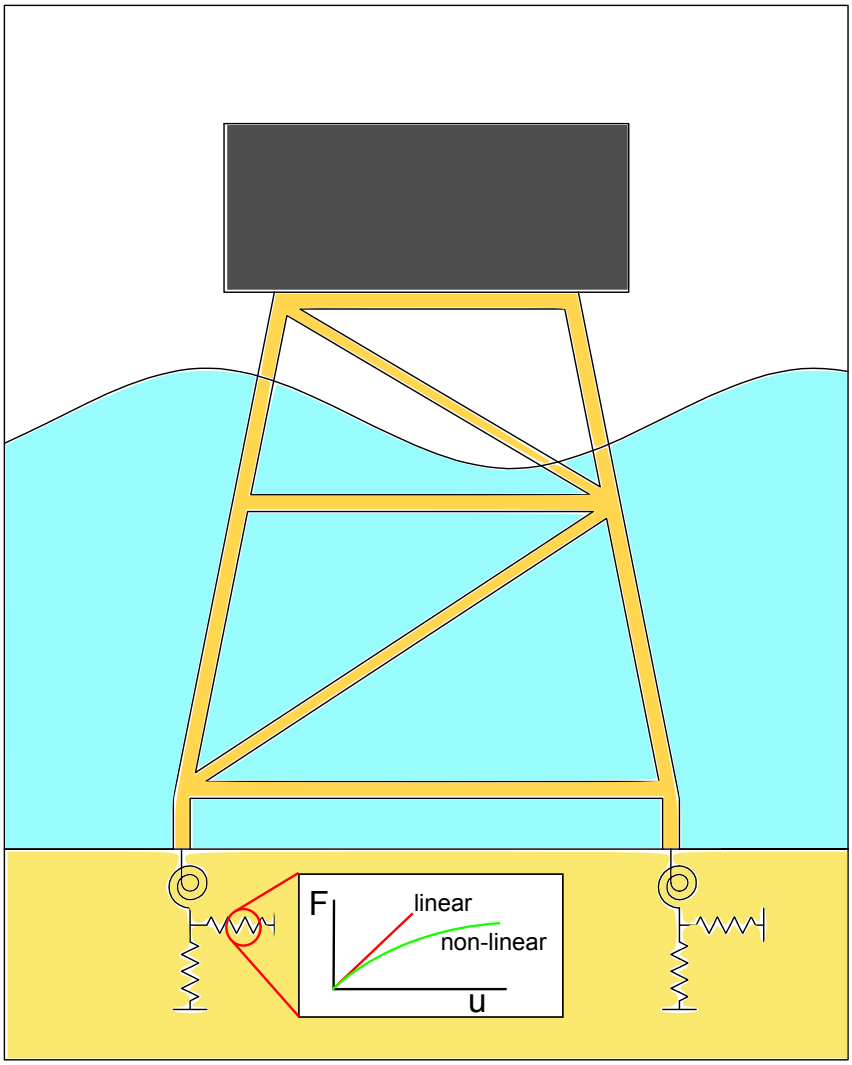

Figure 1: *Sideview of a jacket with suction caisson foundations modelled as springs*

The two caisson models have been implemented in the structural model including the substructure and compared with FEM calculations in Plaxis, again for four different soil stiffnesses that correspond to the same shear moduli as used for the linear-elastic model. The comparison has shown that the non-linear models provide better results than a model using linearized springs. For the loads on the caissons the average difference varies from about 5% for the stiffest soil to approximately 30% for the loosest soil. This is because the foundation behaviour is more sensitive for the exact soil stiffness as the soil stiffness decreases. The average difference in the caisson displacements is in the order of 20 to 30%. The results for the loads on the caissons seem accurate enough to be used for most soil profiles but the results for the displacements contain a significant inaccuracy. The determination of the exact soil stiffness for the correct load conditions is needed to limit the inaccuracy. It has also been attempted to improve the accuracy of the results by applying additional springs between the caissons to account for the interaction effects between the caissons, however the load-displacement curves for these springs could not be obtained with sufficient accuracy to provide useful results.

Stepwise solving method

A different method for the evaluation of non-linear soil-structure interaction that has been investigated is the evaluation of the foundation behaviour in several steps, using stiffness matrices that are updated after each load step. A fraction of the load is applied in the structural model and the loads on the four caissons are determined. These loads are then applied on a FE model of a single caisson in Plaxis and subsequently the updated stiffness matrices for the caissons are determined. These can then be implemented in the structural model and a new load step can be applied to find the updated loads on the caissons. The advantage of this method is that the updated caisson stiffness automatically take the correct load condition into account, as well as the actual position of the centre of rotation. The correct deformations of the jacket substructure are however not included in the model, as the load steps are applied starting from an undeformed initial condition. The jacket deformations could be included by adjusting the caisson springs such that they give the correct deformations in an unloaded condition, however this would make the method far more complex to use and has therefore not been equipped.

The method has been compared with FEM calculations using various numbers of load steps. For the used combination of load case, caisson and jacket geometry and soil stiffness the results showed that five load steps were sufficient to get convergence in the results. The resulting reaction forces on the caissons show good correspondence with the FEM calculations with an average difference of 7%. The caisson displacements vary by 40% on average however, which makes these results unreliable. The results have been obtained for a soil stiffness corresponding to a shear modulus of 60 MPa for an effective stress of 100 kPa. The method using non-linear springs provides results for the caisson displacements that are in a significantly better agreement with the results from the FEM analysis for the same soil stiffness and is therefore considered to be more suited for the evaluation of non-linear foundation stiffness behaviour. The inaccurate results of the stepwise method are most likely caused by not taking the substructure deformations into account, as a comparison for a single caisson without attached substructure gave results from the stepwise method and FEM calculations that varied less than 5%. The stepwise method is thus able to produce quite accurate results, in fact more accurate than when using the non-linear springs, due to the consideration of the actual load combination. The inaccuracies introduced by not accounting for the substructure deformations outweigh this effect however and make the method less suited for applications with multiple caissons.

Conclusions

Of all three methods evaluated the method using non-linear springs is considered the most promising for the design of suction caisson foundations for multi-footed structures. It is able to describe the changing load distribution over the foundations for ultimate load conditions as a result of non-linear soil-structure interaction and provides reliable results for a wide range of soil stiffnesses. The method can and should be improved further however by determining the spring stiffnesses for the correct load conditions, which will lead to more accurate results especially for soil profiles with a small stiffness.

Acknowledgements

I could not have written this thesis without the help of many others. First of all I would like to thank SPT Offshore for offering the interesting topic and supporting me throughout the writing of the thesis. In particular I would like to thank OJ Dijkstra coming up with many useful ideas and always being interested and enthusiastic about my thesis. Furthermore I would like to thank all other colleagues, especially in the 'geo corner', for the great atmosphere and nice lunch breaks in the sun.

I am also very grateful for the help of my supervisors from TU Delft and NTNU, professor Eiksund, professor Metrikine and Jeroen Hoving. Although we have had only a few short meetings the discussions have helped me a great deal to better understand the topic and improve my thesis.

Finally I wouldn't have ended up here without the EWEM programme. Choosing this master was one of the best choices I have ever made and I would like to thank Niels, Simon, Oliver, Traian, Tim, Marius, Bas, Ying, Jinchao and Qiang who followed the Offshore track with me for the great time travelling around and cleaning up the mess in the cabin.

Woerden, The Netherlands — Marijn J. Dekker
15-07-2014

Contents

List of Figures

List of Tables

Chapter 1

Introduction

Suction caissons are a type of offshore foundation that allow for fast and noise-free installation and decommissioning of offshore structures. They have been used for more than 30 years in the oil and gas industry and are also becoming more common in the offshore wind sector as a promising way to cost reduction, potential for re-use and simple decommissioning. SPT is a leading contractor for the installation of both single suction anchor piles and foundations on multiple suction caissons. The suction caissons are installed by applying a differential pressure between the inner and outer sides of the caissons, which pushes the caissons into the soil.

Problem Definition

When a platform is founded on multiple suction caissons, the way the wind and wave loads are transferred through the structure and various caissons into the soil will depend on the stiffness of both the platform and the caissons. The design of the substructure and suction caissons should thus be combined to include the effects of soil-structure interaction. This is currently done by modelling the suction caisson foundations as a set of linear-elastic springs attached to the substructure. However the accuracy of the currently used linear springs is limited for load cases with extreme loading. Linear springs cannot include the effect of load redistribution in the substructure caused by the nonlinear soil stiffness behaviour. Therefore the design loads for the suction caissons for ultimate load conditions that are found are inaccurate, resulting in an inefficient foundation design.

There are some ways of including non-linear soil behaviour, for instance the p-y curves method. However these methods are originally developed for slender foundation piles, so it is questionable whether they can be applied for rigid foundations like suction caissons.

Objective

The goal of this thesis is to develop a method to model the non-linear behaviour of soils in a structural model for suction caisson foundations that is more accurate than the currently used models. This method should then be implemented in the structural programme SACS to be used for design purposes.

Reading Guide

Three different methods for the modelling of suction caisson foundations are evaluated in this thesis, each of which is discussed in a separate chapter.

Chapter 2: Linear Method
First the use of linear springs, currently common practice, is considered. For linear-elastic uniform soils several analytical expressions for the foundation stiffness of embedded foundations are available. These expressions are compared with each other as well as FEM calculations for linear-elastic and other soils. The springs are then applied for a configuration of a jacket substructure resting on 4 suction caissons and compared with results from FEM calculations in Plaxis to see if the spring model can provide decent results.

Chapter 3: Non-linear Spring Method
Secondly more realistic non-linear soil profiles are considered. First the soil model used in the FEM calculations is selected. Next two configurations of non-linear spring foundations are introduced and the limitations of the models are discussed. The foundation configurations are then implemented in the model of the substructure and foundations and compared with FEM calculations in Plaxis to determine the accuracy of the developed models.

Chapter 4: Stepwise Method
In the fourth chapter a different method for the modelling non-linear soil behaviour is discussed, in which the foundation responses are determined in several load steps. The advantages and disadvantages of this method are evaluated and again a comparison with FEM calculations for a complete foundation model is made to determine whether this method can be used for design purposes.

Conclusions
Finally the usability of various methods can be evaluated in the conclusions. Furthermore some recommendations for additional studies are given.

Chapter 2

Linear-Elastic Stiffness Method

2.1 Linear-Elastic Spring Stiffnesses

2.1.1 Introduction

The loads on an offshore structure are transferred through the substructure and the foundation to the soil. The soil will absorb the load and deform as a result of this. These deformations result in displacements of and possibly additional loads on the structure and therefore need to be estimated during the design of the structure. Since soil is an heterogeneous material the properties of the soil vary with the exact location. Furthermore the response of the soil is anisotropic and non-linear. To some extent however the behaviour of the soil can be approximated as linear and uniform, which enables a more simple estimate of the deformations. In this case the relation between the applied load and the resulting deformations is given by

$$\vec{F} = \boldsymbol{K} \cdot \vec{u} \tag{2.1}$$

where $\vec{F}$ is the load vector, $\boldsymbol{K}$ is the stiffness matrix and $\vec{u}$ is the vector containing the resulting displacements of the structure. This equation is equal to the equation for a spring. For a spring with one degree of freedom for instance $\vec{F}$ would be the applied force on the spring, $\boldsymbol{K}$ would be the spring constant and $\vec{u}$ would be the elongation or shortening of the spring. This means that when the response of the soil is assumed to be linear the foundation of an offshore structure can be replaced by a spring with the same characteristics. These characteristics are contained in the stiffness matrix $\boldsymbol{K}$ and the consequent problem is how to determine the entries of the stiffness matrix based on the properties of the foundation that is to be modelled.

2.1.2 The Stiffness Matrix

A rigid foundation for an offshore structure has 6 degrees of freedom; 3 displacements and 3 rotations. Similarly there are 6 load components: 2 horizontal shear forces, 1 vertical force, 2 overturning moments and one torsional moment. The stiffness matrix will therefore be a 6×6 matrix.

If the cylindrical foundation is orientated vertically, that is symmetrically with respect to the normal of the soil surface, most of the degrees of freedom will be uncoupled. This means that there is no interaction between the degrees of freedom, for instance a vertical force will not result in a horizontal displacement. The only exception is the coupling between horizontal displacement and rotation that occurs when the point of loading is different from the centre of rotation. It follows intuitively that these two degrees of freedom are coupled: when a shear force is applied on the structure the load will be countered by a horizontal load on the foundation in the opposite direction. Since these two loads are not acting at the same level this gives an overturning moment and hence a rotation of the foundation. It is assumed that the matrix is symmetrical, meaning that the stiffness term coupling a horizontal load with a rotation is identical to the stiffness term coupling an overturning moment with a horizontal translation. A finite element studies on suction caissons shows that this is a reasonable assumption, as the two coupling terms will generally vary less than 10 % (Liingaard et al., 2007). The full spring equation for a 6 degrees of freedom system with the resulting stiffness matrix is given in Equation 2.2.

$$\begin{bmatrix} F_x \\ F_y \\ F_z \\ M_x \\ M_y \\ M_z \end{bmatrix} = \begin{bmatrix} K_h & 0 & 0 & 0 & -K_{hr} & 0 \\ 0 & K_h & 0 & K_{hr} & 0 & 0 \\ 0 & 0 & K_v & 0 & 0 & 0 \\ 0 & K_{hr} & 0 & K_r & 0 & 0 \\ -K_{hr} & 0 & 0 & 0 & K_r & 0 \\ 0 & 0 & 0 & 0 & 0 & K_t \end{bmatrix} \cdot \begin{bmatrix} u_x \\ u_y \\ u_z \\ \theta_x \\ \theta_y \\ \theta_z \end{bmatrix} \tag{2.2}$$

The axes used for the notation are defined such that the z-axis is orientated vertically and the positive direction pointing upwards and the x-and y-axis are the principal horizontal directions. The origin is located at mudline at the centerline of the caisson. The definition of the axes is shown in Figure 2.1.

The centre of rotation of the caisson will be located below the mudline. This means that a force in positive x-direction will also give a positive moment about the centre of rotation and hence a positive rotation about the y-axis. The positive rotation will increase the horizontal displacement at mudline. When only the lateral stiffness is taken into account this displacement would require a larger horizontal load than is actually the case. Therefore the coupling stiffness should be negative in order to find the correct horizontal load for a given translation and rotation. On the other hand a positive force in the y-direction results in a negative overturning moment about the centre of rotation. Therefore the stiffness for the Fx-My coupling will be negative while for the Fy-Mx coupling it will be positive, as shown in Equation 2.2.

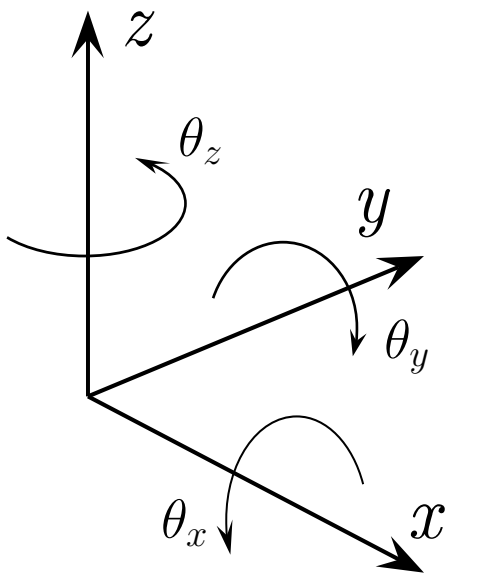

Figure 2.1: *The used right-handed cartesian coordinate system ©Tarquin*

2.1.3 Results from Literature

The various stiffness terms for a cylindrical disc resting on a linear-elastic halfspace with uniform soil properties were initially found by Boussinesq, Mindlin, Borowicka and Reissner (Pais and Kausel, 1988). For a cylindrical foundation that is embedded in the soil the stiffness will increase compared to a surface foundation with the same dimensions and soil properties. There are no theoretical expressions available for embedded foundations, however several approximations have been developed that show good correspondence with more advanced methods such as the boundary integral equation technique (Wolf and Deeks, 2004, chap. 5).

For foundations with an embedment ratio larger than unity a set of stiffness expressions for the lateral and rotational stiffness is given by Carter and Kulhawy (1992). These expressions are currently used in SPT Offshore, together with the expressions by Randolph given below. They give a flexibility matrix instead of a stiffness matrix, which is given in Equation 2.3. The flexibility matrix is derived assuming a rigid foundation.

$$\begin{bmatrix} u_x \\ \theta_y \end{bmatrix} = \begin{bmatrix} \frac{0.4}{G_{eq}D}\left(\frac{2L}{D}\right)^{-1/3} & \frac{0.3}{G_{eq}D^2}\left(\frac{2L}{D}\right)^{-7/8} \\ \frac{0.3}{G_{eq}D^2}\left(\frac{2L}{D}\right)^{-7/8} & \frac{0.8}{G_{eq}D^3}\left(\frac{2L}{D}\right)^{-5/3} \end{bmatrix} \cdot \begin{bmatrix} F_x \\ M_y \end{bmatrix} \tag{2.3}$$

where L is the embedment depth, D is the diameter of the foundation and G_{eq} is given by

$$G_{eq} = G\left(1 + \frac{3\nu}{4}\right) \tag{2.4}$$

with G the shear modulus of the soil and ν the Poisson's ratio. Inverting the flexibility matrix gives

$$K_h = G_{eq}D\left(\frac{0.8\left(\frac{2L}{D}\right)^{-5/3}}{0.32\left(\frac{2L}{D}\right)^{-2} - 0.09\left(\frac{2L}{D}\right)^{-1.75}}\right) \tag{2.5a}$$

$$K_r = G_{eq}D^3\left(\frac{0.4\left(\frac{2L}{D}\right)^{-1/3}}{0.32\left(\frac{2L}{D}\right)^{-2} - 0.09\left(\frac{2L}{D}\right)^{-1.75}}\right) \tag{2.5b}$$

$$K_{hr} = G_{eq}LD\left(\frac{0.6\left(\frac{2L}{D}\right)^{-15/8}}{0.32\left(\frac{2L}{D}\right)^{-2} - 0.09\left(\frac{2L}{D}\right)^{-1.75}}\right) \tag{2.5c}$$

These expressions can be supplemented by vertical and torsional stiffness terms developed by Randolph and Wroth (1978) and Randolph (1981) respectively. These stiffness terms are based on analytical expressions and are validated by FEM calculations for large embedment ratio's ($\frac{L}{D} \geq 10$). As some assumptions are also based on slender foundations the accuracy of the expressions for small embedment ratio's may be limited. The expressions for the vertical and torsional stiffness are given in Equations 2.6 and 2.8 respectively.

$$K_v = \frac{1}{\eta} \cdot \frac{2GD}{1-\nu} \left(1 + \eta\,(1-\nu)\,\frac{\pi}{\zeta}\frac{L}{D}\right) \tag{2.6}$$

$$\text{where } \zeta = \ln\left(5\rho\,(1-\nu)\,\frac{L}{D}\right) \tag{2.7}$$

$$K_t = GD^3\left(\frac{2}{3} + \pi\frac{L}{D}\right) \tag{2.8}$$

In Equation 2.6 η is a depth factor that accounts for the increase in stiffness of the foundation base due to the soil layer that is present between the foundation base and the surface. For small loads the soil layer above the foundation base will deform as a result of the shaft friction and thus cannot prevent the deeper soil layer from settling; hence the stiffness will not vary much from that of the base only and η is approximately equal to 1. For larger loads the shaft friction will be fully mobilized and the load increment will be carried by the foundation base only. In this case the soil above the foundation depth will limit the settling of the soil below the foundation depth and η will be approximately 0.85 (Randolph and Wroth, 1978). This gives a load-displacement behaviour that is bilinear.

The term ρ in Equation 2.7 is a factor that includes the effect of a shear modulus that increases with depth. It is defined as the ratio between the shear modulus at half the foundation depth and at the foundation base. For a uniform soil ρ will be equal to unity, for a shear modulus that is proportional to the depth ρ will be equal to $1/2$.

It can be seen in Equation 2.7 that ζ will be zero when the expression in parentheses on the right hand side is equal to unity. Since ζ appears in the denominator in Equation 2.6 the vertical stiffness will be undefined for an embedment ratio of $\frac{1}{5\rho(1-\nu)}$. A common value of ν for soils is 0.3; for a uniform soil this gives an embedment ratio of approximately 0.3. This means that Equation 2.6 is not suited for shallow foundations.

For shallow foundation two sets of stiffness expressions have been developed by Wolf and Deeks (2004, chap. 5) and Gazetas (1991). The expressions given by Wolf are derived using the cone model, while Gazetas' expressions are based on FEM calculations. Just as for the expressions given by Carter and Randolph their expressions have a limited range of applicability, as they are calibrated to calculation results. The expressions given by Wolf can be used up to an embedment ratio L/D of 1. Gazetas does not give any explicit range of applicability for his expressions but uses embedment ratios up to 1.5 in charts.

The stiffness terms given by Wolf and Gazetas are defined for a point on the centerline of the caisson at foundation depth, not at the mudline. Since a rigid foundation is assumed the displacements at the foundation depth and at mudline for a pure vertical or lateral translation will be equal, as will be the rotations for a torsional or overturning moment. However the distance from the centre of rotation will be different for the two points, and therefore the coupling term will vary as well.

The distance to the centre of rotation can be found by dividing the coupling term by the lateral stiffness term, which gives the moment arm. For the expressions given by Wolf and Gazetas a moment arm of L/3 is found, which means that the centre of rotation is located at a distance of $L/3$ above the foundation depth. The centre of rotation is thus located at $2/3$ of the depth of the pile. This is the depth at which the resultant of the lateral earth pressure acts, assuming that the lateral pressure increases linearly with depth.

In order to change the stiffness matrix such that it is valid for a point at mudline the coupling term should be changed to give a moment arm of $-2/3$L. The coupling terms given by Wolf and Gazetas thus need to be multiplied by -2 to be applicable for a point at mudline and to be able to compare them with the expression given by Carter. Also the rotational stiffness has to be modified as described in Appendix A. This has already been done in the expressions given in Table 2.1. As mentioned before Carters expressions are already given for a point at mudline. The moment arm that follows from Carters coupling and lateral stiffness is equal to $0.65\left(\frac{L}{D}\right)^{-5/24}$L, which for embedment ratios close to unity also gives a centre of rotation located at approximately $2/3$ of the foundation depth.

2.1.4 Comparison of the Suggested Expressions

The various expressions for the stiffness of embedded foundations given have been compared for embedment ratio's varying between 0 and 2, with $\nu = 0.3$, $\eta = 1$ and $\rho = 1$. The results are given in Figure 2.2. The stiffnesses are divided by the stiffnesses for a surface foundation given by Wolf, as these are the exact theoretical expressions (Pais and Kausel, 1988). The coupling term K_{hr} has been omitted as the behaviour is the same as for the lateral stiffness.

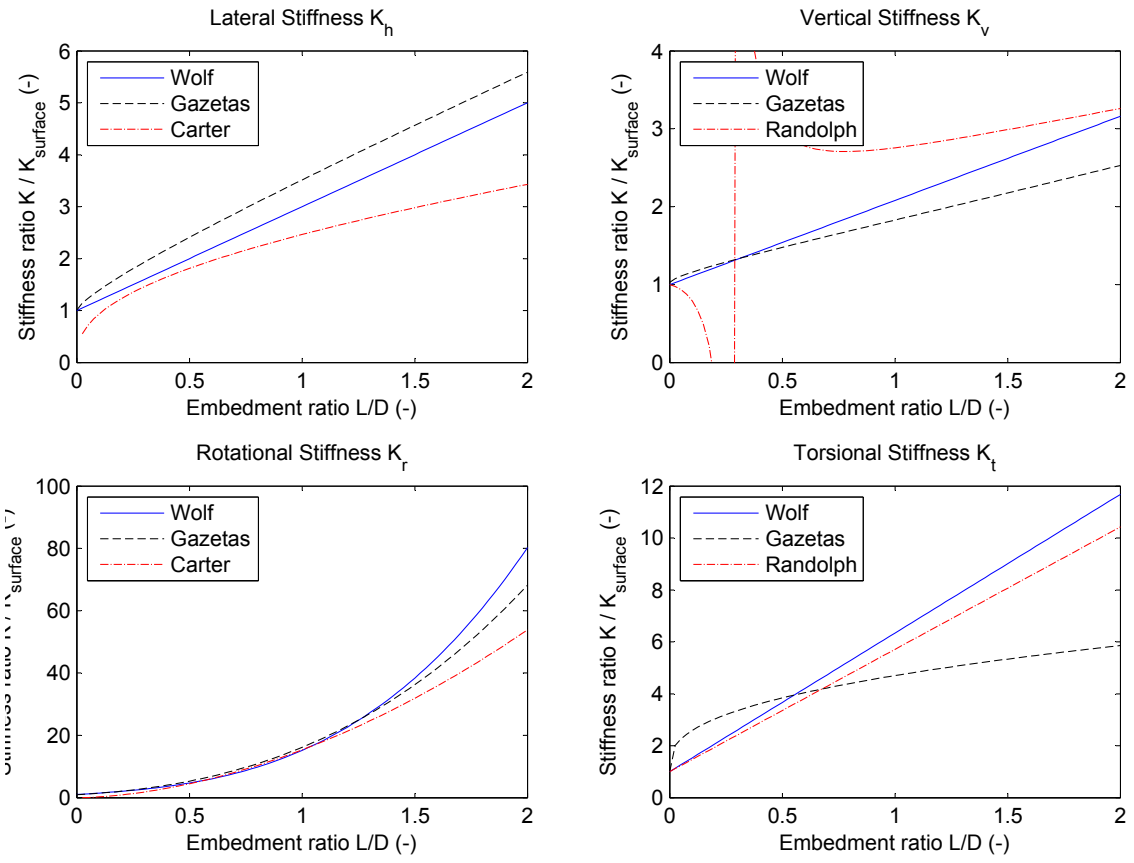

Figure 2.2: *Comparison of the stiffness terms given by Wolf and Deeks, Gazetas, Carter and Kulhawy, Randolph and Wroth*

Table 2.1: *Comparison of the stiffness terms given by Wolf and Deeks, Gazetas, Carter and Kulhawy, Randolph and Wroth*

Entry	Value according to Wolf	Value according to Gazetas	Value according to Carter or Randolph
K_h	$\frac{4GD}{2-\nu}\left(1+2\frac{L}{D}\right)$	$\frac{4.03GD}{2-\nu}\left(1+0.21\left(\frac{L}{D}\right)^{0.5}\right)\left(1+1.88\left(\frac{L}{D}\right)^{0.8}\right)$	$GD\left(1+\frac{3\nu}{4}\right)\left(\frac{0.8\left(\frac{2L}{D}\right)^{-5/3}}{0.32\left(\frac{2L}{D}\right)^{-2}-0.09\left(\frac{2L}{D}\right)^{-1.75}}\right)$
K_v	$\frac{2GD}{1-\nu}\left(1+1.08\frac{L}{D}\right)$	$\frac{2.01GD}{1-\nu}\left(1.02+0.1\frac{L}{D}\right)\left(1+0.51\left(\frac{L}{D}\right)^{2/3}\right)$	$\frac{1}{\eta}\frac{2GD}{1-\nu}\left(1+\eta\left(1-\nu\right)\frac{\pi}{\zeta}\frac{L}{D}\right)$
K_r	$\frac{GD^3}{3(1-\nu)}\left(1+4.6\frac{L}{D}+4.64\left(\frac{L}{D}\right)^3+4\frac{1-\nu}{2-\nu}\left(\frac{L}{D}\right)^2\left(1+2\frac{L}{D}\right)\right)$	$\frac{0.31GD^3}{1-\nu}\left(1+2.52\frac{L}{D}\right)\left(1+2\frac{L}{D}\right)+\frac{1.34GD^3}{2-\nu}\left(\left(\frac{L}{D}\right)^2\left(1+0.21\left(\frac{L}{D}\right)^{0.5}\right)\left(1+1.88\left(\frac{L}{D}\right)^{0.8}\right)\right)$	$GD^3\left(1+\frac{3\nu}{4}\right)\left(\frac{0.4\left(\frac{2L}{D}\right)^{-1/3}}{0.32\left(\frac{2L}{D}\right)^{-2}-0.09\left(\frac{2L}{D}\right)^{-1.75}}\right)$
K_t	$\frac{2GD^3}{3}\left(1+5.34\frac{L}{D}\right)$	$0.67GD^3\left(1+2.11\left(\frac{L}{D}\right)^{0.4}\right)\left(1+0.50\left(\frac{L}{D}\right)^{0.1}\right)$	$GD^3\left(\frac{2}{3}+\pi\frac{L}{D}\right)$
K_{hr}	$2\frac{L}{3}\frac{4GD}{2-\nu}\left(1+2\frac{L}{D}\right)$	$2\frac{L}{3}\frac{4.03GD}{2-\nu}\left(1+0.21\left(\frac{L}{D}\right)^{0.5}\right)\left(1+1.88\left(\frac{L}{D}\right)^{0.8}\right)$	$GLD\left(1+\frac{3\nu}{4}\right)\left(\frac{0.6\left(\frac{2L}{D}\right)^{-15/8}}{0.32\left(\frac{2L}{D}\right)^{-2}-0.09\left(\frac{2L}{D}\right)^{-1.75}}\right)$

It can be seen that the three sets of expressions roughly follow the same trends, but significant differences occur. For the lateral stiffness the expression given by Gazetas gives approximately 50% higher results than the expression from Carter, with the expression from Wolf being closer to Carter's expression for small embedment ratio's and closer to Gazetas' for larger embedment ratio's. For the vertical stiffness the expressions from Wolf and Gazetas give similar results up to an embedment ratio of 0.5, after which the expression given by Wolf gives a significantly higher stiffness. The expression by Randolph clearly cannot be used for embedment ratio's smaller than 1 due to the asymptotic behaviour; for embedment ratio's larger than one it approaches the value given by Wolf. The stiffness terms for the rotational stiffness are all three virtually identical up to an embedment ratio of 1, after which Wolf's expression starts to give a larger stiffness than Carter's and for larger embedment ratio's also Gazetas' expression, with the difference increasing up to 50% for an embedment ratio of 2. The stiffness given by Carter is slightly larger than the stiffness given by Wolf. For the torsional stiffness the expression from Gazetas gives a stiffness that is up to twice as high for small embedment ratio's as the one given by Wolf, while for embedment ratio's larger than unity the expression by Wolf gives a higher stiffness. The expression given by Randolph gives results similar to the expression from Wolf.

The differences between the expressions might be caused by the fact that Gazetas' expressions are valid for any shape of the foundation, while Wolf's expressions are optimized for shallow cylindrical foundations and the expressions from Carter and Randolph for slender cylindrical foundations.

2.1.5 Application for Suction Caisson Foundations

The load-displacement relations from Wolf and Gazetas are given for the centerpoint at the bottom of the foundation, for which it is assumed that the foundation is rigid at the embedment depth. Suction caissons are open at the bottom however, and only consist of skirts and a top plate. This means that the soil inside the caisson is in theory free to have displacements different from the displacements of the caisson itself.

To what extent the soil inside the caisson acts as a part of the foundation depends on whether the valve in the top of the caisson is sealed after installation or not. The difference is shown in Figure 2.3. Usually there is a small layer of water between the top plate of the caisson and the soil. This layer is the result of the fact that there is some safety included in the length of the caisson, to make sure that the required penetration depth is reached despite the soil heave that occurs inside the caisson during installation. The soil heave is the combination of the soil volume displaced by the caisson, which is transported to the interior and exterior of the caisson (DNV, 2005), and the effects of dilatation or contraction of the soil as a result of the changed stress state (Tran et al., 2005). Consequently it is difficult to estimate the exact soil heave that will occur and some margin is needed.

When the top of the caisson is sealed the volume of the water layer will initially remain unchanged during loading due to the incompressibility of the pore water. In the long term the water might dissipate as a result of consolidation. Most waves however will have a wave period that is sufficiently small compared to the consolidation time for the soil to behave undrained, even in sand, meaning that the soil and water inside the caisson will be trapped and the foundation will behave like a rigid foundation.

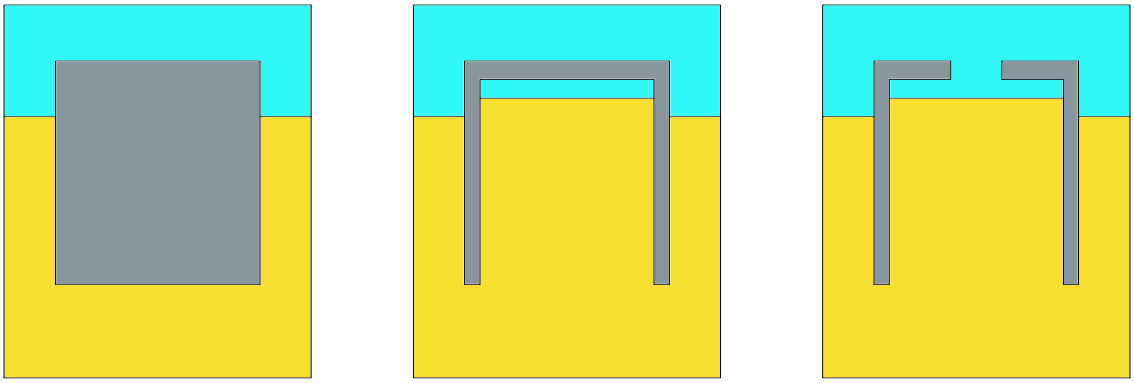

Figure 2.3: *Sketch of the foundation. From left to right: Assumed foundation, suction caisson with closed top plate and suction caisson with open top plate*

If the caisson remains partially opened at the top the water can dissipate upwards when the pressure is increased by additional loading. This will allow the caisson skirts to move relative to the soil inside the caisson and may lead to a significant decrease of the vertical stiffness. The effect on the other stiffness terms will probably be much smaller as other types of loading will not lead to a change of pressure of the water inside the caisson.

As the modelling of a partially opened suction caisson will be quite complex and require a time-dependent analysis the decrease of the stiffness for this case will not be investigated further and it is assumed that the foundation can be modelled as being rigid.

2.2 Dynamic Stiffness

2.2.1 The Dynamic Load-Displacement Relation

When the load applied on the foundation is not constant but varying in time dynamic effects can occur. The dynamic response of the foundation can either be damped or amplified compared to the static load case, depending on the damping of the soil and the excitation frequency. There are two types of soil damping: hysteretic damping, which is the result of energy dissipation by plastic deformation of the soil, and radiation damping, which is the result of waves created by the The damping of the foundation can be included in the model by placing a dashpot parallel to the foundation spring. The load-displacement relation, which is given for a static system in Equation 2.1, thus becomes

$$\vec{F}(\omega, t) = \boldsymbol{S}(\omega) \cdot \vec{u}(\omega, t) \tag{2.9}$$

$$\boldsymbol{S}(\omega) = \boldsymbol{K}(\omega) + i\omega\boldsymbol{C}(\omega) \tag{2.10}$$

Both the stiffness and the damping matrix are functions of the applied excitation frequency ω. This means that the response of the foundation for a dynamic load will not only be altered by dynamic amplification but also by a change in the stiffness and damping of the system itself.

Whether the influence of the dynamic effects is significant or negligible thus depends on the excitation frequency, or more specific on the excitation frequency relative to the characteristic frequency of the system. The relative frequency can for instance be expressed as the frequency factor a_0 (Gazetas, 1991):

$$a_0 = \frac{\omega D}{2V_s} \tag{2.11}$$

where V_s is the shear wave velocity defined by

$$V_s = \sqrt{\frac{G}{\rho}} \tag{2.12}$$

Alternatively the characteristic frequency ω_0, which is not necessarily equal to the eigen-frequency of the system as it is independent of the mass of the structure, can be defined as (Verruijt, 2010, chap. 15):

$$\omega_0^2 = \frac{16G}{\rho D^2} \tag{2.13}$$

$$\frac{\omega}{\omega_0} = \frac{\omega D}{4V_s} = {}^1\!/_2 \cdot a_0 \tag{2.14}$$

2.2.2 Assessment of the Dynamic Response for Ultimate Design Loads

In this section the dynamic effects for a design load case will be assessed. Since the goal of this thesis is to look at non-linear soil behaviour and most soils behave more non-linear for increasing loads and deformations, an ultimate load case should be considered. For offshore structures this will usually be a design wave. The maximum wave height that can occur without breaking increases with the wave period of the wave, so the design wave will have a relatively large wave period, in the order of 10 to 20 seconds. The design wave will be highly non-linear so there will be higher frequencies present as well however. For the assessment a wave period of 6 seconds is assumed.

For the soil a sand layer with a shear modulus of 60 MPa and density of 2000 $^{kg}/_{m^3}$ is assumed. This gives a shear wave velocity of 173 $^{m}/_{s}$, which is the same order as the 150 $^{m}/_{s}$ given by Verruijt (2010, chap. 3). With a caisson diameter of 7 m this gives $a_0 = 0.02$ or $^{\omega}/_{\omega_0} = 0.01$. Gazetas (1991) shows that for this value of a_0 all of the entries in the dynamic stiffness $\boldsymbol{K}(\omega)$ will decrease less than 0.1% and similarly Verruijt (2010, chap. 15) shows that for a uniform surface load the dynamic amplification factor for the given ratio of $^{\omega}/_{\omega_0}$ is practically equal to unity. This means that only a negligible error is introduced when the system is assumed to behave statically. Therefore the dynamic effects of the load on the foundation will be ignored in further calculations.

A case in which the dynamic effects cannot be ignored is when the structure is loaded by slamming loads from breaking waves. Wave slamming can be an ultimate load condition and can cause ringing of the structure, which is a highly dynamic effect (Sheikh and Swan, 2005). Wave breaking mainly occurs in shallow water near the coast however, whereas multifooted platforms are usually designed for intermediate water depths where wave breaking is less of a problem. Jacket structures for offshore wind turbines are also used in more shallow waters with a water depth of 30 to 40 meters and might therefore be affected by breaking waves. Turbulent wind loads can also be an ultimate design condition in this case, so for offshore wind turbines the dynamic effects of the ultimate load state should be taken into account.

2.3 Validation With FEM Calculations

In order to find out which of the proposed expressions for the various stiffnesses gives the most accurate results for reasonable suction caisson applications a series of FEM calculations in the software Plaxis 3D (Plaxis, 2013) has been carried out. In these calculations the modeled foundation is loaded by forces and moments in different directions and the resulting displacements are computed. The stiffnesses can then be found from the resulting load-displacement curves.

The modeled caisson has a diameter of 7 m. The embedment ratio is varied from 0 to 2 in steps of 0.5, so the penetration depth varies from 0 to 14 m in steps of 3.5 m.

The calculations have been performed for three different soil types. The first type is a uniform linear-elastic soil with a shear modulus G of 60 MPa and Poisson's ratio ν of 0.3. This type of soil is assumed in the derivations of the analytical expressions for the stiffness matrix elements and the FEM calculations are thus expected to give results that are similar to the analytical expressions. Since the foundation is also assumed to be rigid the caisson has also been modeled by a rigid linear-elastic cylinder. The shear modulus of this material is 1000 times larger than that of the surrounding soil to make sure that the deformations of the caisson itself are negligible.

The second soil is equal to the first linear-elastic soil, only the stiffness of the soil is now increasing linearly with depth. The Young's Modulus E starts at 0 MPa at mudline and increases with 20 $^{\text{MPa}}/_{m}$ with depth. This means the shear modulus, which is related by

$$G = \frac{E}{2\,(1+\nu)} \tag{2.15}$$

increases with 7.7 $^{\text{MPa}}/_{m}$ depth.

The third soil is a Mohr-Coulomb material with drained behaviour and no cohesion. The Mohr-Coulomb model has been chosen because it can be used with the same set of parameters as the linear-elastic model while including the basic effects of actual soil behaviour. The shear modulus and Poisson's ratio are the same as for the linear-elastic soil. The friction angle ϕ is 35° and the dilation angle ψ is 5°. For this soil the caisson has been modeled by the actual geometry of the steel structure filled with soil. The caisson walls have a plate thickness of 0.05 m and the top plate has a thickness of 3 m. The walls and especially the top plate have been given a larger thickness than actual caissons to account for stiffeners. Since the Mohr-Coulomb model is linear-elastic up to yield the initial stiffness is expected to be similar to that of the linear-elastic soil.

The stiffness matrix has been determined by finding the terms of the flexibility matrix one by one and inverting the flexibility matrix to get the stiffness matrix. The flexibility terms have been determined by applying a unidirectional force or moment on the caisson and determining the displacements and rotations. The flexibility terms are then found by plotting the displacements against the applied load and determining the inclination of the curves. For the linear-elastic soil models the curves will be straight lines, meaning that the flexibility is constant and independent of the applied load, while for the Mohr-Coulomb type soil the flexibility will generally increase (meaning a decreasing stiffness) with increasing load. In this case the flexibility for small loads has been used.

The loads are applied and the displacements measured at mudline. Since Plaxis does not provide any result for rotations they have been determined by looking at the difference in displacement of two opposite points on the edge of the top plate and dividing the difference by the diameter of the caisson. The rotation as a result of an overturning moment is found by looking at the difference in vertical displacement while for a torsion moment the difference in horizontal displacement is used.

The resulting stiffnesses have been divided by the stiffness of a surface foundation with the same diameter, shear modulus and Poisson's ratio given by Wolf to be able to compare them with the previously found analytical expressions. The coupling stiffness for a surface foundation is 0 according to Wolf, so the found values for the coupling stiffness are scaled by $\frac{2}{3} \cdot \frac{4GD^2}{2-\nu}$ (the stiffness for a surface foundation divided by the embedment ratio $^{L}/_{D}$) instead. For the soil with a non-uniform stiffness the average shear modulus, that is the shear modulus at half the foundation depth, is used to compare the results.

2.3.1 Mesh Convergence Study

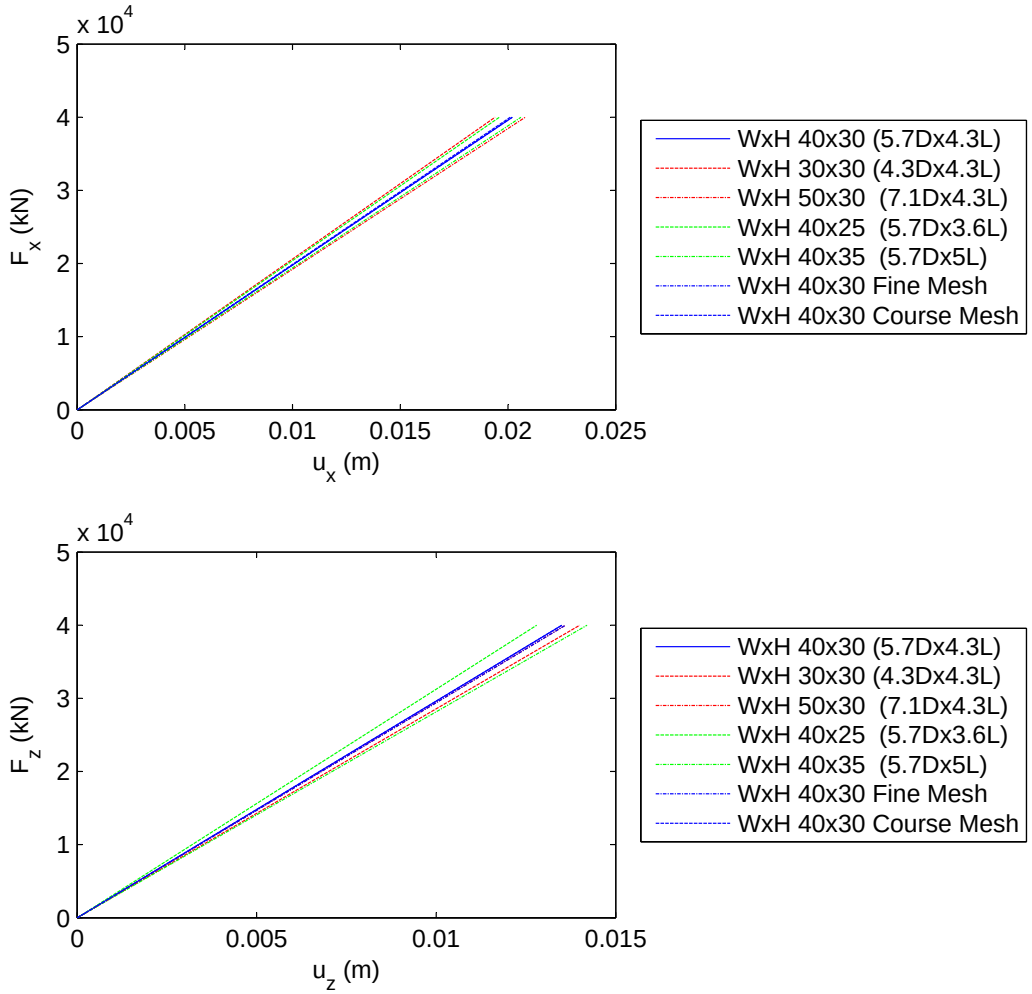

Figure 2.4: *Lateral and axial load-displacement curves for various mesh and model sizes*

The results found in a FEM analysis will depend on the chosen mesh density (the size of the elements) and the chosen boundaries of the model, both in terms of the location of the boundaries and the boundary conditions. This is unphysical, as there will be a single outcome in reality. Therefore the mesh and model size should be chosen such that the results have converged, meaning that any further change in the mesh or model will not lead to a significant change of the output. The boundary conditions should also be chosen such that they correspond with the boundaries of the physical model. The analytical stiffness expressions have been developed for an infinite halfspace, so the boundaries in the FEM model should be located at a distance where they do not influence the results.

Initially a model size of 40 by 30 m (5.7 D by 4.3 L) has been chosen. The mesh size in Plaxis has been chosen as medium (element size is 0.05 times the local volume size), with a local mesh refinement up to 1.5 D and 1.5 L. The width of the FEM model has been varied by 10 m (5 m on either side of the caisson) and the height by 5 m and the results for these models have been compared with the original model. The mesh density is also varied from a mesh defined as fine in Plaxis (element size is 0.035 times the local volume size) to a mesh defined as course (0.075). The resulting load-displacement curves for applied lateral and vertical loads are given in Figure 2.4.

It can be seen that changing the mesh size gives a negligible change in the calculated displacements. Changing the dimensions of the model does lead to a noticeable difference in the results. Since a lateral load will mainly lead to deformations in the soil next to the caisson the lateral displacements are mainly dependent on the mesh width. For a vertical load the soil below the caisson will deform the most and the results are the most sensitive for the height of the FEM model. The change of the model dimensions will give at most a change of 5% in the calculated deformations. This is deemed small enough to consider the results to be converged. Therefore it can be concluded that the chosen combination of mesh and model size gives reliable results.

2.3.2 Results For a Uniform Linear-Elastic Soil

The results from the FEM calculations for a linear-elastic soil model with uniform stiffness are plotted together with the analytical expressions in Figure 2.5 and 2.6.

It can be seen that the FEM calculations give stiffness terms of the same order of magnitude as the analytical expressions. This indicates that the expressions give reasonable results.

The lateral stiffness found in the FEM calculations matches pretty well with the expression given by Gazetas for embedment ratios up to approximately 1.5, with a difference of approximately 10 %. This clearly is the range for which the Gazetas expression has been fitted. For larger embedment ratios the stiffness found in the FEM calculations starts to deviate from the expression given by Gazetas and the results suggest that for embedment ratios above 2 the FEM results will tend to the expression given by Carter, which is indeed calibrated for large embedment ratios.

For the vertical stiffness the FEM calculations show less agreement with the analytical expressions. The expression by Wolf shows the same trend as the FEM results, but the two differ by a constant offset of approximately 0.4 times the vertical stiffness for a surface

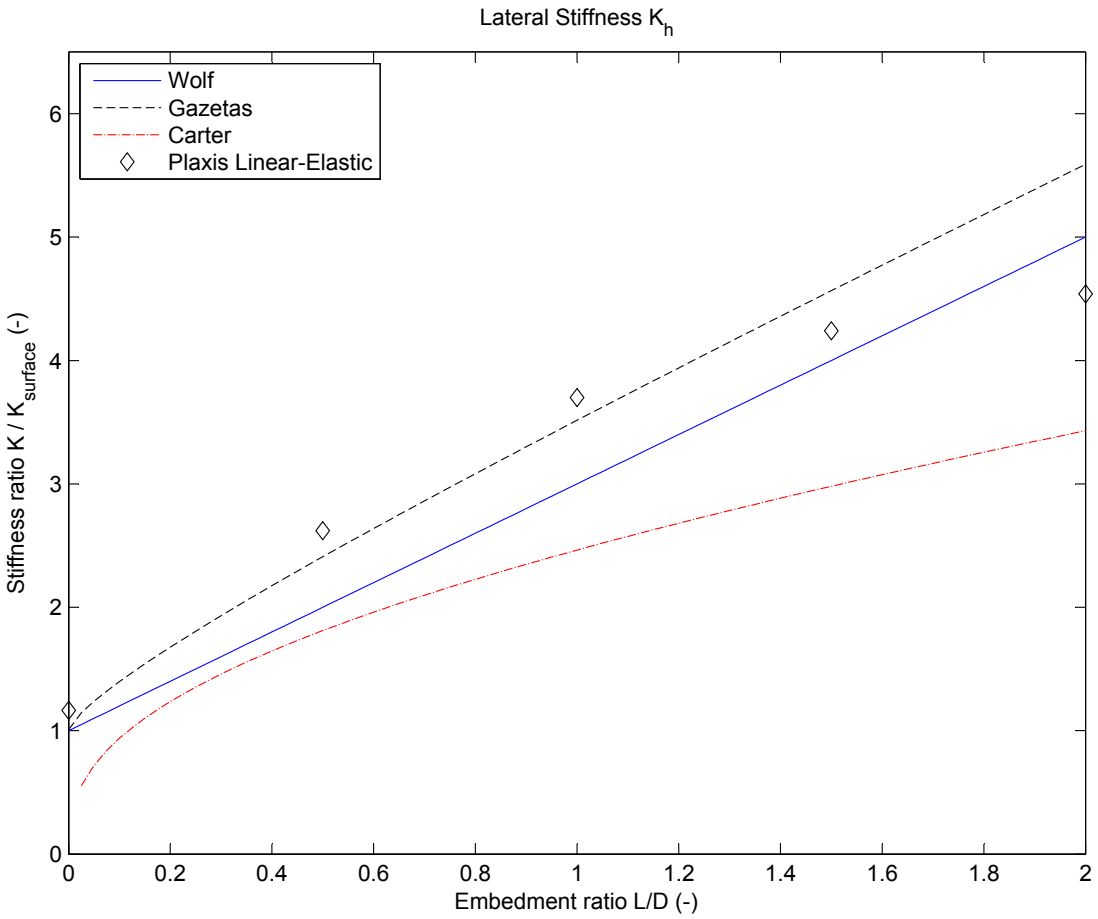

Figure 2.5: *FEM and analytical results for the lateral stiffness for a linear-elastic uniform soil*

foundation ratio for any embedment ratio. For embedment ratio's larger than unity the expression given by Randolph actually matches the FEM results the best, but it shows a different trend and it clearly is unusable for shallow foundations because of the unphysical asymptotic behaviour.

The FEM results for the rotational stiffness correspond very well with the analytical expressions up to an embedment ratios around unity, the difference with the expression from Wolf being approximately 10 %. For embedment ratios larger than one the rotational stiffness found in the FEM results increases significantly less with increasing depth than the analytical expressions suggest. For this range Carters expression matches the FEM results the nearest but still gives a rotational stiffness that is 20 % larger than the FEM results for an embedment ratio of 1.5 and 50 % for an embedment ratio of 2.

For the torsional stiffness the FEM results show a much better correspondence with the analytical expressions than is the case for the vertical and rotational stiffnesses. The FEM results follow the expression from Randolph quite close and match within a 10 % range. The expression given by Wolf gives a good match with the FEM results for small embedment ratio's but starts to deviate from the FEM results for embedment ratio's larger than unity. Gazetas' expression differs significantly from both the FEM results and the expressions given by Randolph and Wolf and seems to overestimate the torsional

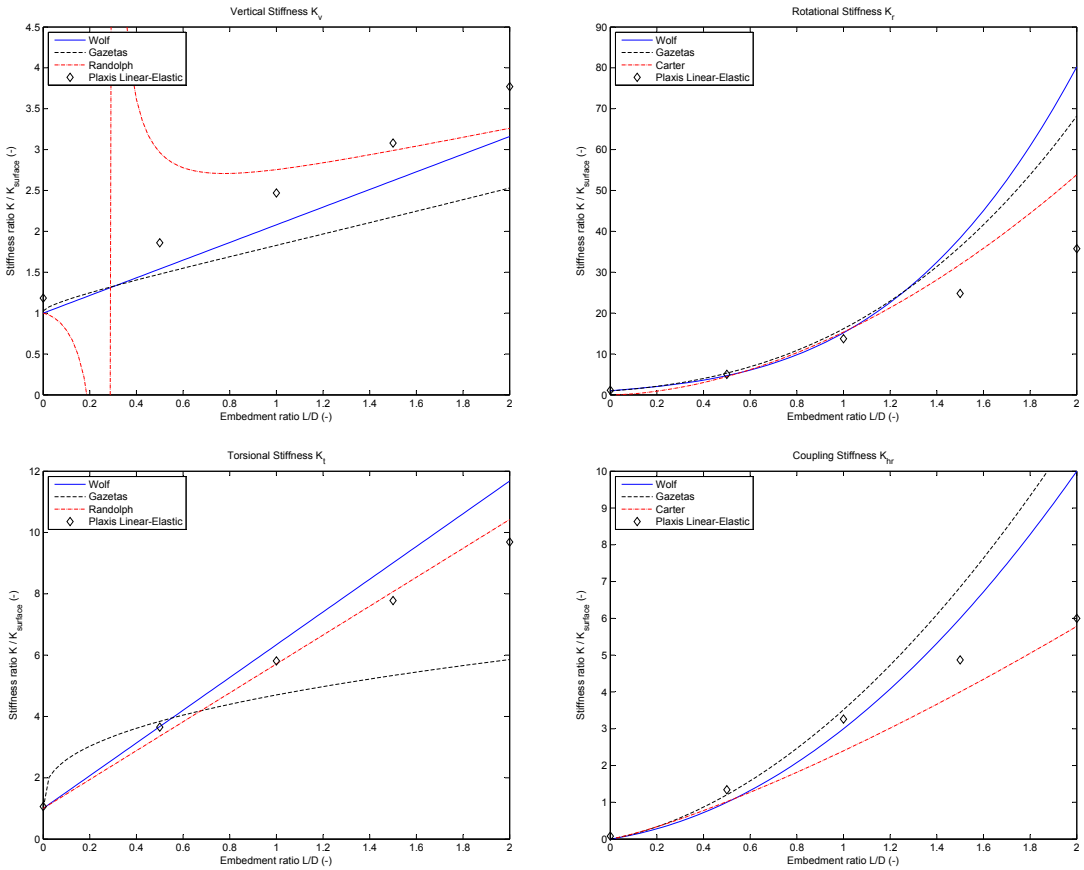

Figure 2.6: *FEM and analytical results for the vertical, rotational, torsional and coupling stiffness*

stiffness for embedment ratio's less than 0.5 and overestimate it for larger embedment ratio's.

For the coupling stiffness the correspondence between the FEM calculations and the analytical expressions gives the same trend as for the lateral stiffness, with the FEM results showing a good match with Gazetas expression for smaller embedment ratios and with Carters expression for larger embedment ratios. The most striking difference between the FEM results and the analytical expressions is that the latter all give give a zero stiffness for a surface foundation, meaning no coupling. This is because only the resistance against rotation from the lateral earth pressure on the caisson skirts is taken into account in the analytical models, while the resistance from the vertical earth pressure on the caisson base is neglected. As mentioned before this results in a centre of rotation that is independent of the embedment ratio in the expressions given by Wolf and Gazetas. Carter does include the effect of the shifting centre of rotation, as can be seen in Figure 2.7, but still gives a zero coupled stiffness for a surface foundation as his expression is fitted for larger embedment ratios. The neglection of the rotation resistance from the caisson base is acceptable for slender piles but Figure 2.7 shows this assumption cannot be made for shallow foundations: the FEM calculations give a centre of rotation that moves closer to the foundation base as the embedment ratio becomes smaller, as for shallow foundations

the base actually gives the largest contribution to the moment resistance. For embedment ratio's close to zero the centre of rotation will actually be located below the foundation. This means that there will still be a misalignment between the point of load application at mudline and the centre of rotation for a surface foundation. Therefore the coupling stiffness will also be non-zero in this case.

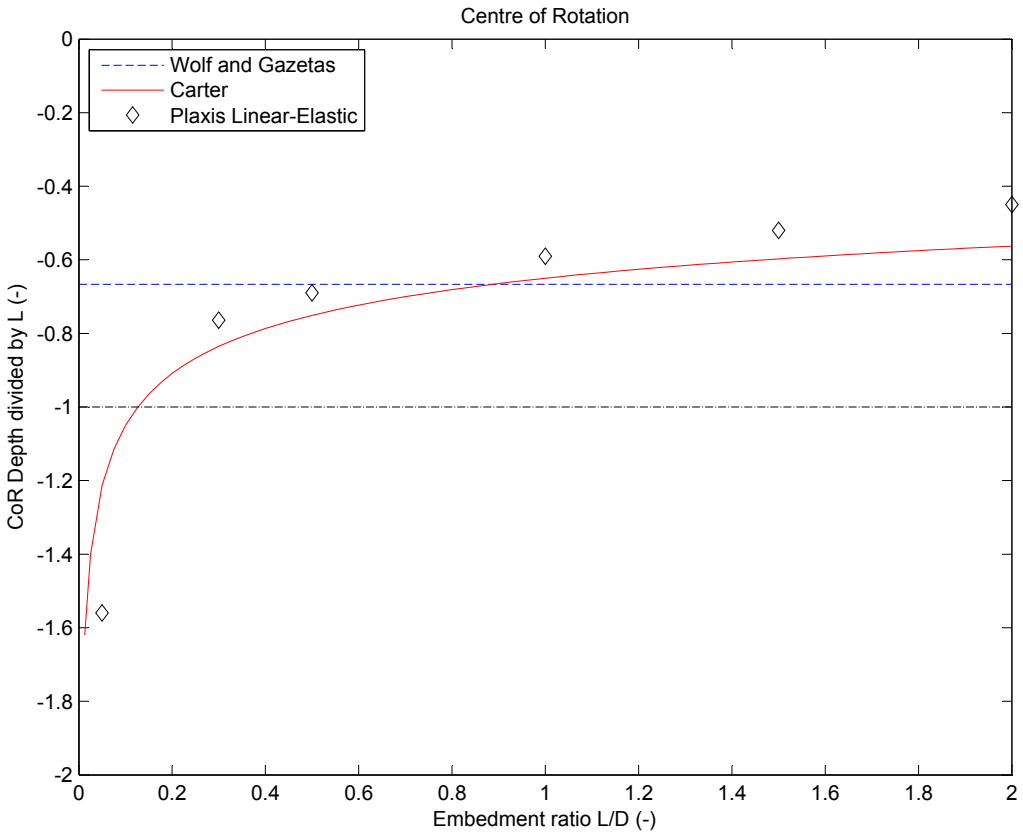

Figure 2.7: *The variation of the centre of rotation with the embedment ratio*

2.3.3 Effects of a Stiffness Increasing With Depth

It is usually assumed that soils have a stress-dependent stiffness, for instance in the hardening soil model (Schanz et al., 1999). In a normally consolidated soil the effective stress increases with depth as a result of gravity. Therefore the stiffness of the soil will also increase with depth. For a simple model the stiffness is often assumed to be proportional to the depth. For the linear-elastic soil with non-uniform stiffness used in the FEM calculations this linearly increasing stiffness is also used. As described in the previous section the Youngs modulus that is used increases with 20 MPa per meter depth, meaning that the shear modulus increases with 7.7 MPa per meter depth. At the mudline the used soil has a stiffness of 1 kPa rather than 0 in order to avoid infinite deformations.

The FEM results for the soil material with non-uniform stiffness are given in Figure 2.8. It can be seen that the stiffnesses for a soil with non-uniform Young's modulus differ quite a lot from the results for the uniform soil, which means that the assumed soil profile has a significant influence on the resulting foundation stiffness.

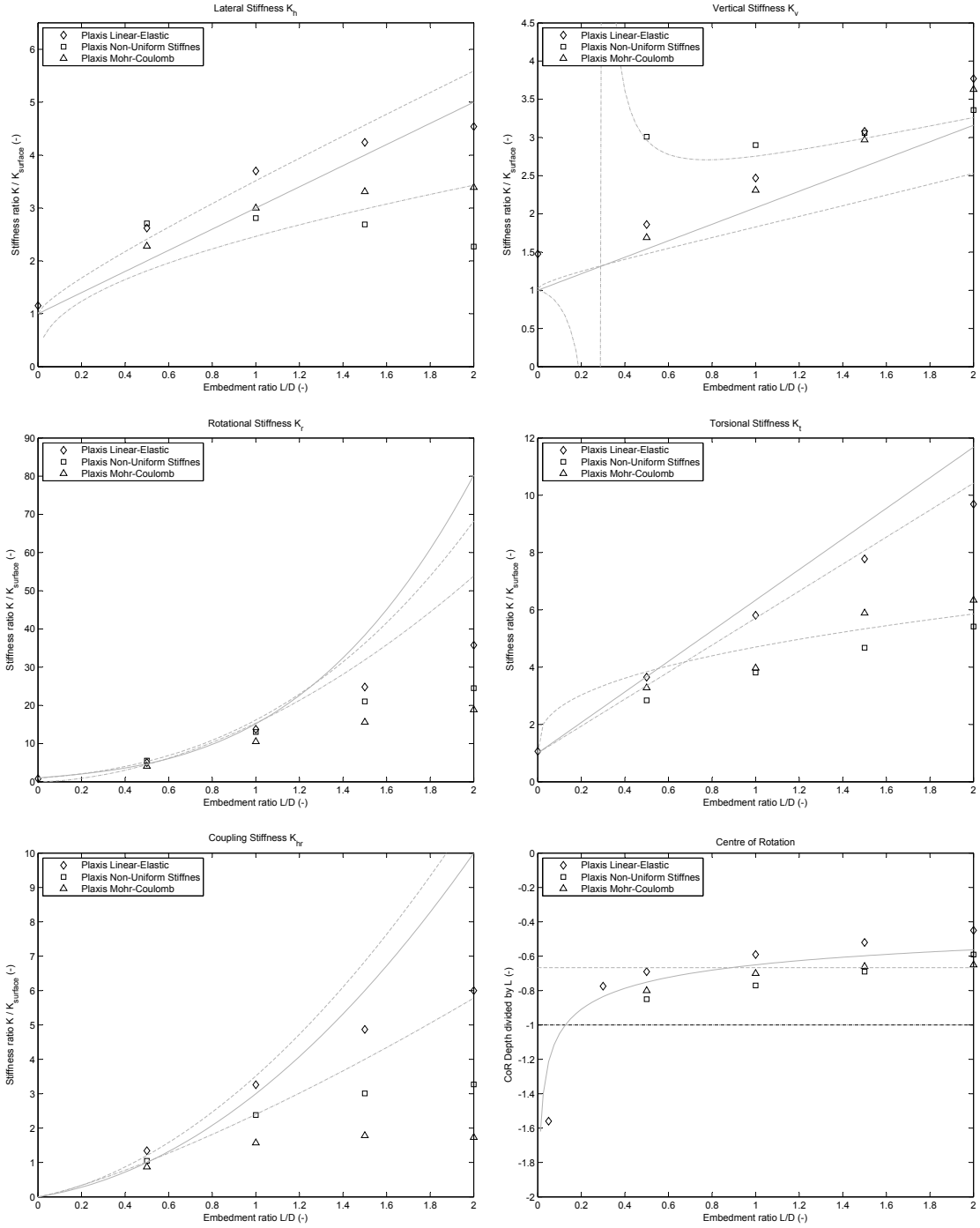

Figure 2.8: *Comparison of stiffnesses and centre of rotation for uniform and non-uniform linear-elastic stiffness and mohr-coulomb model*

For horizontal displacements the non-uniform soil behaves stiffer for small embedment ratio's and less stiff for higher embedment ratio's. For small embedment ratios the foundation behaves stiffer since the base friction has a significant influence on the lateral stiffness and the shear modulus at the pile base is larger for the soil with depth-increasing stiffness than for the uniform soil.

For larger embedment ratios this effect diminishes and the non-uniform soil will actually behave less stiff. The cause for this is that the centre of rotation is located at greater depth than for a uniform soil, as can be seen in the lower right figure in Figure 2.8. This means that a horizontal load at mudline results in a larger overturning moment about the centre of rotation and hence a larger rotation. This in turn gives a larger horizontal displacement at mudline, meaning that the lateral stiffness decreases.

For the vertical stiffness the non-uniform soil profile also gives a higher stiffness for small embedment ratio's. The vertical stiffness is mainly provided by the soil below the caisson. For the non-uniform soil the stiffness below the caisson will be higher than the stiffness at half the foundation depth, which is the stiffness used in the comparison. Therefore the vertical stiffness of the non-uniform soil is relatively high. This effect is especially strong for small embedment ratio's and decreases for smaller embedment ratio's, as can be seen in Figure 2.8. The stiffness expression given by Randolph actually describes this behaviour quite well, although the increasing stiffness for small embedment ratio's in this expression has a completely different background.

The rotational stiffness for a non-uniform soil profile shows the same behaviour as the lateral stiffness. For small embedment ratios the stiffness is slightly larger than for the uniform soil because of the higher base stiffness, while for larger embedment ratios the rotational stiffness will be smailler than that for the uniform soil. This is caused by the downward shift of the centre of rotation. The centre of rotation moves down because for the non-uniform soil the soil is less stiff near mudline and stiffer near the base. Since this means that the stiffest soil is located close to the centre of rotation the resistance against rotation will be small and the rotational stiffness will decrease compared to the uniform soil. The decreased rotational and lateral stiffness also result in a decrease of the coupling stiffness compared to the uniform soil profile, as can be seen in the lower left figure in Figure 2.8.

The torsional stiffness for a non-uniform soil is also lower for all embedment ratio's. The torsional rotation in the FEM calculations is measured at mudline, which is also where the torsional moment is applied. Since the Young's modulus of the non-uniform soil is smaller at mudline than that of the uniform soil the resistance against local torsion of the foundation is smaller and hence there will be some local torsion. Therefore the torsional rotation at mudline is larger than the rotation of the entire foundation and a lower torsional stiffness is found. The local torsion is in contradiction with the assumption of a perfectly rigid foundation. However in reality some local torsion can also be expected, resulting in a lower torsional stiffness.

2.3.4 Effects of Using a More Realistic Foundation Model

The results for the Mohr-Coulomb soil with the non-rigid caisson model are also given in Figure 2.8. It can be seen that the stiffnesses are not necessarily similar to the stiffnesses for a linear-elastic soil with rigid foundation, meaning that these assumptions are not always realistic.

The lateral stiffness for the Mohr-Coulomb soil increases less with increasing embedment ratio as the stiffness for a linear-elastic soil. The reason for this is that the linear-elastic model does not distinguish between tension and compression in the soil. For the used

soil properties without cohesion the Mohr-Coulomb material can handle compression only and will fail when loaded in tension. This means that the active wedge of the soil, which for the linear-elastic soil resists a lateral displacement of the caisson by means of a tensile stress, will not give any tensile load on the caisson for the Mohr-Coulomb material. This means that the total resistance against deformation will be less and hence that the lateral stiffness is smaller.

For the vertical stiffness the resistance comes from compressive and shear stresses only and the difference between the two material types is much smaller. The stiffness for the Mohr-Coulomb soil is slightly lower since there is some local failure of the soil along the shaft near the mudline. The shear strength of the soil is not sufficient at this location to bear the shaft friction. Especially for larger embedment ratio's the influence of this effect is rather small however, so it seems that the assumption of a linear-elastic soil for a vertical load is applicable, at least for small loads.

The rotational stiffness for the Mohr-Coulomb soil is significantly smaller than for the linear-elastic soil, especially for larger embedment ratios. This is because a rotation of the caisson will lead to tensional stresses in the linear-elastic soil, which the Mohr-Coulomb type of soil cannot provide, meaning there will be less resistance against the rotation. For large embedment ratios the displacements near mudline will be larger for a given rotation than for smaller embedment ratios, meaning that a larger area will be in tension and the rotational stiffness will decrease more.

The torsional stiffness shows again a significant difference with the linear-elastic model. This is not so much caused by the Mohr-Coulomb type of soil but by the modeling of the caisson itself. The steel structure used in combination with the Mohr-Coulomb model does not behave perfectly rigid and hence part of the torsional moment is absorbed by local torsion instead of a rotation of the caisson as a whole. The stiffness for local torsion is lower than that for a rigid torsional rotation and will decrease with increasing skirt length, hence the difference with the torsional stiffness for a rigid foundation increases with increasing embedment ratio.

The most important difference between the linear-elastic model and the Mohr-Coulomb model however is the range of applicability of the found stiffness matrices. While the linear-elastic model will show the same behaviour indepent of the amplitude of the load, the load-displacement curve for the Mohr-Coulomb soil will be non-linear. The stiffnesses given in Figure 2.8 are only valid for small loads while for larger loads the stiffness will decrease to almost zero at failure. As an example the load-displacement curve for a vertical load on the caisson with an embedment ratio of 1 calculated in Plaxis is shown in Figure 2.9. The capacity found in Plaxis is an overestimate of the actual capacity as a rather course mesh is used in the calculation to save computing time. The vertical capacity of this caisson is estimated at 296 MN using Terzaghi's formulation for the bearing capacity, modified for axisymmetrical foundations (Dekker, 2013).

Due to the applied safety factors and the gap between the top plate and the mudline only a fraction of the found capacity can actually be utilized, however the load will probably still be outside the linear-elastic range. As the left figure in Figure 2.9 shows the soil can be assumed to behave linear-elastic up to a vertical load of approximately 3 MN, for larger loads the stiffness will decrease significantly. For a load of 20 MN the incremental stiffness is only 0.9 $^{GN}/_{m}$, three times smaller than the initial stiffness. This shows that

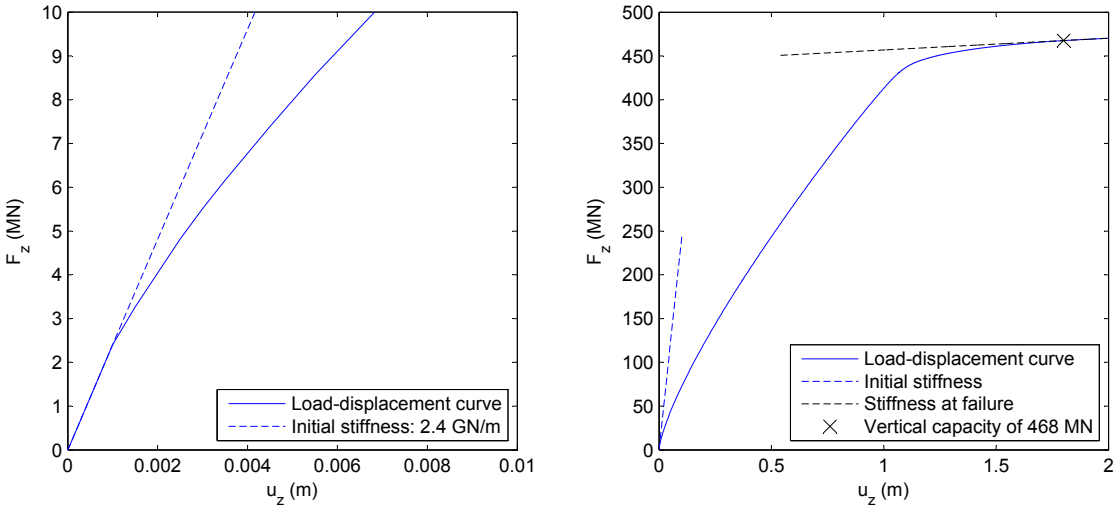

Figure 2.9: *Load-displacement curve for a vertical displacement for the bucket with $l/D = 1$: Detail (left) and complete curve (right)*

the linear-elastic stiffness is not suited for ultimate load cases as it will overestimate the foundation stiffness and therefore give incorrect foundation loads.

2.4 Implementation of a Linear Stiffness Foundation

2.4.1 Comparison of Foundation Types in SACS

In order to see how the foundation stiffness influences the loads on the foundation a series of calculations has been made using the software SACS (Bentley, 2012). The model used in SACS consists of a 4-legged jacket and 4 foundations, 1 for each leg. The jacket is based on a jacket designed for the North Sea in 20 m water depth and has a footprint of 20 by 20 m. 6 different foundation types have been used in the calculations: a clamped foundation, with all degrees of freedom restrained at the mudline, a pinned foundation, with all displacements fixed but no restraints for rotations, and four foundations that are based on a stiffness matrix. The first of these uses a stiffness matrix that is determined using the dimensions of the caisson and the soil parameters that are specified below. The next two foundations use the same stiffness matrix multiplied or divided by a factor $\sqrt{2}$ to account for the uncertainty in the assumed soil parameters. The last foundation uses a stiffness matrix that is a combination of the previous two, as will be discussed later in more detail.

The suction caissons all have a diameter and penetration depth of 7 m, so the dimensions are identical to the caisson with embedment ratio 1 used in the Plaxis calculations in Section 2.3. Therefore, and since the results from the analytical expressions do not correspond too well with the FEM results, the used stiffness matrix is based on the Plaxis calculations for the linear-elastic soil. In these calculations a shear modulus of 60 MPa and Poisson's ratio of 0.3 have been used. The resulting stiffness matrix is given in Equation 2.16. The stiffnesses are given in GN or GNm per m or per radian.

$$\begin{bmatrix} 3.66 & 0 & 0 & 0 & -15.04 & 0 \\ 0 & 3.66 & 0 & 15.04 & 0 & 0 \\ 0 & 0 & 2.96 & 0 & 0 & 0 \\ 0 & 15.04 & 0 & 134.42 & 0 & 0 \\ -15.04 & 0 & 0 & 0 & 134.42 & 0 \\ 0 & 0 & 0 & 0 & 0 & 79.76 \end{bmatrix} \tag{2.16}$$

The jacket is loaded by its own weight, a vertical load representing the topside deadweight and environmental load data representing a storm in the North Sea with a return period of 100 years. The environmental load data are given in Appendix C. The two load directions that give the most severe conditions are the loads coming from the west and south-west. The weather conditions coming from the south-west are more severe than those coming from the west, especially the 100-year current speed is significantly larger. On the other hand the jacket is orientated such that a load coming from the west gives a load in the diagonal direction of the jacket, which may result in a larger load on the most loaded foundation caisson. Therefore both load cases are evaluated, as well as the combination of wind and waves coming from the south-west with a current coming from the west. Since the 100-year wave and current are unlikely to occur simultaneously the current speeds have been halved for the calculation of the total environmental loads, on top of the applied current blockage factor (0.85 for the diagonal direction and 0.8 for other directions).

The weight of the jacket has been determined in SACS as 4200 kN, the submerged weight being 2750 kN. The topside weight is assumed to be 10,000 kN. This load is applied as 4 point loads of 2500 kN, one on top of each leg. The weight of the caissons is not taken into account. The combined weight of jacket and topside has been combined with the three environmental load conditions to get three different oad cases. The loads on each caisson have been determined for each of the load cases. The largest load on any of the caissons for any of the load cases is given for the different foundation types in Table 2.2.

Table 2.2: *Comparison of the foundation loads and displacements for different foundation types*

	Clamped	Pinned	Normal	Low	High	Mixed
F_H (kN)	1335	1059	1157	1113	1197	1071
F_V (kN)	3989	4194	4003	4007	3999	3991
M (kNm)	3187	-	2698	2568	2810	2508
T (kNm)	624	-	629	630	629	635
u_h (m)	-	-	$7.37 \cdot 10^{-4}$	$9.98 \cdot 10^{-4}$	$5.39 \cdot 10^{-4}$	$9.63 \cdot 10^{-4}$
u_z (m)	-	-	$1.35 \cdot 10^{-3}$	$1.92 \cdot 10^{-3}$	$0.96 \cdot 10^{-3}$	$1.91 \cdot 10^{-3}$
θ_h (rad)	-	$19.6 \cdot 10^{-4}$	$1.02 \cdot 10^{-4}$	$1.38 \cdot 10^{-4}$	$0.75 \cdot 10^{-4}$	$1.34 \cdot 10^{-4}$
θ_z (rad)	-	$130 \cdot 10^{-5}$	$0.79 \cdot 10^{-5}$	$1.12 \cdot 10^{-5}$	$0.56 \cdot 10^{-5}$	$1.13 \cdot 10^{-5}$

It can be seen that the pinned and clamped condition are the upper and lower boundary for the maximum foundation loads. In the case of a pinned foundation there will be no overturning moment on the foundation, which results in a slightly larger vertical load than for the clamped condition. The clamped condition does give a moment load on the

foundation and the maximum horizontal load is larger than for the pinned condition as the horizontal load is spread less equally over the four caissons. For the used sets of stiffnesses the caissons behave similar to a fully clamped foundation; the vertical and torsional load for all four stiffness matrices are almost equal to those for the clamped foundation. The moment load is also approximately 80 % of the moment load for a clamped foundation and the lateral load is in between the loads for clamped and pinned foundations.

The results also show that within a certain range, varying the stiffness of all four caissons simultaneously has only little effect on the maximum foundation loads that occur. The vertical and torsional load slow only a negligible difference between the low and the high stiffness matrix, where all the stiffness terms vary by a factor 2. The horizontal and moment load also vary by less than 10%. The results suggest that changing the stiffness of all the foundations does not change the way the load is distributed, the only difference is that the loads result in different displacements of the foundations.

In the case of a non-linear foundation stiffness the four foundations will not all have the same stiffness however, as the stiffness will vary with the load on the caisson. To see how this would influence the load distribution a mixed set of stiffness matrices has been used in the calculations as well. For each stiffness term the two caissons that were loaded most heavily in that load direction for the normal stiffness matrix are given the stiffness term from the low stiffness matrix, simulating a reduced stiffness due to the large load, and the other two caissons are given the stiffness term from the high stiffness matrix. This will lead to a more equally spread load distribution and hence smaller loads on the caisson that is loaded most heavily, as the last column in Table 2.2 confirms. Compared with the results for the normal stiffness matrix the largest horizontal load decreases by 7.5% and the largest overturning moment by 7.0%. This shows that the load distribution can have a significant influence on the caisson design.

2.4.2 Comparison With Plaxis Simulation

Comparison for a Single Caisson

In order to see how well the SACS model with stiffness matrix corresponds with the Plaxis model it is based on, a single caisson is modelled in both and loaded by a series of load combinations. The load cases and resulting displacements are given in Table 2.3.

It can be seen that the results match pretty well. The difference between the displacements found in SACS and Plaxis is less than 10% for most cases and in many cases less than 5%. Especially the vertical displacements show a very good agreement with a difference of 2%. The fact that the vertical displacement found in Plaxis is the same for the various load cases, independent of the applied lateral load, shows that the model behaves perfectly linear-elastic. This will besides not be the case for a real soil.

Since the choice of the load combination thus does not influence the stiffness of the caisson, the larger difference between the SACS and Plaxis results has to be caused by the inaccuracy in the determination of the combination of lateral, rotational and coupling stiffness. The accuracy of these terms can be increased by determining the values based on multiple load cases, instead of the two Plaxis calculations that are used now.

Table 2.3: *Comparison Between SACS and Plaxis Results for a Single Caisson*

	Load				Displacements		
LC	F_x (kN)	F_z (kN)	M_y (kNm)		u_x (m)	u_z (m)	θ_y (rad)
1	1000	-	-	SACS	$5.06{\cdot}10^{-4}$	-	$5.66{\cdot}10^{-5}$
				Plaxis	$5.51{\cdot}10^{-4}$	-	$5.46{\cdot}10^{-5}$
				Difference	*8.89%*	-	*-3.60%*
2	-	-1000	-	SACS	-	$-3.40{\cdot}10^{-4}$	-
				Plaxis	-	$-3.46{\cdot}10^{-4}$	
				Difference	-	*2.37%*	-
3	-	-	4000	SACS	$2.26{\cdot}10^{-4}$	-	$5.51{\cdot}10^{-5}$
				Plaxis	$2.20{\cdot}10^{-4}$	-	$4.89{\cdot}10^{-5}$
				Difference	*0.97%*	-	*-11.32%*
4	1000	-	5000	SACS	$7.89{\cdot}10^{-4}$	-	$1.25{\cdot}10^{-4}$
				Plaxis	$8.27{\cdot}10^{-4}$	-	$1.14{\cdot}10^{-4}$
				Difference	*4.89%*	-	*-9.39%*
5	-	-1000	-2000	SACS	$-1.10{\cdot}10^{-4}$	$-3.40{\cdot}10^{-4}$	$-2.75{\cdot}10^{-5}$
				Plaxis	$-1.03{\cdot}10^{-4}$	$-3.46{\cdot}10^{-4}$	$-2.30{\cdot}10^{-5}$
				Difference	*-8.80%*	*2.38%*	*-16.41%*
6	1000	-1000	-	SACS	$5.06{\cdot}10^{-4}$	$-3.40{\cdot}10^{-4}$	$5.66{\cdot}10^{-5}$
				Plaxis	$5.51{\cdot}10^{-4}$	$-3.46{\cdot}10^{-4}$	$5.36{\cdot}10^{-5}$
				Difference	*8.88%*	*2.35%*	*-5.38%*
7	1000	-1000	5000	SACS	$7.89{\cdot}10^{-4}$	$-3.40{\cdot}10^{-4}$	$1.25{\cdot}10^{-4}$
				Plaxis	$8.27{\cdot}10^{-4}$	$-3.46{\cdot}10^{-4}$	$1.13{\cdot}10^{-4}$
				Difference	*4.88%*	*2.33%*	*-10.20%*
8	1000	-	10000	SACS	$1.07{\cdot}10^{-3}$	-	$1.94{\cdot}10^{-4}$
				Plaxis	$1.10{\cdot}10^{-4}$	-	$1.73{\cdot}10^{-4}$
				Difference	*3.00%*	-	*-11.13%*

Comparison for a Four-Legged Jacket

In order to check whether the found stiffness matrix can actually be used for a structure with multiple caissons the complete jacket with four caissons has also been modelled in Plaxis and compared to SACS calculations. The Plaxis model is shown in Figure 2.10. It has been converted from the SACS model given in Appendix F.2 using the MatLab script codewriter.m given in Appendix F.1.

Since Plaxis has no option to use a seastate as load input a single pointload of 2000 kN in the positive x-direction has been applied on the jacket. In SACS the caissons are modelled by the stiffness matrix found for a single caisson in Plaxis as described in Section 2.3.2, which is given in Equation 2.16. In Plaxis the caissons are modelled by means of the same linear-elastic material as used in the stiffness matrix calculations, with a shear modulus of 60 GPa and Poisson's ratio of 0.3, a 1000 times stiffer than the surrounding soil material.

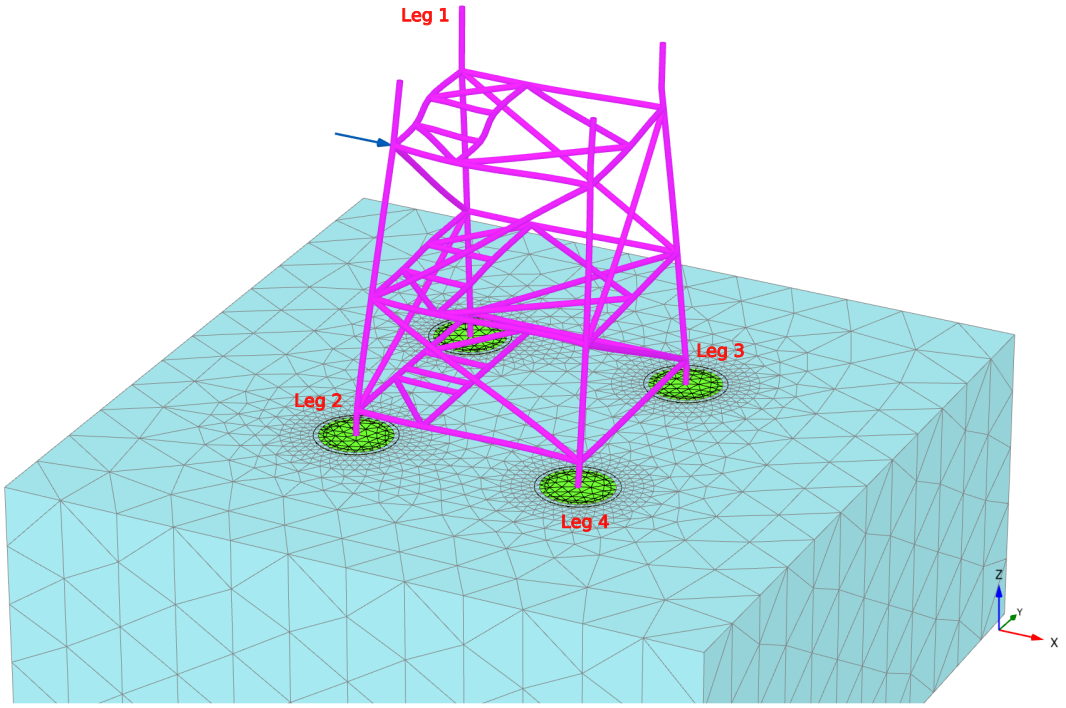

Figure 2.10: *Screenshot of the model of the jacket in Plaxis*

On top of the caissons a rigid top plate is also modelled in order to transfer the rotations of the jacket into the soil. The resulting foundation loads and displacements found in the SACS and Plaxis calculations are compared in Table 2.4 and 2.5.

Table 2.4: *Comparison of foundation loads found in the SACS and Plaxis calculations*

Leg	Results	F_x (kN)	F_y	F_z	M_x (kNm)	M_y	M_z
1	SACS	354.8	-143.8	938.0	415.6	940.6	52.5
	Plaxis	328.6	-140.2	909.0	425.7	905.5	-
	Difference	*-7.4%*	*-2.5%*	*-3.1%*	*2.4%*	*-3.7%*	-
2	SACS	356.1	-182.6	1352.7	622.0	1431.1	-40.4
	Plaxis	407.4	-173.5	1378.3	575.4	1627.9	-
	Difference	*14.1%*	*-5.0%*	*1.9%*	*-7.5%*	*13.8%*	-
3	SACS	193.3	326.5	-940.0	-744.1	619.5	94.6
	Plaxis	206.7	311.0	-910.4	-703.7	637.6	-
	Difference	*7.0%*	*-4.8%*	*-3.2%*	*-5.4%*	*2.9%*	-
4	SACS	1095.1	-0.1	-1350.7	-246.0	2734.9	-23.0
	Plaxis	1057.1	2.7	-1376.9	-265.2	2624.4	-
	Difference	*-3.5%*	*2203.5%*	*1.9%*	*7.8%*	*-4.0%*	-

Table 2.4 shows that the foundation loads found in SACS and in Plaxis correspond very well, with the difference being less than 5% in most cases. As Table 2.2 shows the loads

Table 2.5: *Comparison of foundation displacements found in the SACS and Plaxis calculations*

Leg	Results	u_x (m)	u_y (m)	u_z (m)	θ_x (rad)	θ_y (rad)	θ_z (rad)
1	SACS	$2.3{\cdot}10^{-4}$	$-9.6{\cdot}10^{-5}$	$3.2{\cdot}10^{-4}$	$1.4{\cdot}10^{-5}$	$3.3{\cdot}10^{-5}$	$7.0{\cdot}10^{-7}$
	Plaxis	$3.0{\cdot}10^{-4}$	$-1.1{\cdot}10^{-4}$	$3.5{\cdot}10^{-4}$	$5.6{\cdot}10^{-6}$	$3.8{\cdot}10^{-5}$	$8.8{\cdot}10^{-6}$
	Difference	*29.1%*	*9.4%*	*10.5%*	*-59.8%*	*13.9%*	*1156.2%*
2	SACS	$2.6{\cdot}10^{-4}$	$-1.3{\cdot}10^{-4}$	$4.6{\cdot}10^{-4}$	$1.9{\cdot}10^{-5}$	$4.0{\cdot}10^{-5}$	$-5.0{\cdot}10^{-7}$
	Plaxis	$4.3{\cdot}10^{-4}$	$-1.4{\cdot}10^{-4}$	$5.1{\cdot}10^{-4}$	$1.5{\cdot}10^{-5}$	$5.2{\cdot}10^{-5}$	$-4.8{\cdot}10^{-7}$
	Difference	*62.8%*	*12.3%*	*12.1%*	*-18.9%*	*29.3%*	*-4.0%*
3	SACS	$1.3{\cdot}10^{-4}$	$2.1{\cdot}10^{-4}$	$-3.2{\cdot}10^{-4}$	$-2.9{\cdot}10^{-5}$	$2.0{\cdot}10^{-5}$	$1.2{\cdot}10^{-6}$
	Plaxis	$2.1{\cdot}10^{-4}$	$2.2{\cdot}10^{-4}$	$-3.4{\cdot}10^{-4}$	$-2.7{\cdot}10^{-5}$	$2.6{\cdot}10^{-5}$	$2.8{\cdot}10^{-6}$
	Difference	*56.2%*	*6.0%*	*6.8%*	*-6.5%*	*33.2%*	*130.9%*
4	SACS	$7.1{\cdot}10^{-4}$	$1.4{\cdot}10^{-5}$	$-4.6{\cdot}10^{-4}$	$-3.4{\cdot}10^{-6}$	$1.0{\cdot}10^{-4}$	$-3.0{\cdot}10^{-7}$
	Plaxis	$8.0{\cdot}10^{-4}$	$3.8{\cdot}10^{-5}$	$-4.1{\cdot}10^{-4}$	$-2.9{\cdot}10^{-6}$	$8.2{\cdot}10^{-5}$	$-2.6{\cdot}10^{-7}$
	Difference	*12.8%*	*172.7%*	*-9.2%*	*-14.4%*	*-17.5%*	*-13.2%*

on the caissons are not influenced that much by the stiffness of the caissons, so this result does not necessarily imply that the caissons have the same stiffness in the two models. For the displacements of the caissons the differences are significantly larger, as Table 2.5 shows. Apart from the rotations about the x-axis the displacements found in Plaxis are larger than those found in SACS. This is especially the case for the translation in x-direction and the rotation about the y-axis. For these directions all the caissons have a displacement with the same sign (so in the same direction), as the structure has to withstand the load in x-direction. The result of this is that the soil between the caissons is also displaced the same order of magnitude as the individual caissons. This means that this part of the soil cannot provide as much resistance or stiffness for the caissons as it would for an individual caisson; the caissons are interfering with each other and so-called group effects have to be taken into account when determining the stiffness of the foundation. While many studies have been performed on how the capacity is influenced by pile group effects, for instance Kim et al. (2014), this is not the case for the influence on the soil stiffness. Therefore the effect will be studied by FE analysis.

Comparison Including Pile Group Effects

The effects of the interaction between the caissons through the soil can be included by determining the stiffness matrix in a model that includes all four caissons instead of only one. For this the Plaxis model shown in Figure 2.10 without the actual jacket structure is used. Unidirectional loads are applied on one caisson and the resulting displacements of all four caissons are determined. Because of the symmetry of the foundation and of the linear-elastic soil with regard to the load direction (compression/tension) it can be assumed that the load-displacement relations found for the loads on one caisson will be sufficient to determine the load-displacement relations for loads on each of the four caissons. This way a 24x24 flexibility matrix for the complete foundation can be determined and inverted to find the stiffness matrix. The resulting flexibility matrix is shown in Appendix D.

Not all degrees of freedom are affected by the interaction to the same extent. To study this the interaction terms for each degree of freedom have been included one by one to see how much their inclusion influenced the resulting stiffness matrix and hence the behaviour of the foundation. It turns out that only the lateral translation degrees of freedom are influenced by the interaction. This makes sense, as the soil between the caissons can translate as a whole during loading in lateral direction instead of more complex deformations in the case of rotations, which result in a higher stiffness. Therefore only the bold terms in the flexibility matrix are used to determine the stiffness matrix.

Table 2.6: *Comparison of foundation loads found in the SACS and Plaxis calculations*

Leg	Results	F_x (kN)	F_y	F_z	M_x (kNm)	M_y	M_z
1	SACS	355.7	-144.3	939.7	417.0	945.8	53.4
	Plaxis	328.6	-140.2	909.0	425.7	905.5	-
	Difference	*-7.6%*	*-2.9%*	*-3.3%*	*2.1%*	*-4.3%*	-
2	SACS	357.3	-183.3	1350.3	623.9	1436.0	-39.8
	Plaxis	407.4	-173.5	1378.3	575.4	1627.9	-
	Difference	*14.0%*	*-5.4%*	*2.1%*	*-7.8%*	*13.4%*	-
3	SACS	193.6	327.1	-941.8	-745.3	623.9	95.5
	Plaxis	206.7	311.0	-910.4	-703.7	637.6	-
	Difference	*6.8%*	*-4.9%*	*-3.5%*	*-5.6%*	*2.2%*	-
4	SACS	1093.4	0.5	-1348.2	-247.8	2735.7	-22.6
	Plaxis	1057.1	2.7	-1376.9	-265.2	2624.4	-
	Difference	*-3.3%*	*411.7%*	*2.1%*	*7.0%*	*-4.1%*	-

Table 2.7: *Comparison of foundation displacements found in the SACS and Plaxis calculations*

Leg	Results	u_x (m)	u_y (m)	u_z (m)	θ_x (rad)	θ_y (rad)	θ_z (rad)
1	SACS	$2.9{\cdot}10^{-4}$	$-1.1{\cdot}10^{-4}$	$3.4{\cdot}10^{-4}$	$1.4{\cdot}10^{-5}$	$3.3{\cdot}10^{-5}$	$7.0{\cdot}10^{-7}$
	Plaxis	$3.0{\cdot}10^{-4}$	$-1.1{\cdot}10^{-4}$	$3.5{\cdot}10^{-4}$	$5.6{\cdot}10^{-6}$	$3.8{\cdot}10^{-5}$	$8.8{\cdot}10^{-6}$
	Difference	*5.0%*	*-4.7%*	*0.6%*	*-59.2%*	*15.0%*	*1156.2%*
2	SACS	$3.5{\cdot}10^{-4}$	$-1.4{\cdot}10^{-4}$	$4.8{\cdot}10^{-4}$	$1.9{\cdot}10^{-5}$	$3.9{\cdot}10^{-5}$	$-5.0{\cdot}10^{-7}$
	Plaxis	$4.3{\cdot}10^{-4}$	$-1.4{\cdot}10^{-4}$	$5.1{\cdot}10^{-4}$	$1.5{\cdot}10^{-5}$	$5.2{\cdot}10^{-5}$	$-4.8{\cdot}10^{-7}$
	Difference	*20.3%*	*0.0%*	*1.1%*	*-17.1%*	*33.6%*	*-4.0%*
3	SACS	$1.9{\cdot}10^{-4}$	$2.2{\cdot}10^{-4}$	$-3.4{\cdot}10^{-4}$	$-2.9{\cdot}10^{-5}$	$1.9{\cdot}10^{-5}$	$1.3{\cdot}10^{-6}$
	Plaxis	$2.1{\cdot}10^{-4}$	$2.2{\cdot}10^{-4}$	$-3.4{\cdot}10^{-4}$	$-2.7{\cdot}10^{-5}$	$2.6{\cdot}10^{-5}$	$2.8{\cdot}10^{-6}$
	Difference	*11.1%*	*-1.2%*	*-1.5%*	*-6.2%*	*35.9%*	*113.1%*
4	SACS	$8.0{\cdot}10^{-4}$	$2.8{\cdot}10^{-5}$	$-4.8{\cdot}10^{-4}$	$-3.0{\cdot}10^{-6}$	$9.9{\cdot}10^{-5}$	$-3.0{\cdot}10^{-7}$
	Plaxis	$8.0{\cdot}10^{-4}$	$3.8{\cdot}10^{-5}$	$-4.1{\cdot}10^{-4}$	$-2.9{\cdot}10^{-6}$	$8.2{\cdot}10^{-5}$	$-2.6{\cdot}10^{-7}$
	Difference	*-0.3%*	*32.7%*	*-6.4%*	*-3.0%*	*-16.6%*	*-13.2%*

The stiffness matrix is then entered in SACS as 4 6x6 pile-ground stiffness matrices for the individual caissons plus 6 6x6 pile-pile stiffness matrices for the interaction between two caissons. The results from the SACS calculations are shown in Table 2.6 and 2.7, where they are compared to the results from the Plaxis calculations previously given in Table 2.4 and 2.5.

Comparing Table 2.5 and 2.7 shows that the difference between the displacements found in SACS and in Plaxis is decreased significantly when the interaction between the caissons is included in the SACS model. Especially the translations in x-direction, which are influenced most by the interaction effects since the applied load is also in the x-direction, show a much better correspondence between the SACS and Plaxis calculations. Apart from a few exceptions most differences are below 15% for the model including interaction effects, which is the same order of magnitude as found in Table 2.3 for a single pile. The foundation loads do not change significantly and remain within the 5-10 % difference range from the Plaxis range. This shows that the applied method to include interaction in SACS gives accurate results.

Variation of the Soil Stiffness

So far the comparison between the SACS and Plaxis models has only been made for a shear modulus G of 60 MPa. Before the model can be used for an arbitrary soil profile it should be checked that the behaviour is consistent for different soil types. This has been done by repeating the calculations with a shear modulus of 5, 20 and 240 MPa. With a Poisson's ratio of 0.3 this corresponds with Young's moduli of 13, 52 and 624 MPa, respectively. Offshore soil profiles found in practice will generally not vary over such a large range of soil stiffnesses; especially the Young's modulus of 624 MPa is unrealistic for a soil profile and is more representative for a rock layer in which suction installation is not possible. The large variation has still been chosen as it will not only cover the full range of realistic soil stiffnesses but also help to clarify any trends in the results by using large steps between the used soil stiffnesses.

The soil stiffness has been changed in the Plaxis model and the calculations for the complete jacket loaded by a horizontal load have been repeated. Since the stiffness matrix is proportional to the shear modulus G the stiffness matrices used in the SACS model have not been determined again but the stiffness matrices determined for the shear modulus of 60 MPa have simply been multiplied by a stiffness factor of 1/12, 1/3 and 4 respectively. The resulting loads on and displacements of the caissons found in the Plaxis and SACS models are given and compared in Table 2.9 to 2.14. The average differences are summarized in Table 2.8. For the displacements the difference in rotation about the z-axis (torsion) has not been included in the average, as there are large differences for this degree of freedom for each of the used shear moduli that blur the comparison.

Table 2.8: *Comparison between the SACS and Plaxis models for various shear moduli*

Shear modulus G (MPa)	5	20	60	240
Average difference in loads	5.6%	3.8%	5.4%	6.9%
Average difference in displacements	6.9%	7.2%	10.8%	17.5%

The comparison shows that there are no large differences in the average difference for the various shear moduli. The average difference between the SACS and Plaxis models for the caisson displacements increases with increasing soil stiffness, from approximately 5% for a shear modulus of 5 MPa to approximately 15% for a shear modulus of 240 MPa. This can most likely be attributed to the smaller displacements for high soil stiffnesses: the displacements for a shear modulus of 240 MPa are some 50 times smaller than the displacements for a shear modulus of 5 MPa, meaning that the same absolute difference will lead to a significantly higher relative difference.

Table 2.9: *Comparison of foundation loads for a shear modulus of 5 MPa*

Leg	Results	F_x (kN)	F_y	F_z	M_x (kNm)	M_y	M_z
	Plaxis	309.3	-192.0	1066.6	292.3	885.4	-
1	SACS	332.7	-185.8	1074.6	287.6	969.7	133.4
	Difference	*7.6%*	*-3.2%*	*0.7%*	*-1.6%*	*9.5%*	-
	Plaxis	604.6	-195.2	1257.3	294.8	1665.4	-
2	SACS	585.7	-198.1	1234.8	395.9	1716.0	50.5
	Difference	*-3.1%*	*1.5%*	*-1.8%*	*34.3%*	*3.0%*	-
	Plaxis	294.8	257.0	-1064.9	-299.5	868.4	-
3	SACS	288.8	249.3	-1077.2	-272.9	955.9	206.9
	Difference	*-2.0%*	*-3.0%*	*1.2%*	*-8.9%*	*10.1%*	-
	Plaxis	791.3	130.3	-1259.0	-327.2	1553.4	-
4	SACS	792.8	134.6	-1232.2	-350.0	1660.5	100.0
	Difference	*0.2%*	*3.3%*	*-2.1%*	*7.0%*	*6.9%*	-

Table 2.10: *Comparison of foundation displacements for a shear modulus of 5 MPa*

Leg	Results	u_x (m)	u_y (m)	u_z (m)	θ_x (rad)	θ_y (rad)	θ_z (rad)
	Plaxis	$3.5{\cdot}10^{-3}$	$-1.6{\cdot}10^{-3}$	$4.9{\cdot}10^{-3}$	$1.8{\cdot}10^{-4}$	$4.4{\cdot}10^{-4}$	$2.8{\cdot}10^{-5}$
1	SACS	$3.4{\cdot}10^{-3}$	$-1.5{\cdot}10^{-3}$	$4.6{\cdot}10^{-3}$	$1.8{\cdot}10^{-4}$	$3.8{\cdot}10^{-4}$	$2.2{\cdot}10^{-5}$
	Difference	*-4.3%*	*-7.3%*	*-4.7%*	*-0.4%*	*-13.1%*	*-22.1%*
	Plaxis	$6.4{\cdot}10^{-3}$	$-1.8{\cdot}10^{-3}$	$5.6{\cdot}10^{-3}$	$2.3{\cdot}10^{-4}$	$7.7{\cdot}10^{-4}$	$2.7{\cdot}10^{-7}$
2	SACS	$5.8{\cdot}10^{-3}$	$-1.7{\cdot}10^{-3}$	$5.3{\cdot}10^{-3}$	$2.0{\cdot}10^{-4}$	$6.7{\cdot}10^{-4}$	$8.2{\cdot}10^{-6}$
	Difference	*-9.0%*	*-5.6%*	*-4.7%*	*-12.6%*	*-13.1%*	*2992.8%*
	Plaxis	$3.2{\cdot}10^{-3}$	$2.0{\cdot}10^{-3}$	$-4.8{\cdot}10^{-3}$	$-2.1{\cdot}10^{-4}$	$3.9{\cdot}10^{-4}$	$3.0{\cdot}10^{-5}$
3	SACS	$3.1{\cdot}10^{-3}$	$1.9{\cdot}10^{-3}$	$-4.6{\cdot}10^{-3}$	$-2.2{\cdot}10^{-4}$	$3.5{\cdot}10^{-4}$	$3.4{\cdot}10^{-5}$
	Difference	*-4.4%*	*-7.4%*	*-4.1%*	*3.7%*	*-12.4%*	*13.5%*
	Plaxis	$7.4{\cdot}10^{-3}$	$1.4{\cdot}10^{-3}$	$-5.5{\cdot}10^{-3}$	$-1.5{\cdot}10^{-4}$	$8.8{\cdot}10^{-4}$	$2.1{\cdot}10^{-6}$
4	SACS	$7.0{\cdot}10^{-3}$	$1.3{\cdot}10^{-3}$	$-5.3{\cdot}10^{-3}$	$-1.5{\cdot}10^{-4}$	$8.1{\cdot}10^{-4}$	$1.6{\cdot}10^{-5}$
	Difference	*-5.9%*	*-9.1%*	*-4.4%*	*-3.5%*	*-7.9%*	*690.2%*

No clear trend can be observed for difference in the resulting caisson loads; the difference is approximately 5% for each of the evaluated shear moduli. The results are accurate independent of the used soil stiffness. This confirms the previous conclusion that the representation of a suction caisson foundation by a stiffness matrix provides accurate results, given that the soil can be characterized as being uniform and linear-elastic.

Table 2.11: *Comparison of foundation loads for a shear modulus of 20 MPa*

Leg	Results	F_x (kN)	F_y	F_z	M_x (kNm)	M_y	M_z
	Plaxis	317.9	-164.0	969.5	433.5	882.7	-
1	SACS	341.5	-163.2	992.5	418.4	930.8	69.3
	Difference	*7.4%*	*-0.5%*	*2.4%*	*-3.5%*	*5.4%*	-
	Plaxis	513.3	-183.6	1325.8	527.9	1799.2	-
2	SACS	478.3	-192.0	1300.1	589.0	1692.4	-27.4
	Difference	*-6.8%*	*4.6%*	*-1.9%*	*11.6%*	*-5.9%*	-
	Plaxis	247.4	286.0	-969.5	-595.9	731.4	-
3	SACS	238.4	290.4	-994.3	-594.3	761.1	124.8
	Difference	*-3.6%*	*1.5%*	*2.6%*	*-0.3%*	*4.1%*	-
	Plaxis	921.4	61.6	-1325.9	-367.2	2205.4	-
4	SACS	941.7	64.8	-1298.3	-370.7	2298.4	6.3
	Difference	*2.2%*	*5.2%*	*-2.1%*	*0.9%*	*4.2%*	-

Table 2.12: *Comparison of foundation displacements for a shear modulus of 20 MPa*

Leg	Results	u_x (m)	u_y (m)	u_z (m)	θ_x (rad)	θ_y (rad)	θ_z (rad)
	Plaxis	$8.8{\cdot}10^{-4}$	$-3.9{\cdot}10^{-4}$	$1.1{\cdot}10^{-3}$	$4.4{\cdot}10^{-5}$	$1.1{\cdot}10^{-4}$	$6.7{\cdot}10^{-6}$
1	SACS	$8.4{\cdot}10^{-4}$	$-3.6{\cdot}10^{-4}$	$1.1{\cdot}10^{-3}$	$4.4{\cdot}10^{-5}$	$9.5{\cdot}10^{-5}$	$2.8{\cdot}10^{-6}$
	Difference	*-5.1%*	*-5.6%*	*-4.2%*	*1.2%*	*-13.7%*	*-58.4%*
	Plaxis	$1.5{\cdot}10^{-3}$	$-4.6{\cdot}10^{-4}$	$1.5{\cdot}10^{-3}$	$6.4{\cdot}10^{-5}$	$1.8{\cdot}10^{-4}$	$-2.7{\cdot}10^{-7}$
2	SACS	$1.3{\cdot}10^{-3}$	$-4.4{\cdot}10^{-4}$	$1.4{\cdot}10^{-3}$	$5.6{\cdot}10^{-5}$	$1.5{\cdot}10^{-4}$	$-1.1{\cdot}10^{-6}$
	Difference	*-12.8%*	*-5.0%*	*-5.1%*	*-13.0%*	*-18.9%*	*301.9%*
	Plaxis	$7.0{\cdot}10^{-4}$	$6.0{\cdot}10^{-4}$	$-1.1{\cdot}10^{-3}$	$-7.1{\cdot}10^{-5}$	$8.4{\cdot}10^{-5}$	$7.9{\cdot}10^{-6}$
3	SACS	$6.6{\cdot}10^{-4}$	$5.9{\cdot}10^{-4}$	$-1.1{\cdot}10^{-3}$	$-7.4{\cdot}10^{-5}$	$7.0{\cdot}10^{-5}$	$5.1{\cdot}10^{-6}$
	Difference	*-6.4%*	*-2.7%*	*-3.3%*	*4.3%*	*-15.9%*	*-35.0%*
	Plaxis	$2.2{\cdot}10^{-3}$	$2.3{\cdot}10^{-4}$	$-1.4{\cdot}10^{-3}$	$-2.5{\cdot}10^{-5}$	$2.7{\cdot}10^{-4}$	$7.0{\cdot}10^{-7}$
4	SACS	$2.1{\cdot}10^{-3}$	$2.1{\cdot}10^{-4}$	$-1.4{\cdot}10^{-3}$	$-2.5{\cdot}10^{-5}$	$2.5{\cdot}10^{-4}$	$3.0{\cdot}10^{-7}$
	Difference	*-4.7%*	*-10.7%*	*-3.6%*	*-1.2%*	*-7.3%*	*-57.0%*

Table 2.13: *Comparison of foundation loads for a shear modulus of 240 MPa*

Leg	Results	F_x (kN)	F_y	F_z	M_x (kNm)	M_y	M_z
	Plaxis	338.7	-127.2	873.0	412.2	917.9	-
1	SACS	369.6	-132.3	906.0	403.1	969.4	48.1
	Difference	*9.1%*	*4.1%*	*3.8%*	*-2.2%*	*5.6%*	-
	Plaxis	311.0	-166.6	1414.3	586.9	1412.9	-
2	SACS	252.2	-175.7	1384.1	627.5	1179.3	-38.9
	Difference	*-18.9%*	*5.5%*	*-2.1%*	*6.9%*	*-16.5%*	-
	Plaxis	174.1	335.0	-874.7	-801.5	531.8	-
3	SACS	159.4	355.4	-908.5	-838.9	524.2	80.4
	Difference	*-8.5%*	*6.1%*	*3.9%*	*4.7%*	*-1.4%*	-
	Plaxis	1176.2	-41.2	-1412.6	-157.6	2940.1	-
4	SACS	1218.9	-47.4	-1381.6	-135.2	3065.1	-36.1
	Difference	*3.6%*	*14.9%*	*-2.2%*	*-14.2%*	*4.3%*	-

Table 2.14: *Comparison of foundation displacements for a shear modulus of 240 MPa*

Leg	Results	u_x (m)	u_y (m)	u_z (m)	θ_x (rad)	θ_y (rad)	θ_z (rad)
	Plaxis	$7.7{\cdot}10^{-5}$	$-2.7{\cdot}10^{-5}$	$8.5{\cdot}10^{-5}$	$3.0{\cdot}10^{-6}$	$9.7{\cdot}10^{-6}$	$5.1{\cdot}10^{-7}$
1	SACS	$7.3{\cdot}10^{-5}$	$-2.6{\cdot}10^{-5}$	$8.1{\cdot}10^{-5}$	$3.2{\cdot}10^{-6}$	$8.5{\cdot}10^{-6}$	$2.0{\cdot}10^{-7}$
	Difference	*-4.4%*	*-3.9%*	*-4.6%*	*5.6%*	*-12.7%*	*-60.9%*
	Plaxis	$9.1{\cdot}10^{-5}$	$-3.7{\cdot}10^{-5}$	$1.3{\cdot}10^{-4}$	$5.3{\cdot}10^{-6}$	$1.1{\cdot}10^{-5}$	$-7.3{\cdot}10^{-8}$
2	SACS	$7.2{\cdot}10^{-5}$	$-3.5{\cdot}10^{-5}$	$1.2{\cdot}10^{-4}$	$4.5{\cdot}10^{-6}$	$7.3{\cdot}10^{-6}$	$-1.0{\cdot}10^{-7}$
	Difference	*-21.1%*	*-6.4%*	*-6.7%*	*-15.0%*	*-32.8%*	*37.4%*
	Plaxis	$4.5{\cdot}10^{-5}$	$6.0{\cdot}10^{-5}$	$-8.4{\cdot}10^{-5}$	$-7.6{\cdot}10^{-6}$	$5.2{\cdot}10^{-6}$	$7.3{\cdot}10^{-7}$
3	SACS	$4.1{\cdot}10^{-5}$	$6.0{\cdot}10^{-5}$	$-8.1{\cdot}10^{-5}$	$-7.9{\cdot}10^{-6}$	$4.0{\cdot}10^{-6}$	$3.0{\cdot}10^{-7}$
	Difference	*-10.0%*	*1.0%*	*-3.2%*	*3.9%*	*-23.6%*	*-58.9%*
	Plaxis	$2.3{\cdot}10^{-4}$	$1.5{\cdot}10^{-6}$	$-1.3{\cdot}10^{-4}$	$4.2{\cdot}10^{-7}$	$3.0{\cdot}10^{-5}$	$7.6{\cdot}10^{-8}$
4	SACS	$2.2{\cdot}10^{-4}$	$-7.9{\cdot}10^{-7}$	$-1.2{\cdot}10^{-4}$	$3.0{\cdot}10^{-7}$	$2.8{\cdot}10^{-5}$	$-1.0{\cdot}10^{-7}$
	Difference	*-4.1%*	*-152.1%*	*-3.1%*	*-28.0%*	*-8.4%*	*-232.0%*

2.5 Conclusion

Various analytical expressions to determine the stiffness matrix for a suction caisson have been discussed and compared. They are either developed for shallow foundations or for slender piles. Suction caissons usually have an embedment ratio in between a shallow foundation and a slender pile so some caution is required when the expressions are applied.

A comparison with FEM calculations shows that the analytical results match within 10% with the FEM results for a linear-elastic uniform soil, so it seems that the expressions can be applied for suction caissons. The FEM results for a non-uniform or elastoplastic soil show that the foundation stiffness is very dependent on the assumed soil conditions however, so the analytical expressions will not always give reliable results for realistic soil profiles. Especially the decrease in stiffness with increasing load cannot be captured by a linear model.

The stiffness matrix found from the FEM calculations for the linear-elastic soil has been applied to model a jacket structure with 4 caisson foundations in SACS. The results show that the loads on the caissons are close to the loads that are found for clamped foundations. Varying the stiffness of all the caissons simultaneously does not influence the load distribution of the caisson significantly. When some caissons are made stiffer than others the load on the most heavily loaded caisson will change however.

The jacket and the 4 caissons have also been modelled in Plaxis in order to confirm the results found in SACS. The caisson loads found in the two programs correspond very well, with less than 5% difference in most cases. The displacements found in Plaxis are significantly larger however, most likely because of pile group effects. When additional springs between the caissons are added in SACS to include these effects the displacements show a significantly better agreement. The load distribution is not changed significantly by this method.

A sensitivity study performed by varying the shear modulus of the soil confirmed the accuracy of the use of stiffness matrices for a wide range of soil stiffnesses with the shear modulus varying from 5 to 240 MPa. The difference in the resulting caisson loads is not sensitive for the chosen shear modulus and is approximately 5% for each of the evaluated shear moduli. The difference for the caisson displacements increases with increasing soil stiffness, however this can most likely be attributed to the smaller displacements for large soil stiffnesses which lead to larger relative differences. All in all it can be concluded that modelling a suction caisson foundation by a stiffness matrix gives accurate results for any uniform linear-elastic soil with realistic soil stiffness.

Chapter 3

Non-Linear Stiffness Method

3.1 Choice of the Soil Model

There are several alternatives for the modelling of non-linear soil behaviour in Plaxis. The two models most suited for sandy soils are the Mohr-Coulomb model and the Hardening Soil model (Schanz et al., 1999). These two models will be discussed in the following paragraphs.

3.1.1 The Mohr-Coulomb Model

The Mohr-Coulomb model is a bilinear model; the model behaves linear-elastic up to the failure criterion while for stress states outsidee the failure criterion there is no remaining stiffness, allowing for unlimited plastic deformations. This type of model is called linear-elastic perfectly plastic.

Strain Definition

The strains can be split in an elastic strain ϵ^e and a plastic strain ϵ^p:

$$\epsilon = \epsilon^e + \epsilon^p \tag{3.1}$$

The Mohr-Coulomb model uses a constant, stress-independent Young's Modulus E. This means that the elastic stress-strain relationship will be linear-elastic as follows from Hooke's law, as given for a one and three dimensional stress-state in Equation 3.2 and 3.3.

$$\epsilon^e = \frac{\sigma'}{E} \tag{3.2}$$

$$\begin{bmatrix} \epsilon_1^e \\ \epsilon_2^e \\ \epsilon_3^e \end{bmatrix} = \frac{1}{E} \begin{bmatrix} 1 & -\nu & -\nu \\ -\nu & 1 & -\nu \\ -\nu & -\nu & 1 \end{bmatrix} \begin{bmatrix} \sigma_1' \\ \sigma_2' \\ \sigma_3' \end{bmatrix} \tag{3.3}$$

The plastic strain ϵ^p in the Mohr-Coulomb model will be zero until a certain treshold stress state is reached, and larger than zero beyond this stress state. In principle unlimited plastic strains can develop after failure, but the strains will usually be limited by surrounding particles that are still within the linear-elastic regime and will thus resist large deformations.

The plastic strain can be defined as (Hill, 1998, Chap. 2)

$$\boldsymbol{\epsilon}^p = \lambda \frac{\partial \boldsymbol{g}}{\partial \boldsymbol{\sigma'}} \tag{3.4}$$

where $\boldsymbol{\epsilon}^p$ is the plastic strain vector, $\boldsymbol{\sigma}$ is the stress vector and $\boldsymbol{g}$ is the yield function, which is a function of the stress state and the dilatancy angle ψ. The plasticity in the Mohr-Coulomb model is non-assosiciated, meaning that the yield function $\boldsymbol{g}$ will be different from the failure function $\boldsymbol{f}$. The general forms of $\boldsymbol{f}$ and $\boldsymbol{g}$ used in the Mohr-Coulomb model are

$$f = \tau - \sigma' \cdot \sin\phi - c \cdot \cos\phi \tag{3.5}$$

$$g = \tau - \sigma' \cdot \sin\psi \tag{3.6}$$

where τ is the in-plane shear stress, σ is the average in-plane normal stress (positive in compression), c is the cohesion of the soil, ϕ is the friction angle and ψ is the dilation angle. For a three-dimensional stress state there are three perpendicular planes, with for each normal stress an upper and lower limit for the shear stress, resulting in six failure functions f and six corresponding yield functions g.

Equation 3.4 describes that the plastic strain vector will be perpendicular to the yield function with a magnitude determined by the scalar λ. λ is defined by

$$\lambda = \begin{cases} 0 & \text{if } f < 0 \\ > 0 & \text{if } f = 0 \end{cases} \tag{3.7}$$

The resulting stress-strain relationship for a soil element is sketched in Figure 3.1. Since not all soil elements in a soil volume will have the same stress state and fail at the same time, the resulting load-displacement curve for a certain failure mechanism is not necessarily linear-elastic perfectly plastic and will usually show a gradual development of plastic deformations.

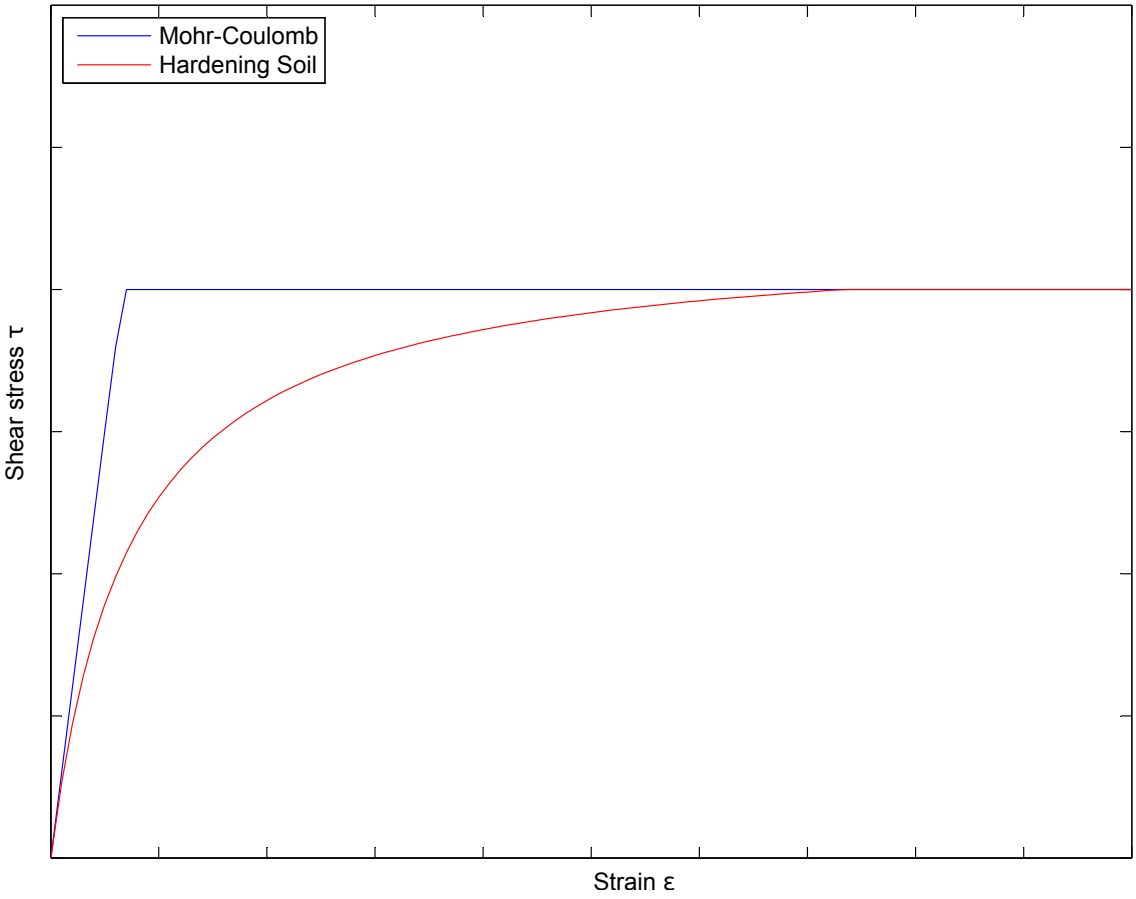

Figure 3.1: *Stress-strain relationship for the Mohr-Coulomb and Hardening Soil model*

3.1.2 The Hardening Soil Model

In contrast to the Mohr-Coulomb model, the Hardening Soil model has no clear distinction between an elastic and plastic region. The plastic deformations develop gradually instead. The Hardening Soil model contains two features that describe the non-linear stress-strain relation: a stress-dependent stiffness and a hyperbolic stress-strain curve.

Stress-dependent Stiffness

The Hardening Soil model uses three different stiffness parameters: E_{50}^{ref} which determines the stiffness for shear loading, E_{oed}^{ref} which determines the stiffness for uniform hydrostatic compression and E_{ur}^{ref} which determines the stiffness during unloading and reloading (Schanz et al., 1999). The first two stiffnesses determine the behaviour of the soil when it is loaded to a higher stress state then it has experienced before, during which there will be both elastic and plastic deformations. The unloading-reloading stiffness determines the behaviour for stress states below the highest stress state during previous louding. In this case the deformations will be purely elastic, although not necessarily linear-elastic. During unloading and reloading the soil is roughly three times as stiff as during primary loading, for which the two stiffness parameters are approximately the same.

Other than for the Mohr-Coulomb model, the stiffness parameters are not used directly but instead are used as input to calculate the stiffness for the given stress-state. The relation between stress and stiffness is given by

$$E = E^{ref} \left(\frac{c \cdot \cos \phi - \sigma_3^{'}}{c \cdot \cos \phi + p^{ref}} \right)^m \tag{3.8}$$

where σ_3 is the principal stress with the smallest magnitude, p^{ref} is a reference pressure usually chosen as 100 kPa and m is a coefficient determining the shape of the stress-stiffness curve. For clays m is approximately equal to 1 while for sands m will be around 0.5. When m is chosen equal to zero the stiffness will be constant and independent of the stress state, resulting in a linear-elastic soil.

Hyperbolic Stress-strain Curve

The Hardening Soil model uses a hyperbolic stress-strain curve based on the hyperbolic model developed by Duncan and Chang (1970). This curve is given by

$$\epsilon_1 = \frac{1}{E_0} \frac{q}{1 - q/q_a} \tag{3.9}$$

with

$$E_0 = \frac{2 \cdot E_{50}}{2 - R_f} \tag{3.10}$$

$$q = |\sigma_1^{'} - \sigma_3^{'}| \tag{3.11}$$

$$q_a = \frac{q_f}{R_f} \tag{3.12}$$

$$q_f = \left(c \cdot \cot \phi - \sigma_3^{'} \right) \frac{2 \cdot \sin \phi}{1 - \sin \phi} \tag{3.13}$$

and R_f is a parameter determining the ratio between the failure shear stress q_f and the assymptotic shear stress q_a. Figure 3.1 shows the hyperbolic stress-strain curve with R_f equal to 0.9 and E_0 equal to the value of E used in the Mohr-Coulomb curve.

3.1.3 Comparison of the Models

In order to find out which of the two models is able to give the most realistic results the models have to be compared to experimental test results. The results of several experimental load tests on suction caissons can be found in literature (Byrne, 2000; Villalobos, 2006; Zhang et al., 2007; Larsen, 2008). These tests are all performed on a small scale in laboratories, with caisson diameters ranging from 50 (Villalobos) to 300 mm (Larsen). A comparison between experiments on laboratory and prototype scale shows that these results scale without significant errors however (Kelly et al., 2006).

The load-displacement curves that are found in the aforementioned tests all closely resemble a hyperbolic curve, as well for vertical as for lateral and moment loading. This is in agreement with the load-displacement curves found in Plaxis using the Mohr-Coulomb and Hardening Soil model, which are shown in Figure 3.2 to 3.4. The curves are found by applying unidirectional loads at the topplate of the 7x7 caisson embedded in a soil modelled with one of the two models. The value of E_{50}^{ref} for a reference pressure of 100 kPa used in the Hardening Soil model is equal to the Young's Modulus used in the Mohr-Coulomb model, which is 156 MPa. m Is chosen as 0.5 in the Hardening Soil model. The soil is unsaturated with an effective weight of 16 $^{kN}/_{m^3}$, Poisson's ratio of 0.3, ϕ equal to 25°, ψ equal to 5° and no cohesion.

It can be seen that the curves for a lateral load and overturning moment are nearly identical. The Mohr-Coulomb model is clearly also able to produce a realistic load curve for the caisson, even if the stress-strain curve for individual elements is bilinear. The tangent stiffnesses of the two curves are also almost the same, as a result of the similar stress states. The vertical effective stress, which will be the minor stress direction for lateral loads, is equal to 7·16 = 112 kPa at the foundation base level, which is close to the reference pressure of 100 kPa. Therefore the stiffness of the soil in the Hardening Soil model will be close to E_{50}^{ref} and to the soil stiffness for the Mohr-Coulomb model.

The vertical load-displacement curve shows a clear difference between the models however. The displacements in the Mohr-Coulomb model are up to 50% larger than the displacements in the Hardening soil model. This will most likely be the result of the fact that the applied vertical load increases the effective stresses in the soil, which leads to an increasing soil stiffness in the Hardening Soil model but not in the Mohr-Coulomb model.

Furthermore the shape of the curves is also different. The Hardening Soil model gives a fluent curve, whereas the curve for the Mohr-Coulomb model shows three separate linear sections with small transition zones in between. This suggests that the zones with elements that violate the Mohr-Coulomb criterion do not increase gradually but instead remain constant in size until a certain treshold load is applied, after which there is a sudden increase of the plastic zones.

Figure 3.2 also shows how well the load-displacement curves found in Plaxis match with the hyperbolic curve fits given in Equation 3.14. Byrne (2000) shows that this curve gives a good correspondence with his experiments. Since the values of the coefficients are dependent on the soil parameters as well as the dimensions of the caisson, it is not possible to directly compare the experimental results with the numerical calculations. Instead curve fits of the hyperbolic curve to the Plaxis results for the two models have been determined in order to see how well these curves match the Plaxis calculations.

$$u_z = u_z^e + u_z^p \tag{3.14}$$

$$u_z^e = \frac{F_z}{k_{el}} \tag{3.15}$$

$$u_z^p = \frac{F_z \cdot (c_{ult} - (2 - s) \cdot F_z)}{k_{pl} \cdot (c_{ult} - F_z)} \tag{3.16}$$

The values of the coefficients found for the curve fits are given in Table 3.1. It can be seen in Figure 3.2 that the load-displacement curve found in Plaxis matches very well with the hyperbolic curve suggested by Byrne. This makes sense since the individual soil elements are also based on a hyperbolic load-displacement curve in the Hardening Soil model.

Table 3.1: *Coefficients found for the curve fits to the Mohr-Coulomb and Hardening Soil model*

Coefficient	Value for MC model	Value for HS model
k_{el}	$2.0 \cdot 10^4$ kN/m	$3.4 \cdot 10^4$ kN/m
c_{ult}	$1.5 \cdot 10^4$ kN	$1.6 \cdot 10^4$ kN
s	2.1	2.0
k_{pl}	$5.2 \cdot 10^5$ kN/m	$2.6 \cdot 10^5$ kN/m
R^2	97.1%	99.6 %

The results for the Mohr-Coulomb model on the other hand show significant deviations from the hyperbolic curve. As mentioned before the curve found in Plaxis is clearly not a smooth hyperbola. This is confirmed by the values of R^2 for the two fits, which are also given in Table 3.1. For the Hardening Soil model a value of 99.6 % is found, while the value for the Mohr-Coulomb model is only 97.1 %. Based on these results it can be concluded that the Hardening Soil model gives results that show a better agreement with the actual behaviour of suction caissons than the Mohr-Coulomb model. Therefore the Hardening Soil model will be used for the development of the non-linear springs.

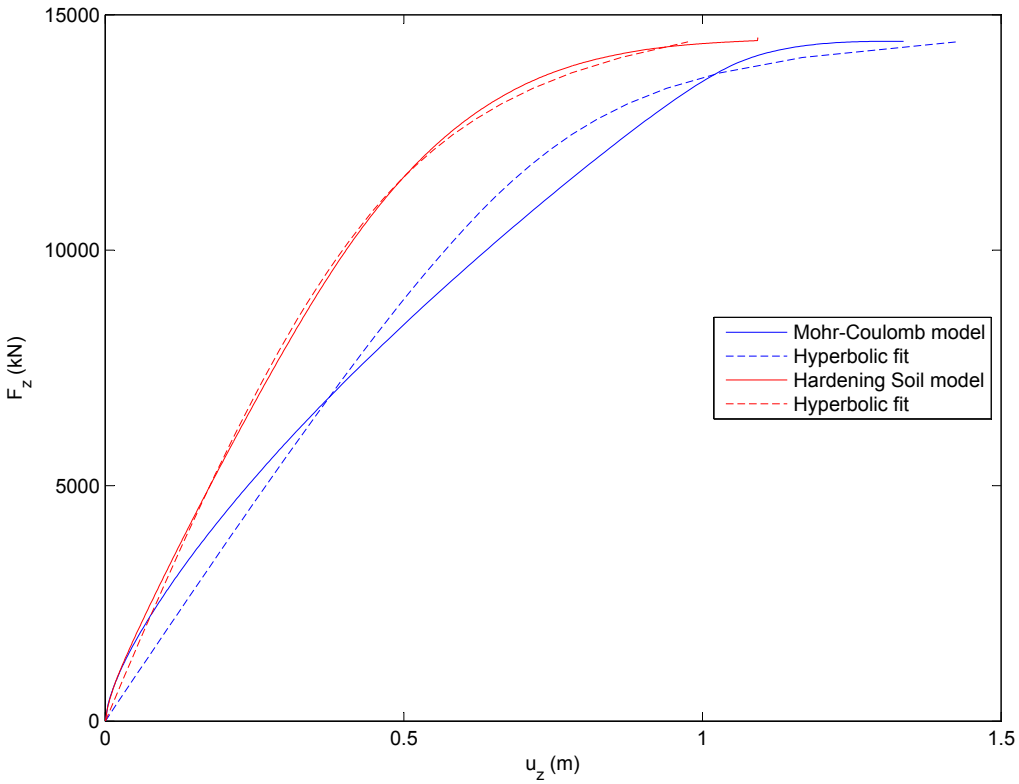

Figure 3.2: *Comparison of the load-displacement curves for a vertical load*

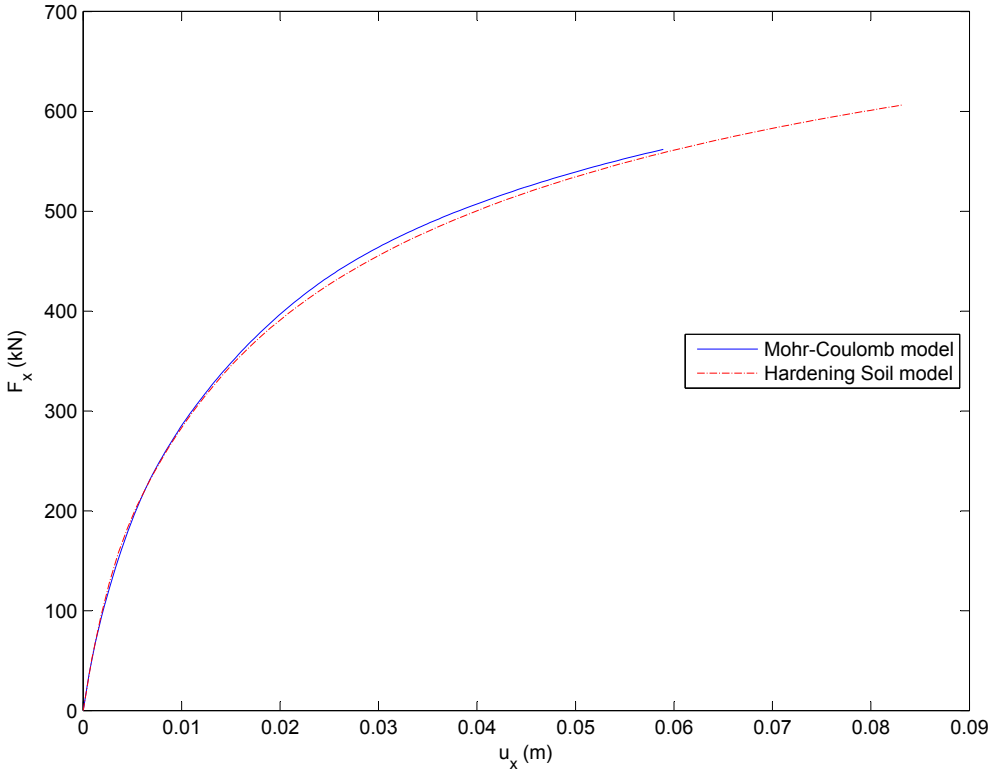

Figure 3.3: *Comparison of the load-displacement curves for a lateral load*

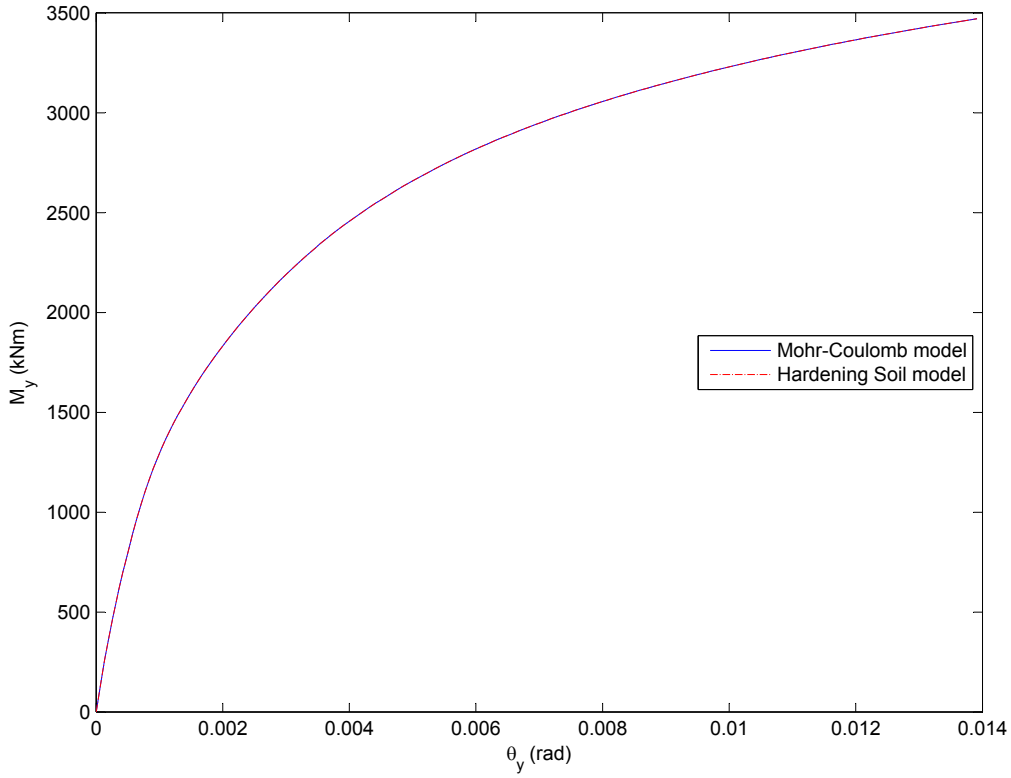

Figure 3.4: *Comparison of the load-displacement curves for an overturning moment*

3.2 Determination of the Load-Displacement Curves in Plaxis

For the determination of the load-displacement curves, the same soil based on the hardening soil model has been used as discussed in the previous section. Since all loads other than the dead weight of the structure will last for only a few seconds the soil will most likely behave undrained, even if it is sandy. Therefore the soil has been modelled as undrained. The same caisson of 7 meter diameter and 7 meter length is also used.

Since it is not possible to use a stiffness matrix for non-linear soil behaviour, the coupling between lateral load and overturning moments cannot be included in the model. Therefore the springs have to be applied at the centre of rotation, meaning that the load-displacement curves have to be determined at the centre of rotation as well. This requires the centre of rotation to be a fixed point however, which is in contrast to a linear-elastic material not necessarily the case for a non-linear soil material. The centre of rotation might shift up or down when the magnitude of the applied load increases. In order to check whether the location of the centre of rotation changes significantly when a larger load is applied the centre of rotation has been determined as a function of the applied load. The result is plotted against the applied overturning moment and the occuring roation in Figure 3.5. The average depth of the centre of rotation determined for the second curve is also plotted.

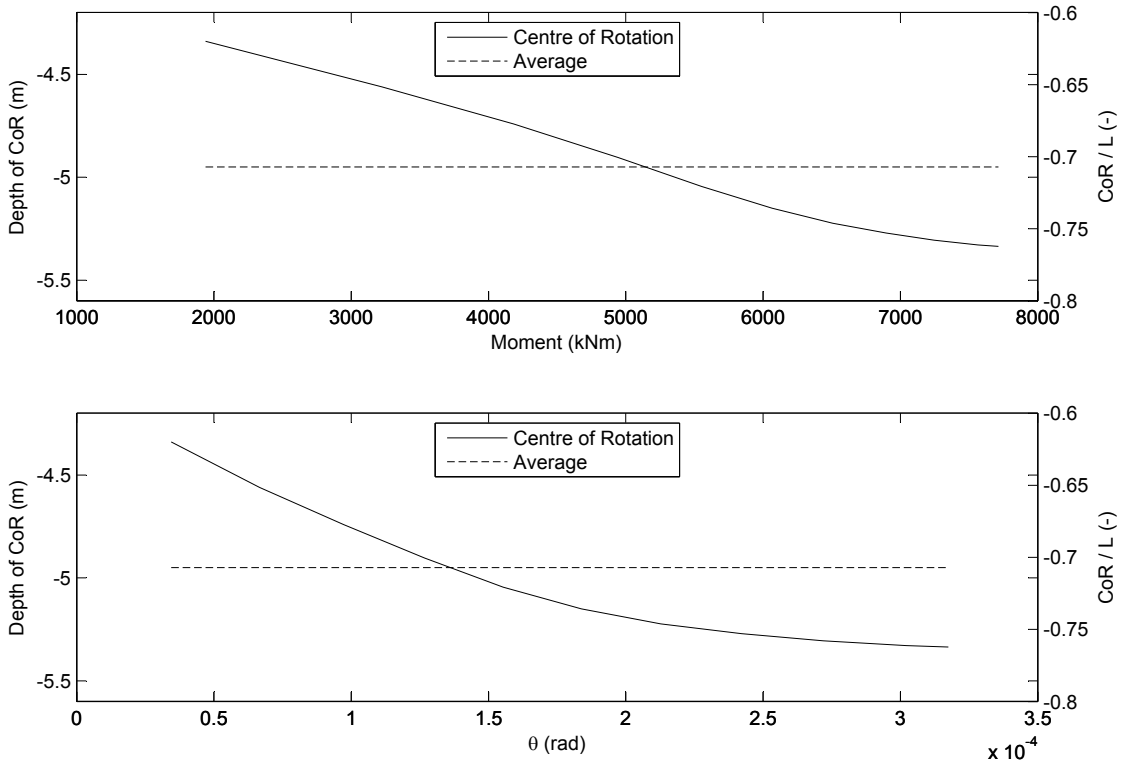

Figure 3.5: *Variation of the depth of the Centre of Rotation with the applied moment and rotation angle*

The location of the centre of rotation has been determined by applying a couple of two opposed vertical loads on two opposite points on the edge of the top plate and determining

the horizontal and vertical displacements for these two points as a result of the load. The difference between the vertical displacements of the two points divided by the diameter of the caisson gives the rotation of the caisson. The horizontal displacement, which is nearly identical at the two points, can then be divided by the rotation to find the position of the centre of rotation.

As can be seen in Figure 3.5, the centre of rotation is initially located at a depth of 4.3 m below mudline and then drops to a depth of 5.3 m for loads close to the capacity. The average depth integrated over the rotation is 4.95 m or 0.71 L. This means that at failure the difference between the actual centre of rotation and the average one is 0.4 m, or 6% of the embedment L.. Since the caisson will not be loaded to full capacity because of the applied safety factors the error will most likely be smaller for realistic load cases. Therefore the fluctuation of the centre of rotation around the average value is considered small enough to model the centre of rotation as a fixed point. Whether this will give accurate results can only be evaluated by comparison to FEM calculations however.

The load-displacement curves have thus been determined at a depth of 4.95 meter below mudline. A lateral load, vertical load, overturning moment have been applied at 4 points along the caisson wall and the displacements have been determined. The results are given in Figure 3.6.

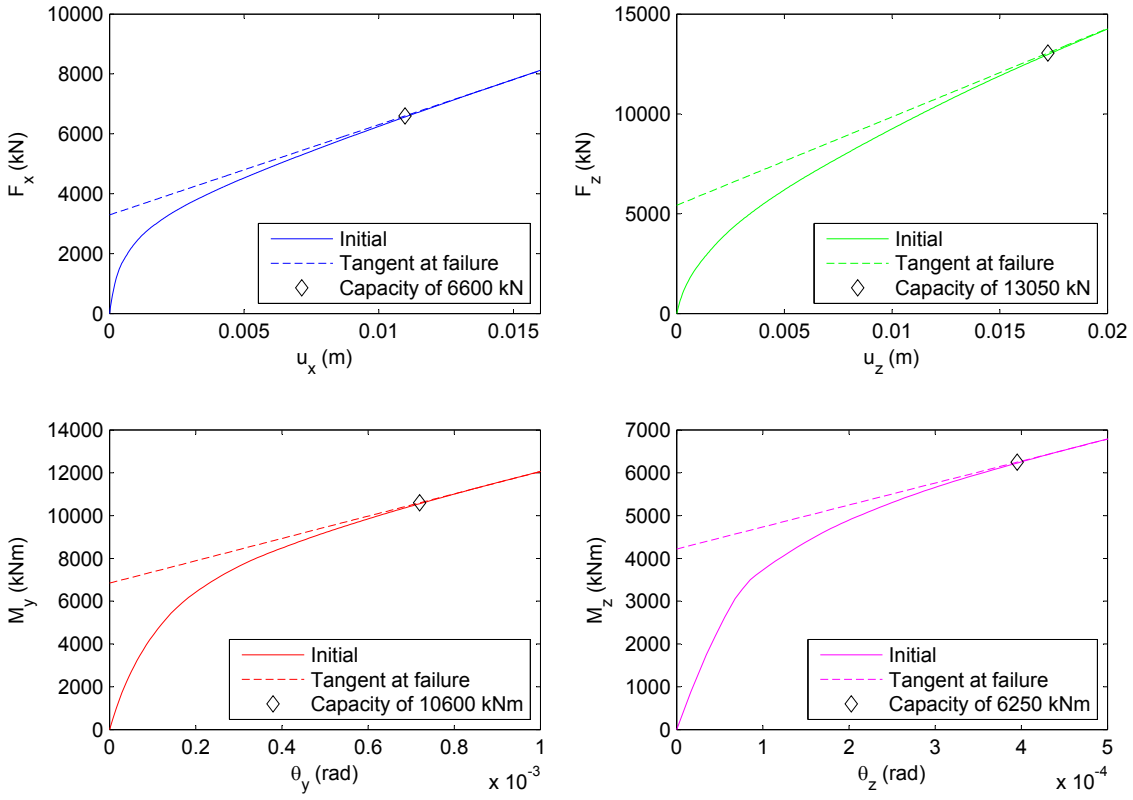

Figure 3.6: *Load-displacement curves for unidirectional loading*

Based on the load-displacement curves the failure loads have also been determined. The curves do not show a clear failure load that is approached asymptotically, but instead the stiffness decreases to a constant positive value, since the dilatancy of the soil leads

to decreasing pore pressures and hence increasing effective stresses and capacity for large shear strains (Gennaro et al., 2004). Therefore the point of failure has been defined as the load for which the inclination of the load-displacement curve becomes constant, as suggested by Meyerhof and Sastry (1985).

Figure 3.6 gives the load-displacement curves in the case of unidirectional loading. The load-displacement curve for one degree of freedom will however be dependent on the loads applied in other load directions since the level of plasticity will depend on the three-dimensional stress state, see for instance Equation 3.4 and 3.9. Therefore the true behaviour of the foundation can only be found when the load-displacement curves are determined for the actual loading conditions. This can be done by defining a model with a three-dimensional yield surface and hardening rule, as developed for instance for spudcan footings by Martin and Houlsby (2001). They define a yield surface given by

$$f(V,M,H) = \left[\left(\frac{M}{M_0}\right)^2 + \left(\frac{H}{H_0}\right)^2 - 2\bar{e}\left(\frac{M}{M_0}\right)\left(\frac{H}{H_0}\right)\right]^{1/2\beta_2} - \bar{\beta}^{1/\beta_2}\left(\frac{V}{V_0}\right)^{\beta_1/\beta_2}\left(1-\frac{V}{V_0}\right) \tag{3.17}$$

together with an associated flow rule. Plastic deformations in the vertical direction then lead to an increase of V_0 which extends the yield surface. The stiffness for loading in one direction now depends on whether the load condition is located on the yield surface and if so, at which location. Thereby it depends on the total stress-state and the influence of combined loading can be included.

The yield surface given by Martin and Houlsby results in ellipsoid which is confined by the origin and the vertical capacity V_0. There is no uplift capacity. As such it is similar to a yield surface for suction caissons in drained cohesionless soil. For undrained conditions the vertical capacity will be roughly identical in tension and compression (Watson and Randolph, 1997), resulting in a yield surface as suggested by for instance Bransby and Randolph (1998):

$$\left(\frac{V}{V_0}\right)^2 + \sqrt{\left(\frac{M}{M_0}\right)^{2.5} + \left(\frac{H}{H_0}\right)^5} - 1 = 0 \tag{3.18}$$

It is however not possible to include a method like this in the current installment of SACS. Therefore it should be investigated to what extent the stiffness is influenced by the loading in other directions. If the influence is small, the error that is introduced by using only a single curve might be acceptable. To find out if this is indeed the case the load-displacement curves have been determined again, but now for cases where the caisson has already been loaded with various loading levels in other directions. For each load direction the caisson has been preloaded with 25, 50 and 75% of the capacities in other load directions, which have been determined in Figure 3.6. The resulting load-displacement curves are given together with the initial curves without any preloading in Figure 3.7.

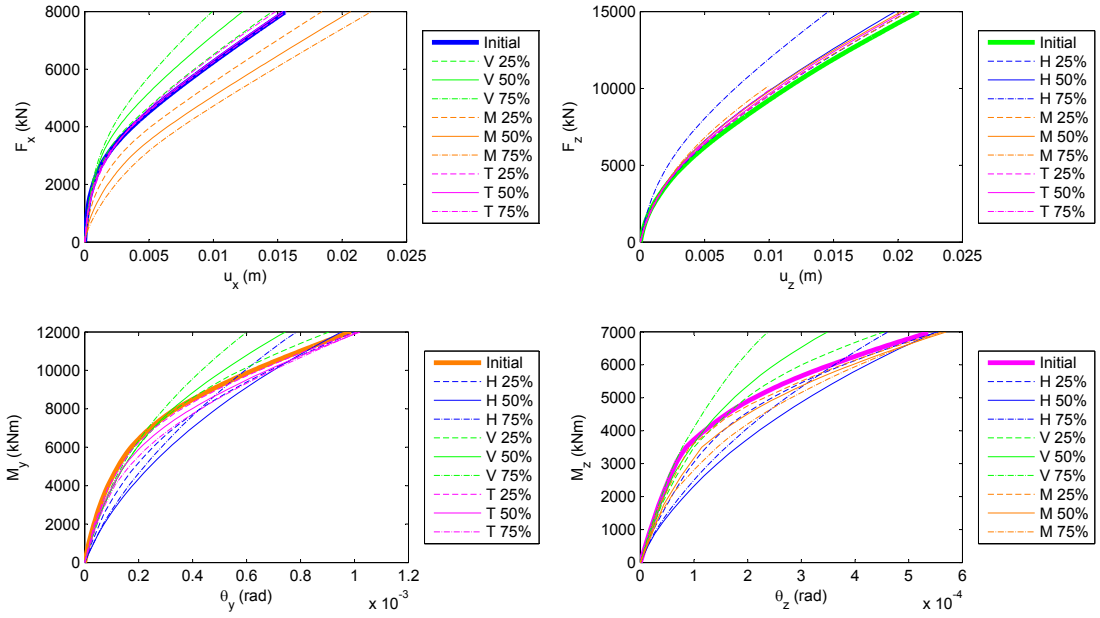

Figure 3.7: *Load-displacement curves for combined loading*

It can be seen that the influence of loading in other directions is significant: the resulting displacements and initial stiffnesses vary up to a factor 2. For the load-displacement curves for lateral loading preloading with a vertical load increases the stiffness, while preloading with an overturning moment leads to a decreasing stiffness. The influence of torsional loading is negligible. This is because a vertical load leads to an increase of the effective stresses, which in the Hardening Soil model leads to an increase of the Youngs modulus as given in Equation 3.8. Preloading with an overturning moment on the other hand leads to lateral displacements, which means the load-displacement curve is already in the plastic regime when the lateral loading starts and the stiffness decreases consequently. Since for realistic load cases both the vertical load and the overturning moment are large compared to the applied lateral load, see for instance Table 2.2, the stiffening effect of the vertical load and the slackening effect of the overturning moment could cancel out each other, in which case the initial load-displacement curve could be used without introducing significant inaccuracies in the results.

The vertical stiffness is influenced less by loading in other directions than the lateral stiffness. Applying a torsional or overturning moment load has little influence on the load-displacement curve, although it does lead to a slight increase of the vertical stiffness. In the case of the overturning moment this is because the caisson will be rotated slightly from the upright position, which means that the shaft is no longer positioned parallel to the displacement direction and will this give a larger resistance against deformations, which leads to a stiffer overall behaviour of the caisson. When a torsional moment is applied this leads to shear stresses along the caisson shaft, which in turn lead to an increase of the lateral stresses along the shaft and thus to an increase of the Youngs modulus. This results in a stiffer behaviour of the shaft when the vertical load is applied. The only loading that has a significant influence on the vertical stiffness is a lateral load. When a lateral load with a magnitude of 75% of the lateral capacity is applied this leads to a loosening of the soil in the active wedge and a strengthening of the soil at the passive

side of the caisson. This asymmetric soil state leads to a rotation of the caisson when a vertical load is applied: the caisson will settle more on the active than on the passive side. Similar to preloading with an overturning moment, this rotation leads to an increase of the vertical stiffness that can reduce the vertical settlement by 30%, but also results an increase of the horizontal displacements.

The rotational stiffnesses for an overturning moment and torsional load show the same behaviour for combined loading. Similarly to the lateral stiffness, preloading with a vertical load leads to a stiffer behaviour of the caisson because of the increased effective stresses, especially for large loads. Applying a moment in another direction leads to a decrease of the stiffness of 30 to 40% around half the capacity, while the stiffness for smaller and larger loads is not influenced significantly. Preloading with a lateral load also results in a less stiff load-displacement relation for most of the load range, while for loads near the capacity the foundation behaves just as stiff or slightly stiffer than without preloading. It is unclear what causes this behaviour.

All in all the influence of combined loading on the individual load-displacement curves is significant. Since loading on other directions can lead to both stiffer and less stiff behaviour the overall effect for a real load case might be limited. The exception is the vertical stiffness, which only increases as a result of other loading. Apart from for large lateral loads the vertical stiffness is not influenced significantly however.

Another issue that one would expect to see in the results is a change of the capacity. As Equation 3.17 and 3.7 show the capacity for loading in one direction will reduce when loads in other directions are applied simultaneously. This is mainly the case in 2D (Bransby and Randolph, 1998), which is why the torsional load is excluded from the curves. Especially lateral and overturning moment loading reduce each others capacity. This effect cannot be clearly observed in the curves in Figure 3.7 however, apart from the lateral capacity that is reduced by up to 30% when an overturning moment is applied. Why this effect is not seen in the relations between vertical and lateral or moment loading is not clear.

Finally it is interesting to compare the capacities and curves of Figure 3.6 and 3.7 to the loads for a realistic load case, for instance the loads found for a design state given in Table 2.2. This comparison is not entirely equitable since the caisson used to determine the load-displacement curves together with the soil parameters used in the Hardening Soil model was not specifically designed for the given load case. However the ratio between the capacities and the maximum loads is approximately 3 for the vertical load and overturning moment, which is a reasonable factor of safety given that a value of 2 is commonly used for deepwater suction anchors (Clukey et al., 2000), and the loading for the various degrees of freedom can at least be compared proportionally.

It can be seen that for the given loads the vertical load-displacement curve is showing significant plastic deformations: for a vertical load of 4000 kN the vertical displacement is rougly twice as large as would be expected based on the initial stiffness. The lateral load and overturning moment curves do not deviate significantly from the initial stiffness for 1100 kN and 2500 kNm respectively, and the torsional stiffness is still in the linear-elastic range for a torsional moment of 600 kNm. Therefore the torsional stiffness can be modelled by a linear spring without introducing any inaccuracy. For the other degrees of freedom non-linear springs will be used, but no large deviations from the results for linear springs are expected.

3.3 Application of the Non-Linear Springs in SACS

3.3.1 Model for a Single Caisson

Non-linear springs can be modelled in SACS by means of force-deflection gap elements. These are elements for which an axial load-elongation curve can be defined (Bentley, 2012). The curve is defined by a set of points, in between which linear interpolation is used. For all load directions other than the axial one the deformations are calculated using the standard linear Timoshenko beam theory. Since the springs are only 1-dimensional multiple springs are needed to model the six degrees of freedom of the foundation. It is also not possible to create coupling springs between the various degrees of freedom, which means that the springs have to be applied at the centre of rotation.

A simple model for a suction caisson that only uses non-linear springs for the translational degrees of freedom and a stiffness matrix for the rotational degrees of freedom is shown in Figure 3.8. The model consists of three non-linear springs, one for each translational degree of freedom, and three linear rotational springs combined into one stiffness matrix. The non-linear springs are attached to each other at one end and to a fixed point at the other end. The supports of the springs are limited-movement bearings that restrain the fixed end of the spring for axial and rotational deformations but allow the spring to move freely in the lateral directions. This way the springs do not restrain any elongation or shortening of the other two translational springs. The point where the three springs meet is connected to the centre of rotation by a short rigid stub that has a hinged connection at one end to make sure that the non-linear springs will not carry any moment loads.

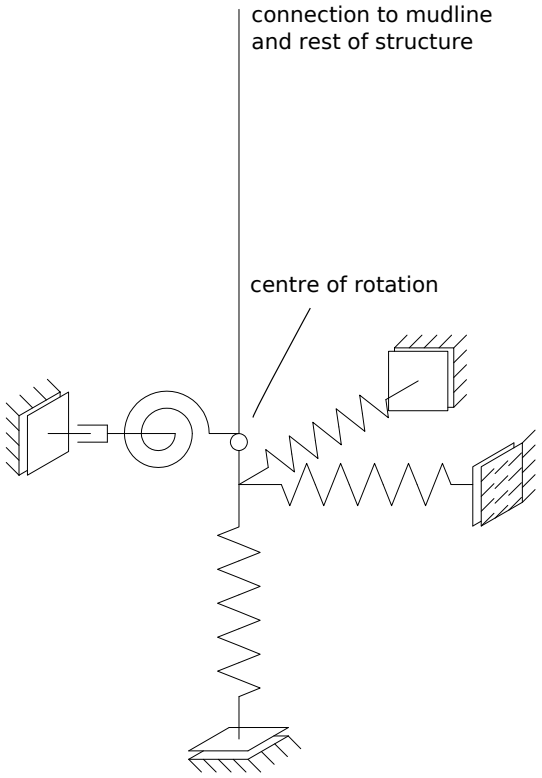

Figure 3.8: *Diagram for a suction caisson with non-linear translational springs*

The rotational springs are connected directly to the centre of rotation on one end and fixed on the other end. The applied stiffness matrix does not provide any resistance against translations, which is represented by the telescopic connection and limited-movement bearing in Figure 3.8. This way a separation of the loads is created: all forces acting on the centre of rotation will be carried by the non-linear springs while all moments will be carried by the linear rotational springs.

This model can be extended further to also include non-linear moment-rotation behaviour. The rotational springs can be modelled by a couple of two axial non-linear springs placed at a certain distance and connected by a rigid beam. This is shown in Figure 3.9, where

the two springs for the overturning moments are also non-linear. The beam connecting the rotational springs is connected to the centre of rotation by a stub that can only transfer bending moments and no translation or torsion. The torsional spring, not shown in Figure 3.9, is still linear and modelled by a stiffness matrix that is attached to the centre of rotation in the same manner as in Figure 3.8. It can also be modelled by a non-linear spring in the same manner as the rotational springs for overturning moments, but as discussed in Section 3.2 a non-linear spring is not needed for the torsional degree of freedom since the applied loads will still be in the linear-elastic range.

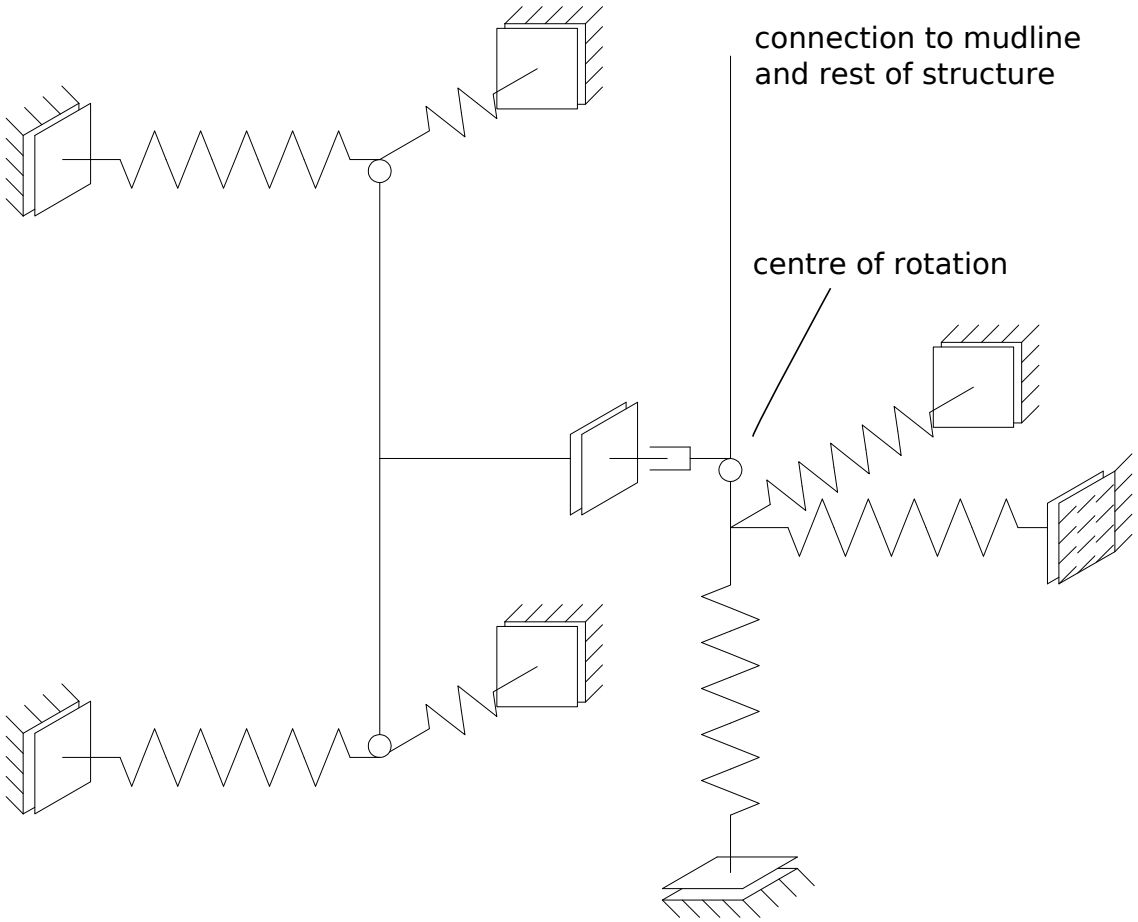

Figure 3.9: *Diagram for a suction caisson with non-linear translational and rotational springs*

Limitations of the Model

As mentioned before the position of the centre of rotation is assumed to be fixed in the model, which is not the case for non-linear soil behaviour as Figure 3.5 shows. This will lead to inaccuracies in the results. The interaction between loads in different directions is also not included in the model, which might lead to inaccuracies in the results.

Another issue is that while the applied springs are non-linear, they are still elastic and as such do not account for permanent deformations of the soil due to plasticity. The model is developed mainly for the evaluation of ultimate load conditions, which will most

likely result in loads that are higher than any of the loads applied before the ultimate load event and thus result in primary loading, which is uneffected by any previous plastic deformations. Still initial deformations might influence the final load distribution, which is something that needs to be investigated in more detail.

The change in stiffness as a result of cyclic loading is also not incorporated in the model. Various methods have been developed that can include the effects of cyclic loading (Dekker, 2013), however it is not possible to apply these models in SACS. Since the ultimate load cases will generally result in only a few load cycles during the life time of the offshore structure the effects of cyclic degradation will most likely be small, however further research on this topic is also required before any conclusions can be drawn.

3.3.2 Alternative Model

The model can be simplified by combining the lateral and rotational stiffness into one set of springs. The principle of this model is shown in Figure 3.10. For each lateral direction two springs are used, one at mudline and one at the depth around which the caisson will rotate when only a lateral load at mudline is applied. These two springs are connected by an infinitely stiff member. The model can be extended to include all 6 degrees of freedom by applying a vertical spring below the lower springs and a torsional spring at mudline.

When the caisson is now loaded by a lateral load applied at mudline the load will be carried by the upper spring, which will deform accordingly, while the lower spring is not loaded. Therefore the caisson will rotate around the lower end. The load-displacement curve for a lateral load applied at mudline can be used directly as input for the non-linear spring stiffness of the upper spring.

When an overturning moment is applied at mudline this will result in equal and opposite lateral loads on the two springs. When the stiffness of the lower lateral spring is related to the upper lateral spring by a factor of $l1/l2$ this will lead to a rotation around the centre of rotation. The model is thus able to give the correct behaviour for both lateral loads and overturning moments acting on the caisson. The rotational stiffness is also modelled correctly in the model, at least in the case of linear springs, as is proven in Appendix B. This is the case because the stiffnesses of the two springs are a combination of both translation and rotation and thus implicitly include the rotational stiffness as well.

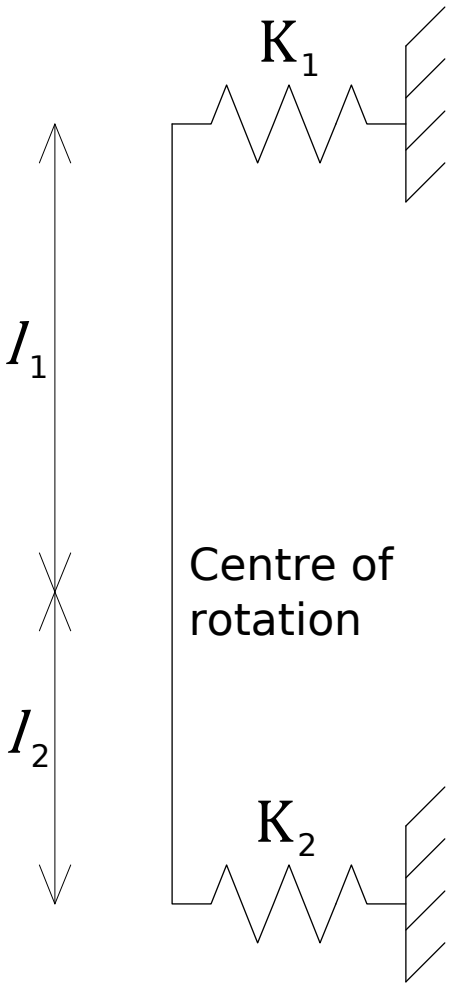

Figure 3.10: *Diagram for a foundation modelled with two translational springs*

Discussion of the Alternative Model

The disadvantage of this model is that the rotation point for a lateral load is assumed to be constant, which is not the case when the non-linearity of the soil is taken into account. This is the same problem as for the position of the centre of rotation in the other model. The centre of rotation for an overturning moment is also assumed to be constant in this model, although the position could be shifted depending on the load level by adjusting the stiffness curve of the lower spring.

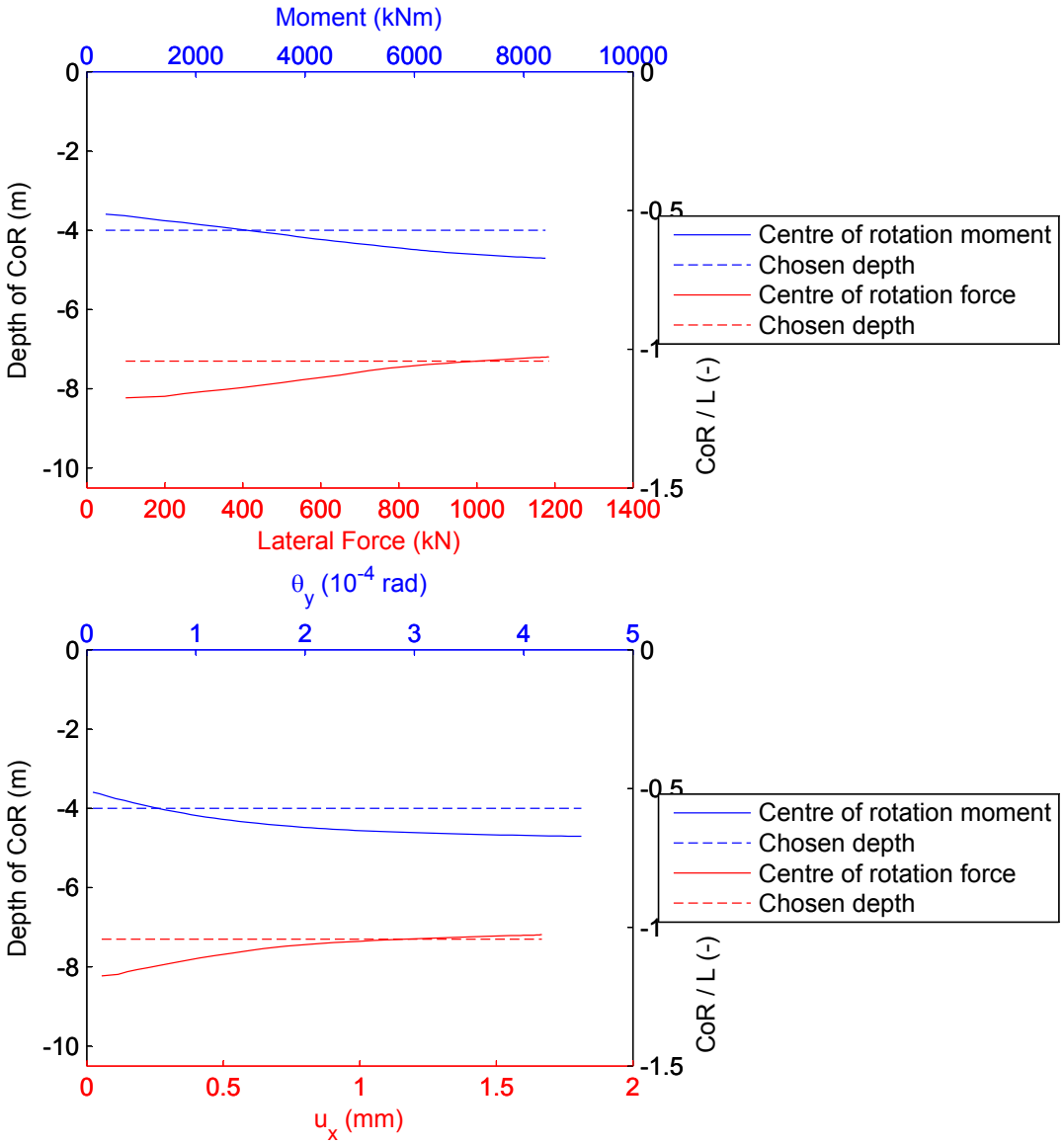

Figure 3.11: *Shifting of the rotation points for a lateral load and overturning moment*

Figure 3.11 shows how the rotation centres for overturning moment and lateral load shift with varying load levels and displacements for the 7 by 7 meter caisson with soil parameters as described for the Hardening Soil model in Section 3.1.3. It can be seen that both rotation centres shift approximately 1 meter or 14% of the caisson height over the

range of applied load levels. They shift in the opposite direction however: the moment centre of rotation shifts down with increasing load, will the centre of rotation for a lateral load moves upwards. This indicates that for large loads most of the soil resistance is provided by the deeper soil layers.

The fixed depths of the rotation centres chosen for the application of the model in SACS are indicated by dashed lines. The values have been chosen such that they correspond with load levels that are expected for a design load case. Based on Table 2.6 a lateral load of 1000 kN and an overturning moment of 3000 kNm are used as reference loads, leading to a centre of rotation for the overturning moment located at 4.0 meter depth or 0.57 L and a rotation point for a lateral load at a depth of 7.3 m or 1.04 L. Since the springs in this model are defined at mudline rather than at the centre of rotation the resulting overturning moment for a design load case will be smaller than for the other model, resulting in a different choice for the depth of the centre of rotation.

Since the rotation of the caisson as a result of an applied lateral load in this model is proportional to the inverse of the chosen distance from mudline to the rotation point for a lateral load, the relative error for the rotation due to a lateral load introduced by assuming a fixed rotation point can be determined in a straightforward way. For small lateral loads the rotation point will be located at a depth of 8.23 rather than 7.3 meter. This means that the rotation of the caisson will be overestimated by 13%. For high lateral loads however the rotation point for the lateral load shifts to a depth of 7.18 meter, which means the rotation will be underestimated by 2%. Since a higher stiffness will result in less redistribution of the load between the caissons and thus in a larger design load, this means that the model is incautious for small loads while cautious for large loads.

In case an overturning moment is applied it is less straightforward to determine whether the chosen locations of the rotation points lead to an over- or underestimate of the resulting rotations, since both the distance between the springs and the ratio between the stiffnesses of the two springs will vary in this case. In order to see how the stiffness is influenced by the choice of the two fixed rotations points a number of overturning moments has been chosen and the resulting rotation has been determined for the shifting rotation points corresponding to various load levels. First the load-displacement curve for the upper spring K_1, determined by applying a lateral load at the topplate of the caisson, has been discretized to a multilinear line consisting of 12 segments. Four loads from this curve have been picked and multiplied by the distance to the rotation point for a lateral load $(l_1 + l_2)$ to find the corresponding overturning moment. For each node on the curve the lateral load in the springs has been determined by dividing these moments by the distance to the rotation point for lateral loads corresponding to the node. The rotation is then found by dividing the deflection of the upper spring corresponding the the load by the distance to the centre of rotation for the node. The rotation for the fixed rotation points can also be found by dividing the deflection corresponding to the chosen load by the fixed distance to the centre of rotation. The resulting rotations are shown in Figure 3.12.

It can be seen that the chosen fixed rotation points lead to rotations that are consistently larger than the actual rotations. This is the case since the rotation points for lateral load and moment loading have been chosen for the loads that are expected on the caisson and do not correspond to the same load level. This leads to a combination that gives too large

rotations and hence a too low stiffness. Therefore the calculated rotations for the fixed roation points have also been reduced by 5.5%. The reduction can be achieved in the model by reducing all displacements in the load-displacement curves by 5.5%. This gives a a better match with the actual rotations, as the graphs show. In this case the difference between the actual and assumed rotations is less than 2% apart from for the unrealistic combination of high loads and rotation points corresponding to small loads. Reducing the displacements in the load-displacement curves will also lead to an increased stiffness for lateral loads however, so the curves should be adjusted such that both the behaviour for lateral loads and overturning moments is modelled accurately.

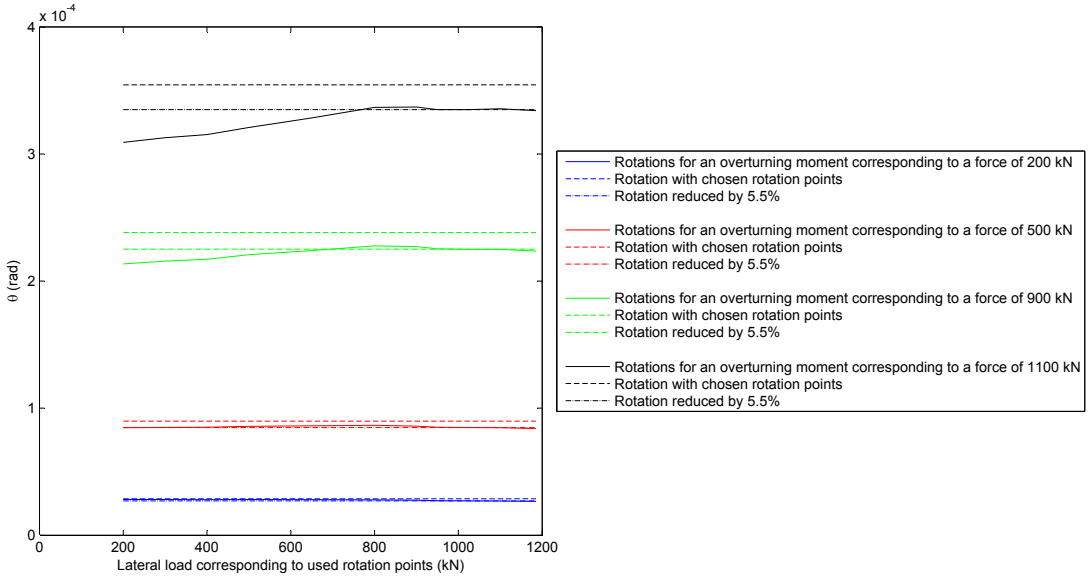

Figure 3.12: *Rotations as a result of various overturning moments for various depths of the rotation points*

Another issue of the model is the fact that the shapes of the load-displacement curves for lateral loads and overturning moments do not have exactly the same shape. Figure 3.6 shows that the ratio between initial stiffness and stiffness at maximum capacity is significantly smaller for the lateral stiffness than it is for the rotational stiffness. Since the applied springs are a combination of the two, this means that the rotational stiffness for large overturning moments will be overestimated.

On the other hand the model does include the effects of combined loading, in the sense that when the caisson is already loaded by an overturning moment, the springs will have deformed into the non-linear regime, meaning that the incremental stiffness of the springs decreases. When a lateral load is applied the lateral stiffness will thus be smaller than it would be if the caisson were unloaded. Whether the combined loading behaviour is modelled correctly this way will follow from the comparison to the Plaxis calculations.

Another advantage of the model is the very straightforward way of determining the spring stiffnesses. An additional FEM calculation is required to determine the position of the centre of rotation but otherwise it is sufficient to run a single calculation to determine the load-displacement curve for a lateral load.

3.3.3 Angle-Dependent Load-Displacement Behaviour

A problem with non-linear load-displacement relations is that when the forces and displacements are decomposed, for instance in components parallel to the x- and y-axes, the resulting load-displacement relationship will change. This is indicated in Figure 3.13.

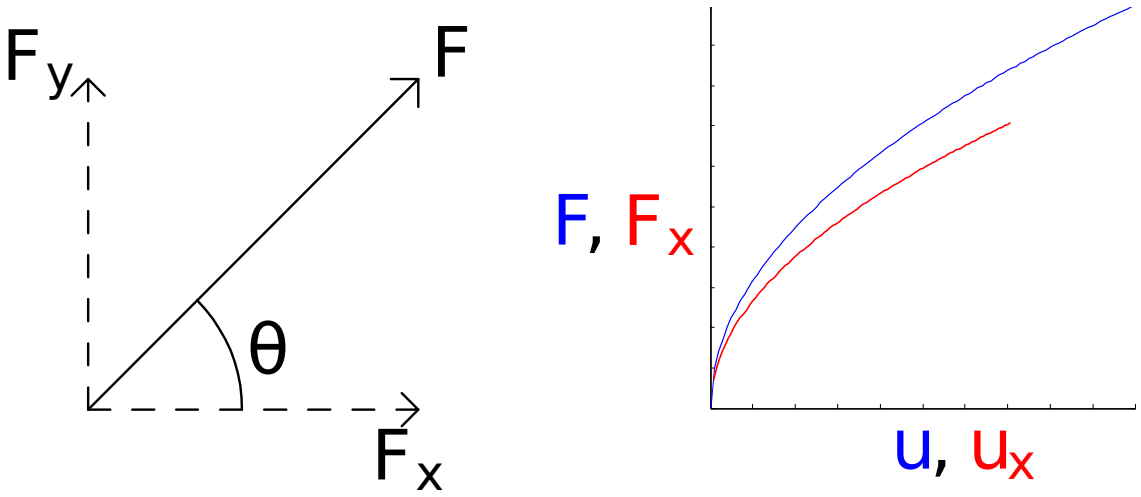

Figure 3.13: *Change of the load-displacement curve for a decomposed load*

For soil behaviour the load-displacement curve will generally become less stiff with increasing load. Thus, when the load-displacement curve for the total load would be used to find the displacements for the decomposed forces, which are smaller, the resulting displacements would be too small and the stiffness of the system would be overestimated. For a load parallel to one of the axes however there would be no decomposition and the used curve would give the correct deformations. This means the behaviour of the system would depend on the chosen orientation of the coordinate system, which is clearly incorrect. Therefore the decomposed load-displacement curves should be function of the angle θ between the applied load and the chosen x-axis:

$$F_x(u,\theta) = F(u) \cdot \cos\theta = F\left(\frac{u_x}{\cos\theta}\right) \cdot \cos\theta \tag{3.19}$$

$$F_y(u,\theta) = F(u) \cdot \sin\theta = F\left(\frac{u_y}{\sin\theta}\right) \cdot \sin\theta \tag{3.20}$$

Only for a linear spring it holds that $F\left(\frac{u_x}{\cos\theta}\right) \cdot \cos\theta = F(u_x)$, in all other cases ignoring the dependency on the load angle will lead to inaccuracies. Assuming for instance a load displacement curve defined by $F(u) = K \cdot \sqrt{u}$, which is a realistic shape for a non-linear load displacement curve, decomposing the load first and then using the uncorrected load-displacement curve to find the deformations overestimates the stiffness of the system by up to 19% for a load that makes a 45° angle with the x- and y- axes.

It is however not possible to make the load-displacement curve dependent on the load direction in SACS. Since the magnitude of the error is not too large, an alternative would be to reduce it to an acceptable range. This could be done by using multiple distributed springs along the circumference of the caisson axis. Instead of 2 springs with a spacing

of 90°, for instance 4 springs with a spacing of 45° could be used. A load parallel to the x-axis is now taken up by 3 springs instead of 1 and a load with an angle of 22.5° with the x-axis is taken up by 4 instead of 2 springs. This leads to a more constant load-displacement behaviour with respect to the load angle and thus smaller errors.

The downside of this method is however that which part of the load is carried by each of the springs will depend on the stiffness of the springs. Initially most of the load will be carried by the springs that are orientated the most parallel to the applied load, however when these springs reach the more non-linear part of their curve and behave less stiff the other springs, which are still in the more stiff regime, will take up a larger portion of the load. This makes it more difficult to choose the right spring stiffnesses for the desired load-displacement behaviour and also results in a too stiff behaviour of the foundation for large loads. Overall the inaccuracies depending on the load direction may reduce when multiple lateral springs are applied, but the method is dubious.

Therefore the multiple springs will not be used and instead the springs for the foundations will be orientated such that one set is parallel to the direction of the applied load. This way the error due to the angle of the structural response with the axes will be small as well. Since a jacket structure is usually positioned such that the governing load directions correspond with the broadside, end-on and diagonal direction of the jacket, the most suited orientations for the springs will for most cases also conveniently coincide with the global coordinate system.

3.4 Comparison with Plaxis Calculations

3.4.1 Comparison for a Single Caisson

The two models for a foundation with non-linear soil behaviour have been implemented in SACS using the code given in Appendix F.2 and compared to calculations in Plaxis to see how accurate the results from the model are. The springs used for the models are based on load-displacement curves determined in Plaxis, as shown for the first model in Figure 3.6, which have been discretized into 10 to 20 points such that they accurately describe the shape of the actual curves. The displacements for the load-displacement curves of the lower springs with stiffness K_2 in the second model are adjusted such compared to the values for K_1 that a rotation centre at a depth of 4.0 meter is established. A linear-elastic foundation based on the initial stiffness of the curves is also used in the comparison in order to assess the non-linearity of the system.

The comparison has first been made for a single caisson, so that the results are not distorted by pile-group effects. The caisson and surrounding soil, with dimensions and soil properties as described in Section 3.1.3, are modelled in Plaxis and SACS and loaded at mudline by various combinations of lateral load, vertical load and overturning moment, as given in Table 3.2. The overturning moments are applied in Plaxis by applying the lateral loads at different heights above the top plate on a rigid beam that is rigidly connected to the caisson. The displacements of the caisson as a result of these loads are given in Table 3.3.

Table 3.2: *Load combinations for the various load cases*

Load case	F_x (kN)	F_x (kN)	F_x (kN)	M_y (kN)
1	1000	-	-	-
2	1000	1000	-	-
3	1000	1000	-1000	-
4	1000	1000	-2000	-
5	1000	-	-	5000
6	500	-	-	5000
7	1000	-	-1000	5000
8	500	-	-500	5000

It can be seen that the correspondence between the Plaxis and SACS results is highly varying, ranging from differences of a few percent to a factor 3. The average agreement is significantly poorer than for the linear-elastic soil behaviour, for which the results are given in Table 2.3. The average difference between the Plaxis and SACS results is 35% for the first model and 45% for the second model, compared to 6.5% for the linear-elastic soil. The non-linear models are not significantly more accurate than the linear-elastic model applied for the non-linear soil behaviour, which gives an average difference with the Plaxis results of 45%.

The large differences seem to be mainly the result of the changing stiffness due to combined loading, which is not included in the SACS models. The resulting lateral translation and rotation for loadcases 6 and 8 for instance, which vary only with regard to the applied vertical load, differ by a factor 2 in the Plaxis calculations, while the SACS models predict the same lateral displacements for both load cases as the lateral load and overturning moment are identical. This cannot result in good results for both of the load cases. In this case especially the results for load case 8 show a very poor match with the Plaxis results and raise the average difference significantly.

Table 3.3: *Comparison of the displacements found for the various load cases*

Load Case	D.o.f.	Plaxis	Model 1	Model 2	LE Model
1	u_x (m)	$6.6{\cdot}10^{-4}$	$8.2{\cdot}10^{-4}$	$1.2{\cdot}10^{-3}$	$5.5{\cdot}10^{-4}$
	Difference	-	*23.4%*	*75.3%*	*-17.0%*
	u_z (m)	-	-	-	-
	Difference	-	-	-	-
	θ_y (rad)	$9.1{\cdot}10^{-5}$	$1.2{\cdot}10^{-4}$	$1.6{\cdot}10^{-4}$	$7.6{\cdot}10^{-5}$
	Difference	-	*34.8%*	*75.3%*	*-16.5%*
2	u_x (m)	$1.1{\cdot}10^{-3}$	$1.1{\cdot}10^{-3}$	$1.6{\cdot}10^{-3}$	$5.5{\cdot}10^{-4}$
	Difference	-	*-3.0%*	*41.7%*	*-51.6%*
	u_z (m)	-	-	-	-
	Difference	-	-	-	-
	θ_y (rad)	$1.7{\cdot}10^{-4}$	$1.8{\cdot}10^{-4}$	$2.2{\cdot}10^{-4}$	$7.6{\cdot}10^{-5}$
	Difference	-	*5.2%*	*32.3%*	*-54.5%*

Table 3.3: *(continued)*

Load Case	D.o.f.	Plaxis	Model 1	Model 2	LE Model
3	u_x (m)	$1.2{\cdot}10^{-3}$	$1.1{\cdot}10^{-3}$	$1.6\cdot10^{-3}$	$5.5{\cdot}10^{-4}$
	Difference	-	*-8.4%*	*33.9%*	*-54.3%*
	u_z (m)	$-4.0{\cdot}10^{-4}$	$-2.8{\cdot}10^{-4}$	$-2.8{\cdot}10^{-4}$	$-2.7{\cdot}10^{-4}$
	Difference	-	*-31.1%*	*-30.8%*	*-31.8%*
	θ_y (rad)	$1.8{\cdot}10^{-4}$	$1.8{\cdot}10^{-4}$	$2.2{\cdot}10^{-4}$	$7.6{\cdot}10^{-5}$
	Difference	-	*-2.1%*	*23.1%*	*-57.7%*
4	u_x (m)	$1.3{\cdot}10^{-3}$	$1.1{\cdot}10^{-3}$	$1.6{\cdot}10^{-3}$	$5.5{\cdot}10^{-4}$
	Difference	-	*-15.3%*	*23.7%*	*-57.7%*
	u_z (m)	$-7.6{\cdot}10^{-4}$	$-7.6{\cdot}10^{-4}$	$-7.7{\cdot}10^{-4}$	$-5.5{\cdot}10^{-4}$
	Difference	-	*-0.1%*	*0.2%*	*-28.3%*
	θ_y (rad)	$2.0{\cdot}10^{-4}$	$1.8{\cdot}10^{-4}$	$2.2{\cdot}10^{-4}$	$7.6{\cdot}10^{-4}$
	Difference	-	*-10.8%*	*12.2%*	*-61.4%*
5	u_x (m)	$2.9{\cdot}10^{-3}$	$3.3{\cdot}10^{-3}$	$3.0{\cdot}10^{-3}$	$9.3{\cdot}10^{-4}$
	Difference	-	*14.4%*	*3.7%*	*-68.0%*
	u_z (m)	-	-	-	-
	Difference	-	-	-	-
	θ_y (rad)	$4.6{\cdot}10^{-4}$	$6.3{\cdot}10^{-4}$	$4.8{\cdot}10^{-4}$	$1.5{\cdot}10^{-4}$
	Difference	-	*35.7%*	*3.6%*	*-67.1%*
6	u_x (m)	$1.1{\cdot}10^{-3}$	$1.5{\cdot}10^{-3}$	$1.7{\cdot}10^{-3}$	$6.5{\cdot}10^{-4}$
	Difference	-	*41.4%*	*52.2%*	*-40.0%*
	u_z (m)	-	-	-	-
	Difference	-	-	-	-
	θ_y (rad)	$1.8{\cdot}10^{-4}$	$2.9{\cdot}10^{-4}$	$2.9{\cdot}10^{-4}$	$1.1{\cdot}10^{-4}$
	Difference	-	*62.5%*	*62.3%*	*-36.8%*
7	u_x (m)	$2.9{\cdot}10^{-3}$	$3.3{\cdot}10^{-3}$	$3.0{\cdot}10^{-3}$	$9.3{\cdot}10^{-4}$
	Difference	-	*13.4%*	*2.8%*	*-68.2%*
	u_z (m)	$-4.6{\cdot}10^{-4}$	$-2.8{\cdot}10^{-4}$	$-2.8{\cdot}10^{-4}$	$-2.7{\cdot}10^{-4}$
	Difference	-	*-39.8%*	*-39.5%*	*-40.4%*
	θ_y (rad)	$4.7{\cdot}10^{-4}$	$6.3{\cdot}10^{-4}$	$4.8{\cdot}10^{-4}$	$1.5{\cdot}10^{-4}$
	Difference	-	*33.2%*	*1.6%*	*-67.7%*
8	u_x (m)	$5.7{\cdot}10^{-4}$	$1{,}5{\cdot}10^{-3}$	$1.7{\cdot}10^{-3}$	$6.5{\cdot}10^{-4}$
	Difference	-	*168.2%*	*188.6%*	*13.9%*
	u_z (m)	$-1.6{\cdot}10^{-4}$	$-1.4{\cdot}10^{-4}$	$-1.4{\cdot}10^{-4}$	$-1.4{\cdot}10^{-4}$
	Difference	-	*-14.9%*	*-14.5%*	*-15.7%*
	θ_y (rad)	$9.4{\cdot}10^{-5}$	$2.9{\cdot}10^{-4}$	$2.9{\cdot}10^{-4}$	$1.1{\cdot}10^{-4}$
	Difference	-	*214.5%*	*214.3%*	*22.4%*

3.4.2 Comparison for a Jacket Foundation

Although the displacements for a single caisson are clearly not estimated correctly by the two SACS models, they might be able to give better results with regard to the load distribution, as Table 2.4 and 2.5 show. Therefore the difference between Plaxis and SACS calculations will also be evaluated for the complete jacket substructure and foundation.

The same springs have been used in the SACS models as for the calculations on the single caisson. The same jacket substructure and load, a single lateral load of 2000 kN applied on leg 2 at the top frame, are used as for the linear-elastic soil. The jacket and the load are shown in Figure 2.10. The resulting loads on and displacements of each of the four caissons found in the Plaxis and SACS models are determined and compared in Table 3.4 and 3.5.

Table 3.4: *Comparison of foundation loads found in the SACS and Plaxis calculations*

Leg	D.o.f.	Plaxis	Model 1	Model 2	LE Model
1	F_x (kN)	384.9	363.0	363.2	382.7
	Difference	-	*6.0%*	*6.0%*	*0.6%*
	F_y (kN)	-172.4	-154.9	-166.5	-173.2
	Difference	-	*11.3%*	*3.5%*	*-0.5%*
	F_z (kN)	969.8	981.9	997.9	1016.5
	Difference	-	*-1.2%*	*-2.8%*	*-4.6%*
	M_x (kNm)	496.7	453.6	471.1	499.4
	Difference	-	*9.5%*	*5.4%*	*-0.5%*
	M_y (kNm)	997.9	939.3	930.4	998.3
	Difference	-	*6.2%*	*7.3%*	*0.0%*
	M_z (rad)	-	61.4	61.9	70.8
2	F_x (kN)	561.3	516.5	523.9	645.5
	Difference	-	*8.7%*	*7.1%*	*-13.0%*
	F_y (kN)	-184.1	-206.2	-202.0	-216.0
	Difference	-	*-10.7%*	*-8.8%*	*-14.7%*
	F_z (kN)	1331.3	1321.5	1308.0	1291.5
	Difference	-	*0.7%*	*1.8%*	*3.1%*
	M_x (kNm)	612.0	689.9	666.6	704.2
	Difference	-	*-11.3%*	*-8.2%*	*-13.1%*
	M_y (kNm)	1896.1	1730.9	1732.6	2005.9
	Difference	-	*9.5%*	*9.4%*	*-5.5%*
	M_z (rad)	-	-34.7	-32.0	-31.7

Table 3.4: *(continued)*

Leg	D.o.f.	Plaxis	Model 1	Model 2	LE Model
3	F_x (kN)	188.9	221.2	228.5	230.6
	Difference	-	*-14.6%*	*-17.3%*	*-18.1%*
	F_y (kN)	329.3	330.2	332.4	349.8
	Difference	-	*-0.3%*	*-0.9%*	*-5.9%*
	F_z (kN)	-972.9	-984.3	-999.9	-1018.0
	Difference	-	*-1.2%*	*-2.7%*	*-4.4%*
	M_x (kNm)	-737.9	-760.4	-751.9	-814.3
	Difference	-	*-3.0%*	*-1.9%*	*-9.4%*
	M_y (kNm)	563.1	667.1	674.3	696.7
	Difference	-	*-15.6%*	*-16.5%*	*-19.2%*
	M_z (rad)	-	105.5	108.3	114.4
4	F_x (kN)	864.9	899.3	884.4	741.2
	Difference	-	*-3.8%*	*-2.2%*	*16.7%*
	F_y (kN)	27.2	30.9	36.1	39.4
	Difference	-	*-12.1%*	*-24.7%*	*-31.0%*
	F_z (kN)	-1328.2	-1319.1	-1306.0	-1290.1
	Difference	-	*0.7%*	*1.7%*	*3.0%*
	M_x (kNm)	-298.8	-328.7	-339.8	-355.9
	Difference	-	*-9.1%*	*-12.1%*	*-16.1%*
	M_y (kNm)	2031.3	2133.4	2042.6	1630.7
	Difference	-	*-4.8%*	*-0.6%*	*24.6%*
	M_z (rad)	-	5.0	9.1	26.2

Table 3.5: *Comparison of foundation displacements found in the SACS and Plaxis calculations*

Leg	D.o.f.	Plaxis	Model 1	Model 2	LE Model
1	u_x (m)	$2.3{\cdot}10^{-4}$	$3.2{\cdot}10^{-4}$	$3.5{\cdot}10^{-4}$	$2.6{\cdot}10^{-4}$
	Difference	-	*37.4%*	*51.9%*	*12.6%*
	u_y (m)	$-1.2{\cdot}10^{-4}$	$-1.3{\cdot}10^{-4}$	$-1.3{\cdot}10^{-4}$	$-1.1{\cdot}10^{-4}$
	Difference	-	*7.5%*	*13.5%*	*-4.8%*
	u_z (m)	$1.4{\cdot}10^{-4}$	$2.7{\cdot}10^{-4}$	$2.8{\cdot}10^{-4}$	$2.6{\cdot}10^{-4}$
	Difference	-	*96.1%*	*99.2%*	*84.9%*
	θ_x (rad)	$1.7{\cdot}10^{-5}$	$2.0{\cdot}10^{-5}$	$2.2{\cdot}10^{-5}$	$1.7{\cdot}10^{-5}$
	Difference	-	*15.8%*	*29.7%*	*0.6%*
	θ_y (rad)	$3.7{\cdot}10^{-5}$	$5.2{\cdot}10^{-5}$	$5.7{\cdot}10^{-5}$	$4.1{\cdot}10^{-5}$
	Difference	-	*39.0%*	*52.4%*	*8.6%*
	θ_z (rad)	$4.7{\cdot}10^{-7}$	$1.2{\cdot}10^{-6}$	$1.3{\cdot}10^{-6}$	$1.1{\cdot}10^{-6}$
	Difference	-	*156.3%*	*177.6%*	*134.9%*

Table 3.5: *(continued)*

Leg	D.o.f.	Plaxis	Model 1	Model 2	LE Model
2	u_x (m)	$5.5{\cdot}10^{-4}$	$5.3{\cdot}10^{-4}$	$7.0{\cdot}10^{-4}$	$3.1{\cdot}10^{-4}$
	Difference	-	*-2.3%*	*28.1%*	*-42.4%*
	u_y (m)	$-1.9{\cdot}10^{-4}$	$-1.7{\cdot}10^{-4}$	$-1.8{\cdot}10^{-4}$	$-1.5{\cdot}10^{-4}$
	Difference	-	*-8.3%*	*-1.2%*	*-22.2%*
	u_z (m)	$2.2{\cdot}10^{-4}$	$4.2{\cdot}10^{-4}$	$4.2{\cdot}10^{-4}$	$3.7{\cdot}10^{-4}$
	Difference	-	*95.8%*	*93.9%*	*72.9%*
	θ_x (rad)	$2.9{\cdot}10^{-5}$	$2.8{\cdot}10^{-5}$	$3.1{\cdot}10^{-5}$	$2.3{\cdot}10^{-5}$
	Difference	-	*-4.0%*	*8.8%*	*-19.9%*
	θ_y (rad)	$8.7{\cdot}10^{-5}$	$9.1{\cdot}10^{-5}$	$1.1{\cdot}10^{-4}$	$5.1{\cdot}10^{-5}$
	Difference	-	*3.9%*	*28.1%*	*-42.3%*
	θ_z (rad)	$-1.6{\cdot}10^{-7}$	$-7.0{\cdot}10^{-7}$	$-6.0{\cdot}10^{-7}$	$-8.0{\cdot}10^{-7}$
	Difference	-	*332.1%*	*270.4%*	*393.9%*
3	u_x (m)	$1.7{\cdot}10^{-4}$	$1.8{\cdot}10^{-4}$	$2.0{\cdot}10^{-4}$	$1.5{\cdot}10^{-4}$
	Difference	-	*7.4%*	*17.9%*	*-10.0%*
	u_y (m)	$3.2{\cdot}10^{-4}$	$2.7{\cdot}10^{-4}$	$3.0{\cdot}10^{-4}$	$2.3{\cdot}10^{-4}$
	Difference	-	*-13.3%*	*-4.8%*	*-27.2%*
	u_z (m)	$-2.7{\cdot}10^{-4}$	$-2.7{\cdot}10^{-4}$	$-2.8{\cdot}10^{-4}$	$-2.6{\cdot}10^{-4}$
	Difference	-	*2.6%*	*4.2%*	*-3.3%*
	θ_x (rad)	$-4.9{\cdot}10^{-5}$	$-4.4{\cdot}10^{-5}$	$-4.8{\cdot}10^{-5}$	$-3.5{\cdot}10^{-5}$
	Difference	-	*-11.5%*	*-2.7%*	*-28.7%*
	θ_y (rad)	$3.2{\cdot}10^{-5}$	$3.0{\cdot}10^{-5}$	$3.4{\cdot}10^{-5}$	$2.4{\cdot}10^{-5}$
	Difference	-	*-7.8%*	*5.2%*	*-24.6%*
	θ_z (rad)	$7.0{\cdot}10^{-7}$	$2.1{\cdot}10^{-6}$	$2.2{\cdot}10^{-6}$	$1.9{\cdot}10^{-6}$
	Difference	-	*198.2%*	*212.4%*	*169.8%*
4	u_x (m)	$1.3{\cdot}10^{-3}$	$1.3{\cdot}10^{-3}$	$1.6{\cdot}10^{-3}$	$8.0{\cdot}10^{-4}$
	Difference	-	*-1.3%*	*20.7%*	*-40.9%*
	u_y (m)	$8.4{\cdot}10^{-5}$	$3.7{\cdot}10^{-5}$	$4.4{\cdot}10^{-5}$	$2.3{\cdot}10^{-5}$
	Difference	-	*-55.7%*	*-46.9%*	*-72.5%*
	u_z (m)	$-5.9{\cdot}10^{-4}$	$-4.2{\cdot}10^{-4}$	$-4.2{\cdot}10^{-4}$	$-3.7{\cdot}10^{-4}$
	Difference	-	*-28.1%*	*-28.8%*	*-36.5%*
	θ_x (rad)	$-1.5{\cdot}10^{-5}$	$-6.7{\cdot}10^{-6}$	$-9.0{\cdot}10^{-6}$	$-4.4{\cdot}10^{-6}$
	Difference	-	*-55.4%*	*-40.0%*	*-70.7%*
	θ_y (rad)	$2.2{\cdot}10^{-4}$	$2.3{\cdot}10^{-4}$	$2.4{\cdot}10^{-4}$	$1.2{\cdot}10^{-4}$
	Difference	-	*4.0%*	*9.9%*	*-44.4%*
	θ_z (rad)	$-2.5{\cdot}10^{-8}$	$1.0{\cdot}10^{-7}$	$2.0{\cdot}10^{-7}$	$-4.0{\cdot}10^{-7}$
	Difference	-	*299.5%*	*698.9%*	*1497.8%*

Table 3.4 shows that the loads on the caissons found in Plaxis and in SACS show a reasonable correspondence. The average difference is 7.1% for the first SACS model and 7.5% for the second SACS model. This is the same order of magnitude as is reached for the linear-elastic soil (see Table 2.6). The linear-elastic model gives significantly poorer results, with an average deviation from the Plaxis results of 14%. The decreasing soil stiffness for large loads leads to a more equal distribution of the lateral force along the x-axis and overturning moment about the y-axis among legs 2 and 4, which is not captured by the linear-elastic model. This clearly shows the necessity of applying a non-linear model in order to get reliable results. The linear-elastic model results in a lateral load and overturning moment on the most heavily loaded caisson that are 25 to 30% larger than the loads found in Plaxis, so the choice of the correct model can have major implications for the foundation design.

The relative difference between the displacements found in the Plaxis and SACS calculations is on average significantly larger than it is for the loads. The largest difference occurs for the rotations about the z-axis, which are the result of torsional moments acting on the caissons. Since the torsional moments cannot be obtained in Plaxis it is not possible to determine whether the loads are different in Plaxis or the torsional stiffness applied in SACS differs from the torsional stiffness in Plaxis. It should however be noted that the torsional rotations of the caissons are 2 orders of magnitude smaller than the other two rotations, so numerical errors could be the cause of the large differences as well. The small torsional moments and rotations also indicate that the torsional behaviour is not defining the overall behaviour of the foundation, which makes the large errors for this degree of freedom acceptable.

Another degree of freedom for which the differences between the Plaxis and SACS results are significantly is the vertical displacement of the caissons. The lateral load on the jacket results in a so-called push-pull mechanism of the foundation, with two caissons loaded in axial tension and two in axial compression. The SACS calculations show reasonable agreement with the Plaxis results for the caissons loaded in compression, while the uplift of the two caissons loaded in tension is found to be roughly twice as high in the SACS models as in Plaxis. This is because the load-displacement curves for the vertical springs used in SACS have been determined for a compressional load but have been applied both for the tension and compression quadrants. The actual soil behaviour is however not symmetrical for the vertical direction, even for undrained behaviour (Gennaro et al., 2004), which leads to errors in the SACS models for tensional loads. Unlike a linear-elastic spring it is possible to define an asymmetrical behaviour for the non-linear springs in SACS, so this issue can be remedied by determining both the tensional and compressional load-displacement curves in Plaxis and combining the two into one spring for use in SACS. This is another advantage of the non-linear models over the linear-elastic model. In reality the load cases for the structure will often contain a significant dead weight load as well however, which means the foundations will rarely be loaded in tension and this issue is thus often not relevant.

When the results for the torsional rotations and uplift vertical displacements are ignored the average difference between the SACS and Plaxis results is 17% for the first model and 22% for the second model. Compared with 11% for the linear-elastic soil this shows that allthough the results for a non-linear soil become less accurate, the SACS models still produce workable results.

The results for the vertical uplift displacements have been improved by adding a different uplift branch to the vertical load-displacement curves. This leads to a significantly smaller difference with the Plaxis results, as Table 3.6 shows. The loads and the displacements for the other degrees of freedom do not change noteworthy and have therefore been omitted from the table.

Table 3.6: *Resulting displacements in the positive z-direction with and without a load-displacement curve determined for uplift*

Leg		Model 1	Model 2
1	Plaxis	$1.4 \cdot 10^{-4}$ m	$1.4 \cdot 10^{-4}$ m
	Without	$2.7 \cdot 10^{-4}$ m	$2.8 \cdot 10^{-4}$ m
	Difference	*96.1%*	*99.2%*
	With	$1.7 \cdot 10^{-4}$ m	$1.7 \cdot 10^{-4}$ m
	Difference	*19.3%*	*20.8%*
2	Plaxis	$2.2 \cdot 10^{-4}$ m	$2.2 \cdot 10^{-4}$ m
	Without	$4.2 \cdot 10^{-4}$ m	$4.2 \cdot 10^{-4}$ m
	Difference	*95.8%*	*93.9%*
	With	$2.4 \cdot 10^{-4}$ m	$2.4 \cdot 10^{-4}$ m
	Difference	*10.3%*	*9.8%*

The results show that the uplift of the caissons becomes smaller when the new curves are implemented, meaning that the caissons behave stiffer in uplift than in compression. This seems remarkable at first, since an uplift load would lead to a decrease of the effective stresses and hence a decrease of the soil stiffness in the Hardening Soil model. The soil is modelled as undrained however, which means that a change of the load will lead to the development of excess pore pressures, while the effective stresses will remain almost unchanged. This means that the load-displacement behaviour will depend on how much deformations are required in order to mobilize the excess pore pressure. Gennaro et al. (2004) have showed that an excess pore pressure in undrained extension will lead to smaller axial strains than an excess pore pressure of the same magnitude in undrained compression, which explains why the caissons behave stiffer in uplift than in compression.

Pile Group Effects in the Non-linear Model

Another way to improve the results from the non-linear spring model is the implementation of springs between the caissons that model the pile group effects. Since for the non-linear model the spring stiffnesses are determined individually instead of from a flexibility matrix, the properties of the springs between the caissons cannot be determined in the same manner as for the linear-elastic soil model. Therefore another approach is pursued. The results for the linear-elastic model given in Appendix D show that mainly the lateral translations are effected by the interaction between the caissons through the soil and that the interaction in the diagonal direction, where the spacing between the caissons is roughly 1.5 times larger, is significantly smaller. It thus seems reasonable to model the pile-group effects for the non-linear model by adding 4 axial non-linear springs between the caissons along the outline of the jacket.

The spring stiffnesses have been determined as shown in Figure 3.14. In the Plaxis model of the four caissons, one caisson is loaded by a force in lateral x-direction applied at the centre of rotation such that the caisson will displace in full translation without rotation. The resulting displacement in x-direction of the caisson and the caisson next to it are determined. The load-displacement curve for the spring between the two caissons can then be formulated with the applied force as load and the difference between the displacements of the two caissons as elongation of the spring. Since for the non-linear soil model the behaviour might be different for the caissons moving towards and away from each other, the compression and extension parts of the curves have been determined separately. It turned out that the resulting curve does not show a clear asymmetry however.

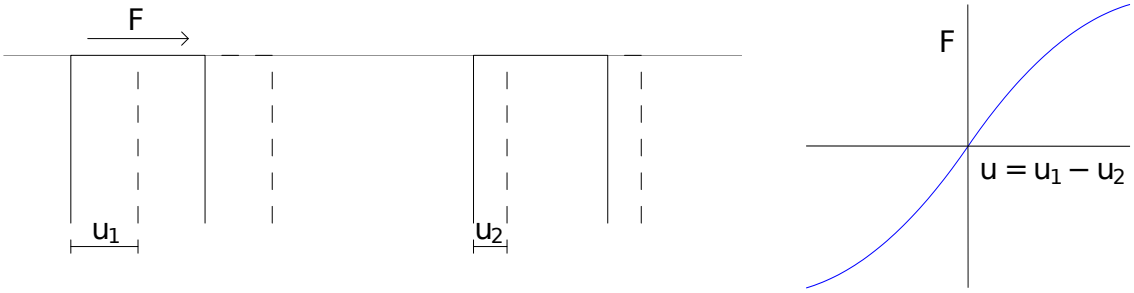

Figure 3.14: *Principle for the determination of the non-linear load-displacement curves for the springs between the caissons*

The four additional springs have been implemented in the two models, but this resulted in loads and displacements for the caissons that were clearly incorrect. Especially the overturning moments about the y-axis were inaccurate and off by up to 1000 kNm, which is the same order of magnitude as the actual load on the caissons. The application of the springs does thus not lead to useful results, let alone an improvement of the results without the additional springs. The cause of this is most likely the inaccuracy in the determination of the springs. The displacement of the caisson that is loaded is 1 to 2 orders of magnitudes larger than the displacements of the other caissons, which as Appendix D shows is also the case for the linear-elastic model. Since the non-linear springs are determined from the difference in displacement between the loaded and unloaded caisson, a small error in the displacement of the loaded caisson in Plaxis can thus have a larger influence on the resulting spring stiffness than the displacement of the unloaded spring, which the spring is supposed to model correctly. The fact that the results for the model using the springs between the caissons deviate that much indicates that the model is very sensitive for the correct stiffness of the springs between the caissons. It seems that the required accuracy of the springs cannot be obtained when the difference between the displacements of two caissons is used for the determination of the spring stiffness.

It is thus not possible to implement non-linear springs for the modelling of the pile group effects based on the calculations in Plaxis. Instead the stiffness matrices determined in the linear-elastic model can be used as coupling between the caissons. The linear-elastic coupling has been implemented and provides results that are not noticeably different from the results without coupling for either of the two models; most differences with the results from Table 3.4 and 3.5 are less than a per cent and the average differences with the Plaxis results remain the same. The reason for this is probably that the displacements in the non-linear models are significantly larger than the displacements in the linear-elastic

model, which means that the change in displacements as a result of the coupling between the caissons is small compared to the total displacements of the caissons and does not have a significant influence. The addition of the linear-elastic springs does thus not seem meaningful and the best option for the non-linear model will be not to add any springs for the modelling of pile group effects.

3.4.3 Variation of the Soil Stiffness

Just as for the linear-elastic model the non-linear models will have to be validated by comparing them with results from the Plaxis model for various soil stiffnesses. The soil parameters for the Hardening Soil model used in Plaxis have been changed for various soil stiffnesses. For the E_{50}^{ref} and E_{oed}^{ref} the same values are used as for the Young's modulus E in the linear-elastic model: 13, 52 and 624 MPa in addition to the previous calculation for 156 MPa. The corresponding value of E_{ur}^{ref} has been chosen approximately 3 times higher (500 MPa for the initial calculations and scaled accordingly for the other soil stiffnesses), but is not used in the calculations as the soil is initially in an unloaded condition without overconsolidation. Just as for the linear-elastic model the load-displacement curves for the SACS models have not determined again but the displacements are simply factored to get the correct spring stiffness. The results for the various spring stiffnesses can be found in Appendix E and are compared in Table 3.7. The torsional rotations have been omitted from the comparison, as well as any differences larger than 500%, in order to get meaningful average differences that are not distorted by large values.

Table 3.7: *Comparison between the SACS and Plaxis models for various shear moduli*

Shear modulus G (MPa)		5	20	60	240
Average difference in loads	Model 1	33.2%	10.3%	7.1%	3.4%
	Model 2	27.0%	12.4%	6.7%	5.7%
Average difference in displacements	Model 1	22.8%	29.6%	16.8%	23.4%
	Model 2	28.6%	42.3%	21.3%	37.8%

It can be seen that for both of the models the loads on the caissons show a better correspondence between the SACS and Plaxis models as the soil stiffness increases. For the loosest soil the average differences are in the order of 30% and it seems the SACS calculations cannot be used as reliable results, while for the stiffest soil the differences between the SACS and Plaxis calculations are in the order of 5%. The cause of this trend is that the behaviour of the foundation becomes less sensitive for variations in the soil stiffness as the stiffness increases. In the extreme case that the soil is infinitely more stiff than the substructure the caissons will effectively clamp the substructure and the load distribution over the foundations will be determined solely by the geometry of the jacket. When the soil stiffness is much smaller than the stiffness of the substructure on the other hand the outcome of the calculations will mainly be determined by the foundation stiffnesses. This means that the determination of the correct spring stiffnesses is very important in order to get accurate results for loose soils. The load-displacement curves used in the current models do not seem to provide the required accuracy.

This can also be seen in the results for the caisson deformations, where the resulting displacements differ on average some 20-25% for the first model and 30% for the second model between the Plaxis and SACS calculations. The results for the first model clearly correspond better with the deformations found in Plaxis over the full range of evaluated soil stiffnesses. Both models give mainly larger deformations than the Plaxis results, especially for the translation parallel to the x-axis and rotation about the y-axis. As Section 3.2 shows the foundation stiffnesses for these degrees of freedom will increase when the caisson is also loaded by a vertical load. This effect is not included in either of the model, which explains why the found deformations are larger than in the Plaxis models. The accuracy of the models can be improved when the load-displacement curves are determined for the load combination that is to expected to act on the caisson. This is something that should be taken into account especially for loose soils, since the influence of the soil stiffness is the largest in this case.

3.5 Conclusion

Two models for the represention of suction caisson foundations by non-linear springs have been created. The non-linear springs have been determined in a Plaxis FE model using the Hardening Soil model. This soil model gives a more realistic soil behaviour than the Mohr-Coulomb model. The first model uses separate springs located at the centre of rotation for each of the 6 degrees of freedom. In the second model the springs for lateral translation and rotation are combined into two springs, one of which is located at mudline and the other at the rotation point for a lateral load.

Both models are based on the assumption that the position of the centre of rotation is fixed and independent of the applied load. Furthermore the spring stiffnesses are assumed not to be influenced by loading in other directions than the one concerned for a given spring, as the springs have been determined starting from an unloaded initial state. Another aspect that is not included in the models is the direction of the loading relative to the used coordinate system. The latter issue can be resolved by orientating the springs in the same direction as the applied load.

A comparison between the two models and results from Plaxis FEM calculations of the complete foundation and substructure for various soil stiffnesses has shown that the results from the models give an acceptable correspondence with the Plaxis results. The difference in the found loads on the caissons increases as the soil stiffness decreases, since the sensitivity of the models for the use of the correct spring stiffnesses becomes larger in this case. For a soil with Young's modulus of 13 MPa the average difference between the loads found in SACS and Plaxis is in the order of 30%, while for a Young's modulus of 624 MPa the average difference has decreased to approximately 5%. The difference for the caisson displacements is in the order of 20 to 30% independent of the soil stiffness, where the first model gives a better agreement with the Plaxis calculations than the second model. All in all it can be concluded that the models give acceptable results, however the results can be improved by determining the spring stiffnesses for the correct load conditions. This is necessary in order to get reliable results for soils with a low soil stiffness. Even with the slightly incorrect spring stiffnesses used the comparison has shown that the non-linear models still give a load distribution over the foundations that matches the Plaxis results considerably better than a model with linear-elastic springs.

Chapter 4

Stepwise Method for Solving of the Non-Linear System

The results from the previous chapter show that the properties of the foundation will vary with the load conditions. The centre of rotation will shift depending on the load level and the stiffness for one degree of freedom does not only depend on the load in that load direction, but also on the loading for the other degrees of freedom. Instead of fixing the properties to one condition around which the real behaviour fluctuates, as has been done in the previous chapter, the system could also be solved in steps with an update of the properties after each step. This method will be investigated in this chapter. First the procedure of the method will be outlined and the advantages and disadvantages will be discussed. Thhe method will then be applied for the jacket structure loaded by a lateral load and the results are evaluated.

4.1 Principles of the Stepwise Method

4.1.1 Numerical Method

As with any numerical problem that is solved in steps, there is a trade-off between the complexity of a stepsize and the maximum stepsize that is allowed for results with a certain accuracy. Higher order methods such as the Runge Kutta 4 scheme and various implicit methods require several iterations for a single step,but in return can be used with a relatively large step size. On the other hand first order methods such as the forward Euler method need only one calculation for a single step but require a smaller step size than a higher order method in order to reach the same accuracy.

Since for the problem of solving the foundation behaviour both Plaxis and SACS need to be used and there is no interface for an efficient cooperation between the programs, using iterations is not a suited option for this problem. Instead an explicit method without iterations will be used. The used iteration procedure is similar to the forward Euler

method in the sense that the tangent to the system behaviour (in this case the foundation stiffnesses) is determined at the starting point and is used directly to determine the next point.

4.1.2 Iteration Procedure

The general idea of the applied method is that the stiffness of the caisson is determined in Plaxis, after which it is applied in SACS to determine the new load on each of the caissons. This load can then be applied in Plaxis again, after which the new stiffness can be determined. This procedure will be continued until the full load is applied.

The first step is determining the initial stiffness of the caissons in Plaxis. The Plaxis model is a single caisson with a mesh size as discussed in Section 2.3.1. Unless the initial (dead weight) load is not distributed evenly over the caissons the initial stiffness will be identical for all four caissons. The flexibility matrix for the caisson can be determined by loading the caisson in each of the degrees of freedom individually and determining the resulting displacements, which can be divided by the applied load to find the flexibility terms. The flexibility matrix can then be inverted to find the stiffness matrix for the caisson.

The resulting stiffness matrices can then be applied in SACS in a model of the complete jacket supported by four caissons. This model will then be loaded by a percentage of the total load case. The SACS model will be loaded by the differential load for each step, in other words the applied load in SACS will not have to be changed if the step size is chosen constant. The resulting loads and displacements found in the SACS model are thus also differential loads and displacements that need to be added to the previous loads and displacements to find the total loads and displacements up to that point.

The total loads on each of the caisson can then be applied in Plaxis one by one to find the new soil states. Then the updated flexibility and stiffness matrices can be determined and applied in SACS, after which the new loads on the caissons can be determined again. This procedure can be repeated until all load steps are completed.

4.1.3 Discussion of the Method

The stepwise method has the advantage over the model with the non-linear springs that the effects of a shifting centre of rotation and a changing stiffness due to loading in other degrees of freedom are incorporated in the method by means of updating the system. This might make the model more accurate than the model with non-linear springs.

The downside of applying the method is that is quite time-consuming. The individual Plaxis calculations are calculated relatively quick since only a single caisson is included instead of the complete foundation, and the caisson is loaded by small loads and not up to failure as is the case for the determination of the load-displacement curves for the model with non-linear springs. However, since multiple load steps are required and the stiffness matrices need to be determined individually for each caisson the total calculation time for the stepwise method will be significantly larger. The method can only be used efficiently when a large database with stiffness matrices for different load conditions is present a

priori so no new Plaxis calculations are required. Since both the soil conditions and the caisson geometry will vary from project to project having a database for this does not seem feasible however.

Since a certain part of the load case that is to be evaluated will generally not represent any real sea state it is not straightforward to apply the load steps as a realistic distributed load on the structure. Instead the load will have to be applied as a lumped load on one point on the structure. This issue will arise as well when a sea state would have to be applied on the full model in Plaxis. Allthough this lumped load will represent the same global load, the local behaviour of the structure will vary depending on how the load is applied, leading to a different distribution of the load over the caissons. Therefore the load should be applied in a point as close to the actual area where the load is acting on as possible. When the lumped load is applied on the middle frame of the jacket, the load distribution for a realistic sea state can be mimicked with an error of 5 to 10% as a comparison has shown. The size of the error will depend on the stiffness of the jacket, since for an infinitely stiff jacket the substructure will behave as a rigid body and the point of load application will not effect the behaviour.

Another approximation made using the stepwise method is that the geometry of the structure and the caissons is not updated in the SACS model. After each load step new deformations are calculated but the next load step is still calculated based on the undeformed structure. This could be solved by using non-linear springs instead of a stiffness matrix and shifting the load-displacement curves such that the unloaded condition corresponds to the displacements found in the previous steps. Using non-linear springs would mean that a shift in the centre of rotation would have to be modelled by updating the geometry of the caisson in the SACS model, which makes the calculations more laborious. Since the deformations of the structure are expected to be small the non-linear springs will therefore not be used and the deformations will be ignored.

4.2 Application of the Stepwise Method

4.2.1 Model Description

For the foundation the same dimensions and soil parameters as described in Section 3.1.3 are used. The jacket structure is loaded by a lateral load of 2000 kN applied at the top frame as shown in Figure 2.10. The number of steps is varied from 2 to 10, resulting in load steps of 200 to 1000 kN.

For the determination of the flexibility matrix the model of the caisson in Plaxis is loaded by loads of 200 kN in x-,y- and z-direction, overturning moments of 700 kNm about the x- and y-axis and a torsional moment of 350 kNm about the z-axis additional to the initial load respectively when 10 or 5 steps are used. When 2 steps are used these loads are multiplied by a factor 2.5 to make sure the load range over which the stiffness is determined corresponds with the differential loads found in the SACS model. The flexibility terms and resulting stiffness matrices are determined from the load-displacement data using the MatLab script processing.m given in Appendix F.1. The resulting differential and total loads on each of the caissons are then calculated and used as input for the new Plaxis stiffness calculations using the MatLab script plaxiscode.m given in Appendix F.1.

4.2.2 Results

The resulting loads on and displacements of the caissons for the various numbers of steps used are given in Table 4.1 and 4.2 and compared with the results from the full FE model in Plaxis. The loads in x-direction on the caissons connected to leg 1 and 4 are also plotted in Figure 4.1. The figure shows that while the results for 5 and 10 steps are similar, the load on leg 4 that is found using 2 steps varies significantly from the resulting loads using more steps and from the results from the full FE model. In this case the chosen stepsize is clearly too large to give accurate results. The initial stiffness matrices result in a load in x-direction on caisson 4 that is too large and consequently loads on the other caissons that are too small. When the updated stiffness matrices are determined this leads to a stiffness matrix for caisson 4 that behaves too soft and stiffness matrices for the other caissons that behave too stiff, which in turn results in a too small load on caisson 4 and larger loads on caissons 1 to 3. As Figure 4.1 shows this effect introduces an instability in the results. For the chosen load it can therefore be concluded that at least 5 steps should be used in order to obtain accurate results. This can also be seen in Table 4.1, where the average difference between the Plaxis results and the models with 5 and 10 steps is on average 7.0%, whereas the difference between Plaxis results and the model with 2 steps is on average 10%. The required stepsize will not only depend on the applied load but also on how much the foundation stiffness will change with changing load.

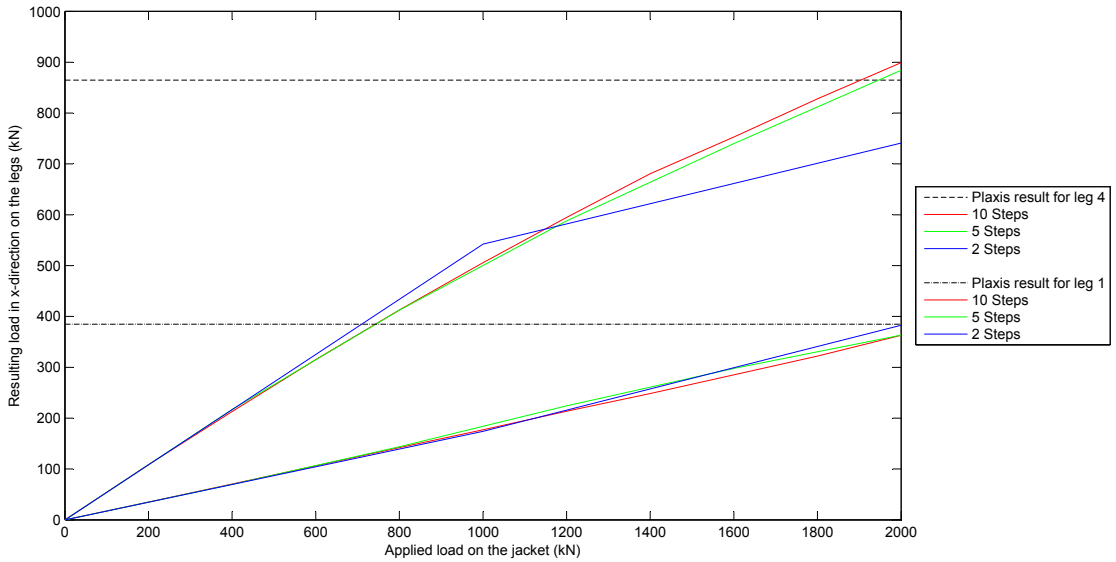

Figure 4.1: *Loads in x-direction on two caissons for various stepsizes*

While the stepwise model gives accurate results for the loads on the caissons, the correspondence of the found displacements with the full FE model seems rather poor. The difference is on average 48% for the results using 10 steps, 40% for 5 steps and 43% for 2 steps. The largest differences occur for the translations in y-direction and rotations about the x- and z-axes, which are the degrees of freedom that are less relevant for the applied load and have small displacements. The large relative differences thus do not necessarily implicate large absolute differences in the found displacements. Still, the displacements

found using the stepwise method seem to be less accurate than the displacements found using the non-linear springs, which resulted in a significantly better correspondence with the FE model results from Plaxis.

Table 4.1: *Comparison of foundation loads found in the SACS and Plaxis calculations*

Leg	D.o.f.	Plaxis	10 Steps	5 Steps	2 Steps
1	F_x (kN)	384.9	363.0	363.2	382.7
	Difference	-	*6.0%*	*6.0%*	*0.6%*
	F_y (kN)	-172.4	-154.9	-166.5	-173.2
	Difference	-	*11.3%*	*3.5%*	*-0.5%*
	F_z (kN)	969.8	981.9	997.9	1016.5
	Difference	-	*-1.2%*	*-2.8%*	*-4.6%*
	M_x (kNm)	496.7	453.6	471.1	499.4
	Difference	-	*9.5%*	*5.4%*	*-0.5%*
	M_y (kNm)	997.9	939.3	930.4	998.3
	Difference	-	*6.2%*	*7.3%*	*0.0%*
	M_z (rad)	-	61.4	61.9	70.8
2	F_x (kN)	561.3	516.5	523.9	645.5
	Difference	-	*8.7%*	*7.1%*	*-13.0%*
	F_y (kN)	-184.1	-206.2	-202.0	-216.0
	Difference	-	*-10.7%*	*-8.8%*	*-14.7%*
	F_z (kN)	1331.3	1321.5	1308.0	1291.5
	Difference	-	*0.7%*	*1.8%*	*3.1%*
	M_x (kNm)	612.0	689.9	666.6	704.2
	Difference	-	*-11.3%*	*-8.2%*	*-13.1%*
	M_y (kNm)	1896.1	1730.9	1732.6	2005.9
	Difference	-	*9.5%*	*9.4%*	*-5.5%*
	M_z (rad)	-	-34.7	-32.0	-31.7
3	F_x (kN)	188.9	221.2	228.5	230.6
	Difference	-	*-14.6%*	*-17.3%*	*-18.1%*
	F_y (kN)	329.3	330.2	332.4	349.8
	Difference	-	*-0.3%*	*-0.9%*	*-5.9%*
	F_z (kN)	-972.9	-984.3	-999.9	-1018.0
	Difference	-	*-1.2%*	*-2.7%*	*-4.4%*
	M_x (kNm)	-737.9	-760.4	-751.9	-814.3
	Difference	-	*-3.0%*	*-1.9%*	*-9.4%*
	M_y (kNm)	563.1	667.1	674.3	696.7
	Difference	-	*-15.6%*	*-16.5%*	*-19.2%*
	M_z (rad)	-	105.5	108.3	114.4

Table 4.1: *(continued)*

Leg	D.o.f.	Plaxis	10 Steps	5 Steps	2 Steps
4	F_x (kN)	864.9	899.3	884.4	741.2
	Difference	-	*-3.8%*	*-2.2%*	*16.7%*
	F_y (kN)	27.2	30.9	36.1	39.4
	Difference	-	*-12.1%*	*-24.7%*	*-31.0%*
	F_z (kN)	-1328.2	-1319.1	-1306.0	-1290.1
	Difference	-	*0.7%*	*1.7%*	*3.0%*
	M_x (kNm)	-298.8	-328.7	-339.8	-355.9
	Difference	-	*-9.1%*	*-12.1%*	*-16.1%*
	M_y (kNm)	2031.3	2133.4	2042.6	1630.7
	Difference	-	*-4.8%*	*-0.6%*	*24.6%*
	M_z (rad)	-	5.0	9.1	26.2

Table 4.2: *Comparison of foundation displacements found in the SACS and Plaxis calculations*

Leg	D.o.f.	Plaxis	10 Steps	5 Steps	2 Steps
1	u_x (m)	$2.3{\cdot}10^{-4}$	$3.9{\cdot}10^{-4}$	$4.7{\cdot}10^{-4}$	$4.3{\cdot}10^{-4}$
	Difference	-	*-39.8%*	*-50.0%*	*-46.0%*
	u_y (m)	$-1.2{\cdot}10^{-4}$	$-1.2{\cdot}10^{-4}$	$-1.6{\cdot}10^{-4}$	$-1.7{\cdot}10^{-4}$
	Difference	-	*-2.1%*	*-26.3%*	*-32.1%*
	u_z (m)	$1.4{\cdot}10^{-4}$	$2.0{\cdot}10^{-4}$	$2.2{\cdot}10^{-4}$	$2.0{\cdot}10^{-4}$
	Difference	-	*-30.6%*	*-36.8%*	*-32.0%*
	θ_x (rad)	$1.7{\cdot}10^{-5}$	$1.5{\cdot}10^{-5}$	$2.1{\cdot}10^{-5}$	$2.1{\cdot}10^{-5}$
	Difference	-	*18.5%*	*-17.0%*	*-18.1%*
	θ_y (rad)	$3.7{\cdot}10^{-5}$	$1.5{\cdot}10^{-5}$	$6.7{\cdot}10^{-5}$	$5.7{\cdot}10^{-5}$
	Difference	-	*157.9%*	*-43.8%*	*-34.2%*
	θ_z (rad)	$4.7{\cdot}10^{-7}$	$9.0{\cdot}10^{-7}$	$1.2{\cdot}10^{-6}$	$1.3{\cdot}10^{-6}$
	Difference	-	*-48.0%*	*-61.0%*	*-64.0%*
2	u_x (m)	$5.5{\cdot}10^{-4}$	$6.0{\cdot}10^{-4}$	$7.9{\cdot}10^{-4}$	$9.6{\cdot}10^{-4}$
	Difference	-	*-8.5%*	*-30.4%*	*-42.8%*
	u_y (m)	$-1.9{\cdot}10^{-4}$	$-1.5{\cdot}10^{-4}$	$-2.3{\cdot}10^{-4}$	$-2.4{\cdot}10^{-4}$
	Difference	-	*22.3%*	*-20.1%*	*-22.4%*
	u_z (m)	$2.2{\cdot}10^{-4}$	$2.7{\cdot}10^{-4}$	$3.8{\cdot}10^{-4}$	$2.6{\cdot}10^{-4}$
	Difference	-	*-19.8%*	*-44.0%*	*-17.2%*
	θ_x (rad)	$2.9{\cdot}10^{-5}$	$1.7{\cdot}10^{-5}$	$2.7{\cdot}10^{-5}$	$3.3{\cdot}10^{-5}$
	Difference	-	*66.8%*	*7.2%*	*-12.0%*
	θ_y (rad)	$8.7{\cdot}10^{-5}$	$9.1{\cdot}10^{-5}$	$1.2{\cdot}10^{-4}$	$1.3{\cdot}10^{-4}$
	Difference	-	*-3.9%*	*-26.4%*	*-33.2%*
	θ_z (rad)	$-1.6{\cdot}10^{-7}$	$-9.0{\cdot}10^{-7}$	$-6.0{\cdot}10^{-7}$	$-8.0{\cdot}10^{-7}$
	Difference	-	*-82.0%*	*-73.0%*	*-79.8%*

Table 4.2: *(continued)*

Leg	D.o.f.	Plaxis	10 Steps	5 Steps	2 Steps
3	u_x (m)	$1.7{\cdot}10^{-4}$	$2.4{\cdot}10^{-4}$	$3.0{\cdot}10^{-4}$	$2.7{\cdot}10^{-4}$
	Difference	-	*-28.5%*	*-43.4%*	*-37.5%*
	u_y (m)	$3.2{\cdot}10^{-4}$	$3.0{\cdot}10^{-4}$	$3.4{\cdot}10^{-4}$	$3.6{\cdot}10^{-4}$
	Difference	-	*5.5%*	*-6.4%*	*-12.2%*
	u_z (m)	$-2.7{\cdot}10^{-4}$	$-3.7{\cdot}10^{-4}$	$-3.1{\cdot}10^{-4}$	$-3.4{\cdot}10^{-4}$
	Difference	-	*-27.4%*	*-13.3%*	*-21.1%*
	θ_x (rad)	$-4.9{\cdot}10^{-5}$	$-2.8{\cdot}10^{-5}$	$-3.9{\cdot}10^{-5}$	$-3.0{\cdot}10^{-5}$
	Difference	-	*79.5%*	*27.9%*	*66.7%*
	θ_y (rad)	$3.2{\cdot}10^{-5}$	$3.7{\cdot}10^{-5}$	$4.5{\cdot}10^{-5}$	$3.8{\cdot}10^{-5}$
	Difference	-	*-12.7%*	*-28.1%*	*-15.7%*
	θ_z (rad)	$7.0{\cdot}10^{-7}$	$1.9{\cdot}10^{-6}$	$2.2{\cdot}10^{-6}$	$2.3{\cdot}10^{-6}$
	Difference	-	*-62.9%*	*-68.0%*	*-69.4%*
4	u_x (m)	$1.3{\cdot}10^{-3}$	$1.5{\cdot}10^{-3}$	$1.7{\cdot}10^{-3}$	$2.2{\cdot}10^{-3}$
	Difference	-	*-7.6%*	*-21.5%*	*-39.7%*
	u_y (m)	$8.4{\cdot}10^{-5}$	$3.6{\cdot}10^{-5}$	$5.3{\cdot}10^{-5}$	$6.2{\cdot}10^{-5}$
	Difference	-	*134.3%*	*56.6%*	*34.8%*
	u_z (m)	$-5.9{\cdot}10^{-4}$	$-5.0{\cdot}10^{-4}$	$-4.7{\cdot}10^{-4}$	$-4.3{\cdot}10^{-4}$
	Difference	-	*16.8%*	*23.2%*	*36.0%*
	θ_x (rad)	$-1.5{\cdot}10^{-5}$	$-5.1{\cdot}10^{-6}$	$-6.4{\cdot}10^{-6}$	$-6.6{\cdot}10^{-6}$
	Difference	-	*194.3%*	*134.5%*	*127.4%*
	θ_y (rad)	$2.2{\cdot}10^{-4}$	$2.2{\cdot}10^{-4}$	$2.6{\cdot}10^{-4}$	$3.2{\cdot}10^{-4}$
	Difference	-	*2.4%*	*-14.0%*	*-30.6%*
	θ_z (rad)	$-2.5{\cdot}10^{-8}$	$1.0{\cdot}10^{-7}$	$3.0{\cdot}10^{-7}$	$8.0{\cdot}10^{-7}$
	Difference	-	*-75.0%*	*-91.7%*	*-96.9%*

There could be various causes for inaccurate results for the displacements found using the stepwise method. Since the results for 5 and 10 steps used are quite similar it seems that linearization of the foundation behaviour, if the interval of the linearization is chosen sufficiently small, is possible with accurate results. In fact, the load-displacement curves for the non-linear springs in SACS are also used for linear interpolation and still provide reasonable results. The linearization is therefore not the cause of the inaccuracy.

Another cause could be the different behaviour of the jacket substructure due to the fact that the deformations of the jacket are not updated. In order to see how much this affects the results the stepwise method has also been applied for a single caisson. The soil parameters and caisson dimensions are kept unchanged and the caisson is loaded by a lateral load of 1000 kN, vertical load of -1000 kN and overturning moment of 3500 kNm. The resulting displacements are given in Table 4.3 and visualized in Figure 4.2. It can be seen that for a single pile the stepwise method provides results that match the results from the FE model in Plaxis very close. For this case the stepwise method also seems to give more accurate results than the method with non-linear springs (see Table 3.3).

Table 4.3: *Resulting displacements for a single caisson loaded by a F_x of 1000 kN, F_z of -1000 kN and M_y of 3500 kNm*

	u_x (mm)	u_z (mm)	θ_y (10^{-4} rad)
Plaxis (FE)	4.15	0.83	6.55
SACS (5 Steps)	4.11	0.83	6.29
Difference	*-0.79%*	*-0.66%*	*-3.97%*

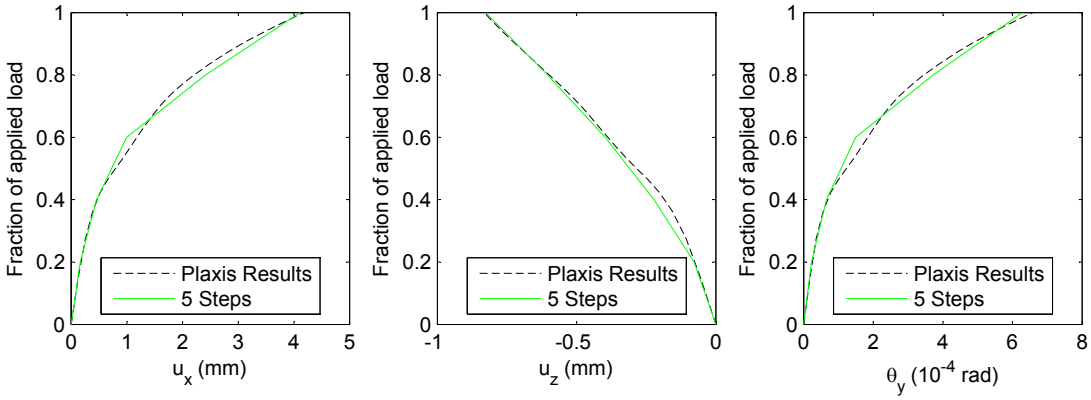

Figure 4.2: *Resulting displacements for a single caisson loaded by a F_x of 1000 kN, F_z of -1000 kN and M_y of 3500 kNm*

This indicates that the large differences found for the displacements of a multi-footed foundation are the results of effects of interaction in the full model that are not included in the model for the stepwise method. Part of this might be the interaction between the caissons through the soil, however since the difference is significantly larger than for the models with linear-elastic and non-linear springs this cannot be the sole cause. It seems that the behaviour of the jacket substructure is also modelled incorrectly due to the fact that the deformations of the jacket are not included in the model. Whether this is actually the cause of the large differences in the results has to be confirmed by further calculations. If this is the case, the incorrect behaviour of the jacket does not result in a significantly different distribution of the loads. As concluded before the load distribution over the caissons is less sensitive to the model conditions than the caisson displacements. This is magnified by the non-linear loosening behaviour of the soil, which makes that a certain relative difference of the load will lead to a larger relative difference of the displacement.

Influence of the Centre of Rotation

The updated stiffness matrices can also be used to assess to what extent the assumptions of a fixed depth of the centre of rotation and a load-displacement behaviour that is independent of loading in other degrees of freedom, that are made in the model with non-linear springs, are acceptable.

The depth of the centre of rotation will shift when the load level changes, as for instance Figure 3.5 shows. This depth is encapsulated in the stiffness matrix as the ratio between the coupling and lateral stiffness, as derived in Appendix A. Thus, assuming that the

centre of rotation is fixed means fixing the ratio between the coupling and lateral stiffness terms. The effect of this on the resulting load distribution can be evaluated by modifying the coupling terms of the stiffness matrices found using 10 load steps, such that the ratio between coupling and lateral stiffness is the same as for the initial stiffness matrix. This has been done and the resulting load on leg 4, the most heavily loaded caisson, with and without fixing the centre of rotation is compared in Figure 4.3.

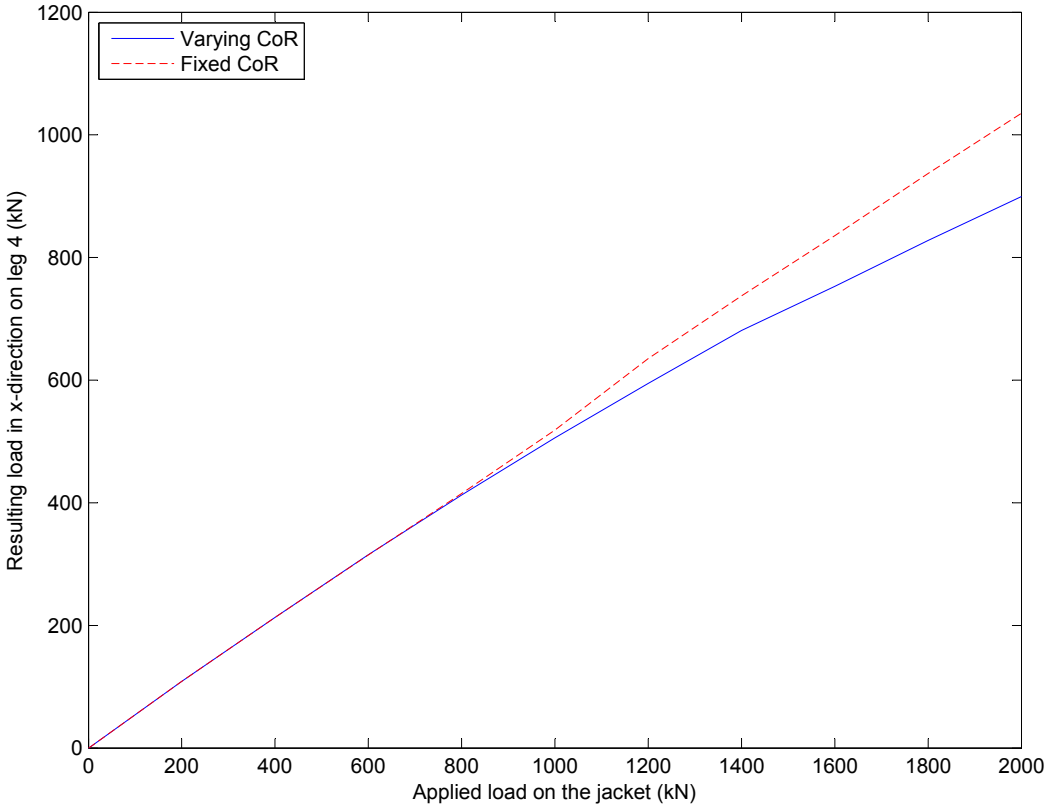

Figure 4.3: *Load on leg 4 using the stepwise method with and without a fixed centre of rotation*

Initially the stiffness matrices do not have to be altered significantly and as a result it can be seen that the difference between the resulting lateral loads on leg 4 is negligible for the first 1000 kN that is applied. When the load is increased further the curves start to deviate. The curve for the varying centre of rotation shows the clear non-linear behaviour of the load distribution over the caissons with increasing load, whereas the curve for a fixed centre of rotation is almost linear. The latter result is interesting, since the lateral stiffness terms do decrease by a factor of 1.4 when the load is increased and the ratio of the lateral stiffness for the individual caissons increases up to 1.2. Still this seems to have little effect on the distribution of the load over the caissons; the load distribution seems to be influenced only by the varying centres of rotation. The centre of rotation does in fact also influence the stiffness of the caisson, since a deeper centre of rotation leads to larger displacements of the caisson top plate for the same rotation. The centre of rotation of the most heavily loaded caisson, connected to leg 4, changes the most during load application, as Figure 4.4 shows. This means that the lateral stiffness of this caisson is increased the most by fixing the depth of the centre of rotation, which results in a smaller redistribution of the load with increasing loads.

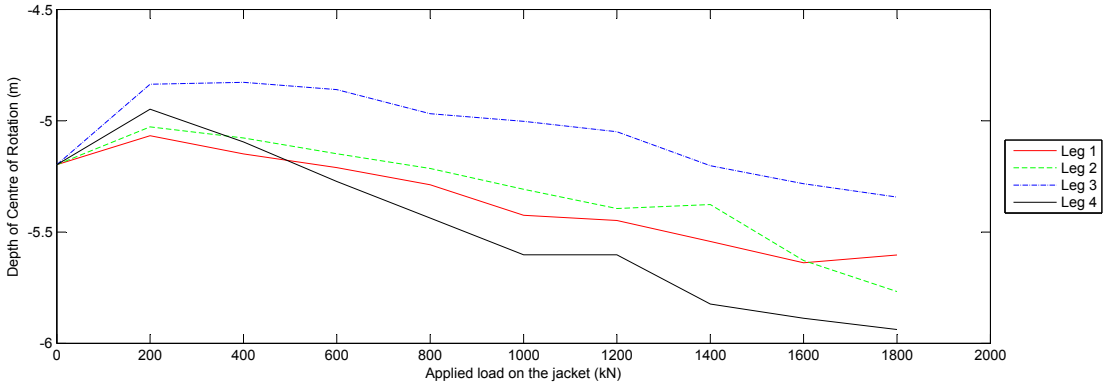

Figure 4.4: *Variation of the centres of rotation for the 4 caissons with increasing load*

Although it has been shown that the fixation of the centre of the rotation can have a significant influence on the resulting load distribution, the question is whether this is also the case for practical applications. For a large range of loads the fixed rotation centre does not change the resulting load distribution noticeably as Figure 4.3 shows, only for loads far from the initial conditions the difference increases to 15%. This difference will be smaller when the fixed centre of rotation is chosen at a location corresponding to the applied load instead of at the initial unloaded position. In this case the error made by fixing the centre of rotation can most likely be deemed acceptable, especially since the fixed centre of rotation leads to larger loads on the most heavily loaded caisson and is thus conservative.

4.3 Conclusion

The non-linear behaviour of suction caissons can be modelled with linear-elastic stiffness matrices if the load is applied in several steps and the stiffness matrices are updated after each step. This method seems however not very efficient since it requires many small but nevertheless time-consuming FE calculations. For a model of the complete substructure and foundation the method gives acceptable results for the load distribution over the caissons, but the resulting displacements of the caissons show poor correspondence with results from the complete FE model. This is likely the result of not including the jacket deformations in the model.

For a single pile the displacements show a much better agreement with FE calculations and actually differ significantly less from the FE calculations than the model with non-linear springs discussed in the previous chapter. This shows once again that the full three-dimensional stress state of the soil, that is taken into account for the stepwise method but not for the non-linear springs, has a major influence on the load-displacement behaviour of the caisson. It should therefore also be considered when determining the non-linear springs by determining them for the correct load conditions.

Chapter 5

Conclusion and Recommendations

Three methods to model a suction caisson foundation for a multi-footed offshore structure in the structural software SACS by means of a multidimensional spring system have been investigated. The three methods are:

1. The use of linear springs
2. The use of non-linear springs
3. The use of linear springs that are updated in several steps.

The methods have been compared to results from an integrated FE model in Plaxis, both for the behaviour of a single caisson and for a jacket substructure resting on four suction caissons. The methods and the obtained results are discussed below.

Linear spring method

Assuming that a suction caisson foundation behaves as a rigid body there are 6 degrees of freedom, resulting in 5 different spring constants. These constants can be combined into a 6x6 stiffness matrix. A comparison of three different sets of analytical expressions for the spring constants with a FEM analysis in Plaxis has shown that although the expressions are not intentionally developed for suction caissons, they give accurate results for the range of aspect ratio's around unity, which is typical for suction caissons. This is only the case if the soil is linear-elastic and uniform, which characteristic soil profiles encountered in practice are not. For the FEM analysis it has been assumed that the caisson and included soil volume act as a rigid body, however in reliality the behaviour may be different due to a void between the soil and the top plate and/or an opening in the top plate through which water may dissipate. Another aspect that is not included in the FEM model is the dynamic behaviour of the caisson. For typical design loads it can be shown that dynamic effects are negligible however.

When the stiffness terms determined in the FEM analysis are implemented in a model of multiple foundations the behaviour of an offshore foundation together with the substructure above can be investigated. The behaviour of the suction caisson foundations is in between a clamped and a pinned foundation, becoming more similar to a clamped foundation as the soil stiffness increases. A comparison with a FE model of the complete foundation has shown that a model with linear springs provides reliable results for a linear-elastic soil. The results can be improved when the interaction between the caissons is included by adding additional springs. The model is consistent over a wide range of soil

stiffnesses with the shear modulus varying from 5 to 240 MPa. The agreement between the FE model and the spring model is very good, with an average difference between the models of 5% for the reaction forces acting on the individual caissons and 5 to 15% for the caisson displacements. For a linear-elastic soil it can therefore be concluded that suction caissons can be modelled efficiently and accurately by use of linear springs represented by stiffness matrices.

Non-linear spring method

For a soil that has a non-linear stiffness the model with linear springs does not provide accurate results however. A comparison has shown that the model is not able to describe the changing load distribution due to changing incremental soil stiffnesses, whereas models that include non-linear springs are. For the considered load case the overturning moment on the governing caisson reduced by more than 20% due to this effect, so the modelling of the foundation stiffness has a considerable impact on the structural design.

Two models that make use of non-linear springs with stiffnesses determined in a FE model have been developed. The difference between the models is that in the first model the response for each degree of freedom is determined by a separate spring while in the second model the lateral and rotational springs are combined. Both models assume that the centre of rotation of the caisson is independent of the applied load and that the spring stiffnesses are not influenced by loading in other directions. Especially the latter assumption is incorrect and leads to inaccuracies in the results. The average difference between the results from the spring and FE models turned out to be larger than for the linear-elastic soil. For the loads on the caissons the difference varied from on average 30% for a soil with an E^{50} of 13 MPa to 5% for an E^{50} of 624 MPa. The inaccuracy of the models increases as the soil stiffness decreases since the behaviour of the system becomes more sensitive to the exact soil stiffness in this case. The displacements showed an average difference in the order of 20 to 30%. This order of magnitude means the results are still usable but not very accurate.

The results of the first model showed a better agreement with the FE results than the second model, especially for the caisson displacements. For the accuracy in the reaction forces on the caissons, which are generally more important for the design than the displacements, the models perform tantamount to each other. Since the determination of the spring stiffnesses is less laborious for the second model it can be concluded that both models have their advantages and neither of the models can be singled out as being clearly preferable above the other.

Just as for the linear-elastic soil the interaction between the caissons has also been tried to model in the non-linear models. Unfortunately the characteristics of the coupling springs could not be determined with the accuracy required for reliable results. The implementation of the linear coupling springs determined for the linear-elastic model did not improve the results noticeably as the resulting change in displacements due to the coupling springs is small compared to the displacements of caissons in the non-linear soil. Therefore there is no real benefit of including the additional springs. For the non-linear models the effects of interaction between the caissons can thus not be included.

Stepwise solving method

As an alternative for the models with non-linear springs a model with linear springs that are updated in steps is also investigated. This model can deal with the changes in

the centre of rotation and the load-displacement curves that are neglected in the other models. This model is however not very efficient as it requires many time-consuming FE calculations. Furthermore the displacements found in the model are inaccurate as the deformations of the jacket substructure are not updated between the steps. For a single pile this is not an issue and in this case the model provides results that are in better agreement with the FE results than the models with non-linear springs. This shows that the influence on the spring stiffnesses of loading in other directions, that is included in this model but not in the models with non-linear springs, is significant. Other than that it can be concluded that this model is not very suited for the use of foundation design.

Conclusions
After comparing the various models it can be concluded that the use of non-linear springs for the modelling of suction caisson foundations is a promising method that is able to provide reliable results. Not all effects of realistic soil behaviour are captured in the springs, which makes the method less accurate for a soil with non-linear behaviour than for a linear-elastic soil, however in all but a few cases the results are accurate enough to be used. Only for very loose soils the accuracy of the used springs needs to be improved. The loss of accuracy is compensated by the possibility to run the models in combination with many realistic load cases, which makes the method more versatile and efficient than the use of FEM calculations and thus very suited for design purposes for suction caisson foundations for multi-footed structures.

5.1 Recommendations for Further Research

In order to improve the accuracy of the non-linear spring method and expand the range of applications several topics need to be explored in more detail than the scope of this thesis allowed. Four of the topics for further research, most of which have been mentioned before, are discussed in more detail in the following paragraphs.

Detailed behaviour of the soil inside the caisson
First of all it has been assumed in this thesis that the suction caisson and the soil that is included inside the caisson act together in a such a way that they can be considered as a single rigid body. Some detailed FEM calculations or model tests are needed to determine for which suction caisson configurations this is actually the case. Configurations that should be considered are a top plate that lays directly on top of the soil surface, a void between the top plate and the soil filled with water and a grouted void between the soil and the top plate. The vertical stiffness of the foundation will mainly be affected by these variations, but whether the other degrees of freedom are also influenced and to what extent needs to be clarified by further studies.

Furthermore the effect of an opening in the top plate should also be considered. This will not only affect the stiffness of the foundation but also the level of drainage that will occur for a given load. The drainage can have a significant effect on the behaviour of the foundation under cyclic loading, something that is not included in this study but needs to be considered for an offshore foundation design. Although it has been shown that the response of the foundation to ultimate load cases can be considered to be static the combination of drainage with cyclic loading can still lead to a frequency-dependent response to loads, which can influence the design. The influence of the drainage can be investigated using an FEM analysis in the time domain including water flow, but since this will result in a very complex model scale tests might be more suited for this research.

Improvement of the load-displacement curves
Another aspect that needs to be improved is the determination of the non-linear load-displacement curves for the correct load conditions. This can lead to an improved accuracy of the model. One approach to do this is to determine the vertical, lateral and rotational stiffness of the model all from the same calculation by applying the load components for these degrees of freedom simultaneously. A lateral load applied on the substructure will lead to a lateral load on the caissons as well as a vertical load to counteract the resulting moment by a push-pull mechanism. If the ratio between the resulting load components is assumed to be independent of the magnitude of the applied load the loads could be applied in this ratio for the determination of the load-displacement curves. This would result in two different sets of lateral and rotational springs, one for the caissons in uplift and one for the caissons in compression. In case of a diagonal load direction a third set without a vertical load component can also be included. The most important issue with this method is the determination of the correct ratio between the load components. This can be determined based on an initial calculation with pinned or clamped foundations, but perhaps some iterations are required for accurate results.

The soil stiffness could be modelled in more detail by defining the displacements in the load-displacement curves not as a function of a single load component but of all six load components. This way the influence of the full three-dimensional stress state on the soil stiffness can be included in the model. In order to get the correct input for this model many FEM calculations for various load conditions would be required, which is not efficient. This could be resolved however by defining a few load curves and using interpolation in between or adjusting the curves analytically based on plasticity theory. There is curently no possibility to implement either of these solutions in SACS so additional modules would have to be developed or another software package would have to be used.

Pile-pile interaction
The effects of interaction between the caissons through the soil is also a topic that deserves further research. For the non-linear spring models a method to include the interaction effects should be pursued, as it could lead to an improvement of the results. The influence of the interaction can also be studied in more detail for the linear-elastic model by performing a parameter study for different caisson diameters and foundation layouts. The soil stiffness should also be varied, as a low soil stiffness will lead to larger relative displacements between the caissons which might cause stronger interaction effects.

Load history
Finally the load history of the foundation will also have an effect on the foundation response and should therefore be studied in more detail. The load history will not only be of importance because of cyclic loading, which has already been mentioned, but also through residual displacements of the caissons as a result of plastic strains in the soil. Since the plastic strains can be presumed to be the largest near the most heavily loaded caissons, this effect might lead to smaller loads on the these caissons and thus reduce the design loads. On the other hand the residual deformations will also mean that the response of the caissons will be determined by a stiff reloading behaviour, which might cancel out the positive effects and even lead to increased fatigue damage for small loads. The actual behaviour could be studied by determining the response of the system for various initial displacements of the caisson. The correct stresses in the substructure due to the residual displacements should also be taken into account in this study.

References

Bentley. Sacs - sacs iv, 2012.

M.F. Bransby and M.F. Randolph. Combined loading of skirted foundations. *Géotechnique*, 48(5):637–655, 1998.

B.W. Byrne. *Investigations of suction caissons in dense sand*. PhD thesis, University of Oxford, 2000.

J.P. Carter and F.H. Kulhawy. Analysis of laterally loaded shafts in rock. *Journal of Geotechnical Engineering*, 118(6):839–855, 1992.

E.C. Clukey, H. Banon, and F.H. Kulhawy. Reliability assessment of deepwater suction caissons. In *Proc. 32nd Offshore Technology Conference, Houston*, 2000.

M.J. Dekker. Modelling the bearing capacity of a suction bucket, 2013.

J.M. Duncan and C. Chang. Nonlinear analysis of stress and strain in soils. *Journal of the Soil Mechanics and Foundations Division*, 96(5):1629–1653, 1970.

G. Gazetas. Formulas and charts for impedances of surface and embedded foundations. *Journal of Geotechnical Engineering*, 117(9):1363–1381, 1991.

V. De Gennaro, J. Canou, J.C. Dupla, and N. Benahmed. Influence of loading path on the undrained behaviour of a medium loose sand. *Canadian Geotechnical Journal*, 41 (1):166–180, 2004.

R. Hill. *The mathematical theory of plasticity*. Oxford university press, Oxford, 1998. ISBN 9780198503675.

R.B. Kelly, G.T. Houlsby, and B.W. Byrne. A comparison of field and laboratory tests of caisson foundations in sand and clay. *Géotechnique*, 56(9):617–626, 2006.

S.R. Kim, L.C. Hung, and M. Oh. Group effect on bearing capacities of tripod bucket foundations in undrained clay. *Ocean Engineering*, 79:1–9, 2014.

K.A. Larsen. *Static behaviour of bucket foundations.* PhD thesis, Department of Civil Engineering, Aalborg University, Denmark, 2008.

M. Liingaard, L. Andersen, and L.B. Ibsen. Impedance of flexible suction caissons. *Earthquake Engineering & Structural Dynamics*, 36(14):2249–2271, 2007.

C.M. Martin and G.T. Houlsby. Combined loading of spudcan foundations on clay: numerical modelling. *Géotechnique*, 51(8):687–699, 2001.

G.G. Meyerhof and V.V.R.N. Sastry. Bearing capacity of rigid piles under eccentric and inclined loads. *Canadian Geotechnical Journal*, 22(3):267–276, 1985.

A. Pais and E. Kausel. Approximate formulas for dynamic stiffnesses of rigid foundations. *Soil Dynamics and Earthquake Engineering*, 7(4):213–227, 1988.

Plaxis. Plaxis 3d reference manual 2013, 2013. URL http://www.plaxis.nl/files/files/3D2013-2-Reference.pdf.

M.F. Randolph. Piles subjected to torsion. *Journal of the Geotechnical Engineering Division*, 107(8):1095–1111, 1981.

M.F. Randolph and C.P. Wroth. Analysis of deformation of vertically loaded piles. *Journal of the Geotechnical Engineering Division*, 104(12):1465–1488, 1978.

T. Schanz, P.A. Vermeer, and P.G. Bonnier. The hardening soil model: formulation and verification. *Beyond 2000 in Computational Geotechnics*, pages 281–296, 1999.

R. Sheikh and C. Swan. Wave slamming on vertical surface-piercing cylinders: the role of nonlinear wave scattering. In *Proc. 15th International Offshore and Polar Engineering Conference, Seoul, South Korea*, pages 652–659, 2005.

M.N. Tran, M.F. Randolph, and D.W. Airey. Study of seepage flow and sand plug loosening in installation of suction caissons in sand. In *Proc. 15th International Offshore and Polar Engineering Conference, Seoul, South Korea*, pages 516–521, 2005.

DNV (Det Norske Veritas). Geotechnical design and installation of suction anchors in clay. *DNV-RP-E303*, 2005.

A. Verruijt. *An introduction to soil dynamics.* Springer, Dordrecht, The Netherlands, 2010. ISBN 9789048134403.

F.A. Villalobos. *Model testing of foundations for offshore wind turbines.* PhD thesis, University of Oxford, 2006.

P.G. Watson and M.F. Randolph. Vertical capacity of caisson foundations in calcareous sediments. In *Proc. 7th International Offshore and Polar Engineering Conference, Honolulu*, pages 784–790, 1997.

J.P. Wolf and A.J. Deeks. *Foundation vibration analysis: A strength of materials approach.* Butterworth-Heinemann, Oxford, 2004.

J.H. Zhang, L.M. Zhang, and X.B. Lu. Centrifuge modeling of suction bucket foundations for platforms under ice-sheet-induced cyclic lateral loadings. *Ocean engineering*, 34(8): 1069–1079, 2007.

Appendix A

Transformation of the Stiffness Matrix

As described in Section 2.3 the stiffness matrix for a certain location on a rigid body can be found by applying a load at that point, measuring the displacements of that point and thus finding the flexibility matrix and consequently the stiffness matrix for that point. Since for a rigid body the displacements in one point directly give the displacements in any other point of the rigid body, a stiffness matrix for a given point can also be utilized to find the stiffness matrix for any other point. This property can be used to transform a stiffness matrix given at mudline to a stiffness matrix in the centre of rotation, which is a uncoupled diagonal matrix, or to transform a stiffness matrix given for the foundation base to one given at mudline, as will be shown later. For both these cases the stiffness matrices are given for a point at the axis of symmetry, which means that there is only coupling between a lateral load and overturning moment. This results in a flexibility and stiffness matrix of the following general form at mudline:

$$\boldsymbol{f} = \begin{bmatrix} f_h & 0 & 0 & 0 & f_{hr} & 0 \\ 0 & f_h & 0 & -f_{hr} & 0 & 0 \\ 0 & 0 & f_v & 0 & 0 & 0 \\ 0 & -f_{hr} & 0 & f_r & 0 & 0 \\ f_{hr} & 0 & 0 & 0 & f_r & 0 \\ 0 & 0 & 0 & 0 & 0 & f_t \end{bmatrix}, \quad \boldsymbol{K} = \begin{bmatrix} K_h & 0 & 0 & 0 & -K_{hr} & 0 \\ 0 & K_h & 0 & K_{hr} & 0 & 0 \\ 0 & 0 & K_v & 0 & 0 & 0 \\ 0 & K_{hr} & 0 & K_r & 0 & 0 \\ -K_{hr} & 0 & 0 & 0 & K_r & 0 \\ 0 & 0 & 0 & 0 & 0 & K_t \end{bmatrix}$$

Transformation from a Coupled to an Uncoupled Stiffness Matrix

First the transformation from a coupled stiffness matrix given at mudline to an uncoupled stiffness matrix given at the centre of rotation will be derived.

Relation between the Lateral and Coupling Stiffness

It can be derived that the ratio between the coupling stiffness K_{hr} and the lateral stiffness K_h gives the distance from the point for which the stiffness matrix is given to the centre of rotation. Figure A.1 shows the rotation and translation at mudline as a result of an overturning moment applied on the caisson. From the geometry it easily follows that for small rotations ϕ the displacement at mudline u is related to the rotation by

$$u = l \cdot \phi \tag{A.1}$$

where l is the distance between the centre of rotation and mudline. The rotation and translation are related to the applied moment by the flexibility terms f_r and f_{hr} respectively:

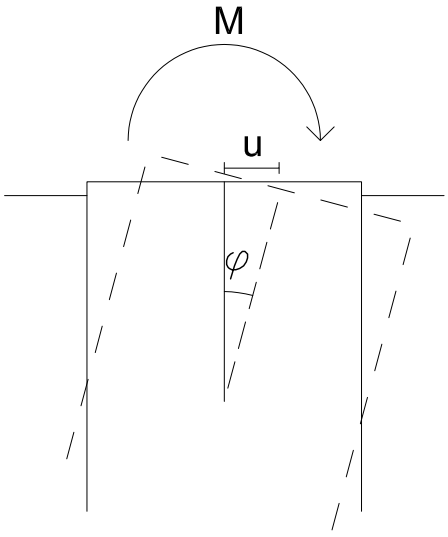

Figure A.1: *Rotation and translation as a result of an overturning moment*

$$\phi = f_r \cdot M \tag{A.2}$$
$$u = f_{hr} \cdot M \tag{A.3}$$

Combined with Equation A.1 this results in

$$f_{hr} = l \cdot f_r \tag{A.4}$$

Since the complete 6 dof flexibility matrix is largely uncoupled, it can be split into several smaller flexibility matrices, including one for the translation in x-direction and the rotation about the y-axis in which the two flexibility terms f_r and f_{hr} are present:

$$\begin{bmatrix} u_x \\ \phi_y \end{bmatrix} = \begin{bmatrix} f_h & f_{hr} \\ f_{hr} & f_r \end{bmatrix} \cdot \begin{bmatrix} F_x \\ M_y \end{bmatrix} \tag{A.5}$$

Inverting this flexibility matrix gives the stiffness matrix for the 2 dof system. Since the flexibility matrix is a 2x2 matrix the inverse can be determined directly as

$$\boldsymbol{K} = \begin{bmatrix} K_h & -K_{hr} \\ -K_{hr} & K_r \end{bmatrix} = \boldsymbol{f}^{-1} = \frac{1}{f_h f_r - f_{hr}^2} \begin{bmatrix} f_r & f_{hr} \\ f_{hr} & f_h \end{bmatrix} \tag{A.6}$$

From this it follows that

$$\frac{K_{hr}}{K_h} = \frac{f_{hr}}{f_r} = l \tag{A.7}$$

Since the lateral stiffness term is independent of the distance to the centre of rotation, as will be shown later, this means that the coupling stiffness term will be proportional to the distance to the centre of rotation and hence zero for a stiffness matrix defined at the centre of rotation, which is thus fully uncoupled.

Relation between the Lateral Stiffness for the Centre of Rotation and at Mudline

Figure A.2 shows the translation u^* at mudline as a result of a lateral load F. This translation can be split into a translation u and rotation ϕ at the centre of rotation:

$$u^* = u + \phi \cdot l \tag{A.8}$$

The load F at mudline is equivalent to an equal lateral load F and overturning moment $M = F \cdot l$ acting at the centre of rotation. Since the stiffness matrix is fully uncoupled at the centre of rotation these loads can be related directly to the displacements at the centre of rotation by means of the lateral and rotational stiffness:

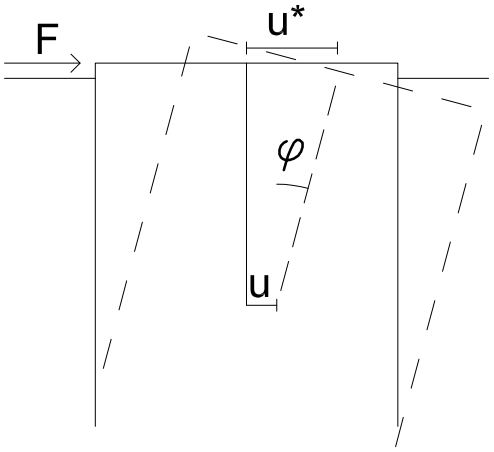

Figure A.2: *Translation at mudline as a result of a lateral load*

$$F = K_h \cdot u \tag{A.9}$$
$$M = K_r \cdot \phi \tag{A.10}$$

At mudline the stiffness matrix is coupled and the load F is given by

$$F = K_h^* \cdot u^* - K_{hr}^* \cdot \phi \tag{A.11}$$

Substituting Equation A.8 in Equation A.11 gives

$$\begin{aligned} F &= K_h^* \cdot u^* - K_{hr}^* \cdot \phi \\ &= K_h^* \cdot (u + \phi \cdot l) - K_{hr}^* \cdot \phi \\ &= K_h^* \cdot u + (K_h^* \cdot l - K_{hr}^*) \cdot \phi \end{aligned} \tag{A.12}$$

When the result from Equation A.7 is substitued it follows that the term in parentheses on the right hand side of Equation A.12 is equal to zero, so that Equation A.12 can be reduced to

$$f = K_h^* \cdot u + \cancel{(K_h^* \cdot l - K_{hr}^*)} \cdot \phi = K_h^* \cdot u \tag{A.13}$$

Comparing Equation A.9 with Equation A.13 shows that K_h^* must be equal to K_h, in other words the lateral stiffness term at mudline or any other point on the centre line of the caisson is equal to the lateral stiffness at the centre of rotation. This term does therefore not have to be altered when the stiffness matrix is moved to a different location.

Relation between the Rotational Stiffness for the Centre of Rotation and at Mudline

An overturning moment applied at mudline will result in the same rotation of the caisson as a moment applied at the centre of rotation. Therefore the rotational flexibilities will be the same. Starting with the same 2x2 stiffness matrix for a point at mudline as given in Equation A.6, the rotational flexibility is found to be

$$\boldsymbol{f} = \boldsymbol{K}^{-1} = \frac{1}{K_h^* K_r^* - \left(K_{hr}^*\right)^2} \begin{bmatrix} K_r^* & K_{hr}^* \\ K_{hr}^* & K_h^* \end{bmatrix} \;,\; f_r = \frac{K_h^*}{K_h^* K_r^* - \left(K_{hr}^*\right)^2} \tag{A.14}$$

Since the flexibility matrix for the centre of rotation is uncoupled, the rotational stiffness can be found by directly inverting the rotational flexibility. This gives

$$K_r = f_r^{-1} = \frac{K_h^* K_r^* - \left(K_{hr}^*\right)^2}{K_h^*} = K_r^* - K_{hr}^* \frac{K_{hr}^*}{K_h^*} = K_r^* - K_{hr}^* \cdot l \tag{A.15}$$

The rotational stiffness at the centre of rotation is thus found by reducing the rotational stiffness at mudline by the coupling stiffness at mudline multiplied by the distance between mudline and centre of rotation. This means that the rotational stiffness term at mudline will be smaller than it is at mudline for the same resulting stiffness.

Resulting Stiffness Matrix at the Centre of Rotation

Combining all previous results, it follows that a stiffness matrix given at mudline can be transformed to a stiffness matrix given at the centre of rotation by removing all coupling terms and deducting the coupling stiffness multiplied by the distance from mudline to the centre of rotation from the rotational stiffness. The lateral, vertical and torsional stiffness terms will remain the same.

Transformation from a Coupled to a Different Coupled Stiffness Matrix

The results found in the previous section can also be used to transform a stiffness matrix defined at the foundation base to one defined at mudline. Given the rotational and coupling stiffness K_r^{**} and K_{hr}^{**} and distance to the centre of rotation l^{**} at the foundation base and K_r^*, K_{hr}^* and l^* at mudline, it follows that the rotational stiffness at the centre of rotation can be expressed as

$$K_r = K_r^{**} - K_{hr}^{**} \cdot l^{**} = K_r^* - K_{hr}^* \cdot l^* \tag{A.16}$$

In the expressions given by Wolf and Deeks (2004) and Gazetas (1991) the centre of rotation is assumed to be at $^2/_3$ of the embedment depth, so that $l^{**} = -^1/_3 L$, $l^* = {}^2/_3 L$ and $K_{hr}^* = -2 \cdot K_{hr}^{**}$. Combining this with Equation A.16 gives the relation between the rotational stiffness terms. With this the new stiffness matrix can be formulated.

$$K_r^* = K_r^{**} - {}^1/_3 L \cdot K_{hr}^{**} - {}^2/_3 L \cdot -2 \cdot K_{hr}^{**} = K_r^{**} + L \cdot K_{hr}^{**} \tag{A.17}$$

Appendix B

Rotational Stiffness of a Model with Translational Springs

In this Appendix it will be proven that it is possible to model both the lateral and the rotational stiffness and rotation points correctly with a combination of two lateral springs, one applied at mudline and one applied at the point around which the foundation will rotate when a lateral load is applied at mudline. This point will be located below the foundation itself. A diagram of the model with the two springs is given in Figure B.1.

When only a lateral load F_1 is applied at mudline the load will be transfered directly to the upper spring, which will thus get a deformation

$$u_1 = \frac{F_1}{K_1} \tag{B.1}$$

Since there will be no load on the lower spring it will not deform and the foundation will rotate around this point. The location of this point should thus be chosen such that the model gives the correct displacements and rotations when a load is applied at mudline. The translation and rotation at mudline as a result of a lateral load applied at mudline are given by

$$u_1 = f_h \cdot F_1 \tag{B.2}$$

$$\theta_1 = f_{hr} \cdot F_1 \tag{B.3}$$

Dividing the displacement by the rotation gives the distance to the rotation centre for a lateral load:

$$l_1 + l_2 = \frac{f_h}{f_{hr}} = \frac{K_r}{K_{hr}} \tag{B.4}$$

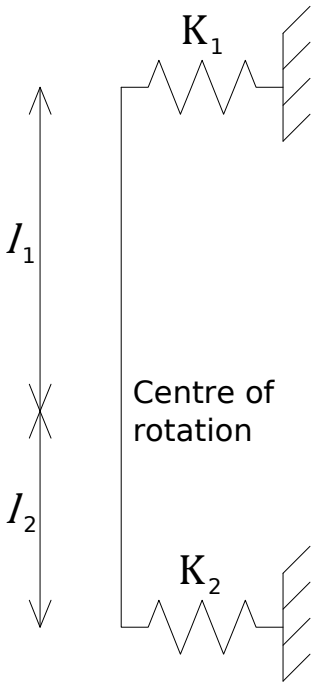

Figure B.1: *Diagram for a foundation modelled with two translational springs*

The latter follows from Equation A.6. The stiffness K_1 relates the displacement at mudline to a lateral load applied at mudline and is hence the inverse of the lateral flexibility f_h. Similar to Equation A.15 this defines K_1 as

$$K_1 = f_h^{-1} = \frac{K_h K_r - K_{hr}^2}{K_r} = K_h - \frac{K_{hr}}{l_1 + l_2} = K_h \cdot \left(1 - \frac{l_1}{l_1 + l_2}\right) = K_h \frac{l_2}{l_1 + l_2} \tag{B.5}$$

When an overturning moment is applied at mudline the foundation should rotate around the centre of rotation. This means that the displacement u_1 should be l_1/l_2 times as large as and in the opposite direction of the displacement u_2. Equilibrium of forces requires that for only an overturning moment, the loads on the two springs are equal and opposite to each other: $F_1 = -F_2$. Therefore the stiffness K_2 has to be related to K_1 as

$$K_2 = \frac{l_1}{l_2} K_1 = \frac{l_1}{l_1 + l_2} K_h \tag{B.6}$$

The rotational stiffness for this model can now be found by

$$\begin{aligned}
K_{\theta\theta} &= \frac{M}{\theta} \\
&= \frac{F_1 \cdot (l_1 + l_2)}{\frac{u_1 - u_2}{l_1 + l_2}} \\
&= \frac{F_1 \cdot (l_1 + l_2)^2}{\frac{F_1}{K_1} - \frac{F_2}{K_2}} \\
&= \frac{F_1 \cdot (l_1 + l_2)^2}{\frac{F_1}{K_1} + \frac{F_1}{K_2}} \\
&= \frac{K_1 \cdot K_2 \cdot (l_1 + l_2)^2}{K_1 + K_2} \\
&= \frac{K_1 \cdot \frac{l_1}{l_2} \cdot K_1 \cdot (l_1 + l_2)^2}{K_1 + \frac{l_1}{l_2} \cdot K_1} \\
&= l_1 \cdot K_1 \cdot (l_1 + l_2) \\
&= l_1 \cdot \left(K_h - \frac{K_{hr}}{l_1 + l_2}\right) \cdot (l_1 + l_2) \\
&= l_1 \cdot (K_h \cdot (l_1 + l_2) - K_{hr}) \\
&= \frac{K_{hr}}{K_h} \left(K_h \cdot \frac{K_r}{K_{hr}} - K_{hr}\right) \\
&= K_r - \frac{K_{hr}^2}{K_h} \\
&= K_r - K_{hr} \cdot l_1
\end{aligned} \tag{B.7}$$

This is indeed the rotational stiffness for the centre of rotation, as it is also given in Equation A.15. The models thus has both the correct lateral and rotational stiffness.

Appendix C

Environmental Load Conditions

100 Year Return Period, Coming from the South-West

Wind

Table C.1: *Design wind speed with a 100 year return period, coming from the south-west*

1 Hour average wind speed at +10 m MSL
24.4 m/s

Wave

Table C.2: *Design wave with a 100 year return period, coming from the south-west*

Maximum waveheight	Wave period
11.7 m	10.2 s

Current

Table C.3: *Design current with a 100 year return period, coming from the south-west*

Distance from mudline	Current Speed
1 %	0.63 m/s
5 %	0.81 m/s
10 %	0.90 m/s
30 %	1.06 m/s
50 %	1.14 m/s
100 %	1.27 m/s

100 Year Return Period, Coming from the West

Wind

Table C.4: *Design wind speed with a 100 year return period, coming from the west*

1 Hour average wind speed at +10 m MSL
26.1 m/s

Wave

Table C.5: *Design wave with a 100 year return period, coming from the west*

Maximum waveheight	Wave period
11.5 m	10.1 s

Current

Table C.6: *Design current with a 100 year return period, coming from the west*

Distance from mudline	Current Speed
1 %	0.13 m/s
5 %	0.17 m/s
10 %	0.18 m/s
30 %	0.22 m/s
50 %	0.23 m/s
100 %	0.26 m/s

Appendix D

Flexibility Matrix Including Caisson Interaction

$$\begin{bmatrix} u^1_{1-6} \\ u^2_{1-6} \\ u^3_{1-6} \\ u^4_{1-6} \end{bmatrix} = \begin{bmatrix} f_{11} & f_{12} & f_{13} & f_{14} \\ f_{21} & f_{22} & f_{23} & f_{24} \\ f_{31} & f_{32} & f_{33} & f_{34} \\ f_{41} & f_{42} & f_{43} & f_{44} \end{bmatrix} \cdot \begin{bmatrix} F^1_{1-6} \\ F^2_{1-6} \\ F^3_{1-6} \\ F^4_{1-6} \end{bmatrix}$$

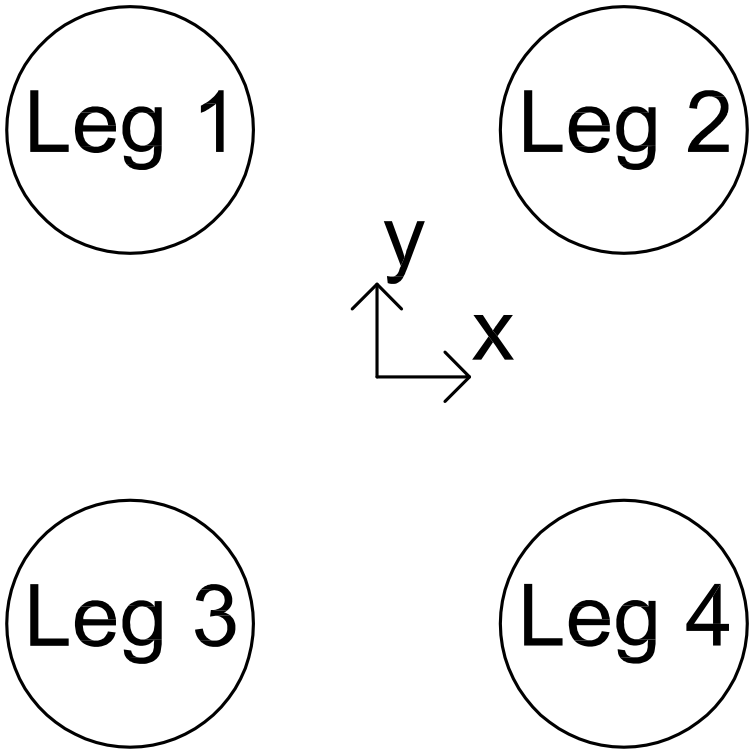

Figure D.1: *Numbering of the Caissons for the Flexibility Matrix*

Table D.1: *The Flexibility Matrix found in Plaxis*

5.55$\cdot10^{-7}$				**6.04**$\cdot10^{-8}$		**5.46**$\cdot10^{-8}$						**1.53**$\cdot10^{-8}$						**1.32**$\cdot10^{-8}$					
	5.55$\cdot10^{-7}$		**-6.04**$\cdot10^{-8}$				**1.53**$\cdot10^{-8}$						**5.46**$\cdot10^{-8}$						**1.32**$\cdot10^{-8}$				
		3.59$\cdot10^{-7}$						1.38$\cdot10^{-8}$						1.38$\cdot10^{-8}$						1.10$\cdot10^{-9}$			
	-6.04$\cdot10^{-8}$		**1.18**$\cdot10^{-8}$						8.66$\cdot10^{-11}$						-2.40$\cdot10^{-10}$						-2.26$\cdot10^{-11}$		
6.04$\cdot10^{-8}$				**1.18**$\cdot10^{-8}$						-2.40$\cdot10^{-10}$						8.66$\cdot10^{-11}$						-2.26$\cdot10^{-11}$	
					1.35$\cdot10^{-8}$																		
5.46$\cdot10^{-8}$						**5.55**$\cdot10^{-7}$				**6.04**$\cdot10^{-8}$		**1.32**$\cdot10^{-8}$						**1.53**$\cdot10^{-8}$					
	1.53$\cdot10^{-8}$						**5.55**$\cdot10^{-7}$		**-6.04**$\cdot10^{-8}$				**1.32**$\cdot10^{-8}$						**5.46**$\cdot10^{-8}$				
		1.38$\cdot10^{-8}$						**3.59**$\cdot10^{-7}$						1.10$\cdot10^{-9}$						1.38$\cdot10^{-8}$			
			8.66$\cdot10^{-11}$				**-6.04**$\cdot10^{-8}$		**1.18**$\cdot10^{-8}$						-2.26$\cdot10^{-11}$						-2.40$\cdot10^{-10}$		
				-2.40$\cdot10^{-10}$		**6.04**$\cdot10^{-8}$				**1.18**$\cdot10^{-8}$						-2.26$\cdot10^{-11}$						8.66$\cdot10^{-11}$	
											1.35$\cdot10^{-8}$												
1.53$\cdot10^{-8}$						**1.32**$\cdot10^{-8}$						**5.55**$\cdot10^{-7}$				**6.04**$\cdot10^{-8}$		**5.46**$\cdot10^{-8}$					
	5.46$\cdot10^{-8}$						**1.32**$\cdot10^{-8}$						**5.55**$\cdot10^{-7}$		**-6.04**$\cdot10^{-8}$				**1.53**$\cdot10^{-8}$				
		1.38$\cdot10^{-8}$						1.10$\cdot10^{-9}$						**3.59**$\cdot10^{-7}$						3.59$\cdot10^{-7}$			
			-2.40$\cdot10^{-10}$						-2.26$\cdot10^{-11}$				**-6.04**$\cdot10^{-8}$		**1.18**$\cdot10^{-8}$						8.66$\cdot10^{-11}$		
				8.66$\cdot10^{-11}$						-2.26$\cdot10^{-11}$		**6.04**$\cdot10^{-8}$				**1.18**$\cdot10^{-8}$						-2.40$\cdot10^{-10}$	
																	1.35$\cdot10^{-8}$						
1.32$\cdot10^{-8}$						**1.53**$\cdot10^{-8}$						**5.46**$\cdot10^{-8}$						**5.55**$\cdot10^{-7}$				**6.04**$\cdot10^{-8}$	
	1.32$\cdot10^{-8}$						**5.46**$\cdot10^{-8}$						**1.53**$\cdot10^{-8}$						**5.55**$\cdot10^{-7}$		**-6.04**$\cdot10^{-8}$		
		1.10$\cdot10^{-9}$						1.38$\cdot10^{-8}$						1.38$\cdot10^{-8}$						**3.59**$\cdot10^{-7}$			
			-2.26$\cdot10^{-11}$						-2.40$\cdot10^{-10}$						8.66$\cdot10^{-11}$				**-6.04**$\cdot10^{-8}$		**1.18**$\cdot10^{-8}$		
				-2.26$\cdot10^{-11}$						8.66$\cdot10^{-11}$						-2.40$\cdot10^{-10}$		**6.04**$\cdot10^{-8}$				**1.18**$\cdot10^{-8}$	
																							1.35$\cdot10^{-8}$

Appendix E

Results of the Sensitivity Study for the Non-Linear Models

Model 1

Table E.1: *Comparison of foundation loads for a shear modulus of 5 MPa*

Leg	Results	F_x (kN)	F_y	F_z	M_x (kNm)	M_y	M_z
	Plaxis	394.3	-237.3	1204.8	142.6	671.7	-
1	SACS	341.5	-201.6	1185.7	50.3	531.7	176.9
	Difference	*-13.4%*	*-15.0%*	*-1.6%*	*-64.7%*	*-20.9%*	-
	Plaxis	685.9	-197.5	1256.6	94.9	809.7	-
2	SACS	604.4	-206.6	1276.0	126.9	592.8	191.2
	Difference	*-11.9%*	*4.6%*	*1.5%*	*33.7%*	*-26.8%*	-
	Plaxis	255.6	263.8	-1221.2	145.3	324.4	-
3	SACS	319.6	246.7	-1190.8	70.5	538.5	248.9
	Difference	*25.0%*	*-6.5%*	*-2.5%*	*-51.5%*	*66.0%*	-
	Plaxis	664.2	171.1	-1240.3	-2.4	52.0	-
4	SACS	734.5	161.5	-1270.9	-129.0	190.3	246.4
	Difference	*10.6%*	*-5.6%*	*2.5%*	*5181.4%*	*265.8%*	-

Table E.2: *Comparison of foundation displacements for a shear modulus of 5 MPa*

Leg	Results	u_x (m)	u_y (m)	u_z (m)	θ_x (rad)	θ_y (rad)	θ_z (rad)
	Plaxis	$4.4{\cdot}10^{-3}$	$-2.7{\cdot}10^{-3}$	$3.3{\cdot}10^{-3}$	$3.5{\cdot}10^{-4}$	$6.9{\cdot}10^{-4}$	$1.5{\cdot}10^{-5}$
1	SACS	$6.1{\cdot}10^{-3}$	$-2.8{\cdot}10^{-3}$	$5.0{\cdot}10^{-3}$	$4.0{\cdot}10^{-4}$	$9.5{\cdot}10^{-4}$	$8.5{\cdot}10^{-5}$
	Difference	*37.9%*	*6.2%*	*53.7%*	*14.3%*	*37.7%*	*481.4%*

Table E.2: *(continued)*

Leg	Results	u_x (m)	u_y (m)	u_z (m)	θ_x (rad)	θ_y (rad)	θ_z (rad)
	Plaxis	$1.0{\cdot}10^{-2}$	$-2.9{\cdot}10^{-3}$	$3.6{\cdot}10^{-3}$	$4.1{\cdot}10^{-4}$	$1.5{\cdot}10^{-3}$	$-3.6{\cdot}10^{-6}$
2	SACS	$1.1{\cdot}10^{-2}$	$-3.1{\cdot}10^{-3}$	$5.4{\cdot}10^{-3}$	$4.4{\cdot}10^{-4}$	$1.8{\cdot}10^{-3}$	$9.2{\cdot}10^{-5}$
	Difference	*10.6%*	*4.1%*	*49.7%*	*7.4%*	*21.5%*	*-2643.1%*
	Plaxis	$4.1{\cdot}10^{-3}$	$3.9{\cdot}10^{-3}$	$-6.3{\cdot}10^{-3}$	$-4.9{\cdot}10^{-4}$	$6.9{\cdot}10^{-4}$	$1.8{\cdot}10^{-5}$
3	SACS	$5.7{\cdot}10^{-3}$	$3.2{\cdot}10^{-3}$	$-8.6{\cdot}10^{-3}$	$-4.4{\cdot}10^{-4}$	$8.9{\cdot}10^{-4}$	$1.2{\cdot}10^{-4}$
	Difference	*40.7%*	*-16.3%*	*36.4%*	*-10.3%*	*28.4%*	*576.1%*
	Plaxis	$1.2{\cdot}10^{-2}$	$3.0{\cdot}10^{-3}$	$-7.7{\cdot}10^{-3}$	$-4.1{\cdot}10^{-4}$	$1.7{\cdot}10^{-3}$	$3.4{\cdot}10^{-6}$
4	SACS	$1.3{\cdot}10^{-2}$	$2.4{\cdot}10^{-3}$	$-9.5{\cdot}10^{-3}$	$-3.6{\cdot}10^{-4}$	$1.9{\cdot}10^{-3}$	$1.2{\cdot}10^{-4}$
	Difference	*12.6%*	*-18.4%*	*22.7%*	*-14.1%*	*12.8%*	*3321.6%*

Table E.3: *Comparison of foundation loads for a shear modulus of 20 MPa*

Leg	Results	F_x (kN)	F_y	F_z	M_x (kNm)	M_y	M_z
	Plaxis	379.2	-217.0	1078.3	482.9	893.0	-
1	SACS	346.3	-192.3	1085.7	395.8	788.7	103.4
	Difference	*-8.7%*	*-11.4%*	*-64.7%*	*-18.0%*	*-11.7%*	-
	Plaxis	646.8	-192.4	1268.2	481.1	1698.5	-
2	SACS	583.3	-211.0	1272.0	526.5	1433.4	49.0
	Difference	*-9.8%*	*9.6%*	*33.7%*	*9.4%*	*-15.6%*	-
	Plaxis	246.1	303.8	-1083.8	-486.2	608.6	-
3	SACS	290.8	277.3	-1089.5	-412.1	733.7	166.9
	Difference	*18.2%*	*-8.7%*	*-51.5%*	*-15.2%*	*20.6%*	-
	Plaxis	728.0	105.6	-1262.8	-350.8	1260.2	-
4	SACS	779.7	125.9	-1268.2	-421.3	1252.0	96.0
	Difference	*7.1%*	*19.2%*	*5181.4%*	*20.1%*	*-0.7%*	-

Table E.4: *Comparison of foundation displacements for a shear modulus of 20 MPa*

Leg	Results	u_x (m)	u_y (m)	u_z (m)	θ_x (rad)	θ_y (rad)	θ_z (rad)
	Plaxis	$1.1{\cdot}10^{-3}$	$-7.2{\cdot}10^{-4}$	$7.5{\cdot}10^{-4}$	$1.0{\cdot}10^{-4}$	$1.8{\cdot}10^{-4}$	$3.4{\cdot}10^{-6}$
1	SACS	$1.7{\cdot}10^{-3}$	$-8.5{\cdot}10^{-4}$	$1.1{\cdot}10^{-3}$	$1.3{\cdot}10^{-4}$	$2.8{\cdot}10^{-4}$	$1.2{\cdot}10^{-5}$
	Difference	*50.4%*	*18.3%*	*53.2%*	*30.2%*	*56.1%*	*267.2%*
	Plaxis	$2.9{\cdot}10^{-3}$	$-8.9{\cdot}10^{-4}$	$9.8{\cdot}10^{-4}$	$1.4{\cdot}10^{-4}$	$4.3{\cdot}10^{-4}$	$-1.3{\cdot}10^{-6}$
2	SACS	$3.5{\cdot}10^{-3}$	$-9.8{\cdot}10^{-4}$	$1.4{\cdot}10^{-3}$	$1.5{\cdot}10^{-4}$	$5.9{\cdot}10^{-4}$	$5.9{\cdot}10^{-6}$
	Difference	*20.5%*	*10.7%*	*38.4%*	*13.4%*	*35.5%*	*-548.9%*

Table E.4: *(continued)*

Leg	Results	u_x (m)	u_y (m)	u_z (m)	θ_x (rad)	θ_y (rad)	θ_z (rad)
	Plaxis	$9.4{\cdot}10^{-4}$	$1.2{\cdot}10^{-3}$	$-1.1{\cdot}10^{-3}$	$-1.7{\cdot}10^{-4}$	$1.6{\cdot}10^{-4}$	$4.7{\cdot}10^{-6}$
3	SACS	$1.4{\cdot}10^{-3}$	$1.2{\cdot}10^{-3}$	$-1.9{\cdot}10^{-3}$	$-1.8{\cdot}10^{-4}$	$2.3{\cdot}10^{-4}$	$2.0{\cdot}10^{-5}$
	Difference	*53.2%*	*-0.7%*	*73.5%*	*6.4%*	*46.6%*	*321.4%*
	Plaxis	$4.0{\cdot}10^{-3}$	$7.0{\cdot}10^{-4}$	$-1.8{\cdot}10^{-3}$	$-1.0{\cdot}10^{-4}$	$6.2{\cdot}10^{-4}$	$2.3{\cdot}10^{-7}$
4	SACS	$4.7{\cdot}10^{-3}$	$6.3{\cdot}10^{-4}$	$-2.4{\cdot}10^{-3}$	$-1.0{\cdot}10^{-4}$	$7.7{\cdot}10^{-4}$	$1.2{\cdot}10^{-5}$
	Difference	*18.2%*	*-10.0%*	*31.7%*	*0.8%*	*23.9%*	*4917.2%*

Table E.5: *Comparison of foundation loads for a shear modulus of 240 MPa*

Leg	Results	F_x (kN)	F_y	F_z	M_x (kNm)	M_y	M_z
	Plaxis	367.5	-149.8	925.7	451.2	962.6	-
1	SACS	368.6	-144.9	946.8	433.0	961.0	54.0
	Difference	*0.3%*	*-3.2%*	*2.3%*	*-4.0%*	*-0.2%*	-
	Plaxis	454.1	-178.8	1367.8	619.1	1702.8	-
2	SACS	426.5	-192.5	1350.0	661.9	1573.0	-42.2
	Difference	*-6.1%*	*7.6%*	*-1.3%*	*6.9%*	*-7.6%*	-
	Plaxis	179.2	341.0	-927.6	-806.8	548.7	-
3	SACS	190.6	349.8	-949.4	-808.8	599.6	93.3
	Difference	*6.4%*	*2.6%*	*2.4%*	*0.3%*	*9.3%*	-
	Plaxis	999.3	-12.4	-1365.8	-217.7	2448.5	-
4	SACS	1014.3	-12.4	-1347.4	-224.4	2452.9	-11.8
	Difference	*1.5%*	*0.4%*	*-1.4%*	*3.1%*	*0.2%*	-

Table E.6: *Comparison of foundation displacements for a shear modulus of 240 MPa*

Leg	Results	u_x (m)	u_y (m)	u_z (m)	θ_x (rad)	θ_y (rad)	θ_z (rad)
	Plaxis	$1.2{\cdot}10^{-4}$	$-5.5{\cdot}10^{-5}$	$7.3{\cdot}10^{-5}$	$8.3{\cdot}10^{-6}$	$1.9{\cdot}10^{-5}$	$2.4{\cdot}10^{-7}$
1	SACS	$1.6{\cdot}10^{-4}$	$-5.9{\cdot}10^{-5}$	$8.5{\cdot}10^{-5}$	$9.4{\cdot}10^{-6}$	$2.7{\cdot}10^{-5}$	$5.0{\cdot}10^{-7}$
	Difference	*38.1%*	*6.9%*	*16.3%*	*13.0%*	*43.4%*	*104.8%*
	Plaxis	$2.1{\cdot}10^{-4}$	$-8.1{\cdot}10^{-5}$	$1.2{\cdot}10^{-4}$	$1.3{\cdot}10^{-5}$	$3.4{\cdot}10^{-5}$	$-1.1{\cdot}10^{-7}$
2	SACS	$2.3{\cdot}10^{-4}$	$-8.3{\cdot}10^{-5}$	$1.2{\cdot}10^{-4}$	$1.4{\cdot}10^{-5}$	$3.9{\cdot}10^{-5}$	$-4.0{\cdot}10^{-7}$
	Difference	*10.4%*	*2.3%*	*2.3%*	*0.8%*	*15.5%*	*257.8%*
	Plaxis	$6.9{\cdot}10^{-5}$	$1.4{\cdot}10^{-4}$	$-1.0{\cdot}10^{-4}$	$9.2{\cdot}10^{-8}$	$-3.1{\cdot}10^{-6}$	$-1.9{\cdot}10^{-5}$
3	SACS	$8.0{\cdot}10^{-5}$	$1.5{\cdot}10^{-4}$	$-1.3{\cdot}10^{-4}$	$-2.4{\cdot}10^{-5}$	$1.3{\cdot}10^{-5}$	$9.0{\cdot}10^{-7}$
	Difference	*14.9%*	*6.6%*	*30.9%*	*-25939.9%*	*-510.9%*	*-104.6%*

Table E.6: *(continued)*

Leg	Results	u_x (m)	u_y (m)	u_z (m)	θ_x (rad)	θ_y (rad)	θ_z (rad)
	Plaxis	$7.2{\cdot}10^{-4}$	$1.2{\cdot}10^{-5}$	$-2.7{\cdot}10^{-4}$	$-6.4{\cdot}10^{-7}$	$1.2{\cdot}10^{-4}$	$-1.5{\cdot}10^{-7}$
4	SACS	$8.4{\cdot}10^{-4}$	$5.2{\cdot}10^{-6}$	$-2.2{\cdot}10^{-4}$	$-1.3{\cdot}10^{-6}$	$1.5{\cdot}10^{-4}$	$-1.0{\cdot}10^{-7}$
	Difference	*16.2%*	*-56.0%*	*-17.9%*	*103.1%*	*25.6%*	*-32.4%*

Model 2

Table E.7: *Comparison of foundation loads for a shear modulus of 5 MPa*

Leg	Results	F_x (kN)	F_y	F_z	M_x (kNm)	M_y	M_z
	Plaxis	394.3	-237.3	1204.8	142.6	671.7	-
1	SACS	350.8	-211.1	1209.0	49.7	481.7	196.4
	Difference	*-11.0%*	*-11.0%*	*0.3%*	*-65.2%*	*-28.3%*	-
	Plaxis	685.9	-197.5	1256.6	94.9	809.7	-
2	SACS	604.9	-215.4	1274.6	118.2	420.4	225.5
	Difference	*-11.8%*	*9.1%*	*1.4%*	*24.6%*	*-48.1%*	-
	Plaxis	255.6	263.8	-1221.2	145.3	324.4	-
3	SACS	332.3	253.0	-1213.6	68.1	483.1	262.4
	Difference	*30.0%*	*-4.1%*	*-0.6%*	*-53.2%*	*48.9%*	-
	Plaxis	664.2	171.1	-1240.3	-2.4	52.0	-
4	SACS	712.1	173.5	-1270.1	-129.0	-28.8	273.4
	Difference	*7.2%*	*1.4%*	*2.4%*	*5180.2%*	*-155.3%*	-

Table E.8: *Comparison of foundation displacements for a shear modulus of 5 MPa*

Leg	Results	u_x (m)	u_y (m)	u_z (m)	θ_x (rad)	θ_y (rad)	θ_z (rad)
	Plaxis	$4.4{\cdot}10^{-3}$	$-2.7{\cdot}10^{-3}$	$3.3{\cdot}10^{-3}$	$3.5{\cdot}10^{-4}$	$6.9{\cdot}10^{-4}$	$1.5{\cdot}10^{-5}$
1	SACS	$6.7{\cdot}10^{-3}$	$-3.1{\cdot}10^{-3}$	$5.1{\cdot}10^{-3}$	$4.3{\cdot}10^{-4}$	$1.0{\cdot}10^{-3}$	$9.4{\cdot}10^{-5}$
	Difference	*52.0%*	*14.6%*	*56.9%*	*22.1%*	*49.4%*	*545.2%*
	Plaxis	$1.0{\cdot}10^{-2}$	$-2.9{\cdot}10^{-3}$	$3.6{\cdot}10^{-3}$	$4.1{\cdot}10^{-4}$	$1.5{\cdot}10^{-3}$	$-3.6{\cdot}10^{-6}$
2	SACS	$1.3{\cdot}10^{-2}$	$-3.3{\cdot}10^{-3}$	$5.4{\cdot}10^{-3}$	$4.8{\cdot}10^{-4}$	$1.9{\cdot}10^{-3}$	$1.1{\cdot}10^{-4}$
	Difference	*29.4%*	*12.1%*	*49.6%*	*15.6%*	*30.4%*	*-3101.7%*
	Plaxis	$4.1{\cdot}10^{-3}$	$3.9{\cdot}10^{-3}$	$-6.3{\cdot}10^{-3}$	$-4.9{\cdot}10^{-4}$	$6.9{\cdot}10^{-4}$	$1.8{\cdot}10^{-5}$
3	SACS	$6.3{\cdot}10^{-3}$	$3.5{\cdot}10^{-3}$	$-8.9{\cdot}10^{-3}$	$-4.7{\cdot}10^{-4}$	$9.7{\cdot}10^{-4}$	$1.3{\cdot}10^{-4}$
	Difference	*55.1%*	*-9.2%*	*40.3%*	*-5.9%*	*40.1%*	*613.6%*

Table E.8: *(continued)*

Leg	Results	u_x (m)	u_y (m)	u_z (m)	θ_x (rad)	θ_y (rad)	θ_z (rad)
	Plaxis	$1.2{\cdot}10^{-2}$	$3.0{\cdot}10^{-3}$	$-7.7{\cdot}10^{-3}$	$-4.1{\cdot}10^{-4}$	$1.7{\cdot}10^{-3}$	$3.4{\cdot}10^{-6}$
4	SACS	$1.5{\cdot}10^{-2}$	$2.6{\cdot}10^{-3}$	$-9.5{\cdot}10^{-3}$	$-3.9{\cdot}10^{-4}$	$2.0{\cdot}10^{-3}$	$1.3{\cdot}10^{-4}$
	Difference	*30.3%*	*-11.6%*	*22.6%*	*-6.0%*	*19.4%*	*3698.9%*

Table E.9: *Comparison of foundation loads for a shear modulus of 20 MPa*

Leg	Results	F_x (kN)	F_y	F_z	M_x (kNm)	M_y	M_z
	Plaxis	379.2	-217.0	1078.3	482.9	893.0	-
1	SACS	353.7	-201.8	1110.9	402.3	781.4	116.6
	Difference	*-6.7%*	*-7.0%*	*-65.2%*	*-16.7%*	*-12.5%*	-
	Plaxis	646.8	-192.4	1268.2	481.1	1698.5	-
2	SACS	591.3	-220.4	1259.1	527.8	1334.6	72.5
	Difference	*-8.6%*	*14.5%*	*24.6%*	*9.7%*	*-21.4%*	-
	Plaxis	246.1	303.8	-1083.8	-486.2	608.6	-
3	SACS	304.6	281.8	-1114.5	-405.7	734.8	177.7
	Difference	*23.8%*	*-7.2%*	*-53.2%*	*-16.6%*	*20.7%*	-
	Plaxis	728.0	105.6	-1262.8	-350.8	1260.2	-
4	SACS	750.4	140.4	-1255.5	-441.0	1079.5	114.1
	Difference	*3.1%*	*32.9%*	*5180.2%*	*25.7%*	*-14.3%*	-

Table E.10: *Comparison of foundation displacements for a shear modulus of 20 MPa*

Leg	Results	u_x (m)	u_y (m)	u_z (m)	θ_x (rad)	θ_y (rad)	θ_z (rad)
	Plaxis	$1.1{\cdot}10^{-3}$	$-7.2{\cdot}10^{-4}$	$7.5{\cdot}10^{-4}$	$1.0{\cdot}10^{-4}$	$1.8{\cdot}10^{-4}$	$3.4{\cdot}10^{-6}$
1	SACS	$1.9{\cdot}10^{-3}$	$-9.3{\cdot}10^{-4}$	$1.2{\cdot}10^{-3}$	$1.5{\cdot}10^{-4}$	$3.1{\cdot}10^{-4}$	$1.4{\cdot}10^{-5}$
	Difference	*68.5%*	*30.1%*	*57.1%*	*49.0%*	*74.0%*	*314.5%*
	Plaxis	$2.9{\cdot}10^{-3}$	$-8.9{\cdot}10^{-4}$	$9.8{\cdot}10^{-4}$	$1.4{\cdot}10^{-4}$	$4.3{\cdot}10^{-4}$	$-1.3{\cdot}10^{-6}$
2	SACS	$4.4{\cdot}10^{-3}$	$-1.1{\cdot}10^{-3}$	$1.3{\cdot}10^{-3}$	$1.8{\cdot}10^{-4}$	$6.7{\cdot}10^{-4}$	$8.7{\cdot}10^{-6}$
	Difference	*50.3%*	*22.0%*	*36.9%*	*30.0%*	*55.2%*	*-762.0%*
	Plaxis	$9.4{\cdot}10^{-4}$	$1.2{\cdot}10^{-3}$	$-1.1{\cdot}10^{-3}$	$-1.7{\cdot}10^{-4}$	$1.6{\cdot}10^{-4}$	$4.7{\cdot}10^{-6}$
3	SACS	$1.6{\cdot}10^{-3}$	$1.3{\cdot}10^{-3}$	$-2.0{\cdot}10^{-3}$	$-2.0{\cdot}10^{-4}$	$2.6{\cdot}10^{-4}$	$2.1{\cdot}10^{-5}$
	Difference	*71.9%*	*8.6%*	*79.8%*	*17.5%*	*66.5%*	*348.8%*
	Plaxis	$4.0{\cdot}10^{-3}$	$7.0{\cdot}10^{-4}$	$-1.8{\cdot}10^{-3}$	$-1.0{\cdot}10^{-4}$	$6.2{\cdot}10^{-4}$	$2.3{\cdot}10^{-7}$
4	SACS	$5.7{\cdot}10^{-3}$	$6.9{\cdot}10^{-4}$	$-2.3{\cdot}10^{-3}$	$-1.2{\cdot}10^{-4}$	$8.4{\cdot}10^{-4}$	$1.4{\cdot}10^{-5}$
	Difference	*42.7%*	*-0.8%*	*29.9%*	*19.0%*	*35.2%*	*5877.0%*

Table E.11: *Comparison of foundation loads for a shear modulus of 240 MPa*

Leg	Results	F_x (kN)	F_y	F_z	M_x (kNm)	M_y	M_z
	Plaxis	367.5	-149.8	925.7	451.2	962.6	-
1	SACS	369.3	-147.6	953.9	439.8	962.5	55.4
	Difference	*0.5%*	*-1.5%*	*3.1%*	*-2.5%*	*0.0%*	-
	Plaxis	454.1	-178.8	1367.8	619.1	1702.8	-
2	SACS	451.4	-195.3	1343.1	667.7	1623.0	-41.5
	Difference	*-0.6%*	*9.2%*	*-1.8%*	*7.9%*	*-4.7%*	-
	Plaxis	179.2	341.0	-927.6	-806.8	548.7	-
3	SACS	195.5	350.2	-956.6	-808.2	610.8	95.4
	Difference	*9.1%*	*2.7%*	*3.1%*	*0.2%*	*11.3%*	-
	Plaxis	999.3	-12.4	-1365.8	-217.7	2448.5	-
4	SACS	983.9	-7.4	-1340.4	-236.8	2385.1	-9.4
	Difference	*-1.5%*	*-40.2%*	*-1.9%*	*8.8%*	*-2.6%*	-

Table E.12: *Comparison of foundation displacements for a shear modulus of 240 MPa*

Leg	Results	u_x (m)	u_y (m)	u_z (m)	θ_x (rad)	θ_y (rad)	θ_z (rad)
	Plaxis	$1.2{\cdot}10^{-4}$	$-5.5{\cdot}10^{-5}$	$7.3{\cdot}10^{-5}$	$8.3{\cdot}10^{-6}$	$1.9{\cdot}10^{-5}$	$2.4{\cdot}10^{-7}$
1	SACS	$1.8{\cdot}10^{-4}$	$-6.0{\cdot}10^{-5}$	$8.6{\cdot}10^{-5}$	$1.0{\cdot}10^{-5}$	$2.9{\cdot}10^{-5}$	$6.0{\cdot}10^{-7}$
	Difference	*51.3%*	*9.7%*	*18.2%*	*23.9%*	*55.1%*	*145.7%*
	Plaxis	$2.1{\cdot}10^{-4}$	$-8.1{\cdot}10^{-5}$	$1.2{\cdot}10^{-4}$	$1.3{\cdot}10^{-5}$	$3.4{\cdot}10^{-5}$	$-1.1{\cdot}10^{-7}$
2	SACS	$2.9{\cdot}10^{-4}$	$-8.8{\cdot}10^{-5}$	$1.2{\cdot}10^{-4}$	$1.5{\cdot}10^{-5}$	$4.7{\cdot}10^{-5}$	$-4.0{\cdot}10^{-7}$
	Difference	*37.3%*	*8.5%*	*2.5%*	*12.8%*	*37.7%*	*257.8%*
	Plaxis	$6.9{\cdot}10^{-5}$	$1.4{\cdot}10^{-4}$	$-1.0{\cdot}10^{-4}$	$9.2{\cdot}10^{-8}$	$-3.1{\cdot}10^{-6}$	$-1.9{\cdot}10^{-5}$
3	SACS	$8.6{\cdot}10^{-5}$	$1.6{\cdot}10^{-4}$	$-1.3{\cdot}10^{-4}$	$-2.6{\cdot}10^{-5}$	$1.5{\cdot}10^{-5}$	$1.0{\cdot}10^{-6}$
	Difference	*23.3%*	*16.9%*	*32.5%*	*-28229.5%*	*-565.4%*	*-105.1%*
	Plaxis	$7.2{\cdot}10^{-4}$	$1.2{\cdot}10^{-5}$	$-2.7{\cdot}10^{-4}$	$-6.4{\cdot}10^{-7}$	$1.2{\cdot}10^{-4}$	$-1.5{\cdot}10^{-7}$
4	SACS	$1.0{\cdot}10^{-3}$	$7.2{\cdot}10^{-6}$	$-2.2{\cdot}10^{-4}$	$-2.1{\cdot}10^{-6}$	$1.5{\cdot}10^{-4}$	$-1.0{\cdot}10^{-7}$
	Difference	*38.8%*	*-38.8%*	*-18.1%*	*228.1%*	*26.8%*	*-32.4%*

Appendix F

MatLab and SACS code

F.1 Matlab code

codewriter.m

```
clear all
close all
clc

%% Input
% Density
gamma = 0; % kN/m^3
% Youngs Modulus
E = 210*10^6; % kN/m^2
% Poison's ratio
nu = 0.3;
% Output file name
outputname = 'plaxiscodewodeadweight.txt';
%% Read data
% read joints
fid = fopen('joints.txt');
jointscoor = fscanf(fid,'%*s %*s %f %f %f',[3,inf]);
fclose(fid);

jointscoor = jointscoor';

fid = fopen('joints.txt');
i = 1;
while 1
    tline = fgetl(fid);
    if ~ischar(tline), break, end %while loop ends when fgetl return
        -1 (which is not a character) after last line
    cleanup = sscanf(tline,'%*6c %4c %*22c'); % removes all text but
        joint name
```

```
28      cleanup(cleanup == '-') = []; % removes minus signs
29      cleanup = sscanf(cleanup,'%s'); % removes space characters
30      jointsname{i,1} = cleanup;
31      i = i + 1;
32  end
33
34  fclose(fid);
35
36  % read members
37  fid = fopen('members.txt');
38  i = 1;
39  while 1
40      tline = fgetl(fid);
41      if ~ischar(tline), break, end
42      cleanup = sscanf(tline,'%*7c %12c'); % removes first chars
43      joint1 = sscanf(cleanup,'%4c %*8c'); % first joint name
44      joint1 = sscanf(joint1,'%s'); % removes space characters
45      joint2 = sscanf(cleanup,'%*4c %4c %*4c'); % second joint name
46      joint2 = sscanf(joint2,'%s'); % removes space characters
47      groupname = sscanf(cleanup,'%*9c %3c'); % group name
48
49      members{i,1} = joint1;
50      members{i,2} = joint2;
51      members{i,3} = groupname;
52      i = i + 1;
53  end
54  fclose(fid);
55
56  % read groups
57  fid = fopen('groups.txt');
58  i = 1;
59  while 1
60      tline = fgetl(fid);
61      if ~ischar(tline), break, end
62      cleanup = sscanf(tline,'%*5c %11c %*64c'); % removes first chars
63      groupname = sscanf(cleanup,'%3c %*8c'); % group name
64      sectionname = sscanf(cleanup,'%*4c %7c'); % section name
65
66
67      groups{i,1} = groupname;
68      groups{i,2} = sectionname;
69      i = i + 1;
70  end
71  fclose(fid);
72
73
74  % read sections
75  fid = fopen('sections.txt');
76  i = 1;
77  while 1
78      tline = fgetl(fid);
79      if ~ischar(tline), break, end
80      cleanup = sscanf(tline,'%*5c %55c'); % removes first chars
```

```
81      sectionname = sscanf(cleanup,'%7c %*48c'); % section name
82      diameter = sscanf(cleanup,'%*44c %6c %*5c'); % diameter (cm)
83      diameter = sscanf(diameter,'%f');
84      thickness = sscanf(cleanup,'%*50c %f'); % wall thickness (cm)
85
86
87      sections{i,1} = sectionname;
88      sections{i,2} = diameter;
89      sections{i,3} = thickness;
90      i = i + 1;
91  end
92  fclose(fid);
93
94  %% Datamining
95  membercoor = zeros(size(members,1),6); % joint coordinates for all
        members
96  for i = 1:size(membercoor,1)
97      comp1 = strcmpi(members{i,1},jointsname); % looks for match in
            name of joint 1
98      [~, loc1] = max(comp1);                   % determines location of
            match
99      membercoor(i,1:3) = jointscoor(loc1,:);   % writes joint
            coordinates to matrix
100
101     comp2 = strcmpi(members{i,2},jointsname);
102     [~, loc2] = max(comp2);
103     membercoor(i,4:6) = jointscoor(loc2,:);
104 end
105
106 membercrosssection = zeros(size(members,1),2); % diameter and wall
        thickness for all members
107 for i = 1:size(membercoor,1)
108     comp1 = strcmpi(members{i,3},groups(:,1)); % looks for match in
            name of group
109     [~, loc1] = max(comp1);                   % determines location of
            match
110
111     comp2 = strcmpi(groups{loc1,2},sections(:,1)); % looks for match
            in name of section
112     [~, loc2] = max(comp2);
113     membercrosssection(i,1) = sections{loc2,2}; % writes diameter
114     membercrosssection(i,2) = sections{loc2,3}; % writes wall
            thickness
115 end
116
117 memberprops = zeros(size(membercrosssection,1),4);
118 memberprops(:,1) = 1:size(membercrosssection,1);
119 innerdiameter = membercrosssection(:,1)-2*membercrosssection(:,2);
120 memberprops(:,2) = pi/4*((membercrosssection(:,1)).^2-(innerdiameter)
        .^2)*10^-4; %area
121 memberprops(:,3) = pi/4*0.5^4*((membercrosssection(:,1)).^4-(
        innerdiameter).^4)*10^-8; %area moment of inertia 1
122 memberprops(:,4) = memberprops(:,3);
```

```
123
124 %% Print Plaxis input code
125 fid = fopen(outputname,'w');
126 fprintf(fid,'_beam (%f %f %f) (%f %f %f)\n',membercoor'); %writes code
      for creating beams
127 fprintf(fid,'\n'); % white line
128 materialprops = sprintf('"w" %5.3f "E" %10.1f',[gamma E]);
129 materialprops2 = sprintf('"nu" %3.2f',nu);
130 fprintf(fid,['_beammat "Comments" "" "MaterialName" "BeamCrosssection%
      i" "Colour" 16721123 "MaterialNumber" 0 "LoadCaseRef0" "" "
      LoadCaseRef1" "" "LoadCaseRef2" "" "LoadCaseRef3" "" "LoadCaseRef4"
       "" "LoadCaseRef5" "" "LoadCaseRef6" "" "LoadCaseRef7" "" "
      LoadCaseRef8" "" "LoadCaseRef9" "" "IsLinear" True "NormalX" 0 "
      NormalY" 1 "NormalZ" 0 "XYListNEpsilon" "[-0.01, 0, 0, 0, 0.01, 0]"
       "XYListMYYKappa" "[-0.01, 0, 0, 0, 0.01, 0]" "XYListMZZKappa"
      "[-0.01, 0, 0, 0, 0.01, 0]" "A" %f ',materialprops,' "Iyy" %f "Izz"
       %f "Iyz" 0 ',materialprops2,' "RayleighAlpha" 0 "RayleighBeta" 0\n
      ',memberprops'); %writes code for beam cross sections
131 fprintf(fid,'\n'); % white line
132 fprintf(fid,'_set Beam_%i.Material BeamCrosssection%i\n',[memberprops
      (:,1) memberprops(:,1)]'); % code for assigning materials to beams
133 fclose(fid);
```

processing.m

```
1 clear all
2 close all
3 clc
4
5 %% input
6 % bucket dimensions
7 D = 7;
8
9 % loads
10 Fh = 200;
11 Fv = 200;
12 M = 700;
13 T = 350;
14
15 % Load-displacement data
16 data = xlsread('Step9ML.xlsx'); % u-F: ux W-E, uy W-E, uz W-E, uy N-S,
      uz N-S
17
18 %% processing
19 lddata = cell(28,1); % cell array containing the l-d data for each
      load phase
20 % 4 legs: Fx, Fy, Fz (uplift for A1 and A2, comp for B1 and B2), Mx,
      My, T
21
22 splits = ones(size(lddata));
23 i = 2;
24
25 % determine where load phases are located
```

```
26 for j = 2:size(data,1)-1
27         if data(j,2) == 1 && data(j+1,2) ~= 1
28             splits(i) = j; % store row at which new load phase starts
29             i = i+1;
30
31             data(j,2) = 0;   % set m_stage to 0 at start of new load
                   phase
32             data(j,4) = 0;   % this is already correct for first load
                   phase
33             data(j,6) = 0;
34             data(j,8) = 0;
35             data(j,10) = 0;
36             data(j,12) = 0;
37             data(j,14) = 0;
38             data(j,16) = 0;
39             data(j,18) = 0;
40             data(j,20) = 0;
41         end
42 end
43
44 % store each load phase in different cell
45 for i = 1:size(lddata,1)
46     if i ~= size(lddata,1)
47         lddata{i} = data(splits(i):splits(i+1)-1,:);
48     else
49         lddata{i} = data(splits(i):end,:);
50     end
51 end
52
53 fvals = zeros(10,4); % fx; frx; fy; fry; fz; fyr; frrx; fxr; frry; ft;
54 Rsq = zeros(size(fvals)); % R squared values
55
56 % determine compliance matrix terms
57 for i = 1:size(lddata,1)
58    j = fix((i-1)/7)+1; % leg number (cols in fvals)
59    k = rem(i-1,7); % load phase
60
61    if k == 1
62        ux = 0.5*(lddata{i}(:,1)+lddata{i}(:,3));
63        thy = (lddata{i}(:,9)-lddata{i}(:,11))/D;
64        F = lddata{i}(:,2)*Fh;
65
66        fvals(1,j) = sum(ux)/sum(F); % gives a curve fit through origin
67        fvals(2,j) = sum(thy)/sum(F);
68
69        s1ux = sum((ux - F*fvals(1,j)).^2);
70        s2ux = sum((ux - mean(ux)).^2);
71        Rsq(1,j) = 1 - s1ux/s2ux;
72
73        s1th = sum((thy - F*fvals(2,j)).^2);
74        s2th = sum((thy - mean(thy)).^2);
75        Rsq(2,j) = 1 - s1th/s2th;
76
```

```
77          % if Rsq smaller than 0.95 create plot with position in Rsq in
78          % title
79
80          if Rsq(1,j) < 0.95
81              figure
82              plot(ux,F,ux,ux/fvals(1,j))
83              title(sprintf('row 1, col %i',j))
84          end
85
86          if Rsq(2,j) < 0.95
87              figure
88              plot(thy,F,thy,thy/fvals(2,j))
89              title(sprintf('row 2, col %i',j))
90          end
91
92      elseif k == 2
93          uy = abs(0.5*(lddata{i}(:,13)+lddata{i}(:,15)));
94          thx = abs((lddata{i}(:,17)-lddata{i}(:,19))/D);
95          F = lddata{i}(:,2)*Fh;
96
97          fvals(3,j) = sum(uy)/sum(F);
98          fvals(4,j) = sum(thx)/sum(F);
99
100         s1uy = sum((uy - F*fvals(3,j)).^2);
101         s2uy = sum((uy - mean(uy)).^2);
102         Rsq(3,j) = 1 - s1uy/s2uy;
103
104         s1th = sum((thx - F*fvals(4,j)).^2);
105         s2th = sum((thx - mean(thx)).^2);
106         Rsq(4,j) = 1 - s1th/s2th;
107
108         % if Rsq smaller than 0.95 create plot with position in Rsq in
109         % title
110
111         if Rsq(3,j) < 0.95
112             figure
113             plot(uy,F,uy,uy/fvals(3,j))
114             title(sprintf('row 3, col %i',j))
115         end
116
117         if Rsq(4,j) < 0.95
118             figure
119             plot(thx,F,thx,thx/fvals(4,j))
120             title(sprintf('row 4, col %i',j))
121         end
122
123     elseif k == 3
124         uz = abs(0.5*(lddata{i}(:,9)+lddata{i}(:,11)));
125         F = lddata{i}(:,2)*Fv;
126
127         fvals(5,j) = sum(uz)/sum(F);
128
129         s1uz = sum((uz - F*fvals(5,j)).^2);
```

```
130         s2uz = sum((uz - mean(uz)).^2);
131         Rsq(5,j) = 1 - s1uz/s2uz;
132
133         if Rsq(5,j) < 0.95
134             figure
135             plot(uz,F,uz,uz/fvals(5,j))
136             title(sprintf('row 5, col %i',j))
137         end
138
139     elseif k == 4
140          uy = abs(0.5*(lddata{i}(:,13)+lddata{i}(:,15)));
141         thx = abs((lddata{i}(:,17)-lddata{i}(:,19))/D);
142         F = lddata{i}(:,2)*M;
143
144         fvals(6,j) = sum(uy)/sum(F);
145         fvals(7,j) = sum(thx)/sum(F);
146
147         s1uy = sum((uy - F*fvals(6,j)).^2);
148         s2uy = sum((uy - mean(uy)).^2);
149         Rsq(6,j) = 1 - s1uy/s2uy;
150
151         s1th = sum((thx - F*fvals(7,j)).^2);
152         s2th = sum((thx - mean(thx)).^2);
153         Rsq(7,j) = 1 - s1th/s2th;
154
155
156         if Rsq(6,j) < 0.95
157             figure
158             plot(uy,F,uy,uy/fvals(6,j))
159             title(sprintf('row 6, col %i',j))
160         end
161
162         if Rsq(7,j) < 0.95
163             figure
164             plot(thx,F,thx,thx/fvals(7,j))
165             title(sprintf('row 7, col %i',j))
166         end
167
168     elseif k == 5
169
170         ux = 0.5*(lddata{i}(:,1)+lddata{i}(:,3));
171         thy = (lddata{i}(:,9)-lddata{i}(:,11))/D;
172         F = lddata{i}(:,2)*M;
173
174         fvals(8,j) = sum(ux)/sum(F);
175         fvals(9,j) = sum(thy)/sum(F);
176
177         s1ux = sum((ux - F*fvals(8,j)).^2);
178         s2ux = sum((ux - mean(ux)).^2);
179         Rsq(8,j) = 1 - s1ux/s2ux;
180
181         s1th = sum((thy - F*fvals(9,j)).^2);
182         s2th = sum((thy - mean(thy)).^2);
```

```
183         Rsq(9,j) = 1 - s1th/s2th;
184
185         if Rsq(8,j) < 0.95
186             figure
187             plot(ux,F,ux,ux/fvals(8,j))
188             title(sprintf('row 8, col %i',j))
189         end
190
191         if Rsq(9,j) < 0.95
192             figure
193             plot(thy,F,thy,thy/fvals(9,j))
194             title(sprintf('row 9, col %i',j))
195         end
196
197     elseif k == 6
198         thz = abs((lddata{i}(:,5)-lddata{i}(:,7))/D);
199         F = lddata{i}(:,2)*T;
200
201         fvals(10,j) = sum(thz)/sum(F);
202
203         s1th = sum((thz - F*fvals(10,j)).^2);
204         s2th = sum((thz - mean(thz)).^2);
205         Rsq(10,j) = 1 - s1th/s2th;
206
207         if Rsq(10,j) < 0.95
208             figure
209             plot(thz,F,thz,thz/fvals(10,j))
210             title(sprintf('row 10, col %i',j))
211         end
212     end
213 end
214
215 % compose and invert matrices
216 k = 1;
217 fA1 = [fvals(1,k) 0 0 0 fvals(8,k) 0; 0 fvals(3,k) 0 -fvals(6,k) 0 0;
       0 0 fvals(5,k) 0 0 0; 0 -fvals(4,k) 0 fvals(7,k) 0 0; fvals(2,k) 0
       0 0 fvals(9,k) 0; 0 0 0 0 0 fvals(10,k)];
218
219 k = 2;
220 fA2 = [fvals(1,k) 0 0 0 fvals(8,k) 0; 0 fvals(3,k) 0 -fvals(6,k) 0 0;
       0 0 fvals(5,k) 0 0 0; 0 -fvals(4,k) 0 fvals(7,k) 0 0; fvals(2,k) 0
       0 0 fvals(9,k) 0; 0 0 0 0 0 fvals(10,k)];
221
222 k = 3;
223 fB1 = [fvals(1,k) 0 0 0 fvals(8,k) 0; 0 fvals(3,k) 0 -fvals(6,k) 0 0;
       0 0 fvals(5,k) 0 0 0; 0 -fvals(4,k) 0 fvals(7,k) 0 0; fvals(2,k) 0
       0 0 fvals(9,k) 0; 0 0 0 0 0 fvals(10,k)];
224
225 k = 4;
226 fB2 = [fvals(1,k) 0 0 0 fvals(8,k) 0; 0 fvals(3,k) 0 -fvals(6,k) 0 0;
       0 0 fvals(5,k) 0 0 0; 0 -fvals(4,k) 0 fvals(7,k) 0 0; fvals(2,k) 0
       0 0 fvals(9,k) 0; 0 0 0 0 0 fvals(10,k)];
227
```

```
228 KA1 = fA1^-1;
229 KA2 = fA2^-1;
230 KB1 = B1^-1;
231 KB2 = fB2^-1;
232 %% output
233 KA1
234 KA2
235 KB1
236 KB2
```

plaxiscode.m

```
1  clear all
2  close all
3  clc
4
5  %% Input
6
7  stepNr = 'Step 9';
8  startPhase = 246; % for stiffness determination steps! First initial
       step = startPhase-4
9  diameter = 7;
10
11 % Mstages
12 Fx = 200;
13 Fy = 200;
14 Fz = 200;
15 Mx = 700;
16 My = 700;
17 T = 350;
18
19 %% Load data
20 xlname = ['loaddata ',stepNr,'.xlsx'];
21 data = xlsread(xlname);
22
23 PlaxisMoments = data(:,4:6)/diameter;
24 PlaxisMoments(:,3) = PlaxisMoments(:,3)/2;
25
26 Outputname = ['Plaxiscode ',stepNr,'.txt'];
27
28 %% Create Initial steps
29 fid = fopen(Outputname,'w');
30 for i = 1:4
31     fprintf(fid,'setcurrentphase Phase_8\n phase Phase_8\n'); %
          creates phase starting from phase 8
32     fprintf(fid,'setcurrentphase Phase_%i\n sps Phase_%i "
          PreviousPhase" Phase_8\n',(startPhase-5+i)*ones(2,1));
33     % load
34         fprintf(fid,'activate PointLoad_1 Phase_%i\n',startPhase-5+i);
35         fprintf(fid,'activate PointLoad_6 Phase_%i\n',startPhase-5+i);
36         fprintf(fid,'activate PointLoad_7 Phase_%i\n',startPhase-5+i);
37         fprintf(fid,'activate PointLoad_8 Phase_%i\n',startPhase-5+i);
38         fprintf(fid,'activate PointLoad_9 Phase_%i\n',startPhase-5+i);
```

```
39          fprintf(fid,'set PointLoad_1_1.Fx Phase_%i %5.3f\n',[
                startPhase-5+i; -data(i,1)]);
40          fprintf(fid,'set PointLoad_1_1.Fy Phase_%i %5.3f\n',[
                startPhase-5+i; -data(i,2)]);
41          fprintf(fid,'set PointLoad_1_1.Fz Phase_%i %5.3f\n',[
                startPhase-5+i; -data(i,3)]);
42          fprintf(fid,'set PointLoad_6_1.Fz Phase_%i %5.3f\n',[
                startPhase-5+i; -PlaxisMoments(i,2)]); %My
43          fprintf(fid,'set PointLoad_8_1.Fz Phase_%i %5.3f\n',[
                startPhase-5+i; PlaxisMoments(i,2)]);
44          fprintf(fid,'set PointLoad_7_1.Fz Phase_%i %5.3f\n',[
                startPhase-5+i; -PlaxisMoments(i,1)]); %Mx
45          fprintf(fid,'set PointLoad_9_1.Fz Phase_%i %5.3f\n',[
                startPhase-5+i; PlaxisMoments(i,1)]);
46          fprintf(fid,'set PointLoad_6_1.Fy Phase_%i %5.3f\n',[
                startPhase-5+i; PlaxisMoments(i,3)]); %T
47          fprintf(fid,'set PointLoad_7_1.Fx Phase_%i %5.3f\n',[
                startPhase-5+i; PlaxisMoments(i,3)]);
48          fprintf(fid,'set PointLoad_8_1.Fy Phase_%i %5.3f\n',[
                startPhase-5+i; -PlaxisMoments(i,3)]); %T
49          fprintf(fid,'set PointLoad_9_1.Fx Phase_%i %5.3f\n',[
                startPhase-5+i; -PlaxisMoments(i,3)]); %T
50
51      %phase settings
52  fprintf(fid,'_set Deform_%i.UseCavitationCutOff True\n',startPhase-5+i
        );
53
54  % renaming
55      if i == 1
56          phaseName = ['sps Phase_%i "Identification" "',stepNr,' A1"\n'
                ];
57          fprintf(fid,phaseName,startPhase-5+i);
58      elseif i ==2
59          phaseName = ['sps Phase_%i "Identification" "',stepNr,' A2"\n'
                ];
60          fprintf(fid,phaseName,startPhase-5+i);
61      elseif i ==3
62          phaseName = ['sps Phase_%i "Identification" "',stepNr,' B1"\n'
                ];
63          fprintf(fid,phaseName,startPhase-5+i);
64      else
65          phaseName = ['sps Phase_%i "Identification" "',stepNr,' B2"\n'
                ];
66          fprintf(fid,phaseName,startPhase-5+i);
67      end
68
69  end
70
71  %% Create stiffness determination steps
72  % loads
73  for i = 1:24
74      k = fix((i-1)/6)+1;
75      j = rem(i,6);
```

```
76 fprintf(fid,'setcurrentphase Phase_%i\n phase Phase_%i\n',(startPhase
   -5+k)*ones(2,1)); % creates phase starting from phase 8
77 fprintf(fid,'setcurrentphase Phase_%i\n sps Phase_%i "PreviousPhase"
   Phase_%i\n',[(startPhase-1+i) (startPhase-1+i) (startPhase-5+k)]);
78         fprintf(fid,'activate PointLoad_1 Phase_%i\n',startPhase-1+i);
79         fprintf(fid,'activate PointLoad_6 Phase_%i\n',startPhase-1+i);
80         fprintf(fid,'activate PointLoad_7 Phase_%i\n',startPhase-1+i);
81         fprintf(fid,'activate PointLoad_8 Phase_%i\n',startPhase-1+i);
82         fprintf(fid,'activate PointLoad_9 Phase_%i\n',startPhase-1+i);
83
84         if j~= 1
85             fprintf(fid,'set PointLoad_1_1.Fx Phase_%i %5.3f\n',[
                startPhase-1+i; -data(k,1)]);
86         else
87             fprintf(fid,'set PointLoad_1_1.Fx Phase_%i %5.3f\n',[
                startPhase-1+i; -data(k,1)+Fx]);
88         end
89
90         if j~= 2
91             fprintf(fid,'set PointLoad_1_1.Fy Phase_%i %5.3f\n',[
                startPhase-1+i; -data(k,2)]);
92         else
93             if -data(k,2) > 0
94                 fprintf(fid,'set PointLoad_1_1.Fy Phase_%i %5.3f\n',[
                    startPhase-1+i; -data(k,2)+Fy]);
95             else
96                 fprintf(fid,'set PointLoad_1_1.Fy Phase_%i %5.3f\n',[
                    startPhase-1+i; -data(k,2)-Fy]);
97             end
98         end
99
100        if j~= 3
101                fprintf(fid,'set PointLoad_1_1.Fz Phase_%i %5.3f\n',[
                   startPhase-1+i; -data(k,3)]);
102        else
103            if -data(k,3) > 0
104                fprintf(fid,'set PointLoad_1_1.Fz Phase_%i %5.3f\n',[
                    startPhase-1+i; -data(k,3)+Fz]);
105            else
106                fprintf(fid,'set PointLoad_1_1.Fz Phase_%i %5.3f\n',[
                    startPhase-1+i; -data(k,3)-Fz]);
107            end
108        end
109
110        if j ~= 4
111            fprintf(fid,'set PointLoad_7_1.Fz Phase_%i %5.3f\n',[
                startPhase-1+i; -PlaxisMoments(k,1)]); %Mx
112            fprintf(fid,'set PointLoad_9_1.Fz Phase_%i %5.3f\n',[
                startPhase-1+i; PlaxisMoments(k,1)]);
113        else
114            if -PlaxisMoments(k,1) > 0
115                fprintf(fid,'set PointLoad_7_1.Fz Phase_%i %5.3f\n',[
                    startPhase-1+i; -PlaxisMoments(k,1)+Mx/diameter]);
```

```
116                 fprintf(fid,'set PointLoad_9_1.Fz Phase_%i %5.3f\n',[
                        startPhase-1+i; PlaxisMoments(k,1)-Mx/diameter]);
117             else
118                 fprintf(fid,'set PointLoad_7_1.Fz Phase_%i %5.3f\n',[
                        startPhase-1+i; -PlaxisMoments(k,1)-Mx/diameter]);
                        %Mx
119                 fprintf(fid,'set PointLoad_9_1.Fz Phase_%i %5.3f\n',[
                        startPhase-1+i; PlaxisMoments(k,1)+Mx/diameter]);
120             end
121         end
122
123         if j ~= 5
124             fprintf(fid,'set PointLoad_6_1.Fz Phase_%i %5.3f\n',[
                    startPhase-1+i; -PlaxisMoments(k,2)]); %My
125             fprintf(fid,'set PointLoad_8_1.Fz Phase_%i %5.3f\n',[
                    startPhase-1+i; PlaxisMoments(k,2)]);
126         else
127             fprintf(fid,'set PointLoad_6_1.Fz Phase_%i %5.3f\n',[
                    startPhase-1+i; -PlaxisMoments(k,2) + My/diameter]);
128             fprintf(fid,'set PointLoad_8_1.Fz Phase_%i %5.3f\n',[
                    startPhase-1+i; PlaxisMoments(k,2) - My/diameter]);
129         end
130
131         if j ~= 0
132             fprintf(fid,'set PointLoad_6_1.Fy Phase_%i %5.3f\n',[
                    startPhase-1+i; PlaxisMoments(k,3)]); %T
133         fprintf(fid,'set PointLoad_7_1.Fx Phase_%i %5.3f\n',[
                startPhase-1+i; PlaxisMoments(k,3)]);
134         fprintf(fid,'set PointLoad_8_1.Fy Phase_%i %5.3f\n',[
                startPhase-1+i; -PlaxisMoments(k,3)]); %T
135         fprintf(fid,'set PointLoad_9_1.Fx Phase_%i %5.3f\n',[
                startPhase-1+i; -PlaxisMoments(k,3)]); %T
136         else
137             if -PlaxisMoments(k,3) > 0
138                 fprintf(fid,'set PointLoad_6_1.Fy Phase_%i %5.3f\n',[
                        startPhase-1+i; PlaxisMoments(k,3)-T/(2*diameter)])
                        ;
139         fprintf(fid,'set PointLoad_7_1.Fx Phase_%i %5.3f\n',[
                startPhase-1+i; PlaxisMoments(k,3)-T/(2*diameter)]);
140         fprintf(fid,'set PointLoad_8_1.Fy Phase_%i %5.3f\n',[
                startPhase-1+i; -PlaxisMoments(k,3)+T/(2*diameter)]); %T
141         fprintf(fid,'set PointLoad_9_1.Fx Phase_%i %5.3f\n',[
                startPhase-1+i; -PlaxisMoments(k,3)+T/(2*diameter)]); %T
142             else
143                 fprintf(fid,'set PointLoad_6_1.Fy Phase_%i %5.3f\n',[
                        startPhase-1+i; PlaxisMoments(k,3)+T/(2*diameter)])
                        ; %T
144         fprintf(fid,'set PointLoad_7_1.Fx Phase_%i %5.3f\n',[
                startPhase-1+i; PlaxisMoments(k,3)+T/(2*diameter)]);
145         fprintf(fid,'set PointLoad_8_1.Fy Phase_%i %5.3f\n',[
                startPhase-1+i; -PlaxisMoments(k,3)-T/(2*diameter)]); %T
146         fprintf(fid,'set PointLoad_9_1.Fx Phase_%i %5.3f\n',[
                startPhase-1+i; -PlaxisMoments(k,3)-T/(2*diameter)]); %T
```

```
147                 end
148             end
149
150 end
151
152 % phase settings
153 A = zeros(24,6);
154
155 for i = 1:size(A,1)
156     A(i,:) = ones(1,size(A,2))*(i+startPhase-1);
157 end
158
159 fprintf(fid,'_set Deform_%i.ResetDisplacementsToZero True\n _set
        Deform_%i.UseCavitationCutOff True\n _set Deform_%i.
        UseDefaultIterationParams False\n _set Deform_%i.UseLineSearch True
        \n _set Deform_%i.ToleratedError 0.001\n _set Deform_%i.
        MaxLoadFractionPerStep 0.1\n',A');
160
161 %% Save
162 q = '"';
163 string = ['_save ',q,'P:\\Plaxis3DstiffnessCheck\\Stepwise loading\\
        HSSingleBucket.P3D',q];
164 fprintf(fid,string);
165 fclose(fid);
```

F.2 SACS code

Linear-Elastic Model

Model Input file

```
1 LDOPT SFINOP  +Z1.0251827.849047    -19.8          GLOBMN
      NPNP    K
2 OPTIONS I    MN          UC   2 2   DC  C    PTPTPT       PTPT
3 UCPART          0.7000.7001.0001.000
4
5 SECT
6 SECT M406127   TUB                                    40.6401.270
7 SECT M406191   TUB                                    40.6401.910
8 SECT M508127   TUB                                    50.8001.270
9 SECT M508191   TUB                                    50.8001.910
10 SECT M508254   TUB                                   50.8002.540
11 SECT M609191   TUB                                   60.9601.910
12 SECT M609254   TUB                                   60.9602.540
13 SECT M609318   TUB                                   60.9603.180
14 SECT M762191   TUB                                   76.2001.910
15 SECT M914254   TUB                                   91.4002.540
16 SECT M914318   TUB                                   91.4403.180
17 SECT N137125   TUB                                   137.162.540
18 SECT N137138   TUB                                   137.163.810
19 SECT N137150   TUB                                   137.165.080
20 SECT N137160   TUB                                   137.166.000
```

```
21
22 GRUP
23 GRUP 111 M609254              21.007.72235.50 1     1.001.00
       7.8500
24 GRUP 112 M609254              21.007.72235.50 1     1.001.00
       7.8500
25 GRUP 112 M609254              21.007.72235.50 1     1.001.00
       7.85001.60
26 GRUP 121 M609254              21.007.72235.50 1     1.001.00
       7.8500
27 GRUP 122 M609191              21.007.72235.50 1     1.001.00
       7.8500
28 GRUP 122 M609254              21.007.72235.50 1     1.001.00
       7.85001.60
29 GRUP 131 M609254              21.007.72235.50 1     1.001.00
       7.8500
30 GRUP 132 M609191              21.007.72235.50 1     1.001.00
       7.8500
31 GRUP 132 M609254              21.007.72235.50 1     1.001.00
       7.85001.60
32 GRUP 211 M609254              21.007.72235.50 1     1.001.00
       7.8500
33 GRUP 212 M609254              21.007.72235.50 1     1.001.00
       7.85001.60
34 GRUP 212 M609191              21.007.72235.50 1     1.001.00
       7.8500
35 GRUP 221 M609254              21.007.72235.50 1     1.001.00
       7.8500
36 GRUP 222 M609254              21.007.72235.50 1     1.001.00
       7.85001.60
37 GRUP 222 M609191              21.007.72235.50 1     1.001.00
       7.8500
38 GRUP 231 M609254              21.007.72235.50 1     1.001.00
       7.8500
39 GRUP 232 M609254              21.007.72235.50 1     1.001.00
       7.8500
40 GRUP 232 M609191              21.007.72235.50 1     1.001.00
       7.85006.00
41 GRUP A11 M609254              21.007.72235.50 1     1.001.00
       7.85001.60
42 GRUP A11 M609191              21.007.72235.50 1     1.001.00
       7.8500
43 GRUP A12 M609254              21.007.72235.50 1     1.001.00
       7.8500
44 GRUP A13 M609191              21.007.72235.50 1     1.001.00
       7.8500
45 GRUP A13 M609254              21.007.72235.50 1     1.001.00
       7.8500.500
46 GRUP A14 M609191              21.007.72235.50 1     1.001.00
       7.8500
47 GRUP A21 M609318              21.007.72235.50 1     1.001.00
       7.85001.60
48 GRUP A21 M609191              21.007.72235.50 1     1.001.00
```

```
      7.8500
49 GRUP A22 M609318          21.007.72235.50 1    1.001.00
      7.8500
50 GRUP A23 M609191          21.007.72235.50 1    1.001.00
      7.8500
51 GRUP A23 M609318          21.007.72235.50 1    1.001.00
      7.85001.60
52 GRUP A31 M609254          21.007.72235.50 1    1.001.00
      7.85001.60
53 GRUP A31 M609191          21.007.72235.50 1    1.001.00
      7.8500
54 GRUP A32 M609254          21.007.72235.50 1    1.001.00
      7.8500
55 GRUP A33 M609191          21.007.72235.50 1    1.001.00
      7.8500
56 GRUP A33 M609254          21.007.72235.50 1    1.001.00
      7.85001.60
57 GRUP B11 M609191          21.007.72235.50 1    1.001.00
      7.8500
58 GRUP B21 M609191          21.007.72235.50 1    1.001.00
      7.8500
59 GRUP B31 M609191          21.007.72235.50 1    1.001.00
      7.8500
60 GRUP C01 M406191          21.007.72235.50 1    1.001.00
      7.8500
61 GRUP C02 M508191          21.007.72235.50 1    1.001.00
      7.8500
62 GRUP D11 M609191          21.007.72235.50 1    1.001.00
      7.8500
63 GRUP D11 M609254          21.007.72235.50 1    1.001.00
      7.8500.500
64 GRUP D12 M609254          21.007.72235.50 1    1.001.00
      7.8500
65 GRUP D13 M609254          21.007.72235.50 1    1.001.00
      7.8500.500
66 GRUP D13 M609191          21.007.72235.50 1    1.001.00
      7.8500
67 GRUP D21 M609191          21.007.72235.50 1    1.001.00
      7.8500
68 GRUP D21 M609254          21.007.72235.50 1    1.001.00
      7.8500.500
69 GRUP D22 M609254          21.007.72235.50 1    1.001.00
      7.8500
70 GRUP D23 M609254          21.007.72235.50 1    1.001.00
      7.8500.500
71 GRUP D23 M609191          21.007.72235.50 1    1.001.00
      7.8500
72 GRUP D31 M508191          21.007.72235.50 1    1.001.00
      7.8500
73 GRUP D31 M508254          21.007.72235.50 1    1.001.00
      7.8500.500
74 GRUP D32 M508254          21.007.72235.50 1    1.001.00
      7.8500
```

```
75 GRUP D33 M508254          21.007.72235.50 1    1.001.00
       7.8500.500
76 GRUP D33 M508191          21.007.72235.50 1    1.001.00
       7.8500
77 GRUP F11 M406127          21.007.72235.50 1    1.001.00
       7.8500
78 GRUP F21 M508127          21.007.72235.50 1    1.001.00
       7.8500
79 GRUP F22 M609191          21.007.72235.50 1    1.001.00
       7.8500
80 GRUP F31 M406127          21.007.72235.50 1    1.001.00
       7.8500
81 GRUP F32 M508127          21.007.72235.50 1    1.001.00
       7.8500
82 GRUP L01 N137160          21.007.72235.50 1    1.001.00
       F7.8500
83 GRUP L04 N137150          21.007.72235.50 1    1.001.00
       F7.8500
84 GRUP L05 N137138          21.007.72235.50 1    1.001.00
       F7.8500
85 GRUP L11 N137150          21.007.72235.50 1    1.001.00
       F7.8500
86 GRUP LA2 N137150          21.007.72235.50 1    1.001.00
       F7.85001.80
87 GRUP LA2 N137125          21.007.72235.50 1    1.001.00
       F7.8500
88 GRUP LA2 N137150          21.007.72235.50 1    1.001.00
       F7.85001.80
89 GRUP LA3 N137150          21.007.72235.50 1    1.001.00
       F7.85002.00
90 GRUP LA3 N137160          21.007.72235.50 1    1.001.00
       F7.8500
91 GRUP LA3 N137150          21.007.72235.50 1    1.001.00
       F7.85004.10
92 GRUP LB2 N137150          21.007.72235.50 1    1.001.00
       F7.85001.80
93 GRUP LB2 N137138          21.007.72235.50 1    1.001.00
       F7.8500
94 GRUP LB2 N137150          21.007.72235.50 1    1.001.00
       F7.85001.80
95 GRUP LB3 N137150          21.007.72235.50 1    1.001.00
       F7.8500
96 GRUP X2A M914254          21.007.72235.50 1    1.001.00
       7.8500
97 GRUP XAB M914254          21.007.72235.50 1    1.001.00
       7.8500
98 GRUP XB2 M914254          21.007.72235.50 1    1.001.00
       7.8500
99 GRUP XBA M914254          21.007.72235.50 1    1.001.00
       7.85009.20
100 GRUP XBA M914318         21.007.72235.50 1    1.001.00
       7.85005.20
101 GRUP XBA M914254         21.007.72235.50 1    1.001.00
```

```
      7.8500
102 GRUP XX1 M762191                21.007.72235.50 1     1.001.00
      7.8500
103
104 MEMBER
105 MEMBER 012001A1 111
106 MEMBER 01B10120 112
107 MEMBER 022002A1 121
108 MEMBER 02B10220 122
109 MEMBER 032003A1 131
110 MEMBER 03B10320 132
111 MEMBER 01A20110 211
112 MEMBER 011001B2 212
113 MEMBER 02A20210 221
114 MEMBER 021002B2 222
115 MEMBER 03A20310 231
116 MEMBER 031003B2 232
117 MEMBER 100101A2 A11
118 MEMBER 10051001 A12
119 MEMBER 10021005 A13
120 MEMBER 01A11002 A14
121 MEMBER 200102A2 A21
122 MEMBER 20022001 A22
123 MEMBER 02A12002 A23
124 MEMBER 300103A2 A31
125 MEMBER 30023001 A32
126 MEMBER 03A13002 A33
127 MEMBER 01B201B1 B11
128 MEMBER 02B22005 B21
129 MEMBER 200502B1 B21
130 MEMBER 03B23005 B31
131 MEMBER 300503B1 B31
132 MEMBER 20032001 C01
133 MEMBER 20042002 C01
134 MEMBER 30033001 C01
135 MEMBER 30043002 C01
136 MEMBER 10031001 C02
137 MEMBER 10061005 C02
138 MEMBER 01101003 D11
139 MEMBER 10031006 D12
140 MEMBER 10061004 D12
141 MEMBER 10040120 D13
142 MEMBER 02102003 D21
143 MEMBER 20032004 D22
144 MEMBER 20040220 D23
145 MEMBER 03103003 D31
146 MEMBER 30033004 D32
147 MEMBER 30040320 D33
148 MEMBER 01101001 F11
149 MEMBER 01201002 F11
150 MEMBER 10041002 F11
151 MEMBER 02102001 F21
152 MEMBER 02202002 F21
```

```
153 MEMBER 02102005 F22
154 MEMBER 02202005 F22
155 MEMBER 03103001 F31
156 MEMBER 03203002 F31
157 MEMBER 03103005 F32
158 MEMBER 03203005 F32
159 MEMBER 0A1 00A1 L01
160 MEMBER 0A2 00A2 L01
161 MEMBER 0B1 00B1 L01
162 MEMBER 0B2 00B2 L01
163 MEMBER 03A104A1 L04
164 MEMBER 03A204A2 L04
165 MEMBER 03B104B1 L04
166 MEMBER 03B204B2 L04
167 MEMBER 04A105A1 L05
168 MEMBER 04A205A2 L05
169 MEMBER 04B105B1 L05
170 MEMBER 04B205B2 L05
171 MEMBER 00A101A1 L11
172 MEMBER 00A201A2 L11
173 MEMBER 00B101B1 L11
174 MEMBER 00B201B2 L11
175 MEMBER 01A102A1 LA2
176 MEMBER 01A202A2 LA2
177 MEMBER 02A103A1 LA3
178 MEMBER 02A203A2 LA3
179 MEMBER 01B102B1 LB2
180 MEMBER 01B202B2 LB2
181 MEMBER 02B103B1 LB3
182 MEMBER 02B203B2 LB3
183 MEMBER 03A202A1 X2A
184 MEMBER 03A102B1 XAB
185 MEMBER 03B102B2 XB2
186 MEMBER 03B202A2 XBA
187 MEMBER 02A101A2 XX1
188 MEMBER 02A201B2 XX1
189 MEMBER 02B101A1 XX1
190 MEMBER 02B201B1 XX1
191
192 JOINT
193 JOINT 0A1  -11.323  11.645 -19.800
194 JOINT 0A2  -11.323 -11.645 -19.800
195 JOINT 0B1   11.323  11.645 -19.800
196 JOINT 0B2   11.323 -11.645 -19.800
197 JOINT 00A1 -11.323  11.645 -18.000
198 JOINT 00A2 -11.323 -11.645 -18.000
199 JOINT 00B1  11.323  11.645 -18.000
200 JOINT 00B2  11.323 -11.645 -18.000
201 JOINT 0110  -4.623 -11.578 -17.300
202 JOINT 0120  -4.623  11.578 -17.300
203 JOINT 01A1 -11.323  11.576 -17.300
204 JOINT 01A2 -11.323 -11.576 -17.300
205 JOINT 01B1  11.259  11.581 -17.300
```

```
206 JOINT 01B2  11.259-11.581-17.300
207 JOINT 0210   -4.623-10.495  -6.000
208 JOINT 0220   -4.623 10.495  -6.000
209 JOINT 02A1 -11.323 10.469  -6.000
210 JOINT 02A2 -11.323-10.469  -6.000
211 JOINT 02B1  10.228 10.551  -6.000
212 JOINT 02B2  10.228-10.551  -6.000
213 JOINT 0310   -4.623 -9.061   9.000
214 JOINT 0320   -4.623  9.061   9.000
215 JOINT 03A1 -11.323  9.000   9.000
216 JOINT 03A2 -11.323 -9.000   9.000
217 JOINT 03B1   8.859  9.182   9.000
218 JOINT 03B2   8.859 -9.182   9.000
219 JOINT 04A1 -11.323  9.000  11.000
220 JOINT 04A2 -11.323 -9.000  11.000
221 JOINT 04B1   8.677  9.000  11.000
222 JOINT 04B2   8.677 -9.000  11.000
223 JOINT 05A1 -11.323  9.000  15.500
224 JOINT 05A2 -11.323 -9.000  15.500
225 JOINT 05B1   8.677  9.000  15.500
226 JOINT 05B2   8.677 -9.000  15.500
227 JOINT 1001 -11.323 -4.000-17.300
228 JOINT 1002 -11.323  2.100-17.300
229 JOINT 1003  -4.623 -4.061-17.300
230 JOINT 1004  -4.623  2.039-17.300
231 JOINT 1005 -11.323 -1.800-17.300
232 JOINT 1006  -4.623 -1.861-17.300
233 JOINT 2001 -11.323 -4.000  -6.000
234 JOINT 2002 -11.323  2.100  -6.000
235 JOINT 2003  -4.623 -4.061  -6.000
236 JOINT 2004  -4.623  2.039  -6.000
237 JOINT 2005  10.228  0.000  -6.000
238 JOINT 3001 -11.323 -4.000   9.000
239 JOINT 3002 -11.323  2.100   9.000
240 JOINT 3003  -4.623 -4.061   9.000
241 JOINT 3004  -4.623  2.039   9.000
242 JOINT 3005   8.859  0.000   9.000
243
244 LOAD
245 LOADCNPNTL
246 LOAD    03A2        2000.                                    GLOB JOIN
        1
247 END
```

Superelement Input file

```
1 SUBOPT INP MN
2 * Individual pile matrices
3 STFHEAD   0A1 0A1 +1.
4 STFR FX        4.29e6                                  -21.98e6
5 STFR FY                  4.29e6              21.98e6
6 STFR FZ                             2.79e6
7 STFR MX                 21.98e6             197.26e6
```

```
 8 STFR MY      -21.98e6                                  197.26e6
 9 STFR MZ                                                          74.07e6
10 STFHEAD   0B1 0B1 +1.
11 STFR FX       4.29e6                                  -21.98e6
12 STFR FY                  4.29e6          21.98e6
13 STFR FZ                              2.79e6
14 STFR MX                 21.98e6         197.26e6
15 STFR MY      -21.98e6                                  197.26e6
16 STFR MZ                                                         74.07e6
17 STFHEAD   0A2 0A2 +1.
18 STFR FX       4.29e6                                  -21.98e6
19 STFR FY                  4.29e6          21.98e6
20 STFR FZ                              2.79e6
21 STFR MX                 21.98e6         197.26e6
22 STFR MY      -21.98e6                                  197.26e6
23 STFR MZ                                                         74.07e6
24 STFHEAD   0B2 0B2 +1.
25 STFR FX       4.29e6                                  -21.98e6
26 STFR FY                  4.29e6          21.98e6
27 STFR FZ                              2.79e6
28 STFR MX                 21.98e6         197.26e6
29 STFR MY      -21.98e6                                  197.26e6
30 STFR MZ                                                         74.07e6
31 * pile interaction matrices
32 STFHEAD   0A2 0B2 +1.
33 STFR FX      -9.36e5                                    4.79e6
34 STFR FY                 -1.88e5         -9.62e5
35 STFR FZ
36 STFR MX                 -9.62e5         -4.93e6
37 STFR MY       4.79e6                                  -24.51e6
38 STFR MZ
39 STFHEAD   0A1 0B1         1.
40 STFR FX      -9.36e5                                    4.79e6
41 STFR FY                 -1.88e5         -9.62e5
42 STFR FZ
43 STFR MX                 -9.62e5         -4.93e6
44 STFR MY       4.79e6                                  -24.51e6
45 STFR MZ
46 STFHEAD   0A2 0A1 +1.
47 STFR FX      -1.88e5                                    9.62e5
48 STFR FY                 -9.36e5         -4.79e6
49 STFR FZ
50 STFR MX                 -4.79e6         -24.51e6
51 STFR MY       9.62e5                                  -4.93e6
52 STFR MZ
53 STFHEAD   0B2 0B1 +1.
54 STFR FX      -1.88e5                                    9.62e5
55 STFR FY                 -9.36e5         -4.79e6
56 STFR FZ
57 STFR MX                 -4.79e6         -24.51e6
58 STFR MY       9.62e5                                  -4.93e6
59 STFR MZ
60 STFHEAD   0A2 0B1 +1.
```

```
61 STFR FX       -1.31e5                                    6.68e5
62 STFR FY                  -1.31e5            -6.68e5
63 STFR FZ
64 STFR MX                  -6.68e5            -3.42e6
65 STFR MY        6.68e5                                   -3.42e6
66 STFR MZ
67 STFHEAD   0B2 0A1 +1.
68 STFR FX       -1.31e5                                    6.68e5
69 STFR FY                  -1.31e5            -6.68e5
70 STFR FZ
71 STFR MX                  -6.68e5            -3.42e6
72 STFR MY        6.68e5                                   -3.42e6
73 STFR MZ
74 END
```

Seastate file

```
 1 LDOPT SFINOP  +Z1.0251827.849047-19.799919.79999GLOBMN
     NPNP     K
 2
 3 FILE B
 4
 5 CDM
 6 CDM         1.   0.65          1.6         1.05          1.2
 7 CDM     1000.0.6501         1.601       1.0501         1.201
 8 *Constant Cd and Cm as specified in BoD
 9
10 MGROV
11 MGROV       0.001   20.925       5.          2.5400-4      1.3
12 *Marine Growth
13
14 LOAD
15
16 LOADCN  DW               1.
17 DEAD       -Z                                  M
18
19 LOADCN   W
20
21 WIND
22 WIND D M     26.1       10.     44.2
23 WAVE
24 WAVE 1.0STRE   11.5          10.1           44.2       D            5.   72
     MM10 1  0
25 CURR
26 CURR            1.     0.13     44.2           0.425         US         WDP
27 CURR            5.     0.17     44.2           0.425         US         WDP
28 CURR           10.     0.18     44.2           0.425         US         WDP
29 CURR           30.     0.22     44.2           0.425         US         WDP
30 CURR           50.     0.23     44.2           0.425         US         WDP
31 CURR          100.     0.26     44.2           0.425         US         WDP
32 DEAD       -Z                                  M
33 *x-axis:SE
34 *y-axis:NE
```

```
35 *100y env loads coming from west. Currentblockage is 0.5*0.85 since
     unlikely to
36
37 LOADCN  SW
38 WIND
39 WIND D M     24.4      10.      90.
40 WAVE
41 WAVE 1.0STRE  11.7         10.2            90.      D           5.  72
     MM10 1  0
42 CURR
43 CURR           1.     0.63      90.             0.4         US        WDP
44 CURR           5.     0.81      90.             0.4         US        WDP
45 CURR          10.     0.90      90.             0.4         US        WDP
46 CURR          30.     1.06      90.             0.4         US        WDP
47 CURR          50.     1.14      90.             0.4         US        WDP
48 CURR         100.     1.27      90.             0.4         US        WDP
49 DEAD       -Z                                  M
50 *100 y loads coming from southwest. Currentblockage = 0.5*0.8 (non-
     diagonal)
51
52 LOADCN WSW
53 WIND
54 WIND D M     26.1      10.     44.2
55 WAVE
56 WAVE 1.0STRE  11.5         10.1            44.2      D           5.  72
     MM10 1  0
57 CURR
58 CURR           1.     0.63      90.             0.4         US        WDP
59 CURR           5.     0.81      90.             0.4         US        WDP
60 CURR          10.     0.90      90.             0.4         US        WDP
61 CURR          30.     1.06      90.             0.4         US        WDP
62 CURR          50.     1.14      90.             0.4         US        WDP
63 CURR         100.     1.27      90.             0.4         US        WDP
64 DEAD       -Z                                  M
65 *100 y wind and wave from west + current from southwest
66
67 END
```

Non-Linear Model 1

Model Input file

```
1 LDOPT SFINOP  +Z1.0251827.849047    -19.8     19.8GLOBMN
     NPNP     K
2 OPTIONS I     MN          UC    2 2    DC  C     PTPTPT       PTPT
3 UCPART           0.7000.7001.0001.000
4 SECT
5 *DUMMY1 - connection of the center of rotation with the top plate -
     infinite sti
6 SECT M406127    TUB                                    40.6401.270
7 SECT M406191    TUB                                    40.6401.910
8 SECT M508127    TUB                                    50.8001.270
9 SECT M508191    TUB                                    50.8001.910
```

```
10 SECT M508254    TUB                                  50.8002.540
11 SECT M609191    TUB                                  60.9601.910
12 SECT M609254    TUB                                  60.9602.540
13 SECT M609318    TUB                                  60.9603.180
14 SECT M762191    TUB                                  76.2001.910
15 SECT M914254    TUB                                  91.4002.540
16 SECT M914318    TUB                                  91.4403.180
17 SECT N137125    TUB                                  137.162.540
18 SECT N137138    TUB                                  137.163.810
19 SECT N137150    TUB                                  137.165.080
20 SECT N137160    TUB                                  137.166.000
21 GRUP
22 GRUP 111 M609254              21.007.72235.50 1     1.001.00
       7.8500
23 GRUP 112 M609254              21.007.72235.50 1     1.001.00
       7.8500
24 GRUP 112 M609254              21.007.72235.50 1     1.001.00
       7.85001.60
25 GRUP 121 M609254              21.007.72235.50 1     1.001.00
       7.8500
26 GRUP 122 M609191              21.007.72235.50 1     1.001.00
       7.8500
27 GRUP 122 M609254              21.007.72235.50 1     1.001.00
       7.85001.60
28 GRUP 131 M609254              21.007.72235.50 1     1.001.00
       7.8500
29 GRUP 132 M609191              21.007.72235.50 1     1.001.00
       7.8500
30 GRUP 132 M609254              21.007.72235.50 1     1.001.00
       7.85001.60
31 GRUP 211 M609254              21.007.72235.50 1     1.001.00
       7.8500
32 GRUP 212 M609254              21.007.72235.50 1     1.001.00
       7.85001.60
33 GRUP 212 M609191              21.007.72235.50 1     1.001.00
       7.8500
34 GRUP 221 M609254              21.007.72235.50 1     1.001.00
       7.8500
35 GRUP 222 M609254              21.007.72235.50 1     1.001.00
       7.85001.60
36 GRUP 222 M609191              21.007.72235.50 1     1.001.00
       7.8500
37 GRUP 231 M609254              21.007.72235.50 1     1.001.00
       7.8500
38 GRUP 232 M609254              21.007.72235.50 1     1.001.00
       7.8500
39 GRUP 232 M609191              21.007.72235.50 1     1.001.00
       7.85006.00
40 GRUP A11 M609254              21.007.72235.50 1     1.001.00
       7.85001.60
41 GRUP A11 M609191              21.007.72235.50 1     1.001.00
       7.8500
42 GRUP A12 M609254              21.007.72235.50 1     1.001.00
```

```
      7.8500
43 GRUP A13 M609191              21.007.72235.50 1     1.001.00
      7.8500
44 GRUP A13 M609254              21.007.72235.50 1     1.001.00
      7.8500.500
45 GRUP A14 M609191              21.007.72235.50 1     1.001.00
      7.8500
46 GRUP A21 M609318              21.007.72235.50 1     1.001.00
      7.85001.60
47 GRUP A21 M609191              21.007.72235.50 1     1.001.00
      7.8500
48 GRUP A22 M609318              21.007.72235.50 1     1.001.00
      7.8500
49 GRUP A23 M609191              21.007.72235.50 1     1.001.00
      7.8500
50 GRUP A23 M609318              21.007.72235.50 1     1.001.00
      7.85001.60
51 GRUP A31 M609254              21.007.72235.50 1     1.001.00
      7.85001.60
52 GRUP A31 M609191              21.007.72235.50 1     1.001.00
      7.8500
53 GRUP A32 M609254              21.007.72235.50 1     1.001.00
      7.8500
54 GRUP A33 M609191              21.007.72235.50 1     1.001.00
      7.8500
55 GRUP A33 M609254              21.007.72235.50 1     1.001.00
      7.85001.60
56 GRUP B11 M609191              21.007.72235.50 1     1.001.00
      7.8500
57 GRUP B21 M609191              21.007.72235.50 1     1.001.00
      7.8500
58 GRUP B31 M609191              21.007.72235.50 1     1.001.00
      7.8500
59 GRUP C01 M406191              21.007.72235.50 1     1.001.00
      7.8500
60 GRUP C02 M508191              21.007.72235.50 1     1.001.00
      7.8500
61 GRUP D11 M609191              21.007.72235.50 1     1.001.00
      7.8500
62 GRUP D11 M609254              21.007.72235.50 1     1.001.00
      7.8500.500
63 GRUP D12 M609254              21.007.72235.50 1     1.001.00
      7.8500
64 GRUP D13 M609254              21.007.72235.50 1     1.001.00
      7.8500.500
65 GRUP D13 M609191              21.007.72235.50 1     1.001.00
      7.8500
66 GRUP D21 M609191              21.007.72235.50 1     1.001.00
      7.8500
67 GRUP D21 M609254              21.007.72235.50 1     1.001.00
      7.8500.500
68 GRUP D22 M609254              21.007.72235.50 1     1.001.00
      7.8500
```

```
69 GRUP D23 M609254          21.007.72235.50 1    1.001.00
       7.8500.500
70 GRUP D23 M609191          21.007.72235.50 1    1.001.00
       7.8500
71 GRUP D31 M508191          21.007.72235.50 1    1.001.00
       7.8500
72 GRUP D31 M508254          21.007.72235.50 1    1.001.00
       7.8500.500
73 GRUP D32 M508254          21.007.72235.50 1    1.001.00
       7.8500
74 GRUP D33 M508254          21.007.72235.50 1    1.001.00
       7.8500.500
75 GRUP D33 M508191          21.007.72235.50 1    1.001.00
       7.8500
76 GRUP F11 M406127          21.007.72235.50 1    1.001.00
       7.8500
77 GRUP F21 M508127          21.007.72235.50 1    1.001.00
       7.8500
78 GRUP F22 M609191          21.007.72235.50 1    1.001.00
       7.8500
79 GRUP F31 M406127          21.007.72235.50 1    1.001.00
       7.8500
80 GRUP F32 M508127          21.007.72235.50 1    1.001.00
       7.8500
81 GRUP L01 N137160          21.007.72235.50 1    1.001.00
       F7.8500
82 GRUP L04 N137150          21.007.72235.50 1    1.001.00
       F7.8500
83 GRUP L05 N137138          21.007.72235.50 1    1.001.00
       F7.8500
84 GRUP L11 N137150          21.007.72235.50 1    1.001.00
       F7.8500
85 GRUP LA2 N137150          21.007.72235.50 1    1.001.00
       F7.85001.80
86 GRUP LA2 N137125          21.007.72235.50 1    1.001.00
       F7.8500
87 GRUP LA2 N137150          21.007.72235.50 1    1.001.00
       F7.85001.80
88 GRUP LA3 N137150          21.007.72235.50 1    1.001.00
       F7.85002.00
89 GRUP LA3 N137160          21.007.72235.50 1    1.001.00
       F7.8500
90 GRUP LA3 N137150          21.007.72235.50 1    1.001.00
       F7.85004.10
91 GRUP LB2 N137150          21.007.72235.50 1    1.001.00
       F7.85001.80
92 GRUP LB2 N137138          21.007.72235.50 1    1.001.00
       F7.8500
93 GRUP LB2 N137150          21.007.72235.50 1    1.001.00
       F7.85001.80
94 GRUP LB3 N137150          21.007.72235.50 1    1.001.00
       F7.8500
95 GRUP X2A M914254          21.007.72235.50 1    1.001.00
```

```
      7.8500
 96 GRUP XAB M914254                21.007.72235.50 1     1.001.00
      7.8500
 97 GRUP XB2 M914254                21.007.72235.50 1     1.001.00
      7.8500
 98 GRUP XBA M914254                21.007.72235.50 1     1.001.00
      7.85009.20
 99 GRUP XBA M914318                21.007.72235.50 1     1.001.00
      7.85005.20
100 GRUP XBA M914254                21.007.72235.50 1     1.001.00
      7.8500
101 GRUP XX1 M762191                21.007.72235.50 1     1.001.00
      7.8500
102 GRUP GAP          X   1+5    3. 2000. 0.77 35.5 1                    N
        1-5
103 GRUP DMY          X   1+5    3.   0.2 2.+0 35.5 1                    N
        1-5
104 GRUP DM2          X   1+5    3.  2.+2 2.+2 35.5 1                    N
        1-5
105
106 MEMBER
107 MEMBER 012001A1 111
108 MEMBER 01B10120 112
109 MEMBER 022002A1 121
110 MEMBER 02B10220 122
111 MEMBER 032003A1 131
112 MEMBER 03B10320 132
113 MEMBER 01A20110 211
114 MEMBER 011001B2 212
115 MEMBER 02A20210 221
116 MEMBER 021002B2 222
117 MEMBER 03A20310 231
118 MEMBER 031003B2 232
119 MEMBER 100101A2 A11
120 MEMBER 10051001 A12
121 MEMBER 10021005 A13
122 MEMBER 01A11002 A14
123 MEMBER 200102A2 A21
124 MEMBER 20022001 A22
125 MEMBER 02A12002 A23
126 MEMBER 300103A2 A31
127 MEMBER 30023001 A32
128 MEMBER 03A13002 A33
129 MEMBER 01B201B1 B11
130 MEMBER 02B22005 B21
131 MEMBER 200502B1 B21
132 MEMBER 03B23005 B31
133 MEMBER 300503B1 B31
134 MEMBER 20032001 C01
135 MEMBER 20042002 C01
136 MEMBER 30033001 C01
137 MEMBER 30043002 C01
138 MEMBER 10031001 C02
```

```
139 MEMBER 10061005 C02
140 MEMBER 01101003 D11
141 MEMBER 10031006 D12
142 MEMBER 10061004 D12
143 MEMBER 10040120 D13
144 MEMBER 02102003 D21
145 MEMBER 20032004 D22
146 MEMBER 20040220 D23
147 MEMBER 03103003 D31
148 MEMBER 30033004 D32
149 MEMBER 30040320 D33
150 MEMBER 01101001 F11
151 MEMBER 01201002 F11
152 MEMBER 10041002 F11
153 MEMBER 02102001 F21
154 MEMBER 02202002 F21
155 MEMBER 02102005 F22
156 MEMBER 02202005 F22
157 MEMBER 03103001 F31
158 MEMBER 03203002 F31
159 MEMBER 03103005 F32
160 MEMBER 03203005 F32
161 MEMBER 0A1 00A1 L01
162 MEMBER 0A2 00A2 L01
163 MEMBER 0B1 00B1 L01
164 MEMBER 0B2 00B2 L01
165 MEMBER 03A104A1 L04
166 MEMBER 03A204A2 L04
167 MEMBER 03B104B1 L04
168 MEMBER 03B204B2 L04
169 MEMBER 04A105A1 L05
170 MEMBER 04A205A2 L05
171 MEMBER 04B105B1 L05
172 MEMBER 04B205B2 L05
173 MEMBER 00A101A1 L11
174 MEMBER 00A201A2 L11
175 MEMBER 00B101B1 L11
176 MEMBER 00B201B2 L11
177 MEMBER 01A102A1 LA2
178 MEMBER 01A202A2 LA2
179 MEMBER 02A103A1 LA3
180 MEMBER 02A203A2 LA3
181 MEMBER 01B102B1 LB2
182 MEMBER 01B202B2 LB2
183 MEMBER 02B103B1 LB3
184 MEMBER 02B203B2 LB3
185 MEMBER 03A202A1 X2A
186 MEMBER 03A102B1 XAB
187 MEMBER 03B102B2 XB2
188 MEMBER 03B202A2 XBA
189 MEMBER 02A101A2 XX1
190 MEMBER 02A201B2 XX1
191 MEMBER 02B101A1 XX1
```

```
192 MEMBER 02B201B1 XX1
193 *Leg A1
194 MEMBER A101A102 GAP
195 MEMBER A101A103 GAP
196 MEMBER A101A104 GAP
197 MEMBER A101A105 DMYSK 000000000111
198 MEMBER A105 0A1 DM2SK
199 MEMBER A107A105 DMYSK 000000111001
200 MEMBER A107A108 DM2SK 000000000111
201 MEMBER A107A109 DM2SK 000000000111
202 MEMBER A108A110 GAP
203 MEMBER A108A112 GAP
204 MEMBER A109A111 GAP
205 MEMBER A109A113 GAP
206 *Leg A2
207 MEMBER A201A202 GAP
208 MEMBER A201A203 GAP
209 MEMBER A201A204 GAP
210 MEMBER A201A205 DMYSK 000000000111
211 MEMBER A205 0A2 DM2SK
212 MEMBER A207A205 DMYSK 000000111001
213 MEMBER A207A208 DM2SK 000000000111
214 MEMBER A207A209 DM2SK 000000000111
215 MEMBER A208A210 GAP
216 MEMBER A208A212 GAP
217 MEMBER A209A211 GAP
218 MEMBER A209A213 GAP
219 *Leg B1
220 MEMBER B101B102 GAP
221 MEMBER B101B103 GAP
222 MEMBER B101B104 GAP
223 MEMBER B101B105 DMYSK 000000000111
224 MEMBER B105 0B1 DM2SK
225 MEMBER B107B105 DMYSK 000000111001
226 MEMBER B107B108 DM2SK 000000000111
227 MEMBER B107B109 DM2SK 000000000111
228 MEMBER B108B110 GAP
229 MEMBER B108B112 GAP
230 MEMBER B109B111 GAP
231 MEMBER B109B113 GAP
232 *Leg B2
233 MEMBER B201B202 GAP
234 MEMBER B201B203 GAP
235 MEMBER B201B204 GAP
236 MEMBER B201B205 DMYSK 000000000111
237 MEMBER B205 0B2 DM2
238 MEMBER B207B205 DMYSK 000000111001
239 MEMBER B207B208 DM2SK 000000000111
240 MEMBER B207B209 DM2SK 000000000111
241 MEMBER B208B210 GAP
242 MEMBER B208B212 GAP
243 MEMBER B209B211 GAP
244 MEMBER B209B213 GAP
```

```
245
246 JOINT
247 JOINT   0A1 -11.323  11.645 -19.800
248 JOINT   0A2 -11.323 -11.645 -19.800
249 JOINT   0B1  11.323  11.645 -19.800
250 JOINT   0B2  11.323 -11.645 -19.800
251 JOINT  00A1 -11.323  11.645 -18.000
252 JOINT  00A2 -11.323 -11.645 -18.000
253 JOINT  00B1  11.323  11.645 -18.000
254 JOINT  00B2  11.323 -11.645 -18.000
255 JOINT  0110  -4.623 -11.578 -17.300
256 JOINT  0120  -4.623  11.578 -17.300
257 JOINT  01A1 -11.323  11.576 -17.300
258 JOINT  01A2 -11.323 -11.576 -17.300
259 JOINT  01B1  11.259  11.581 -17.300
260 JOINT  01B2  11.259 -11.581 -17.300
261 JOINT  0210  -4.623 -10.495  -6.000
262 JOINT  0220  -4.623  10.495  -6.000
263 JOINT  02A1 -11.323  10.469  -6.000
264 JOINT  02A2 -11.323 -10.469  -6.000
265 JOINT  02B1  10.228  10.551  -6.000
266 JOINT  02B2  10.228 -10.551  -6.000
267 JOINT  0310  -4.623  -9.061   9.000
268 JOINT  0320  -4.623   9.061   9.000
269 JOINT  03A1 -11.323   9.000   9.000
270 JOINT  03A2 -11.323  -9.000   9.000
271 JOINT  03B1   8.859   9.182   9.000
272 JOINT  03B2   8.859  -9.182   9.000
273 JOINT  04A1 -11.323   9.000  11.000
274 JOINT  04A2 -11.323  -9.000  11.000
275 JOINT  04B1   8.677   9.000  11.000
276 JOINT  04B2   8.677  -9.000  11.000
277 JOINT  05A1 -11.323   9.000  15.500
278 JOINT  05A2 -11.323  -9.000  15.500
279 JOINT  05B1   8.677   9.000  15.500
280 JOINT  05B2   8.677  -9.000  15.500
281 JOINT  1001 -11.323  -4.000 -17.300
282 JOINT  1002 -11.323   2.100 -17.300
283 JOINT  1003  -4.623  -4.061 -17.300
284 JOINT  1004  -4.623   2.039 -17.300
285 JOINT  1005 -11.323  -1.800 -17.300
286 JOINT  1006  -4.623  -1.861 -17.300
287 JOINT  2001 -11.323  -4.000  -6.000
288 JOINT  2002 -11.323   2.100  -6.000
289 JOINT  2003  -4.623  -4.061  -6.000
290 JOINT  2004  -4.623   2.039  -6.000
291 JOINT  2005  10.228   0.000  -6.000
292 JOINT  3001 -11.323  -4.000   9.000
293 JOINT  3002 -11.323   2.100   9.000
294 JOINT  3003  -4.623  -4.061   9.000
295 JOINT  3004  -4.623   2.039   9.000
296 JOINT  3005   8.859   0.000   9.000
297 *leg A1
```

```
298 JOINT A101 -11.323  11.645 -24.751
299 JOINT A102 -11.323  11.645 -34.000                    001111
300 JOINT A103 -21.323  11.645 -24.751                    100111
301 JOINT A104 -11.323   1.645 -24.751                    010111
302 JOINT A105 -11.323  11.645 -24.750
303 JOINT A107 -11.322  11.645 -24.750
304 JOINT A108 -11.322  11.645 -24.650
305 JOINT A109 -11.322  11.645 -24.850
306 JOINT A110  -1.322  11.645 -24.650                    100111
307 JOINT A111  -1.322  11.645 -24.850                    100111
308 JOINT A112 -11.322  21.645 -24.650                    010111
309 JOINT A113 -11.322  21.645 -24.850                    010111
310 *Leg A2
311 JOINT A201 -11.323 -11.645 -24.751
312 JOINT A202 -11.323 -11.645 -34.000                    001111
313 JOINT A203 -21.323 -11.645 -24.751                    100111
314 JOINT A204 -11.323 -21.645 -24.751                    010111
315 JOINT A205 -11.323 -11.645 -24.750
316 JOINT A207 -11.322 -11.645 -24.750
317 JOINT A208 -11.322 -11.645 -24.650
318 JOINT A209 -11.322 -11.645 -24.850
319 JOINT A210  -1.322 -11.645 -24.650                    100111
320 JOINT A211  -1.322 -11.645 -24.850                    100111
321 JOINT A212 -11.322  -1.645 -24.650                    010111
322 JOINT A213 -11.322  -1.645 -24.850                    010111
323 *Leg B1
324 JOINT B101  11.323  11.645 -24.751
325 JOINT B102  11.323  11.645 -34.000                    001111
326 JOINT B103   1.323  11.645 -24.751                    100111
327 JOINT B104  11.323   1.645 -24.751                    010111
328 JOINT B105  11.323  11.645 -24.750
329 JOINT B107  11.324  11.645 -24.750
330 JOINT B108  11.324  11.645 -24.650
331 JOINT B109  11.324  11.645 -24.850
332 JOINT B110  21.324  11.645 -24.650                    100111
333 JOINT B111  21.324  11.645 -24.850                    100111
334 JOINT B112  11.324  21.645 -24.650                    010111
335 JOINT B113  11.324  21.645 -24.850                    010111
336 *Leg B2
337 JOINT B201  11.323 -11.645 -24.751
338 JOINT B202  11.323 -11.645 -34.000                    001111
339 JOINT B203   1.323 -11.645 -24.751                    100111
340 JOINT B204  11.323 -21.645 -24.751                    010111
341 JOINT B205  11.323 -11.645 -24.750
342 JOINT B207  11.324 -11.645 -24.750
343 JOINT B208  11.324 -11.645 -24.650
344 JOINT B209  11.324 -11.645 -24.850
345 JOINT B210  21.324 -11.645 -24.650                    100111
346 JOINT B211  21.324 -11.645 -24.850                    100111
347 JOINT B212  11.324  -1.645 -24.650                    010111
348 JOINT B213  11.324  -1.645 -24.850                    010111
349
350 LOAD
```

```
351 LOADCNTOPS
352 LOAD    05A1                        -2500.                    GLOB JOIN
          1
353 LOAD    05B1                        -2500.                    GLOB JOIN
          1
354 LOAD    05A2                        -2500.                    GLOB JOIN
          1
355 LOAD    05B2                        -2500.                    GLOB JOIN
          1
356 * Topside weight of 10000 kN (assumed)
357
358 *Leg A1
359 LOADCNA1D3
360 LOAD X A101A103      0.0 -90000.                               MEMB CONC
          DUMMY
361 LOAD X A103A101      0.0  90000.                               MEMB CONC
          DUMMY
362 LOADCNA1D2
363 LOAD X A101A102      0.0 -90000.                               MEMB CONC
          DUMMY
364 LOAD X A102A101      0.0  90000.                               MEMB CONC
          DUMMY
365 LOADCNA1D4
366 LOAD X A101A104      0.0 -90000.                               MEMB CONC
          DUMMY
367 LOAD X A104A101      0.0  90000.                               MEMB CONC
          DUMMY
368 LOADCNA1D6
369 LOAD X A108A110      0.0 -90000.                               MEMB CONC
          DUMMY
370 LOAD X A110A108      0.0  90000.                               MEMB CONC
          DUMMY
371 LOADCNA1D7
372 LOAD X A109A111      0.0 -90000.                               MEMB CONC
          DUMMY
373 LOAD X A111A109      0.0  90000.                               MEMB CONC
          DUMMY
374 LOADCNA1D8
375 LOAD X A108A112      0.0 -90000.                               MEMB CONC
          DUMMY
376 LOAD X A112A108      0.0  90000.                               MEMB CONC
          DUMMY
377 LOADCNA1D9
378 LOAD X A109A113      0.0 -90000.                               MEMB CONC
          DUMMY
379 LOAD X A113A109      0.0  90000.                               MEMB CONC
          DUMMY
380 *Leg A2
381 LOADCNA2D3
382 LOAD X A201A203      0.0 -90000.                               MEMB CONC
          DUMMY
383 LOAD X A203A201      0.0  90000.                               MEMB CONC
          DUMMY
```

```
384 LOADCNA2D2
385 LOAD X A201A202      0.0 -90000.                    MEMB CONC
          DUMMY
386 LOAD X A202A201      0.0  90000.                    MEMB CONC
          DUMMY
387 LOADCNA2D4
388 LOAD X A201A204      0.0 -90000.                    MEMB CONC
          DUMMY
389 LOAD X A204A201      0.0  90000.                    MEMB CONC
          DUMMY
390 LOADCNA2D6
391 LOAD X A208A210      0.0 -90000.                    MEMB CONC
          DUMMY
392 LOAD X A210A208      0.0  90000.                    MEMB CONC
          DUMMY
393 LOADCNA2D7
394 LOAD X A209A211      0.0 -90000.                    MEMB CONC
          DUMMY
395 LOAD X A211A209      0.0  90000.                    MEMB CONC
          DUMMY
396 LOADCNA2D8
397 LOAD X A208A212      0.0 -90000.                    MEMB CONC
          DUMMY
398 LOAD X A212A208      0.0  90000.                    MEMB CONC
          DUMMY
399 LOADCNA2D9
400 LOAD X A209A213      0.0 -90000.                    MEMB CONC
          DUMMY
401 LOAD X A213A209      0.0  90000.                    MEMB CONC
          DUMMY
402 *Leg B1
403 LOADCNB1D3
404 LOAD X B101B103      0.0 -90000.                    MEMB CONC
          DUMMY
405 LOAD X B103B101      0.0  90000.                    MEMB CONC
          DUMMY
406 LOADCNB1D2
407 LOAD X B101B102      0.0 -90000.                    MEMB CONC
          DUMMY
408 LOAD X B102B101      0.0  90000.                    MEMB CONC
          DUMMY
409 LOADCNB1D4
410 LOAD X B101B104      0.0 -90000.                    MEMB CONC
          DUMMY
411 LOAD X B104B101      0.0  90000.                    MEMB CONC
          DUMMY
412 LOADCNB1D6
413 LOAD X B108B110      0.0 -90000.                    MEMB CONC
          DUMMY
414 LOAD X B110B108      0.0  90000.                    MEMB CONC
          DUMMY
415 LOADCNB1D7
416 LOAD X B109B111      0.0 -90000.                    MEMB CONC
```

```
          DUMMY
417 LOAD X B111B109       0.0  90000.                          MEMB CONC
          DUMMY
418 LOADCNB1D8
419 LOAD X B108B112       0.0 -90000.                          MEMB CONC
          DUMMY
420 LOAD X B112B108       0.0  90000.                          MEMB CONC
          DUMMY
421 LOADCNB1D9
422 LOAD X B109B113       0.0 -90000.                          MEMB CONC
          DUMMY
423 LOAD X B113B109       0.0  90000.                          MEMB CONC
          DUMMY
424 *Leg B2
425 LOADCNB2D3
426 LOAD X B201B203       0.0 -90000.                          MEMB CONC
          DUMMY
427 LOAD X B203B201       0.0  90000.                          MEMB CONC
          DUMMY
428 LOADCNB2D2
429 LOAD X B201B202       0.0 -90000.                          MEMB CONC
          DUMMY
430 LOAD X B202B201       0.0  90000.                          MEMB CONC
          DUMMY
431 LOADCNB2D4
432 LOAD X B201B204       0.0 -90000.                          MEMB CONC
          DUMMY
433 LOAD X B204B201       0.0  90000.                          MEMB CONC
          DUMMY
434 LOADCNB2D6
435 LOAD X B208B210       0.0 -90000.                          MEMB CONC
          DUMMY
436 LOAD X B210B208       0.0  90000.                          MEMB CONC
          DUMMY
437 LOADCNB2D7
438 LOAD X B209B211       0.0 -90000.                          MEMB CONC
          DUMMY
439 LOAD X B211B209       0.0  90000.                          MEMB CONC
          DUMMY
440 LOADCNB2D8
441 LOAD X B208B212       0.0 -90000.                          MEMB CONC
          DUMMY
442 LOAD X B212B208       0.0  90000.                          MEMB CONC
          DUMMY
443 LOADCNB2D9
444 LOAD X B209B213       0.0 -90000.                          MEMB CONC
          DUMMY
445 LOAD X B213B209       0.0  90000.                          MEMB CONC
          DUMMY
446 LOADCN  FH
447 LOAD    03A2          2000.                                GLOB JOIN
          1
448 END
```

Gap Element file

```
GAPOPT    5    4    1  MN 600                        PFG
LCSEL                FH TOPS     W    SW   WSW
LCOMB LC1      FH      1.
LCOMB LC2       W      1.TOPS      1.
LCOMB LC3      SW      1.TOPS      1.
LCOMB LC4     WSW      1.TOPS      1.
*Leg A1
*vertical spring
GAPELM A101  A102  A1D2   FD
F-DEL      -20000.      -3.29   -14000.      -1.95   -11500.      -1.42
     -9000.      -0.96
F-DEL       -7000.      -0.62    -6000.      -0.47    -5200.      -0.37
     -4700.      -0.31
F-DEL       -4100.     -0.245    -3600.      -0.19    -3000.      -0.14
     -2700.      -0.12
F-DEL       -2200.    -0.0866    -1600.    -0.0543    -1000.    -0.0274
        0.          0.
F-DEL        794.3     0.0135     1511.     0.0270     2136.     0.0405
     2671.      0.054
F-DEL        3124.     0.0677     3218.      0.071     3307.     0.0745
     3350.      0.076
F-DEL        3383.     0.0775
*horizontal x
GAPELM A101  A103  A1D3   FD
F-DEL      -10000.      -2.23    -8000.      -1.56    -6600.      -1.11
     -5700.      -0.83
F-DEL       -5000.      -0.64    -4300.      -0.44    -3800.      -0.32
     -3400.      -0.24
F-DEL       -3000.      -0.17    -2500.      -0.11    -2100.     -0.076
     -1700.     -0.0475
F-DEL       -1400.     -0.0325    -1100.     -0.024     -600.    -0.0105
        0.          0.
F-DEL         600.     0.0105     1100.      0.024     1400.     0.0325
     1700.     0.0475
F-DEL        2100.      0.076     2500.       0.11     3000.       0.17
     3400.       0.24
F-DEL        3800.       0.32     4300.       0.44     5000.       0.64
     5700.       0.83
F-DEL        6600.       1.11     8000.       1.56    10000.       2.23
*horizontal y
GAPELM A101  A104  A1D4   FD
F-DEL      -10000.      -2.23    -8000.      -1.56    -6600.      -1.11
     -5700.      -0.83
F-DEL       -5000.      -0.64    -4300.      -0.44    -3800.      -0.32
     -3400.      -0.24
F-DEL       -3000.      -0.17    -2500.      -0.11    -2100.     -0.076
     -1700.     -0.0475
F-DEL       -1400.     -0.0325    -1100.     -0.024     -600.    -0.0105
        0.          0.
F-DEL         600.     0.0105     1100.      0.024     1400.     0.0325
     1700.     0.0475
```

```
34 F-DEL        2100.     0.076     2500.      0.11     3000.      0.17
       3400.      0.24
35 F-DEL        3800.      0.32     4300.      0.44     5000.      0.64
       5700.      0.83
36 F-DEL        6600.      1.11     8000.      1.56    10000.      2.23
37 * moment y (rotational stiffness for CoR = 134.42-4.11*15.04 = 72.6
       GNm/rad
38 * With moment arm of 0.2 m this gives Kh = Kr*2/0.2^2= 3630 GN/m
39 GAPELM A108 A110 A1D6  FD
40 F-DEL       -60000. -0.00989   -55000. -0.00797   -44500. -0.00455
       -40000. -0.00343
41 F-DEL       -35000. -0.00247   -31000. -0.00184   -29000. -0.00162
       -27500. -0.00143
42 F-DEL       -23500. -0.00112   -20000.-0.000854   -16000.-0.000635
       -13000. -0.00048
43 F-DEL       -10000.-0.000343    -7500.-0.000243    -2500.-0.000077
           0.         0.
44 F-DEL         2500.0.0000767     7500.0.0002425    10000. 0.000343
       13000.   0.00048
45 F-DEL        16000.0.0006345    20000. 0.000854    23500.  0.00112
       27500.   0.00143
46 F-DEL        29000.  0.00162    31000.  0.00184    35000.  0.00247
       40000.   0.00343
47 F-DEL        44500.  0.00455    55000.  0.00797    60000.  0.00989
48 * moment y
49 GAPELM A109 A111 A1D7  FD
50 F-DEL       -60000. -0.00989   -55000. -0.00797   -44500. -0.00455
       -40000. -0.00343
51 F-DEL       -35000. -0.00247   -31000. -0.00184   -29000. -0.00162
       -27500. -0.00143
52 F-DEL       -23500. -0.00112   -20000.-0.000854   -16000.-0.000635
       -13000. -0.00048
53 F-DEL       -10000.-0.000343    -7500.-0.000243    -2500.-0.000077
           0.         0.
54 F-DEL         2500.0.0000767     7500.0.0002425    10000. 0.000343
       13000.   0.00048
55 F-DEL        16000.0.0006345    20000. 0.000854    23500.  0.00112
       27500.   0.00143
56 F-DEL        29000.  0.00162    31000.  0.00184    35000.  0.00247
       40000.   0.00343
57 F-DEL        44500.  0.00455    55000.  0.00797    60000.  0.00989
58 * moment x
59 GAPELM A108 A112 A1D8  FD
60 F-DEL       -60000. -0.00989   -55000. -0.00797   -44500. -0.00455
       -40000. -0.00343
61 F-DEL       -35000. -0.00247   -31000. -0.00184   -29000. -0.00162
       -27500. -0.00143
62 F-DEL       -23500. -0.00112   -20000.-0.000854   -16000.-0.000635
       -13000. -0.00048
63 F-DEL       -10000.-0.000343    -7500.-0.000243    -2500.-0.000077
           0.         0.
64 F-DEL         2500.0.0000767     7500.0.0002425    10000. 0.000343
       13000.   0.00048
```

```
65 F-DEL      16000.0.0006345   20000. 0.000854   23500.  0.00112
      27500.  0.00143
66 F-DEL      29000.  0.00162   31000.  0.00184   35000.  0.00247
      40000.  0.00343
67 F-DEL      44500.  0.00455   55000.  0.00797   60000.  0.00989
68 * moment x
69 GAPELM A109 A113 A1D9  FD
70 F-DEL     -60000. -0.00989  -55000. -0.00797  -44500. -0.00455
     -40000. -0.00343
71 F-DEL     -35000. -0.00247  -31000. -0.00184  -29000. -0.00162
     -27500. -0.00143
72 F-DEL     -23500. -0.00112  -20000.-0.000854  -16000.-0.000635
     -13000. -0.00048
73 F-DEL     -10000.-0.000343   -7500.-0.000243   -2500.-0.000077
          0.      0.
74 F-DEL       2500.0.0000767    7500.0.0002425   10000. 0.000343
      13000.  0.00048
75 F-DEL      16000.0.0006345   20000. 0.000854   23500.  0.00112
      27500.  0.00143
76 F-DEL      29000.  0.00162   31000.  0.00184   35000.  0.00247
      40000.  0.00343
77 F-DEL      44500.  0.00455   55000.  0.00797   60000.  0.00989
78 *Leg A2
79 *vertical spring
80 GAPELM A201 A202 A2D2  FD
81 F-DEL     -20000.    -3.29  -14000.    -1.95  -11500.    -1.42
     -9000.    -0.96
82 F-DEL      -7000.    -0.62   -6000.    -0.47   -5200.    -0.37
     -4700.    -0.31
83 F-DEL      -4100.   -0.245   -3600.    -0.19   -3000.    -0.14
     -2700.    -0.12
84 F-DEL      -2200.  -0.0866   -1600.  -0.0543   -1000.  -0.0274
          0.      0.
85 F-DEL       794.3   0.0135    1511.   0.0270    2136.   0.0405
      2671.    0.054
86 F-DEL       3124.   0.0677    3218.    0.071    3307.   0.0745
      3350.    0.076
87 F-DEL       3383.   0.0775
88 *horizontal x
89 GAPELM A201 A203 A2D3  FD
90 F-DEL     -10000.    -2.23   -8000.    -1.56   -6600.    -1.11
     -5700.    -0.83
91 F-DEL      -5000.    -0.64   -4300.    -0.44   -3800.    -0.32
     -3400.    -0.24
92 F-DEL      -3000.    -0.17   -2500.    -0.11   -2100.   -0.076
     -1700.  -0.0475
93 F-DEL      -1400.  -0.0325   -1100.   -0.024    -600.  -0.0105
          0.      0.
94 F-DEL        600.   0.0105    1100.    0.024    1400.   0.0325
      1700.   0.0475
95 F-DEL       2100.    0.076    2500.     0.11    3000.     0.17
      3400.     0.24
96 F-DEL       3800.     0.32    4300.     0.44    5000.     0.64
```

```
      5700.      0.83
 97 F-DEL        6600.      1.11     8000.      1.56    10000.      2.23
 98 *horizontal y
 99 GAPELM A201  A204  A2D4   FD
100 F-DEL       -10000.     -2.23    -8000.     -1.56    -6600.     -1.11
      -5700.     -0.83
101 F-DEL        -5000.     -0.64    -4300.     -0.44    -3800.     -0.32
      -3400.     -0.24
102 F-DEL        -3000.     -0.17    -2500.     -0.11    -2100.    -0.076
      -1700.   -0.0475
103 F-DEL        -1400.   -0.0325    -1100.    -0.024     -600.   -0.0105
          0.         0.
104 F-DEL          600.    0.0105     1100.     0.024     1400.    0.0325
       1700.    0.0475
105 F-DEL         2100.     0.076     2500.      0.11     3000.      0.17
       3400.      0.24
106 F-DEL         3800.      0.32     4300.      0.44     5000.      0.64
       5700.      0.83
107 F-DEL         6600.      1.11     8000.      1.56    10000.      2.23
108 * moment y (rotational stiffness for CoR = 134.42-4.11*15.04 = 72.6
      GNm/rad
109 * With moment arm of 0.2 m this gives Kh = Kr*2/0.2^2= 3630 GN/m
110 GAPELM A208  A210  A2D6   FD
111 F-DEL       -60000. -0.00989   -55000. -0.00797   -44500. -0.00455
      -40000. -0.00343
112 F-DEL       -35000. -0.00247   -31000. -0.00184   -29000. -0.00162
      -27500. -0.00143
113 F-DEL       -23500. -0.00112   -20000.-0.000854   -16000.-0.000635
      -13000. -0.00048
114 F-DEL       -10000.-0.000343    -7500.-0.000243    -2500.-0.000077
          0.         0.
115 F-DEL         2500.0.0000767     7500.0.0002425    10000. 0.000343
       13000.   0.00048
116 F-DEL        16000.0.0006345    20000. 0.000854    23500.   0.00112
       27500.   0.00143
117 F-DEL        29000.   0.00162   31000.   0.00184   35000.   0.00247
       40000.   0.00343
118 F-DEL        44500.   0.00455   55000.   0.00797   60000.   0.00989
119 * moment y
120 GAPELM A209  A211  A2D7   FD
121 F-DEL       -60000. -0.00989   -55000. -0.00797   -44500. -0.00455
      -40000. -0.00343
122 F-DEL       -35000. -0.00247   -31000. -0.00184   -29000. -0.00162
      -27500. -0.00143
123 F-DEL       -23500. -0.00112   -20000.-0.000854   -16000.-0.000635
      -13000. -0.00048
124 F-DEL       -10000.-0.000343    -7500.-0.000243    -2500.-0.000077
          0.         0.
125 F-DEL         2500.0.0000767     7500.0.0002425    10000. 0.000343
       13000.   0.00048
126 F-DEL        16000.0.0006345    20000. 0.000854    23500.   0.00112
       27500.   0.00143
127 F-DEL        29000.   0.00162   31000.   0.00184   35000.   0.00247
```

```
      40000.   0.00343
128 F-DEL       44500.   0.00455    55000.   0.00797    60000.   0.00989
129 * moment x
130 GAPELM A208  A212  A2D8   FD
131 F-DEL      -60000.  -0.00989   -55000.  -0.00797   -44500.  -0.00455
      -40000.  -0.00343
132 F-DEL      -35000.  -0.00247   -31000.  -0.00184   -29000.  -0.00162
      -27500.  -0.00143
133 F-DEL      -23500.  -0.00112   -20000. -0.000854   -16000. -0.000635
      -13000.  -0.00048
134 F-DEL      -10000. -0.000343    -7500. -0.000243    -2500. -0.000077
          0.       0.
135 F-DEL        2500. 0.0000767     7500. 0.0002425    10000.  0.000343
      13000.   0.00048
136 F-DEL       16000. 0.0006345    20000.  0.000854    23500.   0.00112
      27500.   0.00143
137 F-DEL       29000.   0.00162    31000.   0.00184    35000.   0.00247
      40000.   0.00343
138 F-DEL       44500.   0.00455    55000.   0.00797    60000.   0.00989
139 * moment x
140 GAPELM A209  A213  A2D9   FD
141 F-DEL      -60000.  -0.00989   -55000.  -0.00797   -44500.  -0.00455
      -40000.  -0.00343
142 F-DEL      -35000.  -0.00247   -31000.  -0.00184   -29000.  -0.00162
      -27500.  -0.00143
143 F-DEL      -23500.  -0.00112   -20000. -0.000854   -16000. -0.000635
      -13000.  -0.00048
144 F-DEL      -10000. -0.000343    -7500. -0.000243    -2500. -0.000077
          0.       0.
145 F-DEL        2500. 0.0000767     7500. 0.0002425    10000.  0.000343
      13000.   0.00048
146 F-DEL       16000. 0.0006345    20000.  0.000854    23500.   0.00112
      27500.   0.00143
147 F-DEL       29000.   0.00162    31000.   0.00184    35000.   0.00247
      40000.   0.00343
148 F-DEL       44500.   0.00455    55000.   0.00797    60000.   0.00989
149 *Leg B1
150 *vertical spring
151 GAPELM B101  B102  B1D2   FD
152 F-DEL      -20000.    -3.29   -14000.    -1.95   -11500.    -1.42
      -9000.    -0.96
153 F-DEL       -7000.    -0.62    -6000.    -0.47    -5200.    -0.37
      -4700.    -0.31
154 F-DEL       -4100.   -0.245    -3600.    -0.19    -3000.    -0.14
      -2700.    -0.12
155 F-DEL       -2200.  -0.0866    -1600.  -0.0543    -1000.  -0.0274
          0.       0.
156 F-DEL        794.3   0.0135     1511.   0.0270     2136.   0.0405
      2671.    0.054
157 F-DEL        3124.   0.0677     3218.    0.071     3307.   0.0745
      3350.    0.076
158 F-DEL        3383.   0.0775
159 *horizontal x
```

```
160 GAPELM B101  B103  B1D3   FD
161 F-DEL      -10000.     -2.23     -8000.     -1.56     -6600.     -1.11
        -5700.     -0.83
162 F-DEL       -5000.     -0.64     -4300.     -0.44     -3800.     -0.32
        -3400.     -0.24
163 F-DEL       -3000.     -0.17     -2500.     -0.11     -2100.    -0.076
        -1700.   -0.0475
164 F-DEL       -1400.   -0.0325     -1100.    -0.024      -600.   -0.0105
           0.        0.
165 F-DEL         600.    0.0105      1100.     0.024      1400.    0.0325
        1700.    0.0475
166 F-DEL        2100.     0.076      2500.      0.11      3000.      0.17
        3400.      0.24
167 F-DEL        3800.      0.32      4300.      0.44      5000.      0.64
        5700.      0.83
168 F-DEL        6600.      1.11      8000.      1.56     10000.      2.23
169 *horizontal y
170 GAPELM B101  B104  B1D4   FD
171 F-DEL      -10000.     -2.23     -8000.     -1.56     -6600.     -1.11
        -5700.     -0.83
172 F-DEL       -5000.     -0.64     -4300.     -0.44     -3800.     -0.32
        -3400.     -0.24
173 F-DEL       -3000.     -0.17     -2500.     -0.11     -2100.    -0.076
        -1700.   -0.0475
174 F-DEL       -1400.   -0.0325     -1100.    -0.024      -600.   -0.0105
           0.        0.
175 F-DEL         600.    0.0105      1100.     0.024      1400.    0.0325
        1700.    0.0475
176 F-DEL        2100.     0.076      2500.      0.11      3000.      0.17
        3400.      0.24
177 F-DEL        3800.      0.32      4300.      0.44      5000.      0.64
        5700.      0.83
178 F-DEL        6600.      1.11      8000.      1.56     10000.      2.23
179 * moment y (rotational stiffness for CoR = 134.42-4.11*15.04 = 72.6
      GNm/rad
180 * With moment arm of 0.2 m this gives Kh = Kr*2/0.2^2= 3630 GN/m
181 GAPELM B108  B110  B1D6   FD
182 F-DEL      -60000. -0.00989   -55000. -0.00797   -44500. -0.00455
        -40000. -0.00343
183 F-DEL      -35000. -0.00247   -31000. -0.00184   -29000. -0.00162
        -27500. -0.00143
184 F-DEL      -23500. -0.00112   -20000.-0.000854   -16000.-0.000635
        -13000. -0.00048
185 F-DEL      -10000.-0.000343    -7500.-0.000243    -2500.-0.000077
           0.        0.
186 F-DEL        2500.0.0000767     7500.0.0002425    10000. 0.000343
        13000.   0.00048
187 F-DEL       16000.0.0006345    20000. 0.000854    23500.  0.00112
        27500.   0.00143
188 F-DEL       29000.  0.00162    31000.  0.00184    35000.  0.00247
        40000.   0.00343
189 F-DEL       44500.  0.00455    55000.  0.00797    60000.  0.00989
190 * moment y
```

```
191 GAPELM B109 B111 B1D7 FD
192 F-DEL -60000. -0.00989 -55000. -0.00797 -44500. -0.00455
      -40000. -0.00343
193 F-DEL -35000. -0.00247 -31000. -0.00184 -29000. -0.00162
      -27500. -0.00143
194 F-DEL -23500. -0.00112 -20000.-0.000854 -16000.-0.000635
      -13000. -0.00048
195 F-DEL -10000.-0.000343 -7500.-0.000243 -2500.-0.000077
      0. 0.
196 F-DEL 2500.0.0000767 7500.0.0002425 10000. 0.000343
      13000. 0.00048
197 F-DEL 16000.0.0006345 20000. 0.000854 23500. 0.00112
      27500. 0.00143
198 F-DEL 29000. 0.00162 31000. 0.00184 35000. 0.00247
      40000. 0.00343
199 F-DEL 44500. 0.00455 55000. 0.00797 60000. 0.00989
200 * moment x
201 GAPELM B108 B112 B1D8 FD
202 F-DEL -60000. -0.00989 -55000. -0.00797 -44500. -0.00455
      -40000. -0.00343
203 F-DEL -35000. -0.00247 -31000. -0.00184 -29000. -0.00162
      -27500. -0.00143
204 F-DEL -23500. -0.00112 -20000.-0.000854 -16000.-0.000635
      -13000. -0.00048
205 F-DEL -10000.-0.000343 -7500.-0.000243 -2500.-0.000077
      0. 0.
206 F-DEL 2500.0.0000767 7500.0.0002425 10000. 0.000343
      13000. 0.00048
207 F-DEL 16000.0.0006345 20000. 0.000854 23500. 0.00112
      27500. 0.00143
208 F-DEL 29000. 0.00162 31000. 0.00184 35000. 0.00247
      40000. 0.00343
209 F-DEL 44500. 0.00455 55000. 0.00797 60000. 0.00989
210 * moment x
211 GAPELM B109 B113 B1D9 FD
212 F-DEL -60000. -0.00989 -55000. -0.00797 -44500. -0.00455
      -40000. -0.00343
213 F-DEL -35000. -0.00247 -31000. -0.00184 -29000. -0.00162
      -27500. -0.00143
214 F-DEL -23500. -0.00112 -20000.-0.000854 -16000.-0.000635
      -13000. -0.00048
215 F-DEL -10000.-0.000343 -7500.-0.000243 -2500.-0.000077
      0. 0.
216 F-DEL 2500.0.0000767 7500.0.0002425 10000. 0.000343
      13000. 0.00048
217 F-DEL 16000.0.0006345 20000. 0.000854 23500. 0.00112
      27500. 0.00143
218 F-DEL 29000. 0.00162 31000. 0.00184 35000. 0.00247
      40000. 0.00343
219 F-DEL 44500. 0.00455 55000. 0.00797 60000. 0.00989
220 *Leg B2
221 *vertical spring
222 GAPELM B201 B202 B2D2 FD
```

```
223 F-DEL      -20000.     -3.29   -14000.     -1.95   -11500.     -1.42
       -9000.     -0.96
224 F-DEL       -7000.     -0.62    -6000.     -0.47    -5200.     -0.37
       -4700.     -0.31
225 F-DEL       -4100.    -0.245    -3600.     -0.19    -3000.     -0.14
       -2700.     -0.12
226 F-DEL       -2200.   -0.0866    -1600.   -0.0543    -1000.   -0.0274
          0.         0.
227 F-DEL        794.3    0.0135     1511.    0.0270     2136.    0.0405
        2671.     0.054
228 F-DEL        3124.    0.0677     3218.     0.071     3307.    0.0745
        3350.     0.076
229 F-DEL        3383.    0.0775
230 *horizontal x
231 GAPELM B201  B203  B2D3   FD
232 F-DEL      -10000.     -2.23    -8000.     -1.56    -6600.     -1.11
       -5700.     -0.83
233 F-DEL       -5000.     -0.64    -4300.     -0.44    -3800.     -0.32
       -3400.     -0.24
234 F-DEL       -3000.     -0.17    -2500.     -0.11    -2100.    -0.076
       -1700.   -0.0475
235 F-DEL       -1400.   -0.0325    -1100.    -0.024     -600.   -0.0105
          0.         0.
236 F-DEL         600.    0.0105     1100.     0.024     1400.    0.0325
        1700.    0.0475
237 F-DEL        2100.     0.076     2500.      0.11     3000.      0.17
        3400.      0.24
238 F-DEL        3800.      0.32     4300.      0.44     5000.      0.64
        5700.      0.83
239 F-DEL        6600.      1.11     8000.      1.56    10000.      2.23
240 *horizontal y
241 GAPELM B201  B204  B2D4   FD
242 F-DEL      -10000.     -2.23    -8000.     -1.56    -6600.     -1.11
       -5700.     -0.83
243 F-DEL       -5000.     -0.64    -4300.     -0.44    -3800.     -0.32
       -3400.     -0.24
244 F-DEL       -3000.     -0.17    -2500.     -0.11    -2100.    -0.076
       -1700.   -0.0475
245 F-DEL       -1400.   -0.0325    -1100.    -0.024     -600.   -0.0105
          0.         0.
246 F-DEL         600.    0.0105     1100.     0.024     1400.    0.0325
        1700.    0.0475
247 F-DEL        2100.     0.076     2500.      0.11     3000.      0.17
        3400.      0.24
248 F-DEL        3800.      0.32     4300.      0.44     5000.      0.64
        5700.      0.83
249 F-DEL        6600.      1.11     8000.      1.56    10000.      2.23
250 * moment y (rotational stiffness for CoR = 134.42-4.11*15.04 = 72.6
      GNm/rad
251 * With moment arm of 0.2 m this gives Kh = Kr*2/0.2^2= 3630 GN/m
252 GAPELM B208  B210  B2D6   FD
253 F-DEL      -60000. -0.00989   -55000. -0.00797   -44500. -0.00455
       -40000. -0.00343
```

```
254 F-DEL      -35000. -0.00247   -31000. -0.00184   -29000. -0.00162
       -27500. -0.00143
255 F-DEL      -23500. -0.00112   -20000.-0.000854   -16000.-0.000635
       -13000. -0.00048
256 F-DEL      -10000.-0.000343    -7500.-0.000243    -2500.-0.000077
           0.      0.
257 F-DEL       2500.0.0000767     7500.0.0002425    10000. 0.000343
       13000.  0.00048
258 F-DEL       16000.0.0006345   20000. 0.000854    23500.  0.00112
       27500.  0.00143
259 F-DEL       29000.  0.00162   31000.  0.00184    35000.  0.00247
       40000.  0.00343
260 F-DEL       44500.  0.00455   55000.  0.00797    60000.  0.00989
261 * moment y
262 GAPELM B209 B211 B2D7  FD
263 F-DEL      -60000. -0.00989   -55000. -0.00797   -44500. -0.00455
       -40000. -0.00343
264 F-DEL      -35000. -0.00247   -31000. -0.00184   -29000. -0.00162
       -27500. -0.00143
265 F-DEL      -23500. -0.00112   -20000.-0.000854   -16000.-0.000635
       -13000. -0.00048
266 F-DEL      -10000.-0.000343    -7500.-0.000243    -2500.-0.000077
           0.      0.
267 F-DEL       2500.0.0000767     7500.0.0002425    10000. 0.000343
       13000.  0.00048
268 F-DEL       16000.0.0006345   20000. 0.000854    23500.  0.00112
       27500.  0.00143
269 F-DEL       29000.  0.00162   31000.  0.00184    35000.  0.00247
       40000.  0.00343
270 F-DEL       44500.  0.00455   55000.  0.00797    60000.  0.00989
271 * moment x
272 GAPELM B208 B212 B2D8  FD
273 F-DEL      -60000. -0.00989   -55000. -0.00797   -44500. -0.00455
       -40000. -0.00343
274 F-DEL      -35000. -0.00247   -31000. -0.00184   -29000. -0.00162
       -27500. -0.00143
275 F-DEL      -23500. -0.00112   -20000.-0.000854   -16000.-0.000635
       -13000. -0.00048
276 F-DEL      -10000.-0.000343    -7500.-0.000243    -2500.-0.000077
           0.      0.
277 F-DEL       2500.0.0000767     7500.0.0002425    10000. 0.000343
       13000.  0.00048
278 F-DEL       16000.0.0006345   20000. 0.000854    23500.  0.00112
       27500.  0.00143
279 F-DEL       29000.  0.00162   31000.  0.00184    35000.  0.00247
       40000.  0.00343
280 F-DEL       44500.  0.00455   55000.  0.00797    60000.  0.00989
281 * moment x
282 GAPELM B209 B213 B2D9  FD
283 F-DEL      -60000. -0.00989   -55000. -0.00797   -44500. -0.00455
       -40000. -0.00343
284 F-DEL      -35000. -0.00247   -31000. -0.00184   -29000. -0.00162
       -27500. -0.00143
```

```
285 F–DEL      −23500. −0.00112   −20000.−0.000854   −16000.−0.000635
      −13000. −0.00048
286 F–DEL      −10000.−0.000343    −7500.−0.000243    −2500.−0.000077
      0.        0.
287 F–DEL       2500.0.0000767     7500.0.0002425    10000. 0.000343
      13000.   0.00048
288 F–DEL      16000.0.0006345    20000. 0.000854    23500.  0.00112
      27500.   0.00143
289 F–DEL      29000.  0.00162    31000.  0.00184    35000.  0.00247
      40000.   0.00343
290 F–DEL      44500.  0.00455    55000.  0.00797    60000.  0.00989
291 END
```

Superelement Input file

```
 1 SUBOPT INP MN
 2 STFHEAD  A105A105 +1.
 3 STFR FX
 4 STFR FY
 5 STFR FZ
 6 STFR MX
 7 STFR MY
 8 STFR MZ                                                    50.12e6
 9 STFHEAD  A205A205 +1.
10 STFR FX
11 STFR FY
12 STFR FZ
13 STFR MX
14 STFR MY
15 STFR MZ                                                    50.12e6
16 STFHEAD  B105B105 +1.
17 STFR FX
18 STFR FY
19 STFR FZ
20 STFR MX
21 STFR MY
22 STFR MZ                                                    50.12e6
23 STFHEAD  B205B205 +1.
24 STFR FX
25 STFR FY
26 STFR FZ
27 STFR MX
28 STFR MY
29 STFR MZ                                                    50.12e6
30 END
```

Non-Linear Model 2

Model Input file

```
 1 LDOPT SFINOP  +Z1.0251827.849047   -19.79    19.79GLOBMN
       NPNP     K
 2 OPTIONS I     MN          UC    2 2    DC  C     PTPTPT        PTPT
 3 UCPART           0.7000.7001.0001.000
 4 SECT
 5 SECT DUMMY1     TUB                                    100.005.000
 6 SECT M406127    TUB                                    40.6401.270
 7 SECT M406191    TUB                                    40.6401.910
 8 SECT M508127    TUB                                    50.8001.270
 9 SECT M508191    TUB                                    50.8001.910
10 SECT M508254    TUB                                    50.8002.540
11 SECT M609191    TUB                                    60.9601.910
12 SECT M609254    TUB                                    60.9602.540
13 SECT M609318    TUB                                    60.9603.180
14 SECT M762191    TUB                                    76.2001.910
15 SECT M914254    TUB                                    91.4002.540
16 SECT M914318    TUB                                    91.4403.180
17 SECT N137125    TUB                                    137.162.540
18 SECT N137138    TUB                                    137.163.810
19 SECT N137150    TUB                                    137.165.080
20 SECT N137160    TUB                                    137.166.000
21
22 GRUP
23 GRUP 111 M609254              21.007.72235.50 1     1.001.00
       7.8500
24 GRUP 112 M609254              21.007.72235.50 1     1.001.00
       7.8500
25 GRUP 112 M609254              21.007.72235.50 1     1.001.00
       7.85001.60
26 GRUP 121 M609254              21.007.72235.50 1     1.001.00
       7.8500
27 GRUP 122 M609191              21.007.72235.50 1     1.001.00
       7.8500
28 GRUP 122 M609254              21.007.72235.50 1     1.001.00
       7.85001.60
29 GRUP 131 M609254              21.007.72235.50 1     1.001.00
       7.8500
30 GRUP 132 M609191              21.007.72235.50 1     1.001.00
       7.8500
31 GRUP 132 M609254              21.007.72235.50 1     1.001.00
       7.85001.60
32 GRUP 211 M609254              21.007.72235.50 1     1.001.00
       7.8500
33 GRUP 212 M609254              21.007.72235.50 1     1.001.00
       7.85001.60
34 GRUP 212 M609191              21.007.72235.50 1     1.001.00
       7.8500
35 GRUP 221 M609254              21.007.72235.50 1     1.001.00
       7.8500
```

```
36 GRUP 222 M609254              21.007.72235.50 1    1.001.00
       7.85001.60
37 GRUP 222 M609191              21.007.72235.50 1    1.001.00
       7.8500
38 GRUP 231 M609254              21.007.72235.50 1    1.001.00
       7.8500
39 GRUP 232 M609254              21.007.72235.50 1    1.001.00
       7.8500
40 GRUP 232 M609191              21.007.72235.50 1    1.001.00
       7.85006.00
41 GRUP A11 M609254              21.007.72235.50 1    1.001.00
       7.85001.60
42 GRUP A11 M609191              21.007.72235.50 1    1.001.00
       7.8500
43 GRUP A12 M609254              21.007.72235.50 1    1.001.00
       7.8500
44 GRUP A13 M609191              21.007.72235.50 1    1.001.00
       7.8500
45 GRUP A13 M609254              21.007.72235.50 1    1.001.00
       7.8500.500
46 GRUP A14 M609191              21.007.72235.50 1    1.001.00
       7.8500
47 GRUP A21 M609318              21.007.72235.50 1    1.001.00
       7.85001.60
48 GRUP A21 M609191              21.007.72235.50 1    1.001.00
       7.8500
49 GRUP A22 M609318              21.007.72235.50 1    1.001.00
       7.8500
50 GRUP A23 M609191              21.007.72235.50 1    1.001.00
       7.8500
51 GRUP A23 M609318              21.007.72235.50 1    1.001.00
       7.85001.60
52 GRUP A31 M609254              21.007.72235.50 1    1.001.00
       7.85001.60
53 GRUP A31 M609191              21.007.72235.50 1    1.001.00
       7.8500
54 GRUP A32 M609254              21.007.72235.50 1    1.001.00
       7.8500
55 GRUP A33 M609191              21.007.72235.50 1    1.001.00
       7.8500
56 GRUP A33 M609254              21.007.72235.50 1    1.001.00
       7.85001.60
57 GRUP B11 M609191              21.007.72235.50 1    1.001.00
       7.8500
58 GRUP B21 M609191              21.007.72235.50 1    1.001.00
       7.8500
59 GRUP B31 M609191              21.007.72235.50 1    1.001.00
       7.8500
60 GRUP C01 M406191              21.007.72235.50 1    1.001.00
       7.8500
61 GRUP C02 M508191              21.007.72235.50 1    1.001.00
       7.8500
62 GRUP D11 M609191              21.007.72235.50 1    1.001.00
```

```
      7.8500
63 GRUP D11 M609254              21.007.72235.50 1     1.001.00
      7.8500.500
64 GRUP D12 M609254              21.007.72235.50 1     1.001.00
      7.8500
65 GRUP D13 M609254              21.007.72235.50 1     1.001.00
      7.8500.500
66 GRUP D13 M609191              21.007.72235.50 1     1.001.00
      7.8500
67 GRUP D21 M609191              21.007.72235.50 1     1.001.00
      7.8500
68 GRUP D21 M609254              21.007.72235.50 1     1.001.00
      7.8500.500
69 GRUP D22 M609254              21.007.72235.50 1     1.001.00
      7.8500
70 GRUP D23 M609254              21.007.72235.50 1     1.001.00
      7.8500.500
71 GRUP D23 M609191              21.007.72235.50 1     1.001.00
      7.8500
72 GRUP D31 M508191              21.007.72235.50 1     1.001.00
      7.8500
73 GRUP D31 M508254              21.007.72235.50 1     1.001.00
      7.8500.500
74 GRUP D32 M508254              21.007.72235.50 1     1.001.00
      7.8500
75 GRUP D33 M508254              21.007.72235.50 1     1.001.00
      7.8500.500
76 GRUP D33 M508191              21.007.72235.50 1     1.001.00
      7.8500
77 GRUP F11 M406127              21.007.72235.50 1     1.001.00
      7.8500
78 GRUP F21 M508127              21.007.72235.50 1     1.001.00
      7.8500
79 GRUP F22 M609191              21.007.72235.50 1     1.001.00
      7.8500
80 GRUP F31 M406127              21.007.72235.50 1     1.001.00
      7.8500
81 GRUP F32 M508127              21.007.72235.50 1     1.001.00
      7.8500
82 GRUP L01 N137160              21.007.72235.50 1     1.001.00
      F7.8500
83 GRUP L04 N137150              21.007.72235.50 1     1.001.00
      F7.8500
84 GRUP L05 N137138              21.007.72235.50 1     1.001.00
      F7.8500
85 GRUP L11 N137150              21.007.72235.50 1     1.001.00
      F7.8500
86 GRUP LA2 N137150              21.007.72235.50 1     1.001.00
      F7.85001.80
87 GRUP LA2 N137125              21.007.72235.50 1     1.001.00
      F7.8500
88 GRUP LA2 N137150              21.007.72235.50 1     1.001.00
      F7.85001.80
```

```
 89 GRUP LA3 N137150                21.007.72235.50 1     1.001.00
       F7.85002.00
 90 GRUP LA3 N137160                21.007.72235.50 1     1.001.00
       F7.8500
 91 GRUP LA3 N137150                21.007.72235.50 1     1.001.00
       F7.85004.10
 92 GRUP LB2 N137150                21.007.72235.50 1     1.001.00
       F7.85001.80
 93 GRUP LB2 N137138                21.007.72235.50 1     1.001.00
       F7.8500
 94 GRUP LB2 N137150                21.007.72235.50 1     1.001.00
       F7.85001.80
 95 GRUP LB3 N137150                21.007.72235.50 1     1.001.00
       F7.8500
 96 GRUP X2A M914254                21.007.72235.50 1     1.001.00
       7.8500
 97 GRUP XAB M914254                21.007.72235.50 1     1.001.00
       7.8500
 98 GRUP XB2 M914254                21.007.72235.50 1     1.001.00
       7.8500
 99 GRUP XBA M914254                21.007.72235.50 1     1.001.00
       7.85009.20
100 GRUP XBA M914318                21.007.72235.50 1     1.001.00
       7.85005.20
101 GRUP XBA M914254                21.007.72235.50 1     1.001.00
       7.8500
102 GRUP XX1 M762191                21.007.72235.50 1     1.001.00
       7.8500
103 GRUP GAP          X   1+5    3. 2000. 0.77 35.5 1                    N
         1-5
104 GRUP DMY          X   1+5    3.    0.2 2.+0 35.5 1                    N
         1-5
105 GRUP DM2          X   1+5    3.  2.+2 2.+2 35.5 1                    N
         1-5
106
107 MEMBER
108 MEMBER 012001A1 111
109 MEMBER 01B10120 112
110 MEMBER 022002A1 121
111 MEMBER 02B10220 122
112 MEMBER 032003A1 131
113 MEMBER 03B10320 132
114 MEMBER 01A20110 211
115 MEMBER 011001B2 212
116 MEMBER 02A20210 221
117 MEMBER 021002B2 222
118 MEMBER 03A20310 231
119 MEMBER 031003B2 232
120 MEMBER 100101A2 A11
121 MEMBER 10051001 A12
122 MEMBER 10021005 A13
123 MEMBER 01A11002 A14
124 MEMBER 200102A2 A21
```

```
125 MEMBER 20022001  A22
126 MEMBER 02A12002  A23
127 MEMBER 300103A2  A31
128 MEMBER 30023001  A32
129 MEMBER 03A13002  A33
130 MEMBER 01B201B1  B11
131 MEMBER 02B22005  B21
132 MEMBER 200502B1  B21
133 MEMBER 03B23005  B31
134 MEMBER 300503B1  B31
135 MEMBER 20032001  C01
136 MEMBER 20042002  C01
137 MEMBER 30033001  C01
138 MEMBER 30043002  C01
139 MEMBER 10031001  C02
140 MEMBER 10061005  C02
141 MEMBER 01101003  D11
142 MEMBER 10031006  D12
143 MEMBER 10061004  D12
144 MEMBER 10040120  D13
145 MEMBER 02102003  D21
146 MEMBER 20032004  D22
147 MEMBER 20040220  D23
148 MEMBER 03103003  D31
149 MEMBER 30033004  D32
150 MEMBER 30040320  D33
151 MEMBER 01101001  F11
152 MEMBER 01201002  F11
153 MEMBER 10041002  F11
154 MEMBER 02102001  F21
155 MEMBER 02202002  F21
156 MEMBER 02102005  F22
157 MEMBER 02202005  F22
158 MEMBER 03103001  F31
159 MEMBER 03203002  F31
160 MEMBER 03103005  F32
161 MEMBER 03203005  F32
162 MEMBER 0A1  00A1  L01
163 MEMBER 0A2  00A2  L01
164 MEMBER 0B1  00B1  L01
165 MEMBER 0B2  00B2  L01
166 MEMBER 03A104A1  L04
167 MEMBER 03A204A2  L04
168 MEMBER 03B104B1  L04
169 MEMBER 03B204B2  L04
170 MEMBER 04A105A1  L05
171 MEMBER 04A205A2  L05
172 MEMBER 04B105B1  L05
173 MEMBER 04B205B2  L05
174 MEMBER 00A101A1  L11
175 MEMBER 00A201A2  L11
176 MEMBER 00B101B1  L11
177 MEMBER 00B201B2  L11
```

```
178 MEMBER 01A102A1 LA2
179 MEMBER 01A202A2 LA2
180 MEMBER 02A103A1 LA3
181 MEMBER 02A203A2 LA3
182 MEMBER 01B102B1 LB2
183 MEMBER 01B202B2 LB2
184 MEMBER 02B103B1 LB3
185 MEMBER 02B203B2 LB3
186 MEMBER 03A202A1 X2A
187 MEMBER 03A102B1 XAB
188 MEMBER 03B102B2 XB2
189 MEMBER 03B202A2 XBA
190 MEMBER 02A101A2 XX1
191 MEMBER 02A201B2 XX1
192 MEMBER 02B101A1 XX1
193 MEMBER 02B201B1 XX1
194 *Leg A1
195 MEMBER A101A102 DM2SK
196 MEMBER A102A103 GAP    000111000000
197 MEMBER A102A104 GAP    000111000000
198 MEMBER A102A105 GAP    000111000000
199 MEMBER A101 0A1 DM2SK 000000000100
200 MEMBER A107 0A1 GAP    000000000111
201 MEMBER A108 0A1 GAP    000000000111
202 *Leg A2
203 MEMBER A201A202 DM2SK
204 MEMBER A202A203 GAP    000111000000
205 MEMBER A202A204 GAP    000111000000
206 MEMBER A202A205 GAP    000111000000
207 MEMBER A201 0A2 DM2SK 000000000100
208 MEMBER A207 0A2 GAP    000000000111
209 MEMBER A208 0A2 GAP    000000000111
210 *Leg B1
211 MEMBER B101B102 DM2SK
212 MEMBER B102B103 GAP    000111000000
213 MEMBER B102B104 GAP    000111000000
214 MEMBER B102B105 GAP    000111000000
215 MEMBER B101 0B1 DM2SK 000000000100
216 MEMBER B107 0B1 GAP    000000000111
217 MEMBER B108 0B1 GAP    000000000111
218 *Leg B2
219 MEMBER B201B202 DM2SK
220 MEMBER B202B203 GAP    000111000000
221 MEMBER B202B204 GAP    000111000000
222 MEMBER B202B205 GAP    000111000000
223 MEMBER B201 0B2 DM2SK 000000000100
224 MEMBER B207 0B2 GAP    000000000111
225 MEMBER B208 0B2 GAP    000000000111
226
227 JOINT
228 JOINT   0A1  -11.323  11.645 -19.800
229 JOINT   0A2  -11.323 -11.645 -19.800
230 JOINT   0B1   11.323  11.645 -19.800
```

```
231 JOINT   0B2   11.323 -11.645 -19.800
232 JOINT  00A1  -11.323  11.645 -18.000
233 JOINT  00A2  -11.323 -11.645 -18.000
234 JOINT  00B1   11.323  11.645 -18.000
235 JOINT  00B2   11.323 -11.645 -18.000
236 JOINT  0110   -4.623 -11.578 -17.300
237 JOINT  0120   -4.623  11.578 -17.300
238 JOINT  01A1  -11.323  11.576 -17.300
239 JOINT  01A2  -11.323 -11.576 -17.300
240 JOINT  01B1   11.259  11.581 -17.300
241 JOINT  01B2   11.259 -11.581 -17.300
242 JOINT  0210   -4.623 -10.495  -6.000
243 JOINT  0220   -4.623  10.495  -6.000
244 JOINT  02A1  -11.323  10.469  -6.000
245 JOINT  02A2  -11.323 -10.469  -6.000
246 JOINT  02B1   10.228  10.551  -6.000
247 JOINT  02B2   10.228 -10.551  -6.000
248 JOINT  0310   -4.623  -9.061   9.000
249 JOINT  0320   -4.623   9.061   9.000
250 JOINT  03A1  -11.323   9.000   9.000
251 JOINT  03A2  -11.323  -9.000   9.000
252 JOINT  03B1    8.859   9.182   9.000
253 JOINT  03B2    8.859  -9.182   9.000
254 JOINT  04A1  -11.323   9.000  11.000
255 JOINT  04A2  -11.323  -9.000  11.000
256 JOINT  04B1    8.677   9.000  11.000
257 JOINT  04B2    8.677  -9.000  11.000
258 JOINT  05A1  -11.323   9.000  15.500
259 JOINT  05A2  -11.323  -9.000  15.500
260 JOINT  05B1    8.677   9.000  15.500
261 JOINT  05B2    8.677  -9.000  15.500
262 JOINT  1001  -11.323  -4.000 -17.300
263 JOINT  1002  -11.323   2.100 -17.300
264 JOINT  1003   -4.623  -4.061 -17.300
265 JOINT  1004   -4.623   2.039 -17.300
266 JOINT  1005  -11.323  -1.800 -17.300
267 JOINT  1006   -4.623  -1.861 -17.300
268 JOINT  2001  -11.323  -4.000  -6.000
269 JOINT  2002  -11.323   2.100  -6.000
270 JOINT  2003   -4.623  -4.061  -6.000
271 JOINT  2004   -4.623   2.039  -6.000
272 JOINT  2005   10.228   0.000  -6.000
273 JOINT  3001  -11.323  -4.000   9.000
274 JOINT  3002  -11.323   2.100   9.000
275 JOINT  3003   -4.623  -4.061   9.000
276 JOINT  3004   -4.623   2.039   9.000
277 JOINT  3005    8.859   0.000   9.000
278 *leg A1
279 JOINT A101  -11.323  11.645 -23.800
280 JOINT A102  -11.323  11.645 -27.100
281 JOINT A103  -11.323  11.645 -44.000                    001111
282 JOINT A104  -11.323   1.645 -27.100                    010111
283 JOINT A105  -21.323  11.645 -27.100                    100111
```

```
284 JOINT A107 -11.323   1.645-19.800                          010111
285 JOINT A108 -21.323  11.645-19.800                          100111
286 *leg A2
287 JOINT A201 -11.323-11.645-23.800
288 JOINT A202 -11.323-11.645-27.100
289 JOINT A203 -11.323-11.645-44.000                           001111
290 JOINT A204 -11.323-21.645-27.100                           010111
291 JOINT A205 -21.323-11.645-27.100                           100111
292 JOINT A207 -11.323-21.645-19.800                           010111
293 JOINT A208 -21.323-11.645-19.800                           100111
294 *leg B1
295 JOINT B101  11.323  11.645-23.800
296 JOINT B102  11.323  11.645-27.100
297 JOINT B103  11.323  11.645-44.000                          001111
298 JOINT B104  11.323   1.645-27.100                          010111
299 JOINT B105   1.323  11.645-27.100                          100111
300 JOINT B107  11.323   1.645-19.800                          010111
301 JOINT B108   1.323  11.645-19.800                          100111
302 *Leg B2
303 JOINT B201  11.323-11.645-23.800
304 JOINT B202  11.323-11.645-27.100
305 JOINT B203  11.323-11.645-44.000                           001111
306 JOINT B204  11.323-21.645-27.100                           010111
307 JOINT B205   1.323-11.645-27.100                           100111
308 JOINT B207  11.323-21.645-19.800                           010111
309 JOINT B208   1.323-11.645-19.800                           100111
310
311 LOAD
312 LOADCNTOPS
313 LOAD    05A1                        -2500.                    GLOB JOIN
          1
314 LOAD    05B1                        -2500.                    GLOB JOIN
          1
315 LOAD    05A2                        -2500.                    GLOB JOIN
          1
316 LOAD    05B2                        -2500.                    GLOB JOIN
          1
317 * Topside weight of 10000 kN (assumed)
318
319 *Leg A1
320 LOADCNA1D3
321 LOAD X A102A103      0.0-90000.                               MEMB CONC
          DUMMY
322 LOAD X A103A102      0.0 90000.                               MEMB CONC
          DUMMY
323 LOADCNA1D4
324 LOAD X A102A104      0.0-90000.                               MEMB CONC
          DUMMY
325 LOAD X A104A102      0.0 90000.                               MEMB CONC
          DUMMY
326 LOADCNA1D5
327 LOAD X A102A105      0.0-90000.                               MEMB CONC
          DUMMY
```

```
328 LOAD X A105A102      0.0  90000.                    MEMB CONC
        DUMMY
329 LOADCNA1D7
330 LOAD X  0A1A107      0.0 -90000.                    MEMB CONC
        DUMMY
331 LOAD X A107 0A1      0.0  90000.                    MEMB CONC
        DUMMY
332 LOADCNA1D8
333 LOAD X  0A1A108      0.0 -90000.                    MEMB CONC
        DUMMY
334 LOAD X A108 0A1      0.0  90000.                    MEMB CONC
        DUMMY
335 *Leg A2
336 LOADCNA2D3
337 LOAD X A202A203      0.0 -90000.                    MEMB CONC
        DUMMY
338 LOAD X A203A202      0.0  90000.                    MEMB CONC
        DUMMY
339 LOADCNA2D4
340 LOAD X A202A204      0.0 -90000.                    MEMB CONC
        DUMMY
341 LOAD X A204A202      0.0  90000.                    MEMB CONC
        DUMMY
342 LOADCNA2D5
343 LOAD X A202A205      0.0 -90000.                    MEMB CONC
        DUMMY
344 LOAD X A205A202      0.0  90000.                    MEMB CONC
        DUMMY
345 LOADCNA2D7
346 LOAD X  0A2A207      0.0 -90000.                    MEMB CONC
        DUMMY
347 LOAD X A207 0A2      0.0  90000.                    MEMB CONC
        DUMMY
348 LOADCNA2D8
349 LOAD X  0A2A208      0.0 -90000.                    MEMB CONC
        DUMMY
350 LOAD X A208 0A2      0.0  90000.                    MEMB CONC
        DUMMY
351 *Leg B1
352 LOADCNB1D3
353 LOAD X B102B103      0.0 -90000.                    MEMB CONC
        DUMMY
354 LOAD X B103B102      0.0  90000.                    MEMB CONC
        DUMMY
355 LOADCNB1D4
356 LOAD X B102B104      0.0 -90000.                    MEMB CONC
        DUMMY
357 LOAD X B104B102      0.0  90000.                    MEMB CONC
        DUMMY
358 LOADCNB1D5
359 LOAD X B102B105      0.0 -90000.                    MEMB CONC
        DUMMY
360 LOAD X B105B102      0.0  90000.                    MEMB CONC
```

```
        DUMMY
361 LOADCNB1D7
362 LOAD X   0B1B107       0.0 -90000.                          MEMB CONC
        DUMMY
363 LOAD X B107 0B1        0.0  90000.                          MEMB CONC
        DUMMY
364 LOADCNB1D8
365 LOAD X   0B1B108       0.0 -90000.                          MEMB CONC
        DUMMY
366 LOAD X B108 0B1        0.0  90000.                          MEMB CONC
        DUMMY
367 *Leg B2
368 LOADCNB2D3
369 LOAD X B202B203        0.0 -90000.                          MEMB CONC
        DUMMY
370 LOAD X B203B202        0.0  90000.                          MEMB CONC
        DUMMY
371 LOADCNB2D4
372 LOAD X B202B204        0.0 -90000.                          MEMB CONC
        DUMMY
373 LOAD X B204B202        0.0  90000.                          MEMB CONC
        DUMMY
374 LOADCNB2D5
375 LOAD X B202B205        0.0 -90000.                          MEMB CONC
        DUMMY
376 LOAD X B205B202        0.0  90000.                          MEMB CONC
        DUMMY
377 LOADCNB2D7
378 LOAD X   0B2B207       0.0 -90000.                          MEMB CONC
        DUMMY
379 LOAD X B207 0B2        0.0  90000.                          MEMB CONC
        DUMMY
380 LOADCNB2D8
381 LOAD X   0B2B208       0.0 -90000.                          MEMB CONC
        DUMMY
382 LOAD X B208 0B2        0.0  90000.                          MEMB CONC
        DUMMY
383
384 LOADCN   FH
385 LOAD    03A2          2000.                                GLOB JOIN
         1
386 END
```

Gap Element file

```
1 GAPOPT    5    4    1   MN1200                          PFG
2 LCSEL                  FH TOPS     W    SW   WSW
3 LCOMB LC1      FH       1.
4 LCOMB LC2       W       1.TOPS      1.
5 LCOMB LC3      SW       1.TOPS      1.
6 LCOMB LC4     WSW       1.TOPS      1.
7 *Leg A1
8 *vertical spring
```

```
 9 GAPELM A102 A103 A1D3 FD
10 F-DEL -20000. -3.29 -14000. -1.95 -11500. -1.42
     -9000. -0.96
11 F-DEL -7000. -0.62 -6000. -0.47 -5200. -0.37
     -4700. -0.31
12 F-DEL -4100. -0.245 -3600. -0.19 -3000. -0.14
     -2700. -0.12
13 F-DEL -2200. -0.0866 -1600. -0.0543 -1000. -0.0274
     0. 0.
14 F-DEL 794.3 0.0135 1511. 0.0270 2136. 0.0405
     2671. 0.054
15 F-DEL 3124. 0.0677 3218. 0.071 3307. 0.0745
     3350. 0.076
16 F-DEL 3383. 0.0775
17 *K2y
18 GAPELM A102 A104 A1D4 FD
19 F-DEL -10000. -2.10 -1185.16 -0.137 -1100. -0.117
     -1025. -0.10065
20 F-DEL -950. -0.0866 -900. -0.0786 -800. -0.0636
     -650. -0.04397
21 F-DEL -500. -0.0296 -400. -0.02186 -300. -0.01535
     -200. -0.00949
22 F-DEL 0. 0. 200. 0.00949 300. 0.01535
     400. 0.02186
23 F-DEL 500. 0.0296 650. 0.04397 800. 0.0636
     900. 0.0786
24 F-DEL 950. 0.0866 1025. 0.10065 1100. 0.117
     1185.16 0.137
25 F-DEL 10000. 2.10
26 *K2x
27 GAPELM A102 A105 A1D5 FD
28 F-DEL -10000. -2.10 -1185.16 -0.137 -1100. -0.117
     -1025. -0.10065
29 F-DEL -950. -0.0866 -900. -0.0786 -800. -0.0636
     -650. -0.04397
30 F-DEL -500. -0.0296 -400. -0.02186 -300. -0.01535
     -200. -0.00949
31 F-DEL 0. 0. 200. 0.00949 300. 0.01535
     400. 0.02186
32 F-DEL 500. 0.0296 650. 0.04397 800. 0.0636
     900. 0.0786
33 F-DEL 950. 0.0866 1025. 0.10065 1100. 0.117
     1185.16 0.137
34 F-DEL 10000. 2.10
35 *K1y
36 GAPELM 0A1 A107 A1D7 FD
37 F-DEL -10000. -2.55 -1185.16 -0.166 -1100. -0.142
     -1025. -0.122
38 F-DEL -950. -0.105 -900. -0.0953 -800. -0.0771
     -650. -0.0533
39 F-DEL -500. -0.0359 -400. -0.0265 -300. -0.0186
     -200. -0.0115
40 F-DEL 0. 0. 200. 0.0115 300. 0.0186
```

```
      400.    0.0265
41 F-DEL         500.    0.0359      650.    0.0533      800.    0.0771
      900.    0.0953
42 F-DEL         950.     0.105     1025.     0.122     1100.     0.142
      1185.16     0.166
43 F-DEL       10000.      2.55
44 *K1x
45 GAPELM  0A1 A108 A1D8  FD
46 F-DEL      -10000.     -2.55 -1185.16    -0.166    -1100.    -0.142
      -1025.    -0.122
47 F-DEL         -950.    -0.105     -900.   -0.0953     -800.   -0.0771
      -650.   -0.0533
48 F-DEL         -500.   -0.0359     -400.   -0.0265     -300.   -0.0186
      -200.   -0.0115
49 F-DEL            0.          0.      200.    0.0115      300.    0.0186
      400.    0.0265
50 F-DEL         500.    0.0359      650.    0.0533      800.    0.0771
      900.    0.0953
51 F-DEL         950.     0.105     1025.     0.122     1100.     0.142
      1185.16     0.166
52 F-DEL       10000.      2.55
53 *Leg A2
54 *vertical spring
55 GAPELM A202 A203 A2D3  FD
56 F-DEL      -20000.     -3.29 -14000.     -1.95 -11500.     -1.42
      -9000.     -0.96
57 F-DEL       -7000.     -0.62    -6000.     -0.47    -5200.     -0.37
      -4700.     -0.31
58 F-DEL       -4100.    -0.245    -3600.     -0.19    -3000.     -0.14
      -2700.     -0.12
59 F-DEL       -2200.   -0.0866    -1600.   -0.0543    -1000.   -0.0274
      0.          0.
60 F-DEL        794.3    0.0135     1511.    0.0270     2136.    0.0405
      2671.     0.054
61 F-DEL        3124.    0.0677     3218.     0.071     3307.    0.0745
      3350.     0.076
62 F-DEL        3383.    0.0775
63 *K2y
64 GAPELM A202 A204 A2D4  FD
65 F-DEL      -10000.     -2.10 -1185.16    -0.137    -1100.    -0.117
      -1025. -0.10065
66 F-DEL         -950.   -0.0866     -900.   -0.0786     -800.   -0.0636
      -650. -0.04397
67 F-DEL         -500.   -0.0296     -400. -0.02186     -300. -0.01535
      -200. -0.00949
68 F-DEL            0.          0.      200.  0.00949      300.  0.01535
      400.  0.02186
69 F-DEL         500.    0.0296      650.  0.04397      800.    0.0636
      900.    0.0786
70 F-DEL         950.    0.0866     1025.  0.10065     1100.     0.117
      1185.16     0.137
71 F-DEL       10000.      2.10
72 *K2x
```

```
GAPELM A202 A205 A2D5 FD
F-DEL -10000. -2.10 -1185.16 -0.137 -1100. -0.117
      -1025. -0.10065
F-DEL  -950. -0.0866  -900. -0.0786  -800. -0.0636
       -650. -0.04397
F-DEL  -500. -0.0296  -400. -0.02186 -300. -0.01535
       -200. -0.00949
F-DEL     0.    0.   200.  0.00949   300.  0.01535
       400.  0.02186
F-DEL   500.  0.0296   650.  0.04397   800.  0.0636
       900.  0.0786
F-DEL   950.  0.0866  1025.  0.10065  1100.  0.117
      1185.16  0.137
F-DEL 10000.  2.10
*K1y
GAPELM 0A2 A207 A2D7 FD
F-DEL -10000. -2.55 -1185.16 -0.166 -1100. -0.142
      -1025. -0.122
F-DEL  -950. -0.105  -900. -0.0953  -800. -0.0771
       -650. -0.0533
F-DEL  -500. -0.0359  -400. -0.0265  -300. -0.0186
       -200. -0.0115
F-DEL     0.    0.   200.  0.0115   300.  0.0186
       400.  0.0265
F-DEL   500.  0.0359   650.  0.0533   800.  0.0771
       900.  0.0953
F-DEL   950.  0.105  1025.  0.122  1100.  0.142
      1185.16  0.166
F-DEL 10000.  2.55
*K1x
GAPELM 0A2 A208 A2D8 FD
F-DEL -10000. -2.55 -1185.16 -0.166 -1100. -0.142
      -1025. -0.122
F-DEL  -950. -0.105  -900. -0.0953  -800. -0.0771
       -650. -0.0533
F-DEL  -500. -0.0359  -400. -0.0265  -300. -0.0186
       -200. -0.0115
F-DEL     0.    0.   200.  0.0115   300.  0.0186
       400.  0.0265
F-DEL   500.  0.0359   650.  0.0533   800.  0.0771
       900.  0.0953
F-DEL   950.  0.105  1025.  0.122  1100.  0.142
      1185.16  0.166
F-DEL 10000.  2.55
*Leg B1
*vertical spring
GAPELM B102 B103 B1D3 FD
F-DEL -20000. -3.29 -14000. -1.95 -11500. -1.42
      -9000. -0.96
F-DEL  -7000. -0.62  -6000. -0.47  -5200. -0.37
       -4700. -0.31
F-DEL  -4100. -0.245  -3600. -0.19  -3000. -0.14
       -2700. -0.12
```

```
105 F–DEL       −2200.   −0.0866    −1600.   −0.0543    −1000.   −0.0274
        0.         0.
106 F–DEL        794.3    0.0135     1511.    0.0270     2136.    0.0405
        2671.     0.054
107 F–DEL        3124.    0.0677     3218.     0.071     3307.    0.0745
        3350.     0.076
108 F–DEL        3383.    0.0775
109 *K2y
110 GAPELM B102  B104  B1D4   FD
111 F–DEL      −10000.     −2.10 −1185.16    −0.137    −1100.    −0.117
        −1025.  −0.10065
112 F–DEL        −950.   −0.0866     −900.   −0.0786     −800.   −0.0636
        −650.  −0.04397
113 F–DEL        −500.   −0.0296     −400. −0.02186     −300. −0.01535
        −200.  −0.00949
114 F–DEL           0.         0.      200.  0.00949      300.  0.01535
        400.   0.02186
115 F–DEL         500.    0.0296      650.  0.04397      800.   0.0636
        900.    0.0786
116 F–DEL         950.    0.0866     1025.  0.10065     1100.    0.117
        1185.16    0.137
117 F–DEL       10000.      2.10
118 *K2x
119 GAPELM B102  B105  B1D5   FD
120 F–DEL      −10000.     −2.10 −1185.16    −0.137    −1100.    −0.117
        −1025.  −0.10065
121 F–DEL        −950.   −0.0866     −900.   −0.0786     −800.   −0.0636
        −650.  −0.04397
122 F–DEL        −500.   −0.0296     −400. −0.02186     −300. −0.01535
        −200.  −0.00949
123 F–DEL           0.         0.      200.  0.00949      300.  0.01535
        400.   0.02186
124 F–DEL         500.    0.0296      650.  0.04397      800.   0.0636
        900.    0.0786
125 F–DEL         950.    0.0866     1025.  0.10065     1100.    0.117
        1185.16    0.137
126 F–DEL       10000.      2.10
127 *K1y
128 GAPELM   0B1  B107  B1D7   FD
129 F–DEL      −10000.     −2.55 −1185.16    −0.166    −1100.    −0.142
        −1025.   −0.122
130 F–DEL        −950.    −0.105     −900.  −0.0953     −800.  −0.0771
        −650.  −0.0533
131 F–DEL        −500.  −0.0359     −400.  −0.0265     −300.  −0.0186
        −200.  −0.0115
132 F–DEL           0.         0.      200.   0.0115      300.   0.0186
        400.   0.0265
133 F–DEL         500.   0.0359      650.   0.0533      800.   0.0771
        900.   0.0953
134 F–DEL         950.    0.105     1025.    0.122     1100.    0.142
        1185.16    0.166
135 F–DEL       10000.      2.55
136 *K1x
```

```
137 GAPELM  0B1 B108 B1D8  FD
138 F-DEL      -10000.     -2.55 -1185.16    -0.166    -1100.    -0.142
       -1025.    -0.122
139 F-DEL        -950.    -0.105     -900.   -0.0953     -800.   -0.0771
       -650.   -0.0533
140 F-DEL        -500.   -0.0359     -400.   -0.0265     -300.   -0.0186
       -200.   -0.0115
141 F-DEL           0.        0.      200.    0.0115      300.    0.0186
       400.    0.0265
142 F-DEL         500.    0.0359      650.    0.0533      800.    0.0771
       900.    0.0953
143 F-DEL         950.     0.105     1025.     0.122     1100.     0.142
       1185.16     0.166
144 F-DEL       10000.      2.55
145 *Leg B2
146 *vertical spring
147 GAPELM B202 B203 B2D3  FD
148 F-DEL      -20000.     -3.29 -14000.     -1.95 -11500.     -1.42
       -9000.     -0.96
149 F-DEL       -7000.     -0.62  -6000.     -0.47  -5200.     -0.37
       -4700.     -0.31
150 F-DEL       -4100.    -0.245  -3600.     -0.19  -3000.     -0.14
       -2700.     -0.12
151 F-DEL       -2200.   -0.0866  -1600.   -0.0543  -1000.   -0.0274
       0.         0.
152 F-DEL        794.3    0.0135   1511.    0.0270   2136.    0.0405
       2671.     0.054
153 F-DEL        3124.    0.0677   3218.     0.071   3307.    0.0745
       3350.     0.076
154 F-DEL        3383.    0.0775
155 *K2y
156 GAPELM B202 B204 B2D4  FD
157 F-DEL      -10000.     -2.10 -1185.16    -0.137    -1100.    -0.117
       -1025.  -0.10065
158 F-DEL        -950.   -0.0866     -900.   -0.0786     -800.   -0.0636
       -650.  -0.04397
159 F-DEL        -500.   -0.0296     -400.  -0.02186     -300.  -0.01535
       -200.  -0.00949
160 F-DEL           0.        0.      200.   0.00949      300.   0.01535
       400.   0.02186
161 F-DEL         500.    0.0296      650.   0.04397      800.    0.0636
       900.    0.0786
162 F-DEL         950.    0.0866     1025.   0.10065     1100.     0.117
       1185.16     0.137
163 F-DEL       10000.      2.10
164 *K2x
165 GAPELM B202 B205 B2D5  FD
166 F-DEL      -10000.     -2.10 -1185.16    -0.137    -1100.    -0.117
       -1025.  -0.10065
167 F-DEL        -950.   -0.0866     -900.   -0.0786     -800.   -0.0636
       -650.  -0.04397
168 F-DEL        -500.   -0.0296     -400.  -0.02186     -300.  -0.01535
       -200.  -0.00949
```

```
169 F-DEL          0.        0.      200.   0.00949      300.   0.01535
       400.   0.02186
170 F-DEL        500.    0.0296      650.   0.04397      800.    0.0636
       900.    0.0786
171 F-DEL        950.    0.0866     1025.   0.10065     1100.     0.117
       1185.16     0.137
172 F-DEL       10000.      2.10
173 *K1y
174 GAPELM  0B2 B207 B2D7  FD
175 F-DEL      -10000.     -2.55  -1185.16    -0.166    -1100.    -0.142
       -1025.    -0.122
176 F-DEL        -950.    -0.105     -900.   -0.0953     -800.   -0.0771
       -650.   -0.0533
177 F-DEL        -500.   -0.0359     -400.   -0.0265     -300.   -0.0186
       -200.   -0.0115
178 F-DEL          0.        0.      200.   0.0115      300.    0.0186
       400.    0.0265
179 F-DEL        500.    0.0359      650.   0.0533      800.    0.0771
       900.    0.0953
180 F-DEL        950.     0.105     1025.    0.122     1100.     0.142
       1185.16     0.166
181 F-DEL       10000.      2.55
182 *K1x
183 GAPELM  0B2 B208 B2D8  FD
184 F-DEL      -10000.     -2.55  -1185.16    -0.166    -1100.    -0.142
       -1025.    -0.122
185 F-DEL        -950.    -0.105     -900.   -0.0953     -800.   -0.0771
       -650.   -0.0533
186 F-DEL        -500.   -0.0359     -400.   -0.0265     -300.   -0.0186
       -200.   -0.0115
187 F-DEL          0.        0.      200.   0.0115      300.    0.0186
       400.    0.0265
188 F-DEL        500.    0.0359      650.   0.0533      800.    0.0771
       900.    0.0953
189 F-DEL        950.     0.105     1025.    0.122     1100.     0.142
       1185.16     0.166
190 F-DEL       10000.      2.55
191 END
```

Superelement Input file

```
 1 SUBOPT INP MN
 2 STFHEAD    0A1 0A1 +1.
 3 STFR FX
 4 STFR FY
 5 STFR FZ
 6 STFR MX
 7 STFR MY
 8 STFR MZ                                                        50.12e6
 9 STFHEAD    0A2 0A2 +1.
10 STFR FX
11 STFR FY
12 STFR FZ
```

```
13 STFR MX
14 STFR MY
15 STFR MZ                                                    50.12e6
16 STFHEAD    0B1  0B1  +1.
17 STFR FX
18 STFR FY
19 STFR FZ
20 STFR MX
21 STFR MY
22 STFR MZ                                                    50.12e6
23 STFHEAD    0B2  0B2  +1.
24 STFR FX
25 STFR FY
26 STFR FZ
27 STFR MX
28 STFR MY
29 STFR MZ                                                    50.12e6
30 END
```